

# Applications of Computer Modelling to Landfill Processes.

DoE Report Number : CWM 039A/92.

*Contractor*

Dr. Alan Young,  
188 Divinity Road,  
Oxford,  
OX4 1LR,

*Sub-Contractor*

Dr. David Davies,  
Aspinwall & Company,  
Walford Manor,  
Baschurch,  
Shrewsbury,  
SY4 2HH.

**Principal Keywords.**

Gas, landfill, methane, modelling.

**Secondary Keywords.**

Acidogenesis, atmosphere, Darcy flow, decomposition, degradation, emissions, leachate, migration, pressure, simulation, temperature, venting, water.

**Official Disclaimer.**

The opinions expressed in this report are those of the author (Alan Young) and may not reflect those of the Department of the Environment. The results of this work may be used in the formulation of government policy, but at this stage they do not necessarily represent government policy.

**Staff.**

At the Mathematical Institute of Oxford University the staff involved with this project were Alan Young, Nigel J. Gay and Leslie C. Woods. At Aspinwall & Company the principal staff connected with this project have been David R. Davies, Philippa Towler, Brian Latham and Peter Young.

**Acknowledgements.**

Funding for this project was provided by the Department of the Environment (U.K.). Earlier work was funded jointly by Aspinwall & Company, the U.S. Army Corps of Engineers, and the SERC. Irene Watson-Craik and Sandra Goldie at Strathclyde University were responsible for the microbial investigation. The author would like to thank the many individuals and organisations who have given freely of their time and expertise, without whom this project could not have been successful.

## Contents.

### Chapters.

Chapter		Page
1	Executive summary	1
2	Project Background	7
3	Continuum Models	9
4	Gas Composition and Migration	22
5	Gas Extraction Systems	64
6	The Methanogenic Ecosystem	84
7	Temperature and Moisture	109
8	Additional Topics	133
9	Overall Summary	143

Appendices		Page
3A	Finite Element Algorithm	156
3B	Three Dimensional ADI Method	158
4A	The Loscoe Explosion	161
4B	Experimental Results from Sleaf	164
5A	Solution of Network Equations	174
5B	Analytical Gas Flow Solution	176
6A	Biochemical Approximations	180
6B	Effects of Temperature and pH	183
7A	Solution of Gas Flow Equations	187
N	Main Notation	189
R	References	192

## **Chapter 1 : Executive Summary.**

This report describes the results of a 3-year research project funded by the Department of the Environment. Its aim has been to gain an improved understanding of landfill behaviour through the development of mathematical models, and to apply these to specific problems in site management. This executive summary is based on the overall conclusions and recommendations presented in Chapter 9.

It is our firm contention that all the mechanisms involved in regulating landfill degradation interact and cannot ultimately be considered in isolation from each other. The model results support this belief and we advocate a more holistic approach to landfill management, rather than concentrating on one or two supposedly key parameters as most previous studies have done. Computer simulations are used to demonstrate the interactions of various factors within landfills and to offer insights into feasible management strategies.

The theory that has been developed is sufficiently comprehensive to allow many of the physical, chemical and microbiological characteristics of landfills to be better understood. It also provides a powerful tool for the accurate modelling of gas extraction systems. The models which have been produced are capable of being applied to a wide range of underground pollution problems, though most of the practical emphasis of the present project has been directed specifically towards landfill gas.

## 1.1 Gas Monitoring — Chapter 4.

Current practise in landfill gas monitoring relies on measuring gas composition to assess environmental safety and the internal state of a landfill. However, measurements of emissions from a single site frequently show large variations in chemical composition and magnitude, often on the same time scale as the monitoring interval, and these have been generally ascribed to faulty instrumentation or mysterious alterations in the internal biological processes. Such data will eventually be used as evidence to determine when a site deserves a Certificate of Completion, and it is important to know to what extent it can be trusted. The model has shown that the present methods are both intrinsically unreliable and inaccurate as presently applied.

Results from the model, and a supporting field experiment, show that gas flux and composition is affected by changes in atmospheric pressure. In particular the size of gas emissions is linearly related to the rate at which the surface pressure is changing, and has little correlation with the actual value of atmospheric pressure as is often supposed. The model demonstrates how factors such as pH, void fraction, moisture distribution, depth, permeability, and gas evolution/production rates affect these changes. It is shown that the void fractions are much more important than the permeability. An experimental investigation was conducted at Sleaf, which produced a number of important results showing broad consistency with the model.

Amongst our conclusions are that gas monitoring should be done much more frequently than at present (at least daily), that atmospheric pressure changes must be taken into account, and that monitoring for safety purposes is especially important during periods when atmospheric pressure is falling rapidly. Variations in landfill gas concentration are greatest near the surface of a site, and the model predicts that volumetric changes in surface flux are much larger than the fluctuations in internal composition. We were unable to find suitable instruments for either continuous monitoring of gas composition or flux, and their development should be regarded as a priority.

Simple statistical tests for analysing gas data are demonstrated, and a new method of graphically presenting monitoring data has been developed. It is recommend that these become part of standard site characterisation practises.

The model also looked at the effect of aquifers beneath a site and the effect this has on gas yield. In particular it was shown that they may be responsible for the observed phenomena of sites which have an average internal pressure below atmospheric. Predicted spatial variations in carbon-dioxide are highlighted as a possible diagnostic test for the presence of aquifers within or near to sites.

## 1.2 Gas Extraction Systems — Chapter 5.

Gas extraction systems are currently designed on a rule-of-thumb basis using the radius of influence of a gas well as a single parameter relating gas yield to applied suction, and ignoring the interactions between wells and surface equipment. The model has been used to develop a parameter (the yield reduction coefficient, YRC) which quantifies the degree to which one well affects another. The use of YRCs reduces the need for underground gas flow computations which has previously hindered the prediction of extraction network performance.

The model allows systems composed of any number of pumps, pipes and wells to be assessed before installing them on a site, and can predict the effect of component failures on gas recovery. An illustrative example is given, consisting of 28 wells, 2 pumps and 62 pipes, which took under 2 seconds to compute on a Vax6000 — making the system fast enough for interactive design use by landfill engineers.

### 1.3 Methanogenic Ecosystem — Chapter 6.

Waste management policies in Europe and the UK are placing pressure on packaging wastes, encouraging higher recycling rates and the development of energy reclamation schemes. These changes will have a profound influence on the nature of the residual materials requiring landfill disposal, and the subsequent course of events within sites.

In studying the biochemical degradation of landfills and the establishment of the methanogenic ecosystem, the primary aim has been to predict the conditions under which methanogenesis is able to become established, the time scales required for this to happen, and ways of influencing the processes. The main influences on anaerobic bacterial activity are temperature, pH, Eh, substrate availability, and moisture level. These, together with their associated rate controlling factors are taken into account in the model. To provide flexibility in specifying composition, waste is divided into 10 separate categories. The methanogenic bacteria are considered as two separate species: acetoclasts and hydrogen consumers. A special laboratory study was conducted at Strathclyde University to provide data on the pH and temperature behaviour of methanogens, and it was found that the bacteria are more tolerant of low pH values than is usually assumed.

Low alkali metal concentrations have been associated with a failure of methanogenesis and the model indicates that this is due to insufficient pH buffering during acidogenesis, rather than nutritional deficiencies as has previously been supposed. This pH buffering seems to be essential for the populations to be able to reach a self regulating size. The model also demonstrated that it may be useful to reduce the fraction of highly-degradable wastes present in a site, possibly by aerobic pre-composting.

## **1.4 Temperature and Moisture — Chapter 7.**

The internal heat balance of landfills is one of the primary factors regulating their behaviour. A section of the model calculates the opposing effects of exothermic bacterial reactions and physical heat losses (including evaporation) and the way in which these are affected by such factors as emplacement temperature, site layout, and long-term site management practises. Amongst the results is a recommended minimum depth for new landfills.

One outcome of this is a study comparing the consequences of changes in capping regulations which would favour the creation of either wet or dry sites. The simulations indicate that although dry sites have fewer operational problems in the short-term, they represent a much greater long-term hazard and consequently wetter sites are recommended. The investigation also found that, for reasons of speed and convenience, microbial experiments have only been done with very wet wastes and the state of knowledge regarding dry wastes is inadequate.

A scheme is proposed for increasing gas production rates and accelerating site stabilization by partially re-circulating extracted gas. This technique would be most likely to find application at sites where gas flow rates are insufficient to warrant exploitation, and simulations indicate that it should be possible to substantially raise the internal temperature, perhaps even to thermophilic levels. Other potential advantages of this process include the maintenance of anaerobic conditions and shorter completion times. A field study is needed before this can be attempted at a real site.

## **1.5 Settlement and Water Flow — Chapter 8.**

Landfill settlement is an issue of growing importance to operators, and an initial aim of the project was to explain the major factors affecting its rate and magnitude and to produce a predictive model based on them. However despite the belief in the industry that good data exists, none of it is useful: the only thing measured is the rate at which the surface height at a site decreases with time, and nothing is known of the extent to which interior layers have been compressed or displaced. Before a model can be constructed, an investigation is required into the bulk modulus of waste and how it varies with the composition of the material present. Such a project has now been initiated by the DoE.

Several models for landfill moisture flow were compared, including a sophisticated approach based on a doubly-porous media formulation. It was concluded that, except during periods of sudden flooding, a basic single-media model represents the optimum balance between ease of parametrisation and accuracy.



## **1.6 Summary, Recommendations and Future Work — Chapter 9.**

A major benefit of the approach adopted has been the highlighting of deficiencies in current knowledge and consequent recommendations for data acquisition. The final chapter suggests changes in landfill practise based on model results, and details the experimental evidence that is currently lacking.

## **Chapter 2 : Project Background.**

Immediately following its deposition within a landfill most of the organic fraction of waste will begin to undergo degradation through chemical and bacterial action. In the earliest phase this takes place via aerobic metabolic pathways, but as more material is added and overlying strata begin to significantly impede the flow of oxygen into the landfill then the dominant reactions within the interior will become anaerobic. After the first year or so of decomposition the major gaseous products are normally carbon dioxide and methane, and the reactions producing them will continue at a gradually decreasing rate for at least fifteen, and often upwards of fifty, years. It is during this latter phase that the majority of the degradable waste will decompose.

The onset of large-scale methane production is of great importance when managing a site, both in terms of its environmental impact and financial opportunities for exploitation. Before this occurs the gas vented is largely carbon dioxide with an admixture of hydrogen, and the leachate (the liquid from within the site, which may leak from some uncontrolled landfills) is highly acidic. When the methane producing phase is entered, hydrogen ceases to be found in the gas, and the leachate becomes much less acidic (and consequently less harmful in the event it escapes past the site walls).

The aim of this project was to produce a mathematical model for landfill processes which could be implemented on computers to produce predictions of site behaviour.

It is our firm contention that all the mechanisms involved in regulating landfill degradation interact and cannot ultimately be considered in isolation from each other. However the number of variables involved makes the production of a single unified model difficult, and it is initially necessary to separate out the primary aspects and to develop and verify them individually. Hence this report describes a modular set of models which could eventually be combined to produce a single scheme.

The difficulties in gathering data regarding the contents of a particular site make it difficult to produce specific predictions of the sites future behaviour — in addition to which the amount of computer time required for some aspects would be prohibitive. Most of our effort was therefore concentrated on producing generic models to identify the primary in-situ interactions and any feasible methods of controlling them. The advantage of modelling over experimentation for these purposes is that there are no uncontrollable factors and full information is available when trying to understand simulation results.

A significant by-product of the modelling process has been the identification of areas in which fundamental data is lacking, and of the need to perform experiments before further progress can be made.

## **2.1 How To Read This Report.**

It has been my intention that each of Chapters 4–8 should, as far as possible, be able to be read as a stand-alone essay. To minimise unnecessary duplication of the mathematics, the common modelling elements have been gathered together into Chapter 3, however the general reader should be able to omit this Chapter without detracting from the content overmuch.

## **2.2 History.**

The project was originally conceived in 1981 between Professor L.C. Woods and Dr. David R. Davies. In 1983 a short M.Sc dissertation was produced at the Mathematical Institute of Oxford University by Mark Cooker, primarily as a literature review.

In October 1986, Alan Young began a D.Phil at Oxford entitled “Mathematical Models for Active Landfills” as a CASE award between the SERC and Aspinwall & Company, with Peter Young acting as the Industrial Liaison. This was completed in February 1989.

In April 1989 the Department of the Environment (in the person of Dr. Janet Gronow) agreed to fund the research for a 3-year period, and to allow the recruitment of additional staff. Nigel Gay joined the Oxford team in September 1989. Dr. Philippa Towler was the principal contact at Aspinwall & Company during the early phase, with Brian Latham taking over part of this role in the later stages. The contract was eventually extended by six months till the end of September 1992.

Although there is necessarily some overlap, Alan Young was responsible for most of the material in Chapters 3, 4, 5 and 6, while Nigel Gay did the majority of the work for Chapters 7 and 8.

## **Chapter 3 : Continuum Models.**

In this section we explain the main mathematical techniques upon which this report is based, in the hope of improving the lucidity of the other Chapters by concentrating most of the formal derivations here. Readers without a mathematical background may thus omit this Chapter.

### **3.1 Introduction.**

All the models used rely on the continuum hypothesis, which is that the landfill interior can be approximated by piecewise ‘smooth’ functions. Our strategy is first to formulate a general transport equation for gases and solutes, then to deduce specific cases from it. Generally we have preferred to solve equations using analytical techniques, but when this has not been possible numerical finite element and ADI methods have been employed (which are documented briefly in Appendices 3A and 3B).

The large number of parameters involved in the various aspects of the landfill model mean that some symbols have different meanings in different Chapters. However,  $P$  is always pressure,  $t$  is time,  $x, y, z$  are Cartesian space co-ordinates,  $u$  is gas velocity,  $v$  is liquid velocity,  $\varphi$  is the void fraction available to gas,  $\theta$  is the void fraction available to water, and  $K$  is the permeability. Appendix N lists the meanings of the individual variables used in each Chapter.

### 3.2 The General Flow Equation.

This is formulated by considering the amount of some substance present in a ‘typical’ arbitrary volume  $\Omega$  inside the region bounded by surface  $\partial\Omega$ . This will obey the following mass balance

$$\begin{aligned}
 \text{Rate of change of mass within } \Omega &= \text{Convective flux through } \partial\Omega \\
 &+ \text{Diffusive flux through } \partial\Omega \\
 &+ \text{Rate of formation/destruction} \\
 &+ \text{Rate of artificial injection/extraction.}
 \end{aligned} \tag{1}$$

Mathematically this can be phrased as

$$\frac{\partial}{\partial t} \iiint_{\Omega} C \varphi \, d\tau = \oint_{\partial\Omega} -C \underline{u} \cdot d\underline{S} + \oint_{\partial\Omega} \underline{\underline{E}} \nabla C \cdot d\underline{S} + \iiint_{\Omega} Q \, d\tau + \iiint_{\Omega} W \, d\tau, \tag{2}$$

where  $C$  is the concentration of the substance,  $t$  is the time,  $\varphi$  is the void fraction accessible,  $\underline{u}$  is the Darcy fluid velocity (ie. the volume of fluid passing through unit area per unit time),  $\underline{\underline{E}}$  is the combined diffusion/dispersion tensor,  $Q$  is the rate of mass formation/destruction, and  $W$  is the rate of mass injection/extraction by which the substance enters/leaves  $\Omega$  without passing through the boundary  $\partial\Omega$ . Since the region  $\Omega$  is arbitrary, we may apply the divergence theorem and remove the integral signs thus

$$\frac{\partial}{\partial t}(C\varphi) + \text{div}(C\underline{u}) = \text{div}(\underline{\underline{E}}\nabla C) + Q + W. \tag{3}$$

The main categories of applicable boundary conditions for such equations are

$$\begin{aligned}
 \text{Specified concentration} &\Rightarrow C = A, \\
 \text{Specified normal gradient} &\Rightarrow \frac{\partial C}{\partial n} = A, \\
 \text{Specified flux} &\Rightarrow C \underline{u} \cdot \underline{n} + \frac{\partial C}{\partial n} = A,
 \end{aligned}$$

where  $\underline{n}$  is the unit outward normal to the surface  $\partial\Omega$ , and  $A$  is some function. For one dimensional flow, parallel to the  $z$ -axis, the governing equation simplifies to the form

$$\frac{\partial}{\partial t}(C\varphi) + \frac{\partial}{\partial z}(Cu) = \frac{\partial}{\partial z} \left( E \frac{\partial C}{\partial z} \right) + Q + W, \tag{4}$$

where  $u$  is assumed positive if flow is in the direction of  $z$  increasing.

### 3.3 Slow Single Species Gas Flow.

The most elementary model for landfill gas flow treats the gas as being a composite with properties near to those of an equimolar mixture of carbon dioxide and methane (though if any result derived using this assumption predicts the ingress of gas from the atmosphere into a site then we must treat it with care). Fully coupled models for the simultaneous flow of liquid and gas are possible, but their solution is often difficult (and in any case requires unavailable detail on internal geometry), and as the effects of landfill water movement are usually on a much longer time scale than those of gas migration we shall neglect the former wherever convenient.

Applying our general mass flow relation gives the equation

$$\frac{\partial}{\partial t}(\rho\varphi) + \text{div}(\rho\underline{u}) = Q + W, \quad (5)$$

where  $\rho$  is the composite gas density in  $\text{kg m}^{-3}$ . The term  $Q$  ( $\text{kg m}^{-3} \text{s}^{-1}$ ) will usually be distributed due to biological activity and gas solution/exsolution, whereas the mass sink term  $W$  ( $\text{kg m}^{-3} \text{s}^{-1}$ ) is highly localised since gas enters an extraction pipe only at its surface.

At this point we make a ‘smoothing’ approximation by supposing that it is possible to define a global<sup>†</sup> gas permeability  $\underline{K}$  within the region, and we allow for the possibility of differing values in different directions by assigning it the tensor form

$$\underline{K} = \begin{pmatrix} K_v & 0 & 0 \\ 0 & K_h & 0 \\ 0 & 0 & K_h \end{pmatrix}, \quad (6)$$

where  $K_v$  and  $K_h$  are the vertical and horizontal permeabilities respectively in  $\text{m}^2 \text{s}^{-1} \text{Pa}^{-1}$ .

Within the landfill interior, high internal friction and geometrical complexity mean that the standard Navier-Stokes equations for fluid flow cannot be applied. When gas flows slowly through a porous medium, friction is usually the major factor restricting its motion, and this rather than conservation of momentum is the feature which must be used to model the gas velocity. Darcy’s law gives an empirical relation between the pressure gradient and the gas velocity for slow flows as

$$\underline{u} = -\underline{K} \cdot \nabla p, \quad (7)$$

where  $p$  is the gas pressure (Pa), and combining this with equation (5) gives

$$\frac{\partial(\varphi\rho)}{\partial t} = \text{div}(\rho\underline{K} \cdot \nabla P) + Q + W. \quad (8)$$

---

<sup>†</sup> Obviously on a sufficiently small scale  $\underline{K}$  would be very dependent on the location.

We also make use of the Ideal Gas Law

$$P_a + P = p = \frac{RT_K \rho}{m} = \alpha \rho \quad \text{say,} \quad (9)$$

where  $P_a$  is the steady mean background atmospheric pressure,  $P$  the deviation from this,  $R$  the Ideal Gas constant,  $T_K$  the absolute temperature and  $m$  the composite molar gas mass. Other studies carried out as part of our model indicate that the heat carrying capacity of the gas is negligible compared with that of the waste, and field data shows that the absolute temperature within the fill tends to be fairly uniform, so that we may take  $\alpha$  as fixed. Similarly  $\varphi$  will change insignificantly except during periods of rapid inundation.

Lastly, in order to linearize the equation (and hence make its solution easier), we would like the term  $|\nabla P|^2$  to be dominated by the behaviour of  $P_a \nabla^2 P$ . If  $h$  is a 'typical length' over which  $p$  varies from zero to its maximum value  $p_{max}$  then the comparison we want is

$$P_a \nabla^2 P \sim P_a P_{max} / h^2 \quad \gg \quad (P_{max} / h)^2 \sim |\nabla P|^2, \quad (10)$$

and this is a reasonable assumption, since within the landfill environment  $p_{max}$  is unlikely to be greater than 0.5% of  $P_a$ . Combining the results of (8–10) we arrive at

$$(\varphi / P_a) \frac{\partial P}{\partial t} = \text{div}(\underline{\underline{K}} \cdot \nabla P) + \lambda Q + \lambda W, \quad (11)$$

where  $\lambda = \alpha / P_a$ . The term  $\lambda Q / P_a$  is measured in  $\text{m}^3 \text{m}^{-3} \text{s}^{-1}$  and thus gives the fractional increase in gas pressure due to new production.

If there is significant leachate present, then a fraction of the gas molecules will be held in solution, so that the effective void fraction has to be modified thus

$$\frac{(\varphi + \gamma \theta)}{P_a} \frac{\partial P}{\partial t} = \text{div}(\underline{\underline{K}} \cdot \nabla P) + \lambda Q + \lambda W, \quad (12)$$

where  $\theta$  is the void fraction occupied by water, and  $\gamma$  is Henry's Constant (see below). For a gas comprised of equal proportions of carbon dioxide and methane at 30 °C, with leachate pH= 6.5, we have

$$\gamma = 0.86, \quad \lambda = 8.4 \times 10^4 \text{ N m kg}^{-1}. \quad (13, 14)$$

For a site which has a relatively thin capping layer, of thickness  $l$  and permeability  $K_l$ , the upper boundary condition is formulated under the reasonable assumption that the flow in the capping layer is predominantly vertical. Thus the gas velocity within it is equal to the exit velocity of the gas leaving the landfill body beneath, and hence at the interface

$$K_l \left[ \frac{p - P_a}{l} \right] = K_v \frac{\partial P}{\partial z} \quad \Rightarrow \quad P = L \frac{\partial P}{\partial z}, \quad (15)$$

with  $P_a$  being the atmospheric pressure, and  $L$  defined as  $lK_v / K_l$ .

### 3.4 Gas Extraction Wells.

The ideal way of incorporating extraction wells into gas flow problems would be to define surfaces within the landfill at which a specified pressure is maintained. However this approach leads to a multiply connected region which, except in cases of unusual symmetry, cannot be solved economically.

Instead we use the device of delta functions (for a fuller explanation of which see Champeney, 1973), assuming that along the centre of each pipe there is a line sink (i.e. a one dimensional region through which mass can vanish or appear). Since such an artifact has no direct physical counterpart we cannot expect our modelled gas flow equations to hold there, but this anomalous region is confined to the centre of a pipe, and provided the requisite conditions hold on the pipe's surface then the solutions generated by this method will still be valid.

Using this approximation, the extraction term for a system of wells may be given as

$$W = \sum_{wells} S_i(\underline{r}) \delta(\underline{r} - \underline{s}), \quad (16)$$

where  $S_i$  gives the strength of the  $i$ th well at any location, and  $\underline{s}$  is a locus of co-ordinates defining the position of the well.



### 3.5 Multiple Species Gas Flow.

It is sometimes necessary to study the individual components of the landfill gas, and a more sophisticated model is required, composed of several equations which must be solved simultaneously. We assume that there are  $M$  different species of gas molecules present and apply our general flow equation. Individual gas molecules are transported either by diffusion/dispersion within the mixed multi-species gas or through convection at some net velocity. Also gas molecules may dissolve in the leachate, or be exsolved from it. Hence

$$\varphi \frac{\partial \rho_i}{\partial t} + \text{div}(\rho_i \underline{u}) = \text{div}(\underline{E}_i \nabla \rho_i) + Q_i, \quad (17)$$

where  $\rho_i$  is the density of the  $i$ th gas,  $\underline{u}$  is now the mean gas velocity,  $E_i$  is the combined diffusion and dispersion coefficient of the  $i$ th species, and  $Q_i$  is the mass rate at which gas molecules leave the leachate. Assume as before that the void fractions occupied by gas and water change very slowly compared with the typical period of variations in the atmospheric pressure. This may be simplified further using the conversion factors  $\alpha_i$  defined by

$$\alpha_i = \frac{m_i}{RT} \quad \Rightarrow \quad P_i = \alpha_i \rho_i, \quad (18)$$

where  $m_i$  is the molar mass of gas  $i$ . The equation for predominantly vertical flow is thus

$$\varphi \frac{\partial P_i}{\partial t} + \frac{\partial}{\partial z}(P_i u) = \frac{\partial}{\partial z} \left( E_i \frac{\partial P_i}{\partial z} \right) + \alpha_i Q_i, \quad (19)$$

with the mean gas velocity being given by Darcy's Law  $u = -K_v \frac{\partial P}{\partial z}$ , where  $P$  is the sum of the individual gas pressures. The effect of the gas composition on its viscosity can be neglected as being insignificant compared to the uncertainties in the permeability, and (as far as compositional changes are concerned) the latter will later also be shown to be relatively unimportant since it primarily influences the net velocity of the gases rather than affecting the individual species.

Note that the values of each of the  $E_i$  coefficients are dependent on the local composition and velocity of the gas, so that they cannot be treated as constants (see below).

### 3.5.1 Mixing Coefficients for Multi-Species Flow in Porous Media.

In an unobstructed region with uniform pressure, Chapman and Cowling (1970) give the momentum equation for the  $i$ th gas in a mixture of  $M$  gases as being

$$\rho_i \left( \frac{\partial \underline{u}_i}{\partial t} + (\underline{u}_i \cdot \nabla) \underline{u}_i \right) = \rho_i \underline{F}_i - \nabla P_i + \sum_{j=1}^M \frac{P_i P_j}{P D_{ij}^b} (\underline{u}_j - \underline{u}_i), \quad (20)$$

where  $\underline{u}_i$  is the velocity of the  $i$ th species of gas molecules, and  $D_{ij}^b$  is the binary diffusion coefficient for the  $i$ - $j$  gas pair.

The formulation (20) may be applied to the landfill interior if the apparent body force  $\rho_i \underline{F}_i$  is replaced by the frictional drag from the static landfill medium. Summing (20) for  $i = 1, \dots, M$  we have the relation  $\sum_{i=1}^n \rho_i \underline{F}_i \approx \nabla P$  so that, for one-dimensional flow, the apparent body force on the  $i$ th gas can be taken as

$$\rho_i \underline{F}_i = \frac{P_i u_i}{PK}. \quad (21)$$

The binary diffusion coefficients can also be modified to take account of the medium thus

$$D_{ij} = \tau \varphi D_{ij}^b + \sigma |vL|, \quad (22)$$

where  $D_{ij}$  is the modified binary diffusion coefficient,  $\tau$  is the tortuosity for gas flow, and  $L$  is the characteristic dispersion length.

Equations (20,21) can be combined to obtain a closed expression for the mixing coefficients  $E_k$  that appear in Equation (4). Writing  $P_i v_i = -E_k \frac{\partial P_i}{\partial z} + u P_i$  gives

$$-\frac{P_i u}{PK} - \frac{\partial P_i}{\partial z} - \sum_{j=1}^M \frac{P_i}{P D_{ij}} E_j \frac{\partial P_j}{\partial z} + \sum_{j=1}^M \frac{P_j}{P D_{ij}} E_i \frac{\partial P_i}{\partial z} = 0, \quad i = 1, \dots, M, \quad (23)$$

which is equivalent to the set of simultaneous algebraic linear equations

$$\begin{pmatrix} \sum_{k \neq 1} S_{k,1} & -S_{1,2} & -S_{1,3} & \dots & -S_{1,M} \\ -S_{2,1} & \sum_{k \neq 2} S_{k,2} & -S_{2,3} & \dots & -S_{2,M} \\ -S_{3,1} & -S_{3,2} & \sum_{k \neq 3} S_{k,3} & \dots & -S_{3,M} \\ \vdots & \vdots & \vdots & \ddots & \vdots \\ -S_{M,1} & -S_{M,2} & \dots & -S_{M,M-1} & \sum_{k \neq M} S_{k,M} \end{pmatrix} \begin{pmatrix} E_1 \\ E_2 \\ E_3 \\ \vdots \\ E_M \end{pmatrix} = \begin{pmatrix} \frac{\partial P_1}{\partial z} + \frac{P_1 u}{PK} \\ \frac{\partial P_2}{\partial z} + \frac{P_2 u}{PK} \\ \frac{\partial P_3}{\partial z} + \frac{P_3 u}{PK} \\ \vdots \\ \frac{\partial P_M}{\partial z} + \frac{P_M u}{PK} \end{pmatrix}, \quad (24)$$

writing  $S_{i,j} = P_i \frac{\partial P_j}{\partial z} / P D_{ij}$  for convenience. These equations are not independent, and to calculate the  $E_i$  we use  $M - 1$  of them (chosen to maximize numerical stability), together with the continuity equation

$$E_1 \frac{\partial P_1}{\partial z} + E_2 \frac{\partial P_2}{\partial z} + E_3 \frac{\partial P_3}{\partial z} + \dots + E_M \frac{\partial P_M}{\partial z} = 0. \quad (25)$$

Note that simpler formulations (which are faster to compute) are available for cases in which all but two of the gases are present in trace concentrations only. However, throughout the depth of the landfill the composition and dominant gases will vary widely, so that such approximations are invalid and will give incorrect results.

### 3.6 Solute Transport.

We can repeat this approach when considering the gas molecules which are dissolved in the water inside a site, giving the formulation

$$\theta \frac{\partial C_i}{\partial t} + \frac{\partial}{\partial z}(vC_i) = \frac{\partial}{\partial z} \left( E_i^w \frac{\partial C_i}{\partial z} \right) - q_i + S_i, \quad (26)$$

with  $\theta$  being the void fraction occupied by water,  $v$  the vertical Darcy water velocity,  $C_i$  the concentration of the  $i$ th species of dissolved molecules,  $E_i^w$  their combined diffusion and dispersion coefficient in the water, and  $S_i$  the rate of mass formation due to chemical and biological processes.

Because the solutes are present in relatively small amounts compared to the volume of water, their mixing coefficients may be taken as

$$E_i^w = \tau^w \theta D_i^w + \sigma |vL|, \quad (27)$$

where  $D_i^w$  is the normal molecular diffusion coefficient,  $\tau^w$  is the tortuosity factor,  $L$  is a characteristic length scale for dispersion within the porous landfill medium, and  $\sigma \approx 1.8$  is the dispersion scaling constant.

### 3.7 Molecular Transfer between Gas and Liquid Phases.

Landfill gas is formed by reactions which probably take place within the body of the liquid (which includes moist surfaces) and molecules must migrate from these sites before they can be evolved into the gas phase. In a medium consisting solely of water and gas this movement is rapid, but the presence of solid material will greatly lengthen many of the migration pathways and thus delay equilibration. Ultimately, in the absence of further production, the dissolved concentration ( $C$ ) and partial pressure ( $P$ ) of a gas would reach a ratio determined by Henry's Law

$$C = HP, \quad (28)$$

where  $H$  is called Henry's constant — though the value of  $H$  changes according to temperature and the presence of other solutes, and the actual amount of gas which dissolves will increase if it reacts chemically with the solute (e.g. by hydration or ionization).

Suppose this process can be characterised by some 'half-life'  $T_{1/2}$  such that, in the absence of further production or venting, the deviation from equilibrium conditions will halve every  $T_{1/2}$  seconds. Denoting  $P_o, C_o$  as the partial pressure and dissolved concentration of a gas at  $t = 0$  and  $P_T, C_T$  as their value at  $t = T$ , we have the relations

$$C_T - HP_T = \exp(-kT)(C_o - HP_o), \quad (29)$$

$$\theta(C_o - C_T) = \Omega \int_0^T \exp(-kt) dt, \quad \varphi(HP_o - HP_T) = -\Omega \int_0^T \exp(-kt) dt, \quad (30, 31)$$

where  $\Omega$  is the initial rate of mass transfer from the dissolved to gaseous phases,  $H$  is Henry's constant, and  $k = \ln(2)/T_{1/2}$ . We may eliminate  $P_T$  and  $C_T$  from these to give

$$\Omega = \frac{k\theta\varphi}{\theta + \varphi}(C_o - HP_o). \quad (32)$$

### 3.7.1 Yield Reduction Coefficients.

Using our equation for gas flow within a landfill containing several extraction wells, we show the conditions under which the flow can be considered as the sum of individual flows due to each of the wells plus a background term. This formulation enables the flux through any single well to be expressed as a function of the suction pressures at all of the wells.

Under the main assumptions that the landfill does not change shape on a time-scale of days and that the deviation of the internal pressure from atmospheric is less than 10%, we earlier derived the basic linearised equation for gas flow in landfill to be

$$\varphi \frac{\partial P}{\partial t} = P_a \operatorname{div}(\underline{K}P) + Q - S. \quad (33)$$

where  $\underline{K}$  is the gas permeability in tensor form,  $P_a$  is atmospheric pressure,  $P$  is the deviation of the gas pressure from atmospheric,  $Q$  is the volume rate of gas generation, and  $S$  is the volume-averaged rate of gas extraction,

Provided the extraction wells occupy only a very small fraction of the landfill volume (ie. we are not considering ‘blanket’ type systems) then under steady operating conditions the overall equation for a site containing  $M$  wells may be re-written as

$$P_a \operatorname{div}(\underline{K}P) + Q = \sum_{i=1}^M V_i S_i, \quad (34)$$

where  $V_i$  is the mass of gas extracted by well  $i$ , and  $S_i$  defines the location of that well. This equation is subject to boundary conditions determined by the nature of the environment surrounding the landfill, and these will generally have the linear form

$$f_1 P + f_2 \frac{\partial P}{\partial \underline{n}} = f_3, \quad (35)$$

where  $f_1$ ,  $f_2$ ,  $f_3$  are functions of position and  $\underline{n}$  is the outward normal to the landfill boundary.

Equations (34,35) may be split into  $M + 1$  sub-problems

$$P = \sum_{j=0}^M P_j, \quad (36)$$

$$P_a \operatorname{div}(\underline{K} \nabla P_0) + Q = 0, \quad f_1 P_0 + f_2 \frac{\partial P_0}{\partial \underline{n}} = f_3, \quad (37, 38)$$

$$P_a \operatorname{div}(\underline{K} \nabla P_i) = V_i S_i, \quad f_1 P_i + f_2 \frac{\partial P_i}{\partial \underline{n}} = 0, \quad i = 1, \dots, M. \quad (39, 40)$$

The pressure solution for each  $P_i$  will be the product of  $V_i$  with some function  $F_i(x, y, z)$  which is independent of  $V_i$ , so that

$$P = P_0 + \sum_{j=1}^M V_j F_j. \quad (41)$$

This procedure is illustrated more fully in Appendix 5B for the specific case of a set of vertical wells in a rectangular landfill.

Writing  $W_i$  as the extraction pressure at  $i$ th well, and applying relation (41) to each of the wells produces a set of  $M$  simultaneous linear equations which express  $W_1, \dots, W_M$  in terms of the yields  $V_1, \dots, V_M$ . This set of equations can be inverted to give each flux  $V_i$  as a function of the extraction pressures  $W_1, \dots, W_M$  thus

$$V_i = \alpha_i + \beta_i \left( W_i - \sum_{j \neq i} \mu_{ij} W_j \right), \quad (42)$$

where  $\alpha_i$ ,  $\beta_i$  and  $\mu_{ij}$  are constants depending on the physical characteristics of the site.

From equation (42) it can be seen that if the suction pressure  $W_j$  at well  $j$  is increased by  $p$ , then the yield at well  $i$  decreases by the same amount as would occur if  $W_j$  were held constant and  $W_i$  were instead reduced by  $\mu_{ij}p$ . Thus  $\mu_{ij}$  quantifies the effect of changing the pressure at well  $j$  on the yield produced by its neighbour well  $i$ .

We therefore define the parameter  $\mu_{ij}$  as the yield reduction coefficient at well  $i$  due to well  $j$ . The greater the interaction between two wells, the larger the YRC will be.

### 3.8 Simultaneous Flow of Heat, Gas and Moisture.

Thermal regulation cannot be considered without including terms for heat transport due to gas and moisture. Since water can exist in one of two phases, we choose variables with the same units for both phases. Hence we use density/concentration as our variable for the amount of water, water vapour and landfill gas at each 'point'. The four variables modelled are:

- [1]  $\rho$ , the saturated landfill gas density ( $\text{kg m}^{-3}$ ),
- [2]  $\theta$ , the moisture density ( $\text{kg m}^{-3}$ ),
- [3]  $T$ , the temperature ( $^{\circ}\text{C}$ ).
- [4]  $\rho_v$ , the water vapour density ( $\text{kg m}^{-3}$ ),

The heat flow equation considers the processes of conduction, transport by gas and moisture, generation (by chemical and microbiological reactions) and the release/taking up of latent heat. Other mechanisms such as radiation play a minimal role within the site and can therefore be omitted. The heat equation is therefore

$$C \frac{\partial T}{\partial t} = \text{div}(\underline{h}\nabla)T + \rho c_g \underline{v} \cdot \nabla T + H_0 R - L_0 E, \quad (43)$$

where  $\underline{h}(\theta)$  is the thermal conductivity,  $Q_0 R(T, \theta)$  is the rate of methane production,  $E$  is the evaporation rate. The heat capacity ( $C$ ), is given by the expression,

$$C = \theta_s \rho_s c_s + \theta \rho_w c_w + \rho c_g. \quad (44)$$

The landfill gas is modelled as a single species, being an equimolar mix of methane and carbon dioxide which is assumed always to be fully saturated with water vapour. The saturation point is a known variable of both the moisture content and the temperature. The mass balance governing its density  $\rho$  obeys the differential equation

$$\frac{\partial \rho_g}{\partial t} = \text{div}(\underline{u}\rho_g) + Q_0 R(T, \theta) + E + W, \quad (45)$$

where  $\underline{u}$  is the gas velocity.

### 3.8.1 Moisture Flow.

Since the movement of moisture inside a landfill is by seepage at low velocities we model the moisture flux,  $\underline{v}$ , using a Darcy relation

$$\underline{v} = -(\underline{M}(\theta)\nabla)\psi, \quad (46)$$

where  $\psi$  is the total potential and  $M$  is the permeability to moisture. For unsaturated flow the total potential may be expressed as the sum of the matric potential,  $h$ , and the gravitational potential  $z$ ,

$$\psi = h(\theta) + z. \quad (47)$$

(For saturated flow we must also consider the overburden potential.) The matric potential models the effect of capillarity (sometimes called the suction potential) and is often expressed as

$$h(\theta) = h_0 \left( \frac{\theta}{\theta_{max}} \right)^{-b}, \quad (48)$$

from which we derive the equation

$$\frac{\partial \theta}{\partial t} = \text{div} \underline{v} - E. \quad (49)$$

To model the transport of water vapour, we assume that the gas is always at its saturated equilibrium level. This level is dependent on  $T$  and  $\theta$  (since for very dry media the normal Saturation Vapour Pressure relation is not valid), and we define  $f(\theta, T)$  as the mass fraction of vapour in the landfill gas, so that  $\rho_v = f(\theta, T)\rho$ . In order to find the evaporation rate, we now consider a mass balance for vapour on an arbitrary element  $\Omega$  (which is not at a well),

$$\text{Rate of Increase of Vapour in } \Omega = \text{Convection through } \delta\Omega + \text{Evaporation } \Omega, \quad (50)$$

which gives rise to the equation for the evaporation rate

$$E = \frac{\partial f\rho}{\partial t} - \text{div}(\underline{v}f\rho). \quad (51)$$



## **Chapter 4 : Gas Composition and Migration.**

---

### **4.1 Introduction.**

The need to control gas emissions from landfill sites is an increasingly important facet of site operations, governed by increasingly stringent waste management licence conditions. Because of the difficulties involved in measuring the total quantity of gas escaping from a site, it is normal practice to monitor its chemical composition and to use this both as a means of assessing the environmental impact and of estimating the internal state of a site. Such measurements frequently show significant changes in the relative fractions of the gases vented, and for lack of any other explanation these changes have been attributed either to inaccurate instrumentation or to variations in the internal biological processes. It is thus important to know to what extent current gas monitoring practices represent a reliable method of determining the status and safety of a site.

Some recent experimental evidence, for instance Rettenberger (1990) and Bogner et.al. (1987), has suggested linkage between the stoichiometric (ie. the chemical composition) changes and atmospheric pressure, but there has been no quantitative explanation for the relationship. This Chapter aims to clarify this situation by describing a fundamental physical mechanism, common to all sites, which is able to cause many of these changes without the need to invoke hidden extra factors.

### **4.2 Volumetric Changes Due to Atmospheric Pressure.**

We first aimed to develop a quantitative model relating volumetric changes in landfill gas emissions to variations in the surface atmospheric pressure. It is thought that this phenomena may have been a contributory factor in some landfill gas incidents (such as the Loscoe explosion — see later), since a sudden drop in atmospheric pressure can cause a rapid rise of methane concentrations in surrounding regions.

This model considers gas emissions as the sum of two terms, one constant over a period of weeks, and the other able to vary on a scale of hours. Results from computer simulations are given below which indicate that the magnitude of the variable term is proportional to the rate at which surface pressure is changing, rather than the actual value of the surface pressure.

### 4.2.1 Assumptions.

We assume, in accordance with Chapter 3, that changes in the physical configuration of a site happen slowly compared with the daily time-scale of weather effects, and we assume that the void fractions occupied by gas and water remain steady, as does the medium's permeability (though the latter turns out to be a relatively unimportant factor).

Carbon dioxide and methane are formed by bacterial action within the landfill liquid (both in the saturated and unsaturated regions) and molecules pass into the gaseous phase when their dissolved concentrations exceed the equilibrium values given by Henry's law. It is probable that this process occurs much faster than changes in atmospheric pressure, and we initially treated the dissolved and gaseous concentrations as always being in local equilibrium.

There is no evidence to suggest that small perturbations in pressure can cause a measurable direct effect on the rates of the anaerobic chemical and biological reactions within a landfill (assuming that oxygen is not drawn in). Secondary mechanisms, such as a shift in pH due to altered levels of dissolved carbon dioxide, should also be negligible for pressure changes of the size we are concerned with. We thus suppose that the rate of internal gas generation is roughly constant over periods of a few days.

The mathematics required, and the interpretation of results, can be greatly simplified by treating the gas flow as being predominantly vertical, and from Chapter 3 we have the following equation

$$\frac{(\varphi + \gamma\theta)}{P_a} \frac{\partial P}{\partial t} = \text{div}(\underline{K} \cdot \nabla P) + \lambda Q. \quad (1)$$

The model's results show that of the physical parameters it is the void fractions that dominate the transient behaviour rather than the permeability — so that differing values for the horizontal and vertical permeabilities influence where the gas escapes rather than how much is vented. Thus the conclusions we draw later in this section can confidently be extended to fully three-dimensional situations.

Note that the non-linearity of equation (1) means that for equal drops in atmospheric pressure the actual amount of additional gas vented would not be precisely the same — but for realistic conditions the fractional deviation due to this would be less than 5% of the total flux.

It was decided to solve this equation using the finite element numerical algorithm described in Appendix 3A, subject to the boundary conditions

$$P|_{z=0} = P_0 + p(t), \quad \left. \frac{\partial P}{\partial z} \right|_{z=d} = 0, \quad (2, 3)$$

where  $P_0$  is the constant mean atmospheric pressure, and  $p(t)$  is the time varying deviation from this. To apply this method to equation (1) we take  $C = \{\varphi + \gamma\theta\}$ ,  $D = KP^{(0)}$  and  $G = \lambda q$ . Analytical solutions are available for the case of time-independent boundary conditions, and our numerical approximations agree with these to within 1%.

#### 4.2.2 An example simulation.

Using our model we carried out a series of computer simulations exploring the effects of atmospheric variations for sites having different values of permeability, depth, void fractions and gas generation rate.

An illustrative example of the type of results produced by the model is given in Figure 4.1 below. This relates to a site 20 m deep in which liquid and gas both occupy void fractions of 0.2, the permeability is  $10^{-7} \text{ m}^2 \text{ s}^{-1} \text{ Pa}^{-1}$ , the temperature is  $30^\circ\text{C}$  and the gas generation rate is  $6.8 \times 10^{-7} \text{ kg s}^{-1} \text{ m}^{-3}$  (roughly equivalent to  $0.05 \text{ m}^3$  of gas being generated each day per  $\text{m}^3$  of landfill volume).

We look at the effect of three successive ‘lows’ passing over a landfill during an 8 day period, and compare the changes they induce in the gas flux. For clarity the changes in atmospheric pressure have been made abrupt, but the model and its conclusions hold equally well for gradual transitions.

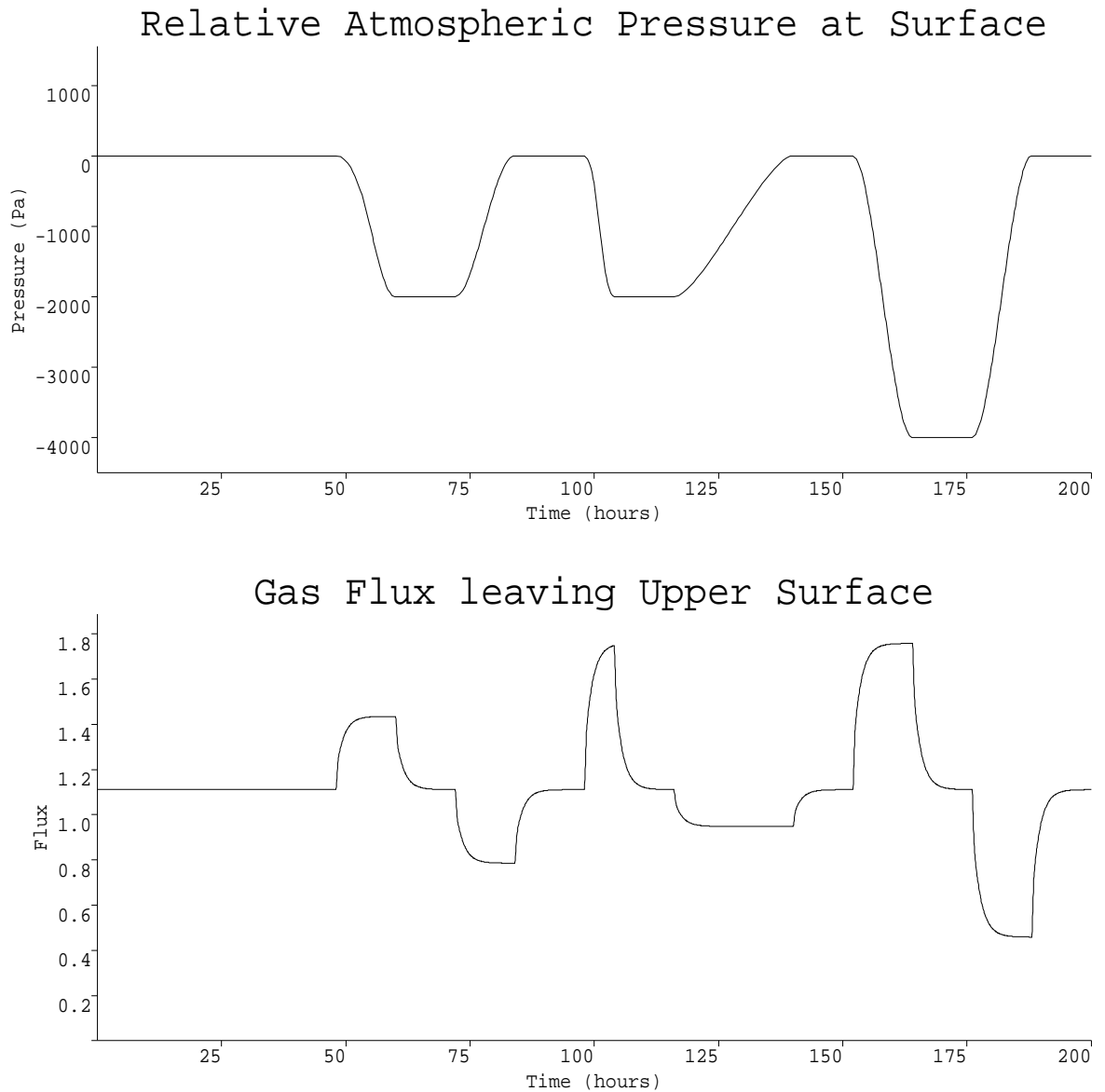


**Figure 4.1 :** Predicted flux for simulation with idealised barometric pressure.

Table 4.1 (below) shows the barometric pressure imposed at the surface of the site over a 200 hour period. The rate at which gas is being vented from the site over the same interval is given by the exit velocity (in  $\text{m s}^{-1}$ ).

**Table 4.1 : Atmospheric pressure imposed during simulation.**

Time ( hours )	Duration	Pressure conditions
0 - 48	48	Initial steady phase at 100kPa (= 1000mbar)
48 - 60	12	decrease from 100kPa to 98kPa
60 - 72	12	Steady at 98kPa
72 - 84	12	rise from 98kPa to 100kPa
84 - 98	14	steady at 100kPa
98 - 104	4	rapid decrease from 100kPa to 98kPa
104 - 116	12	steady at 98kPa
116 - 140	24	slow rise from 98kPa to 100kPa
140 - 152	12	steady at 100kPa
152 - 164	12	decrease from 100kPa to 96kPa
164 - 176	12	steady at 96kPa
176 - 188	12	rise from 96kPa to 100kPa
188 - 200	12	steady at 100kPa

During the first low (48–84 hours) the flux rises while the pressure drops, it then returns to the normal steady value once the pressure has stabilised, and falls while the pressure rises back to the initial level. This general pattern is repeated during each of the other two lows from 98–140 and 152–188 hours.

The extra amount of gas which is vented during any period is proportional to the area between the flux curve and a horizontal line through the initial pressure. Comparing the periods 48–60, 98–104 and 152–164 hours, we see that the additional gas vented is the same during the first two drops, and doubled over the third. The extra gas vented during each fall is also seen to be equal to the deficit which occurs when the pressure returns to the initial value. This implies that the total amount of extra gas vented over any period is proportional to the total decrease in pressure.

The magnitude of the increases in flux during the periods 98–104 and 152–164 hours are equal (though it persists for longer in the latter case) and twice that observed during the first fall. This indicates that at any time the amount by which the flux is increased is proportional to the rate at which the atmospheric pressure is falling, rather than the actual value of the pressure.

### 4.2.3 Conclusions about Volumetric Flux.

From the results of our simulations it seems that changes in gas emissions are transient effects due to gas storage within the landfill void space, and that they follow three general rules :

[1] When the atmospheric pressure is steady, the rate of gas venting is constant and independent of the pressure.

[2] When the atmospheric pressure is rising, the rate of venting decreases by an amount proportional to the rate at which the pressure is rising.

[3] When the atmospheric pressure is falling, the rate of venting increases by an amount proportional to the rate at which the pressure is falling.

These conclusions can be stated more concisely as

$$\text{Gas flux} \approx \alpha + \beta \frac{dP_{atm}}{dt}, \quad (4)$$

where  $P_{atm}$  is the atmospheric pressure,  $\alpha$  is the total rate of gas generation within the site, and  $\beta$  is a constant depending on the physical parameters of the landfill.

The implications of these results are that gas emissions on or adjacent to landfill sites are highest during times of rapid atmospheric pressure decrease. This effect will enhance the build up of methane concentrations in confined or poorly ventilated spaces during such periods, making them especially dangerous with respect to the hazards of explosions and asphyxiation.

The form of equation (4) raises the possibility of being able to indirectly estimate the total rate of gas production within a site. The term  $\beta$  is dominated by the values of the gas and liquid void fractions within a site, and can be evaluated if these are known. If the relative magnitude of the gas flux is measured as the atmospheric pressure fluctuates, then the ratio  $\beta/\alpha$  can be estimated. This allows us to determine a value for  $\alpha$ , which is equal to the total rate of gas generation within the landfill — though one must be wary of errors due to inhomogeneities within the site.

### 4.3 Compositional Changes Due to Atmospheric Pressure.

The volume-flux model was extended to cover multi-species gas flows by considering each of the gases in the multi-component system as a separate entity, and paying especial attention to the ways in which the different molecular species can exhibit different behaviour. A total of 5 equations were linked together — 3 for the gases, and 2 for the dissolved forms of  $CO_2$  and  $CH_4$ .

The equations (3.19,3.26) derived in Chapter 3 are valid for complex forms of the equation coefficients, such as would occur in a heterogeneous site, however we wish to focus attention on the effects of atmospheric changes alone and prefer not to confuse the issue by introducing too much internal detail. The model equations were solved using an extended variant of the finite element algorithm described in Appendix 3A, with the mesh nodes concentrated towards the upper end of the region. A large series of runs were performed to gauge the effect of the various physical parameters involved.

#### 4.3.1 Multi-Species Simulation.

At the surface of the region, the gas compositions were fixed to be typical of those found in the air above a landfill site, where both  $CH_4$  and  $CO_2$  are only marginally above the normal atmospheric levels — the solution was found to be relatively insensitive to the actual values assumed, provided they were less than about 10% of atmospheric pressure. The base of the site was assumed to be impermeable to gas flow. The water was allowed a small downwards velocity.

One example simulation is given to illustrate the type of behaviour obtained. This is based on a hypothetical site with the following characteristics: the depth is 20 m, the vertical permeability was taken to be  $10^{-7} \text{ m}^2 \text{ s}^{-1} \text{ Pa}^{-1}$ , with the void fractions of gas and water being 0.1 and 0.3, respectively. The internal temperature was fixed at  $30^\circ\text{C}$ . The water velocity was taken to be  $0.3 \text{ m yr}^{-1}$ . Gas production was assumed to be  $0.01 \text{ m}^3$  per cubic metre of waste per day of an equimolar mixture of  $CO_2$  and  $CH_4$  — except within the uppermost 2 m where methanogenic activity was taken to be zero. Any air present in the site below the 2 m level is assumed not to react with the solid material there, and this is justified retrospectively from the results. The characteristic length for dispersion was taken to be 0.05 m in both the gas and liquid phases, with a value of 0.5 assumed for the tortuosity. The pH was fixed at 7, and the half-lives for gas evolution were set at 2 hr.

For the numerical solution the site was divided into 60 elements, and a variable time step used. To maintain uniform accuracy, the size of the time step must be decreased as the rate of change of atmospheric pressure increases, with a range of 0.1 to 0.5 hr being

suitable for the example shown.

Figure 4.2 illustrates a simplified pressure profile for a 10 day period, consisting of a 'low' followed by a 'high' (both in the range  $\pm 3\text{kPa}$ ) after a long period of constant pressure, and also shows the corresponding predicted rate of gas venting at the surface of the site measured in  $\text{mol m}^{-2} \text{d}^{-1}$ .



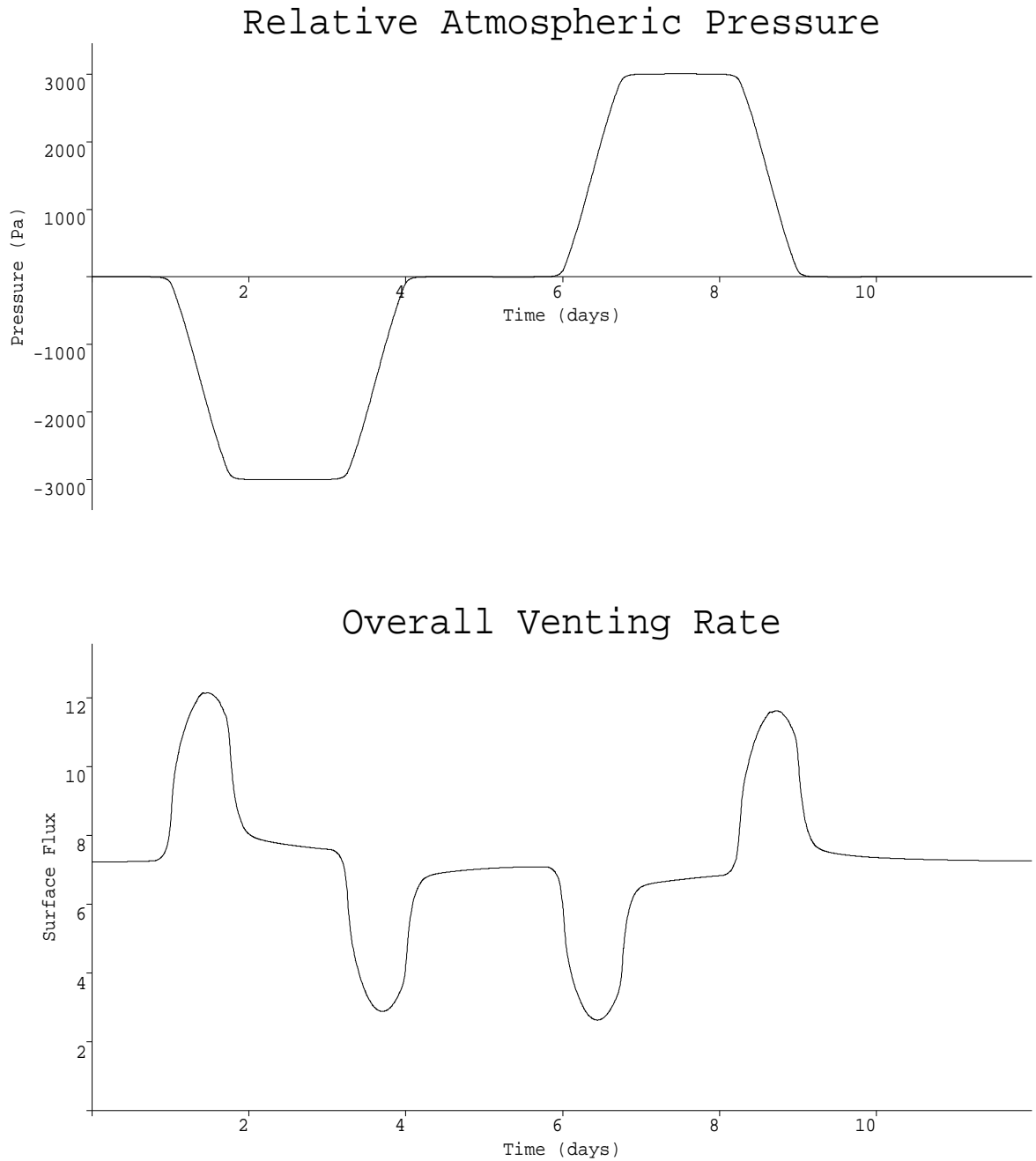


**Figure 4.2 :** Basic weather profile and predicted total flux.

Figure 4.3 shows the fraction of this flux composed of  $CH_4$ ,  $CO_2$  and air (given the physical characteristics of  $N_2$ ). Figure 4.4 is a plot of the percentage of  $CH_4$  (relative to the total volume of  $CH_4$  and  $CO_2$  combined) in the vented gas over this time period.

# Surface Gas Fluxes

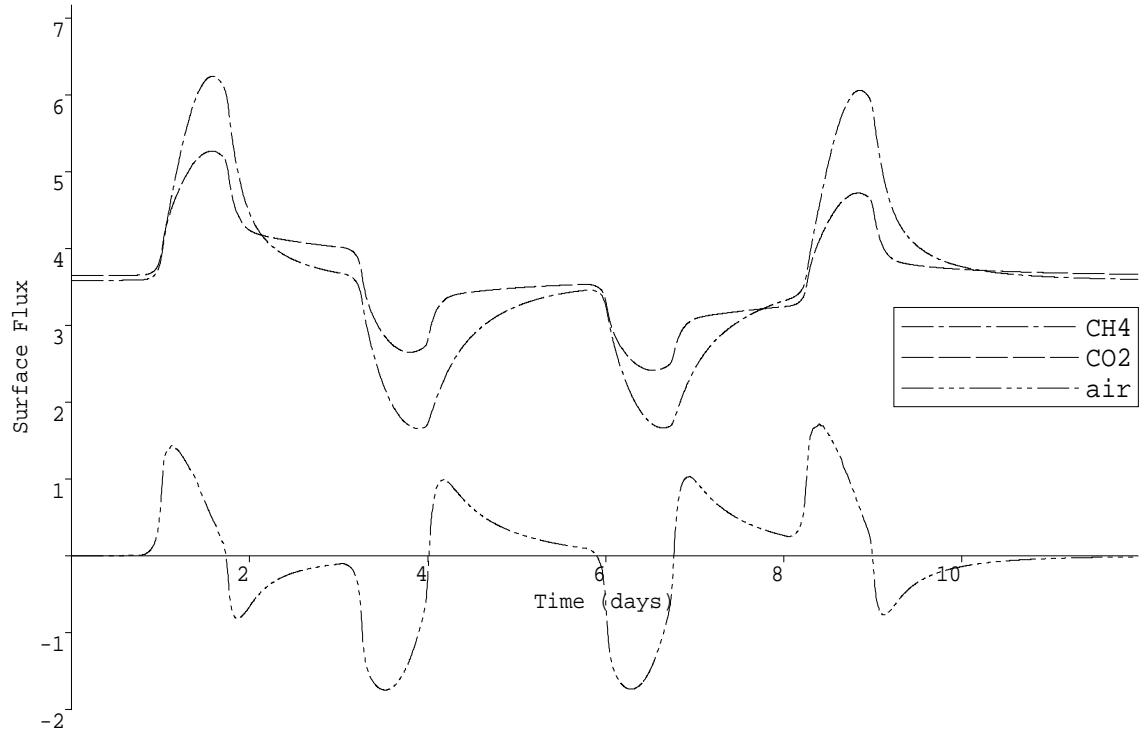


**Figure 4.3 :** Predicted fluxes of gas through upper surface of landfill.

## Apparent Gas Composition

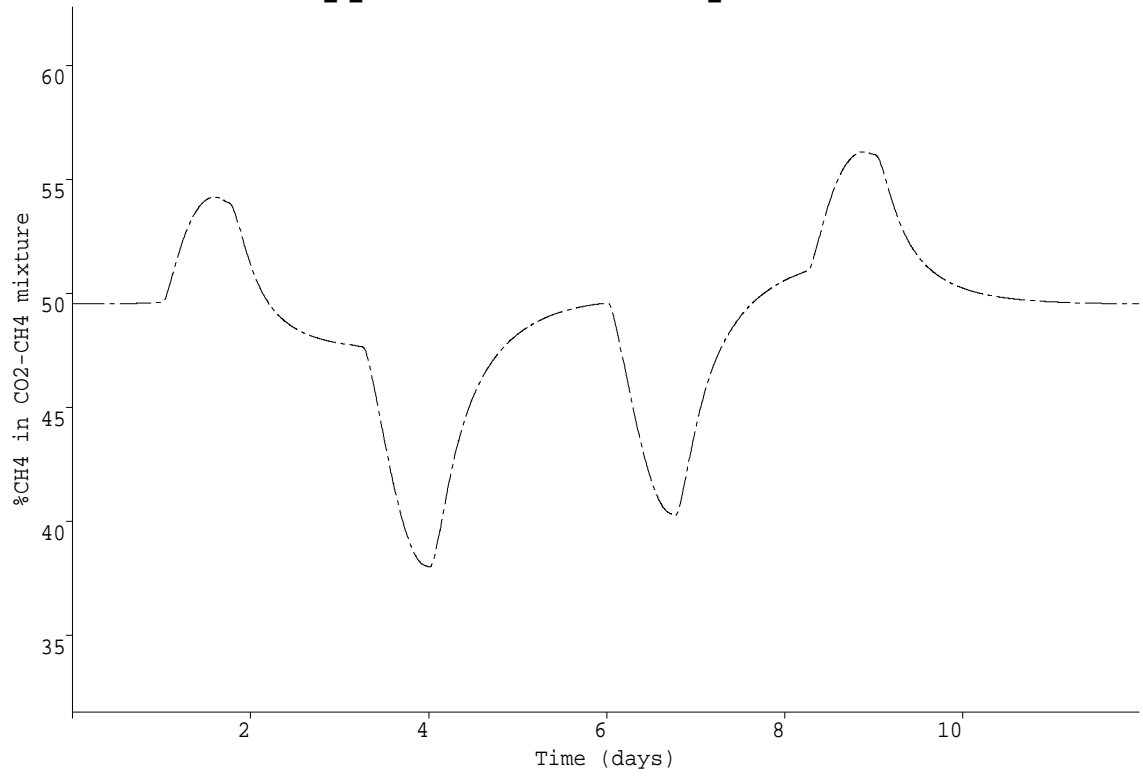


**Figure 4.4 :** Apparent percentage of methane in metabolic gases.

### 4.3.2 Results and Interpretation.

As expected from our single-species results, when the surface pressure is dropping there is a rise in the amounts of each of the gases vented, and conversely when the atmospheric pressure is rising the rate of venting decreases, so that our approximate relation (4) remains valid — though the approximation to a linear relationship is less precise due to the extra delays introduced by our assumption of a finite time for gas exsolution and dissolution.

However the three gases present respond to the surface changes in different ways, so that the composition of this total flux varies in time, and we now look at how the various mechanisms interact using the simulation results show in Figures 4.2 to 4.6 to illustrate these phenomena.

During the initial pressure drop a large amount of air is flushed out of the site, and the rate of flushing diminishes although the rate at which the pressure decreases is constant. Simultaneously, the venting rates of  $CH_4$  and  $CO_2$  gradually rise. These effects are mainly due to the initial distribution of the gases when the pressure begins to drop, as shown in Figure 4.5. The upper region contains the highest proportion of air, and as a surge of gas is exsolved in the lower regions the near-surface molecules tend to be vented first. This tails off since the reservoir of air is relatively small. Meanwhile  $CH_4$  and  $CO_2$  molecules from further down in the site move upwards and as more of them reach the surface their respective venting rates rise.

Note that, against one's initial intuition, the increase in  $CH_4$  venting is greater than that for  $CO_2$  — although within the body of the site the transient rate of evolution of  $CO_2$  will be greater than that of  $CH_4$ . This is because the extra  $CO_2$  evolved takes a considerable time to reach the surface so that the actual molecules vented are those which were in the upper region when the pressure began to drop. As the gases pass through the upper layers, the increased partial pressure of  $CO_2$  causes some of it to dissolve in the near-surface water, whereas almost none of the  $CH_4$  is trapped in this way. Hence the apparent percentage of  $CH_4$  in the landfill gas increases, as shown in Figure 4.4.

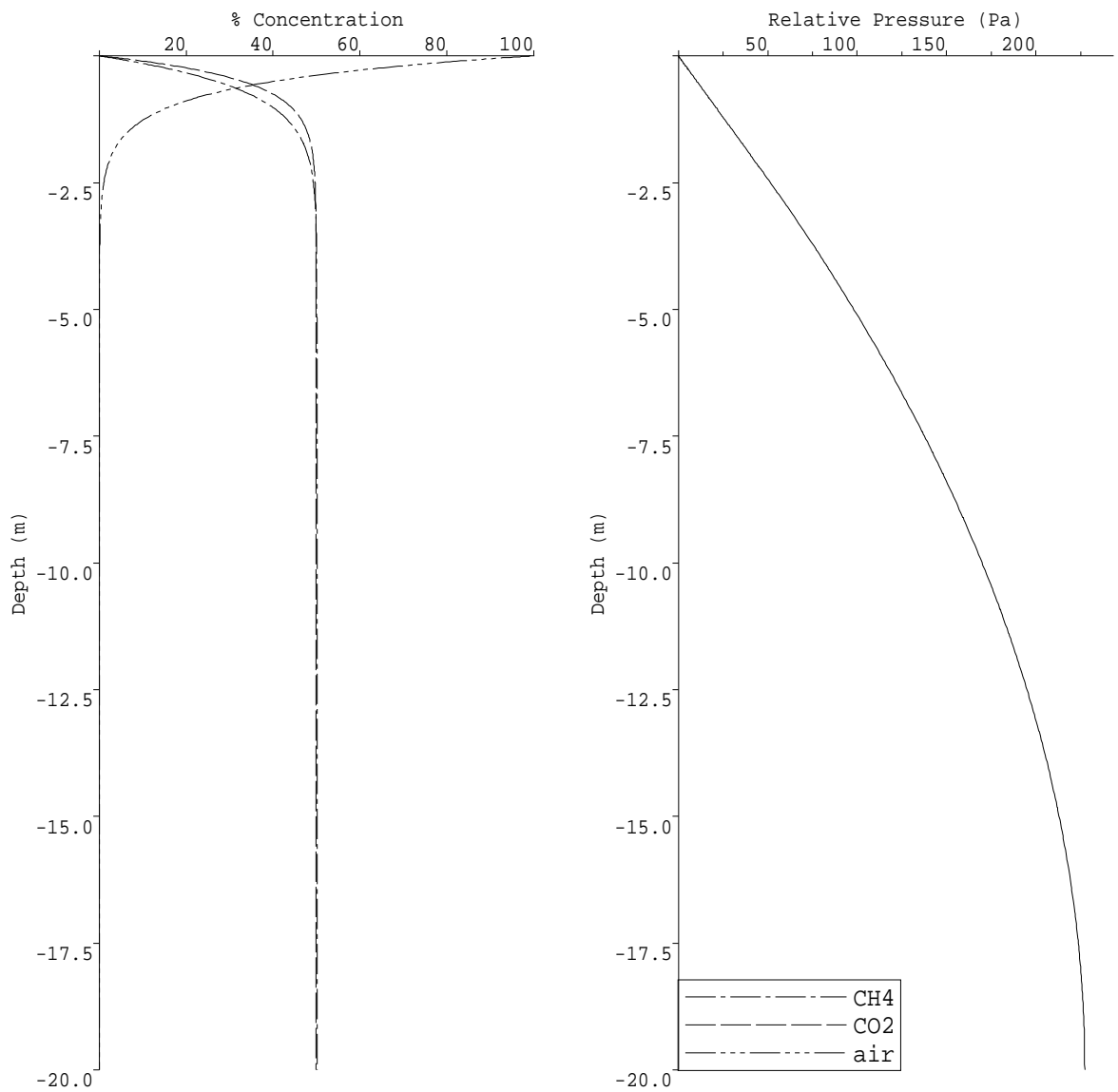


**Figure 4.5 :** Internal Gas Concentrations Total Gas Pressure  
Initial partial pressures of gases inside model landfill.

The depletion of the air and buffering of the  $CO_2$  levels by exsolution/solution are evident in Figure 4.6, which shows the predicted gas composition at a depth of 1 metre below the surface.

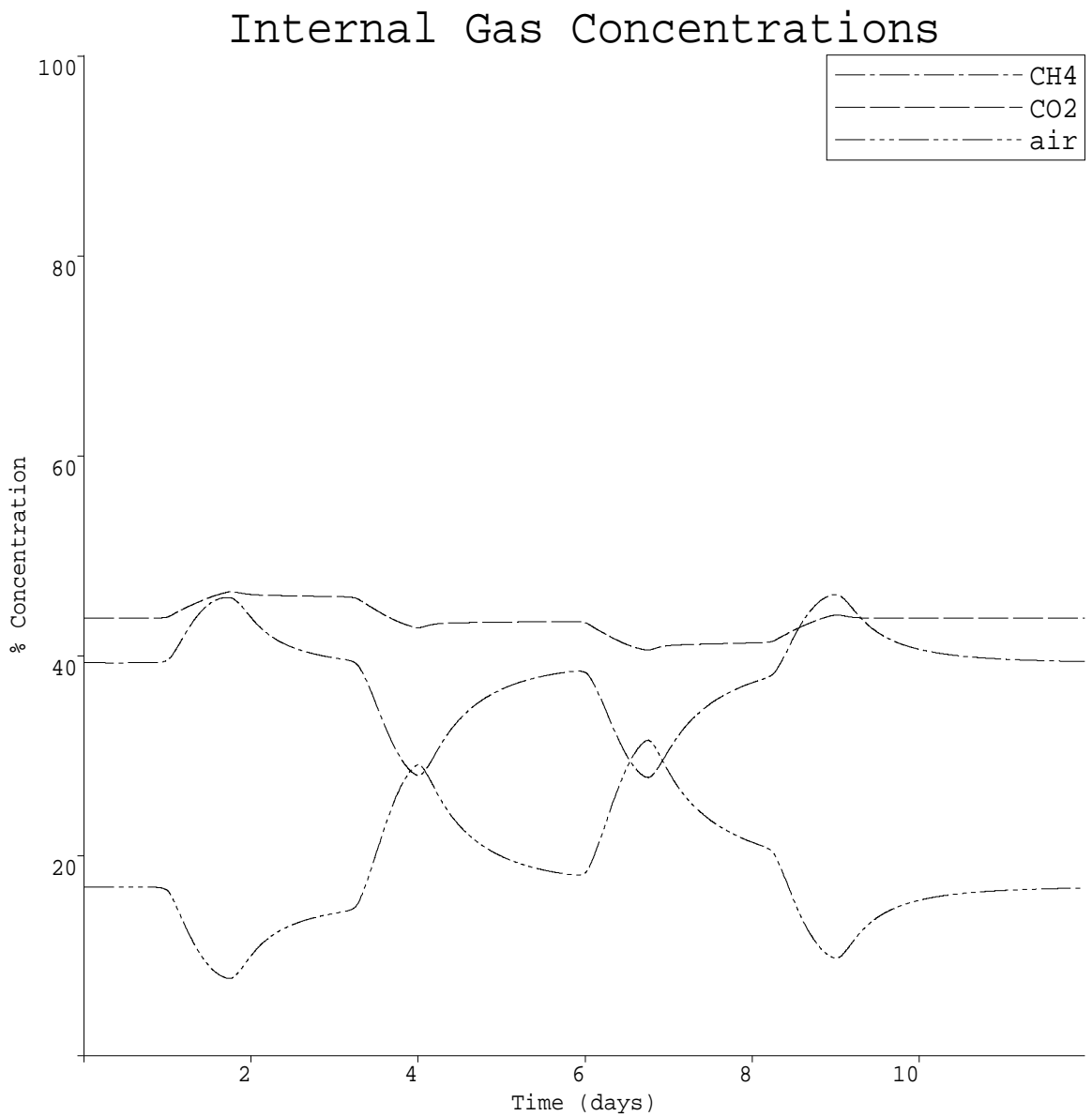


**Figure 4.6 :** Predicted gas composition at depth of 1 m below surface.

During the subsequent steady phase of reduced pressure the internal composition begins to return to its initial state. The net upward gas velocity decreases, so air is able to diffuse back into the upper layers, and together with a slight residual excess internal pressure this results in  $CH_4$  and  $CO_2$  still being vented faster than at equilibrium for a while. If the pressure remained steady for a long enough period, the  $CO_2:CH_4$  ratio would rise above 1 as the extra  $CO_2$  liberated in the interior eventually reached the surface in sufficient quantities to overcome the absorption in the upper layers.

Note that the time-scale for gas composition to approach equilibrium under steady external conditions is several weeks, whereas the net internal pressure reaches equilibrium within a matter of hours. This is because compositional equilibrium requires specific molecules of each type to migrate throughout the site to change the local gas composition, whereas to equilibrate only the net pressure, a smaller movement of adjacent gas molecules is sufficient (their species being irrelevant in this respect).

When the pressure begins to rise we see a large influx of air, whilst the outflow of  $CH_4$  and  $CO_2$  is reduced. Due to this influx the partial pressures of  $CO_2$  and  $CH_4$  in the upper layers decrease (even though their net flux is still upwards) and more  $CO_2$  is evolved from the near-surface leachate — resulting in the ratio  $CO_2:CH_4$  exceeding one.

The same phenomena are repeated, in reverse order, in the following interval when a high pressure front moves over the landfill.

It is important to note that, although the pressure changes and time scales involved are the same, the pattern of gas fluxes is only similar rather than identical. This illustrates that the gas composition is influenced not just by the instantaneous pressure changes, but also by the history of the weather over the preceding days or weeks which determines the initial position of the molecules of the individual component gases.

### 4.3.3 Site-Specific Factors.

Having described the particular case illustrated in the example simulation, we now discuss the effect of various parameters as indicated by running a large number of simulations with different weather profiles, liquid pH, void fractions, wetness, depths, permeabilities, gas evolution rates, water velocities, and gas production rates.

For two identical sites with the same pressure history, the response to a given constant rate of change of pressure depends almost linearly on the speed of the change. However if the recent weather has been different, then the sites will respond less predictably even to the same pressure change — although their qualitative behaviour will usually be similar.

The model indicates that the disparity between the behaviour of the  $CH_4$  and  $CO_2$  will be greater in sites where the leachate pH is more alkaline. This is because leachates with high pHs have a greater capacity to store dissolved  $CO_2$  due to the larger fraction which is held in the form of carbonate and bicarbonate ions. Increasing the moisture content of the site will cause a similar rise in the magnitude of the effects, due also to the increased carbonate storage capacity available.

Increasing the void fraction available for gas flow damps down the stoichiometric fluctuations, although the total volume of each of the gases vented rises — this is mainly due

to the relatively reduced importance of the leachate as a reservoir for  $CO_2$ , together with a small effect caused by the increase in the gaseous diffusion coefficients resulting from wider migration pathways. The compositional variations will also decrease slightly as the temperature is increased due to alterations in the Henry's constants and solute pKs, but the difference caused by a  $10^\circ C$  change is minimal.

The moisture distribution within a site is important for the stoichiometric effects, not just the total amount of water present. The increase in the ratio  $CH_4/CO_2$  as the pressure falls is due to absorption in the upper layers, and if the surface is very dry then this will be reduced and may be reversed if a sufficient excess of  $CO_2$  is being liberated in the lower regions.

The effect increases with the depth of the site since this increases the amount of gas which must move around in order to restore equilibrium when the surface conditions change. The depth to which air penetrates decreases for deeper sites (assuming that the rate of gas production per unit volume of the site remains constant) because their greater net production convects more of the air molecules out.

For the majority of landfill sites (both in actuality and as predicted by the model) air fails to penetrate below the top few metres, and thus one can justify the earlier assumptions that there is insignificant internal  $O_2$  consumption and that the methanogenic bacteria (which are obligate anaerobes) are unaffected by the atmospheric fluctuations.

Increasing the gas evolution half-lives (ie. reducing the modelled rate of molecular transfer responsible for bringing the dissolved and gaseous concentrations into equilibrium) results in the surface flux curves becoming shallower and smoother, however this does not become very noticeable until the half-life approaches a significant fraction (say a quarter) of the period of the barometric pressure fluctuations.

The permeability, whilst affecting the net pressure excess, makes little difference to the stoichiometric behaviour, except for very impermeable sites when it exerts a minor damping effect — hence neglecting the slight dependence of gas viscosity on composition is reasonable. This is because changing the permeability affects only the gas velocity, it cannot cause the individual molecules to be vented in a different order.

The steady vertical water velocity is too slow to produce noticeable effects in the surface emissions. The only difference it seems to make is at the base of the site where the partial pressure of  $CO_2$  is slightly elevated due to dissolved carbonate being brought from higher regions, however this perturbation is very small.

The fluctuations become more pronounced as the underlying biological rate of gas generation decreases, since the transient amounts of  $CO_2$  evolved from the leachate are inde-



pendent of biological activity (except insofar as this influences the nature of the leachate). In particular this means that the composition of vented gas should be most variable in relatively old inactive sites and in the strata surrounding landfills.

#### **4.3.4 Implications for Monitoring Strategies.**

The results above demonstrate that the composition of gas vented from a landfill may change even when the underlying biochemical generation rate is steady. The existence of these short term stoichiometric changes mean that the prevailing barometric conditions must always be taken into account when using field data to assess gas generation rates and environmental hazards. Ideally, a monitoring program should cover a period in which there are several rapid falls and rises in atmospheric pressure, as it is only during such circumstances that the extremes of gas concentration and flux will be exhibited.

As a more realistic example, Figure 4.7 shows a pressure profile observed in England during the month of December (from the Brogborough site, courtesy of Barry Croft) and the predicted total gas flux associated with it. The model landfill illustrated in this simulation has the same physical and biological parameters as the previous example.

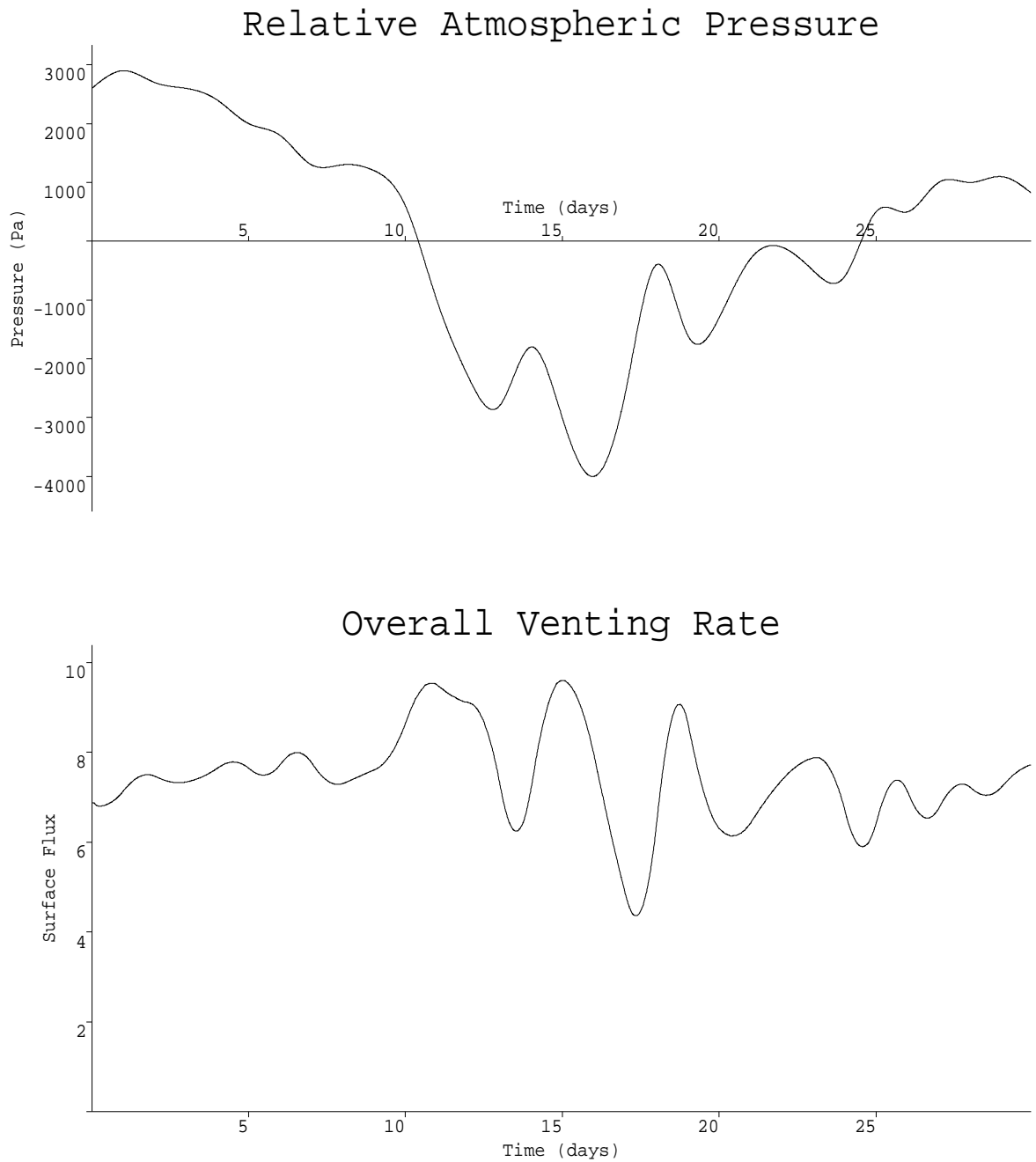


**Figure 4.7 :** Atmospheric pressure and predicted flux during December.

Figure 4.8 gives the fractionated gas fluxes over this 30 day period, and Figure 4.9 shows the apparent percentage level of  $CH_4$  in the landfill gas as predicted for this site.

## Surface Gas Fluxes

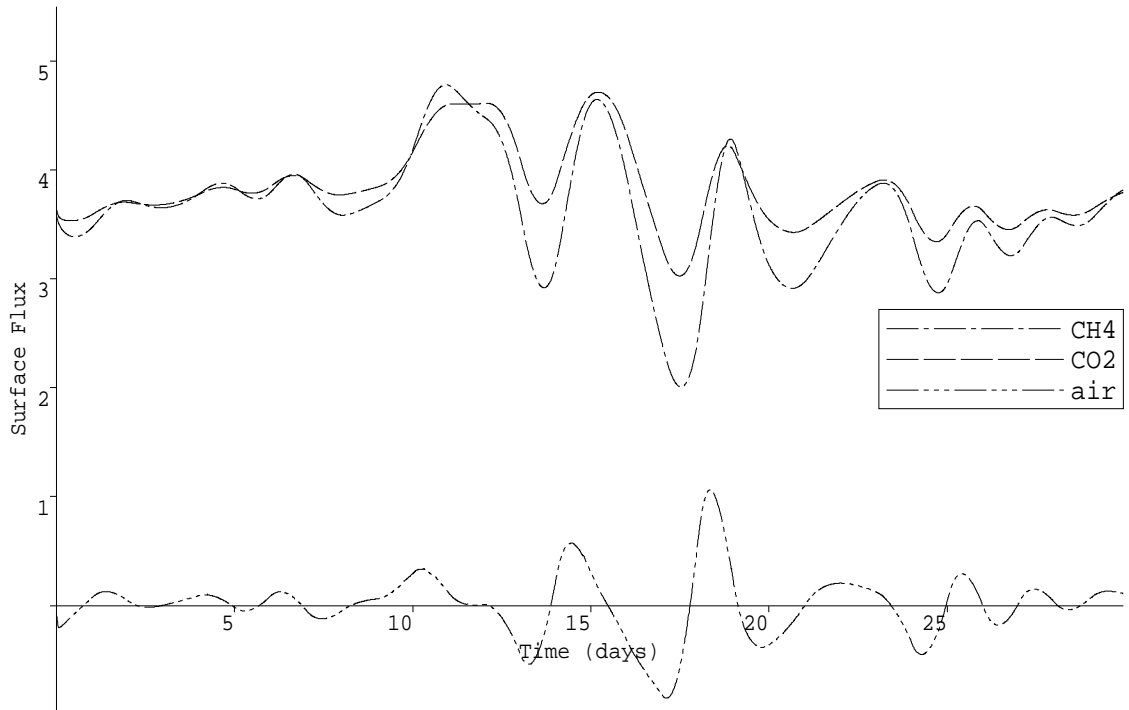


**Figure 4.8** : Individual fluxes in vented gas.

From these we see that successive measurements taken on the 11th and 18th days respectively would show an apparent halving of the  $CH_4$  concentration, which doubles again by the end of the month. Hence monitoring at weekly intervals could show large fluctuations, which would be inexplicable if the atmospheric changes were not known. Conversely, the individual peaks and troughs in the  $CO_2:CH_4$  ratio last only 1 to 3 days, and could easily be missed — which is dangerous since the peaks in total venting and  $CH_4$  concentration represent the times of maximum gas migration (see Appendix 4A for an analysis of the events at Loscoe in 1986).

## Apparent Gas Composition

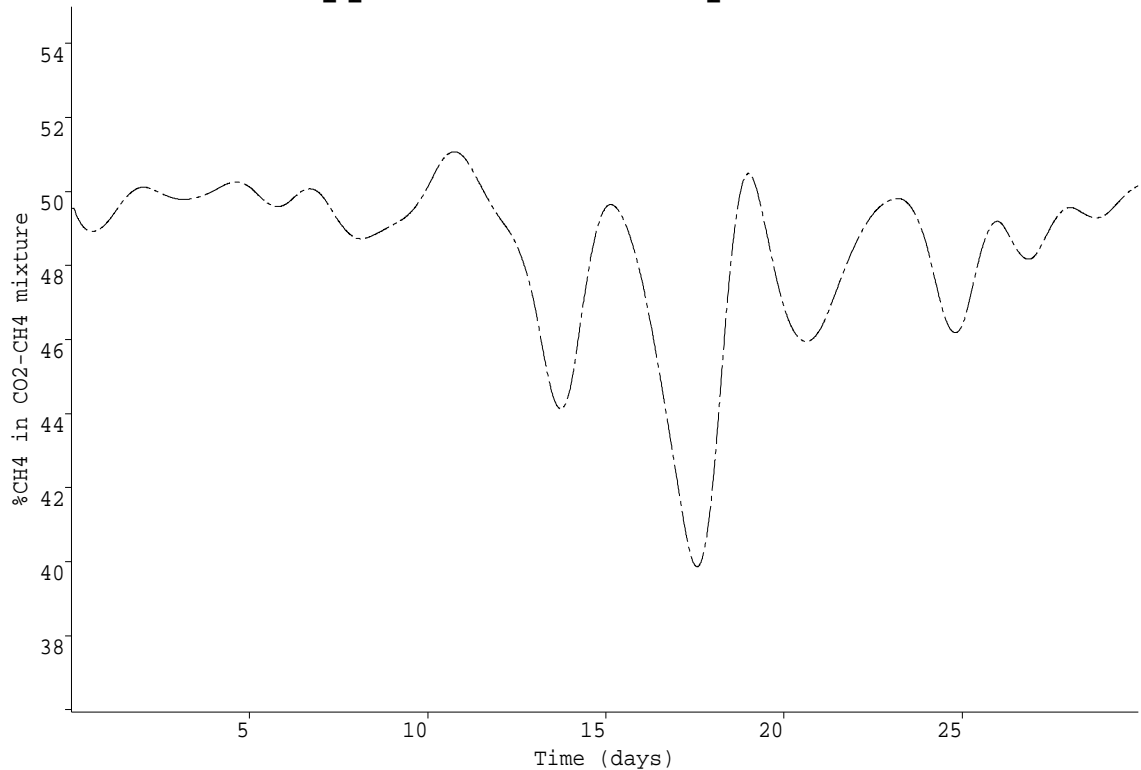


**Figure 4.9 :** Apparent percentage of  $CH_4$  in vented gas.

Note that during periods when the pressure is dropping, not only does the total flux of landfill gas increase but so does the fraction of  $CH_4$  it contains, and conversely during periods of rising pressure the net gas outflow decreases and the  $CH_4$  flux is suppressed even further. In sites with low methanogenic activity this means that  $CH_4$  could not be detected by surface measurements if the atmospheric pressure was rising sufficiently fast. As a general guideline, the model suggests that if only a small number of measurements can be made then they should be conducted during periods when the atmospheric pressure is falling — ideally when it has been falling for several days to allow  $CH_4$  and  $CO_2$  to migrate to the surface.

Any trace gases produced within the landfill are subject to the same mechanisms as the  $CO_2$  and  $CH_4$  molecules, and will therefore show analogous alterations in concentration. Highly soluble gases, such as  $H_2S$ , should show less variation than relatively insoluble gases like  $H_2$ . The influence of the site parameters on the size of these fluctuations will be different for some of the trace gases — for instance, ammonia becomes more soluble as the leachate pH rises rather than less.

Although the particular example simulations given are for the surface of a landfill, the same phenomena will occur in the regions surrounding a site. In these areas there will probably be no methanogenesis so they are analogous to an inactive site, with the  $CO_2$  storage capacity being influenced by the intrinsic properties of the solid medium (for instance, alkaline or acid soils). To complicate the interpretation of monitoring data, areas near peat or coal measures may have an intrinsic background level of soil  $CH_4$ , and this should be determined before infilling is commenced at any new site.

The compositional shifts become smaller as the distance from the surface of the site increases. Thus if one wishes to assess the actual fractions of  $CH_4$  and  $CO_2$  being generated, it is preferable to draw samples from deep within the landfill.

Ideally some form of continuous (at least daily) monitoring should be installed at sites. At present, with limited financial and technical resources, the model implies that it is most efficient to concentrate measurements during periods of falling pressure — especially if there is a requirement to issue hazard warnings to adjacent properties.

## 4.4 Further Work.

Several simplifications were made when deriving the model, and these are considered briefly below. Note that the stoichiometric changes predicted are not an artifact caused by these simplifications, and if anything the mechanism and size of the changes may have been damped down by them.

Some bacteria living in soil are able to oxidize  $CH_4$  aerobically to  $CO_2$  and  $H_2O$ . In regions which have a low throughput of landfill gas it is possible that all of the  $CH_4$  could be consumed in this fashion, thus hiding its production and making a site seem more quiescent than it really is. However rapid pressure drops could pull  $CH_4$  through such a region faster than it could dissolve into the soil water for the bacteria to consume it.

Our assumption that the air entering the site behaves as though it were inert should be valid under most circumstances, but for inactive sites during periods of rapid pressure rise  $O_2$  may be able to penetrate into deeper regions and be consumed there or hinder methanogenesis.

The tortuosity of the landfill medium (ie. the factor by which diffusion coefficients are reduced due to the internal geometry) is unknown. Most soil models take values between 1.0 and 0.3 for this. It was found in the model that reducing the tortuosity meant that air penetrated less deeply, so that the near-surface concentrations of  $CH_4$  and (especially)  $CO_2$  become larger, which in turn magnifies the size of the compositional changes in the surface flux (the preceding simulations were run with a value of 1.0). Some simple laboratory experiments would provide suitable values for this.

It is possible that temperature differences between the landfill interior, the surrounding strata, and the atmosphere could result in the formation of convection cells which would influence gas migration (though if it did exist, it would probably be a very minor effect). Also, the thermal gradients mean that water vapour will evaporate from within the site interior and may condense as the gas cools on its way out of the site. Hence as the atmospheric moisture level varies with the diurnal cycle so may the amount of moisture leaving the site and this could affect the partial pressures of the other gases.

It would be useful to have some experimental evidence to determine the time scales for gas evolution. Although it is unlikely that the half-lives are long enough to seriously alter the compositional shifts, they could result in the dissolved concentrations being considerably out of equilibrium with the partial pressures so that measurements of bacterial metabolism based on gas concentrations would be misleading.

Although the steady mean velocity of the leachate has a negligible effect on the compositional fluctuations, it is possible that sudden large inundations of water might —

especially if they occur in the upper layers and change the pH of the water there. This may mean that there is some correlation between variations in gas concentration and incidences of rain (the analysis of which is complicated by the fact that sudden drops in pressure tend to be associated with rainfall).

## 4.5 Negative Pressure Zones inside Landfills.

During landfill surveys (carried out independently of this project), engineers from Aspinwall & Company had found that some boreholes consistently produce anomalous pressure readings below the surface atmospheric value. These sites seemed to be associated with underground aquifers, and our gas migration model was employed to try to explain this phenomena.

### 4.5.1 Formulation.

At an early stage, the idea that gas might be being sucked out of a site through the ‘venturi effect’ of flowing water was proposed. However, the water velocities involved seemed too low to support this hypothesis and it was discarded.

The best candidate explanation was that gas was dissolving in the aquifer and being removed from the site in this form.

Since methane, oxygen and nitrogen have approximately the same solubilities, the model was simplified by considering only two gases (suffix  $c$  for  $CO_2$ , and suffix  $g$  for the sum of all the other species). The upper boundary condition is one of fixed concentration, whereas at the lower boundary (writing  $F_i$  for the flux of gas  $i$  passing from the site into the aquifer) we have

$$F_i = -uP_i + E_i \frac{\partial P_i}{\partial z} = \Upsilon_i(P_i - A_i/H_i), \quad \text{on } z = d, \quad (5)$$

where  $\Upsilon_i$  is a transfer coefficient describing how rapidly each gas is exsolved or dissolved,  $H_i$  is Henry’s constant,  $A_i$  is the concentration at the upper surface of the aquifer. The values of  $u$ ,  $E_i$ , and  $P_i$  are evaluated at the interface between the landfill and aquifer.

Under the assumption that the aquifer is well-mixed (so that we not need be concerned with internal concentration gradients), and that the concentration of solute  $i$  is  $A_{i0}$  in the aquifer before it enters the site, then the average flux  $\bar{F}_i$  of gas  $i$  into it can be expressed as

$$\bar{F}_i = \frac{\Upsilon_i d_a (P - A_{i0}/H_i)}{d_a + (\Upsilon_i t_a / H_i \lambda_i)}, \quad (6)$$

where  $t_a$  is the average residence time of aquifer water passing through the site, and  $d_a$  is the mean depth of the aquifer over the site base (allowing for dry regions where the depth may be taken as zero). The mass-flux into the aquifer is thus given by  $F_i/\lambda_i$  (in  $\text{kg m}^{-2}$ ).

The overall gas pressure equation is

$$\varphi \frac{\partial P}{\partial t} = \text{div}(P \underline{K} \cdot \nabla P) + Q, \quad (7)$$

where  $Q = \alpha_c Q_c + \alpha_g Q_g$ . This is subject to the boundary conditions

$$P = P_{atm} \quad \text{on } z = 0, \quad -PK_v \frac{\partial P}{\partial z} = \bar{F}_c + \bar{F}_g, \quad \text{on } z = d. \quad (8, 9)$$



#### 4.5.2 Results and Conclusions.

A large number of simulations were run for varying values of  $\Upsilon_i$ ,  $t_a$  and  $d_a$ . It was found that the presence of an aquifer invariably reduced the internal site pressure and the surface flux. The gas escaping from the surface was enriched with respect to methane, so that the ratio  $CH_4:CO_2$  was higher in the vented gas than would be expected from the production rates. Furthermore, the value of  $CH_4:CO_2$  generally increased with depth below the surface, reaching a low at the boundary with the aquifer (though the actual  $CO_2$  concentration normally peaked somewhere within the site away from either boundary). These spatially dependent changes in the ratio  $CH_4:CO_2$  could form the basis of a diagnostic test for the presence of aquifers near to (or within) a site.

The phenomena of internal pressures being consistently below atmospheric could be reproduced by suitable choice of the aquifer parameters, but there was no physical evidence available with which to decide whether the values required were plausible. Our general conclusion is that the presence of aquifers can cause enrichment of the methane content and some lowering of internal pressure, but that the magnitudes of these effects cannot be determined without additional experimental evidence.

## **4.6 Field Investigations at Sleaf Landfill.**

The conclusions of the gas migration model suggest that there is an intrinsic variability in gas monitoring data based on compositional measurements, and hence considerable unreliability in using it for site assessment purposes. This has important ramifications for all landfill monitoring, and could result in modifications to waste management codes of practise and legislation. Accordingly it was decided to run a field experiment to assess to what degree the predicted effects are actually manifested on a site.

### **4.6.1 Experimental Specification.**

The model predicts that compositional variations are greatest nearest to the surface, and that the changes in the flux are larger than those inside the landfill. Accordingly the original specification called for gas composition to be monitored at depths of 0 m, 0.3 m and 1 m below the surface (ideally at the same horizontal location), and for some method of assessing the surface flux to be employed. It proved impractical to provide such near-surface facilities, and the final experiment consisted of a surface sampler and 3 separate boreholes sampling gas at 1 m, 2 m and 5 m, each displaced horizontally by about 3 m. No form of continuous flux monitoring could be devised, and this aspect of the experiment had to be abandoned. For the trial, Aspinwall & Company selected a site at Sleaf in Shropshire. This site was used for the disposal of household waste during the 1960s and '70s, being restored and grassed over by Shropshire County Council in the late '80s. This site had the desired characteristics of being remote from habitation with no gas venting system installed.

An interval of 3 hours between measurements was thought to be ideal, and this required automated equipment able to process small sample sizes (to avoid disturbing the landfill interior by sucking gas around). The experiment was delayed for a year while such equipment was sought, but the only instrument available at the time proved unreliable. Instead monitoring was carried out manually at 12 hourly intervals using a portable infra-red device to measure methane, carbon-dioxide and oxygen. A portable pressure gauge was also used at the surface and within each borehole simultaneously with the other monitoring.

Independent data on atmospheric pressure was obtained from a nearby meteorological station, and showed the on-site barometric gauge to be accurate to within the manufacturers tolerances. Facilities were installed to monitor surface temperature also, but the instrumentation was destroyed by cattle grazing the on site. Monitoring was carried out over a 3 month period from 5th September to 2nd December in 1991. Some of the early data proved unreliable and was discarded, leaving a total of 175 data points for each of

the monitored variables.

#### 4.6.2 Results.

It is seen from the various plots (see below and Appendix 4B) that the landfill gas concentrations tend to remain fixed near a mean level — except for isolated periods when they fall significantly below this. Figure 4.10 shows the total pressure in the 1 m borehole during the study, together with the concentrations of methane and carbon-dioxide recorded over the same period. Table 4.2 below gives a statistical summary of the concentration data from the three boreholes (the ‘St.Dev’ and ‘Cor’ terms are defined in Appendix 4B).

**Table 4.2 : Concentrations (%) at 1m Depth.**

Gas	Minimum	Maximum	Range	Mean	St.Dev	Cor( $P$ )	Cor( $dP/dt$ )
$CH_4$	15.7	72	56.3	62.97	6.71	-0.040	-0.336
$CO_2$	6.5	29.1	22.6	24.5	2.71	-0.104	-0.023
$O_2$	0.4	15.2	14.8	0.88	1.59	0.022	0.200

**Table 4.3 : Concentrations (%) at 2m Depth.**

Gas	Minimum	Maximum	Range	Mean	St.Dev	Cor( $P$ )	Cor( $dP/dt$ )
$CH_4$	33.4	75.5	42.1	65.5	3.72	-0.107	-0.180
$CO_2$	12.8	27.1	14.3	24.3	1.34	-0.104	-0.023
$O_2$	0.3	10.0	9.7	0.619	0.81	0.004	0.063

Note that the variation (as indicated by the range) is greatest in the 1 m borehole, and that the small standard deviation indicates that only a few points varied significantly from the mean value. After experimenting with several graphical methods of presenting the data, it was found that scatterplots were by far the most useful since the degree of clustering near the mean is immediately obvious as are the number and deviation of outlying data points.

**Table 4.4 : Concentrations (%) at 5m Depth.**

Gas	Minimum	Maximum	Range	Mean	St.Dev	Cor( $P$ )	Cor( $dP/dt$ )
$CH_4$	23.9	69.8	45.9	61.1	4.38	-0.060	-0.059
$CO_2$	11.4	31.2	19.8	28.1	2.04	-0.009	-0.032
$O_2$	0.2	11.9	11.7	0.696	1.167	0.013	0.096

No surges in concentration were recorded during the experiment — however, since the typical combined concentrations of methane and carbon-dioxide were in the range 90–95%, such surges were impossible under any circumstances. This is caused by the normal rate of gas production being large compared to the rate of air diffusion into the site, so that most of the air is pushed out. The majority of sites currently being monitored are less active than the Sleaf landfill (due either to greater age or to a larger fraction of inert wastes) and lack a capping layer, and the model predicts that the compositional variations would be significantly larger in such sites.

The inability to study the effects of pressure drops could have been overcome had it been possible to install continuous flux monitoring equipment. Also, monitoring nearer to the surface would have eliminated this problem by sampling from a region in which back-diffusion maintained a higher mean air concentration.

It can be seen from Figure 4.10 that the troughs in  $CH_4/CO_2$  concentrations are associated with periods of rising pressure, and this is borne out and emphasized by the scatterplot analysis below.

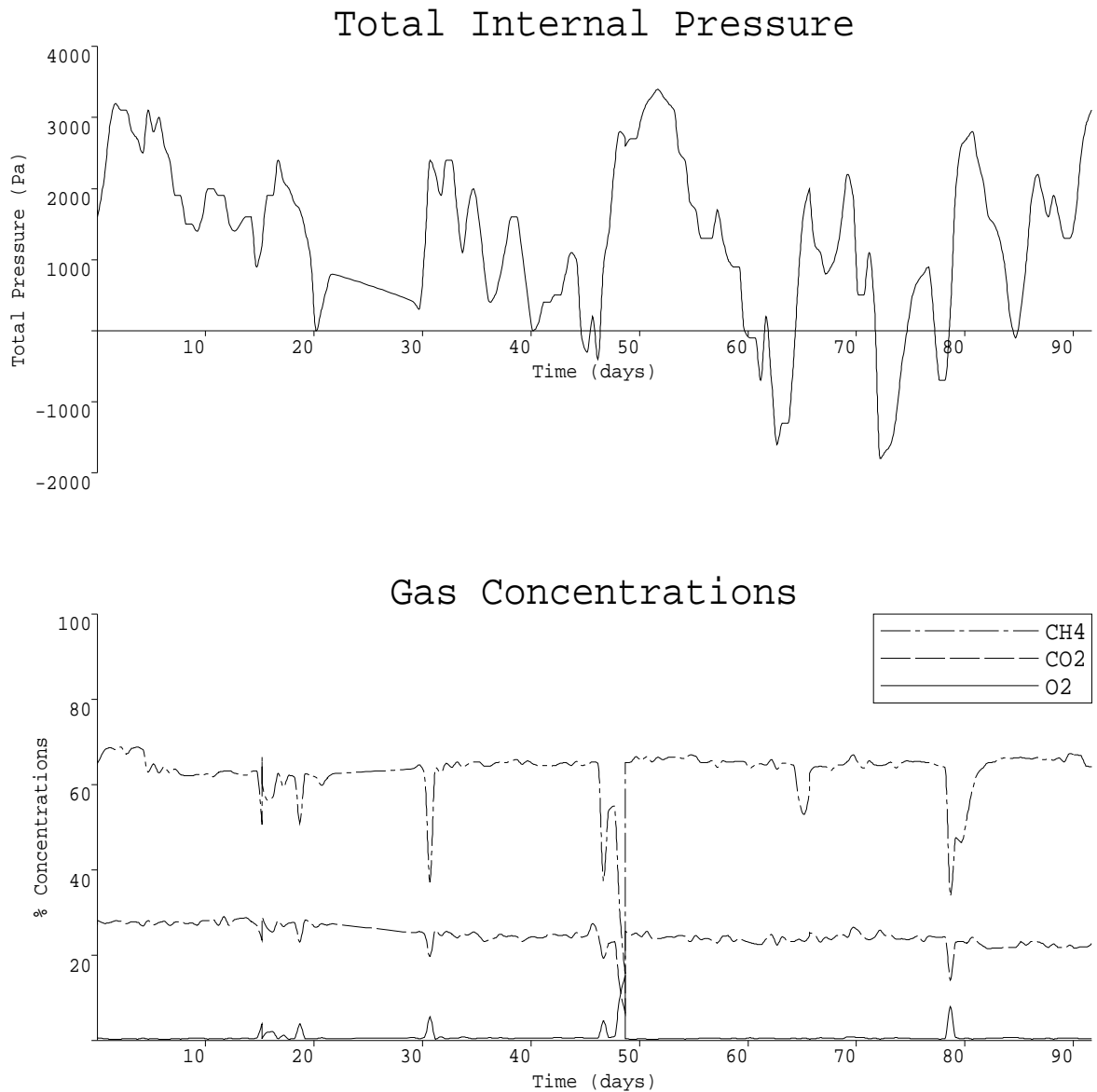


**Figure 4.10** : Recorded concentrations of  $CH_4$ ,  $CO_2$  and  $O_2$  in 1 m borehole.

To assess the influence of atmospheric pressure on gas composition, a series of scatter-plots were created, showing the gas concentration against either the barometric pressure or its rate of change at each monitoring time. A  $\chi^2$ -fit (the method of ‘least squares’) was performed on each of the data sets, and is indicated by a dotted line. The centroid of the data is marked by a large cross. Points marked “+” indicate that the interpolated derivative of the pressure variable ( $dP/dt$  for the upper graphs, and  $d^2P/dt^2$  for the lower ones) was positive at that time, “Y” indicates a negative derivative, and “o” indicates either

that the derivative was zero or could not be determined due to invalid or missing adjacent points.

Figure 4.11 shows the total pressure at 1 m mapped against its time derivative ( $dp/dt$  denotes the rate of change of atmospheric pressure). This indicates that there is a some correlation between the atmospheric pressure and its derivative over the monitoring period, and is presumably an artifact of the sampling interval. This apparent correlation (which would not exist over a longer time period) is unhelpful — it hinders our attempts to demonstrate that minor fluctuations are due to the derivative of the pressure rather than the instantaneous pressure.

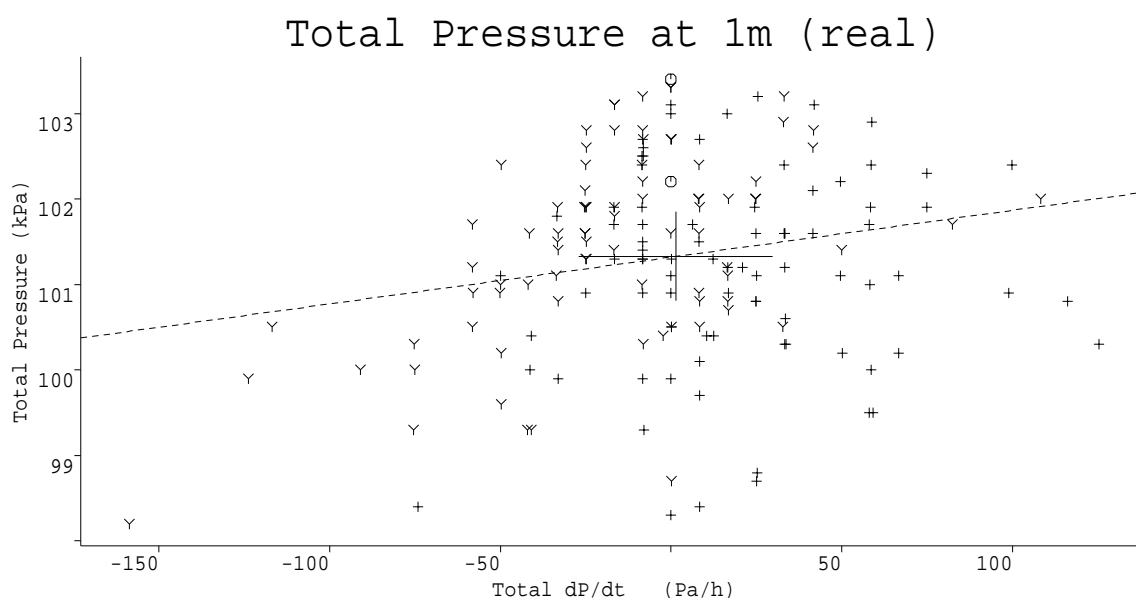


**Figure 4.11** : Total pressure at 1 m depth.

Graphs of the data from the other depths are given in Appendix 4B. A statistical analysis in term of  $\chi^2$ -fits and Standard Deviations is also listed.

Note that the data is subject to considerable ‘noise’ caused by changes in the physical nature of the site — for instance; episodes of rain alter the permeability (both to gas and water) and saturation level and may introduce new gases into the site, changing temperatures influence gas solubilities. Hence, we must expect some perturbations not predicted by the computer model (see below) which only considered the variations due to changes in atmospheric pressure — these additional fluctuations will appear random as we cannot assign particular mechanisms to them.

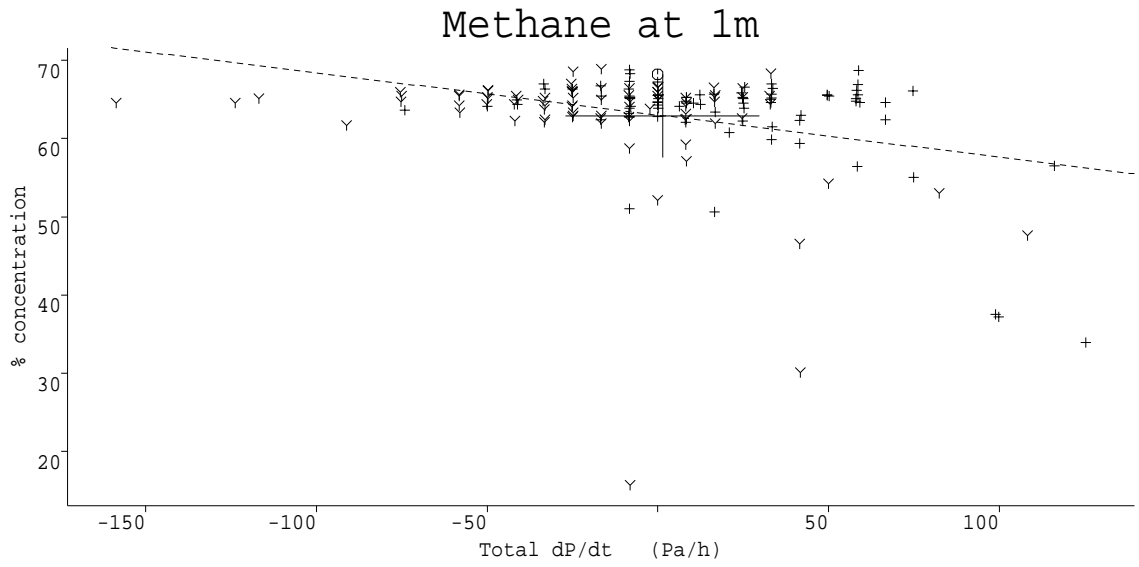
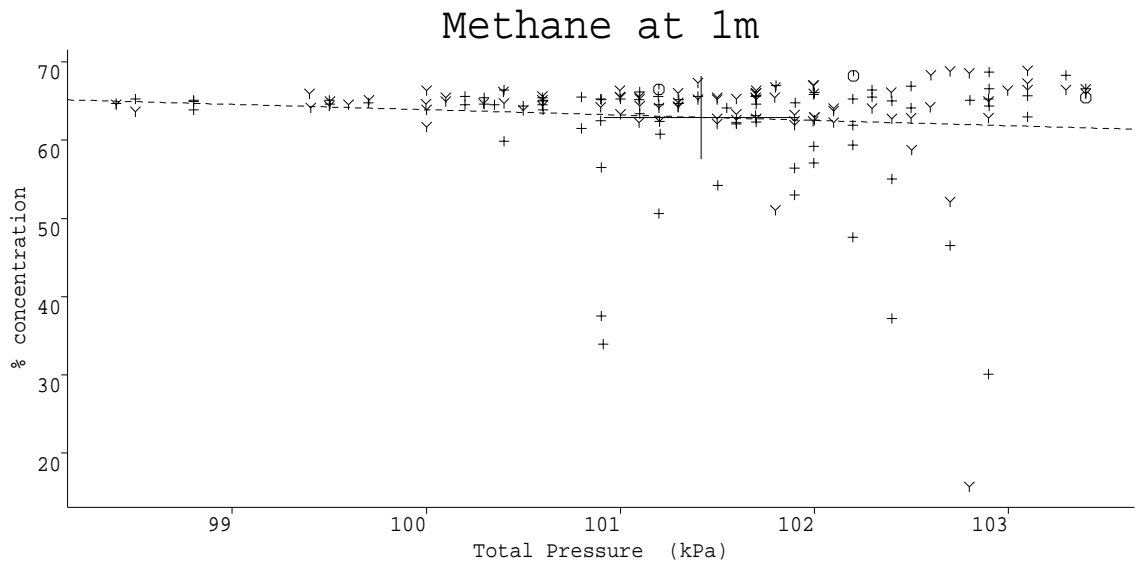


**Figure 4.12 : Methane at 1 m depth.**

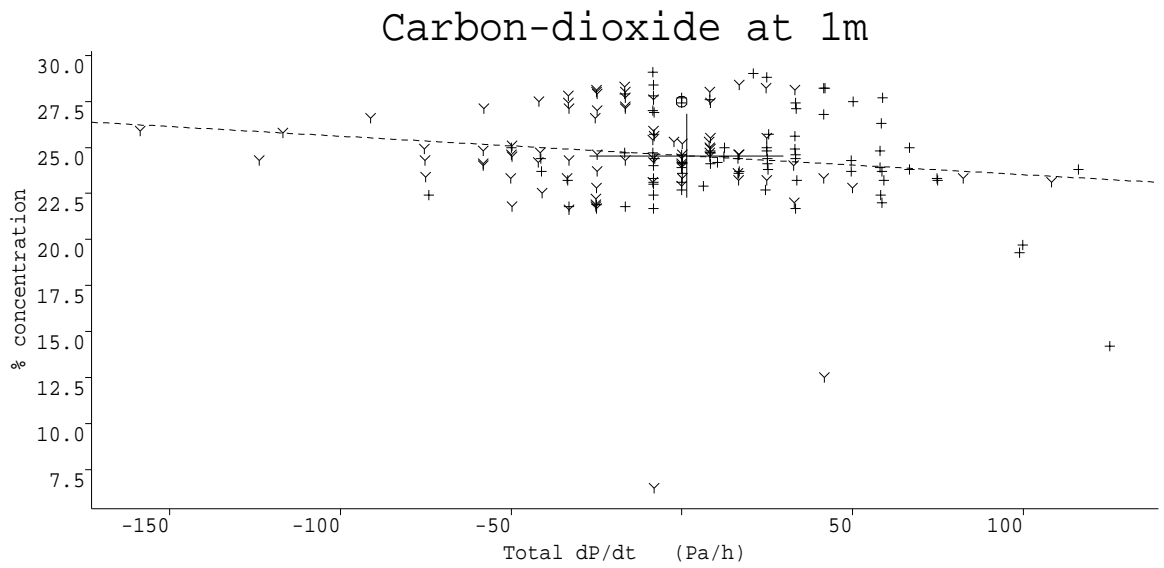
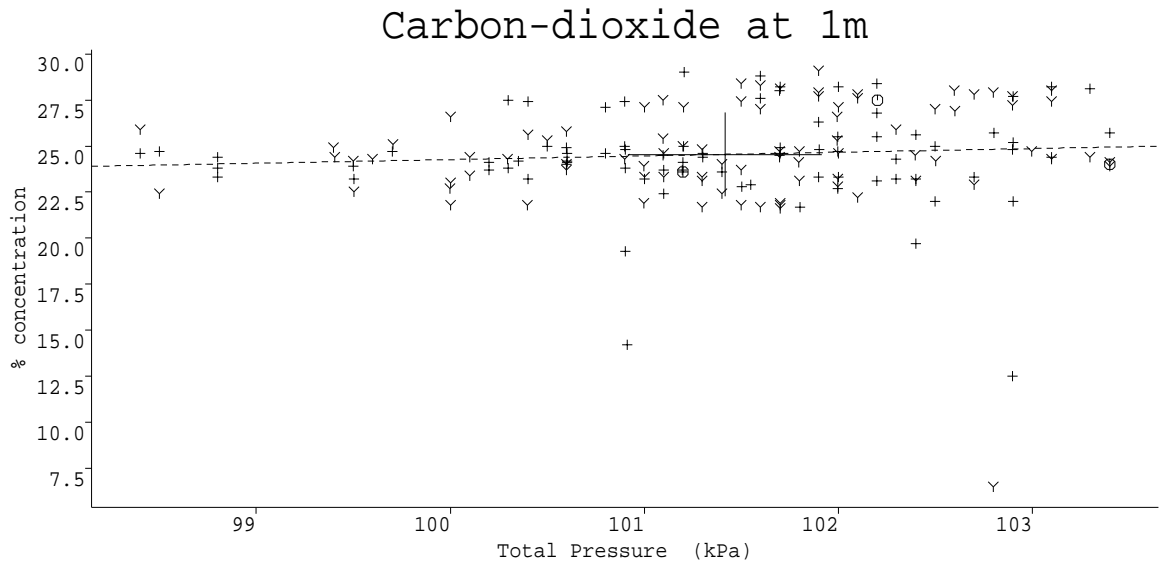


**Figure 4.13 :** Carbon-dioxide at 1m depth.

Figure 4.14 shows a plot of the instantaneous pressures of carbon-dioxide and methane measured. These generally lie along a line, with clustering about the saturation values.



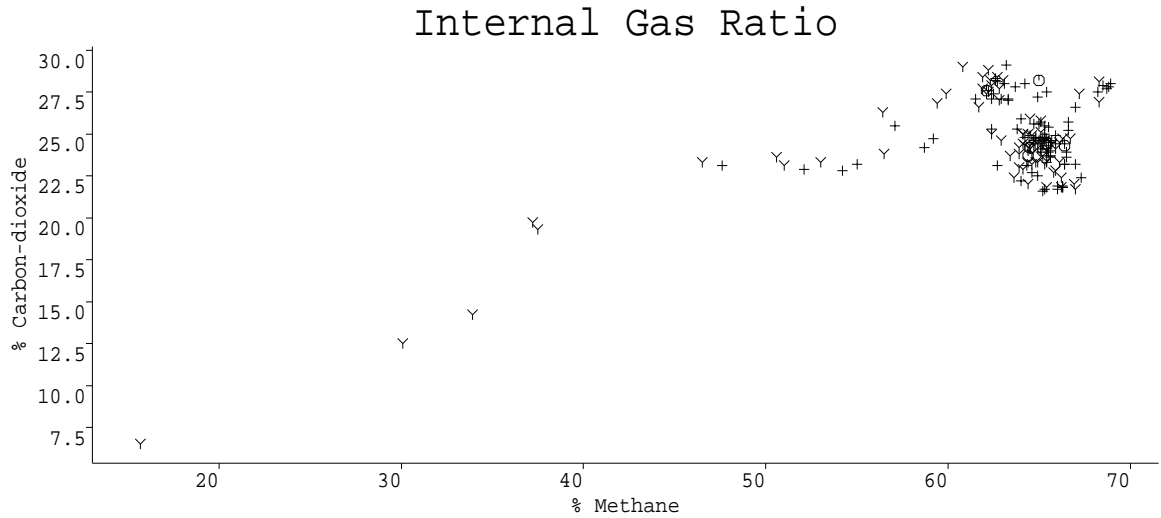


**Figure 4.14 :** Carbon-dioxide versus methane in 1 m borehole.

The 1 m borehole was found to exhibit more variation than either of the others, although the mean concentrations at all three depths were fairly similar. The concentrations of methane found were on average 2.4 times higher than carbon-dioxide, and this ratio decreased from 2.6 at 1 m to 2.2 at 5 m. The variation in methane concentration (based on Standard Deviations) was on average 2.4 times that of carbon-dioxide, with the ratio decreasing from 2.7 at 1 m to 2.1 at 5 m. Thus, allowing for the different means, no significant difference in the generic behaviours of the two gases was observed — however, methane did show more instances of exceptionally low concentrations (the model would explain this in terms of the greater solubility of carbon-dioxide providing a buffer against rapid falls, but this may not necessarily be the only explanation).

The plots against instantaneous atmospheric pressure seem to indicate that typical gas concentrations are marginally higher during periods of high pressure — they supply no evidence to indicate any link between low atmospheric pressure and high gas fluxes. The instances of very low gas concentration seem slightly common during periods of higher pressure, but the bias is negligible and probably due to random effects.

Considering the plots against rate of change of atmospheric pressure, most of the concentration readings lie in a central cluster with the highest values centred around periods of static weather. It is notable that all of the instances of unusually low gas concentrations occur when the surface pressure is rising.

### 4.6.3 Model Comparison.

The site consisted of 20 m of waste, capped by 1 m of soil. The upper 30 cm of the cap gradually became more compressed due to trampling by people and cattle. The 'best guess' site parameters are shown in Table 4.5 below.

**Table 4.5 : Parameters for simulation of Sleaf site.**

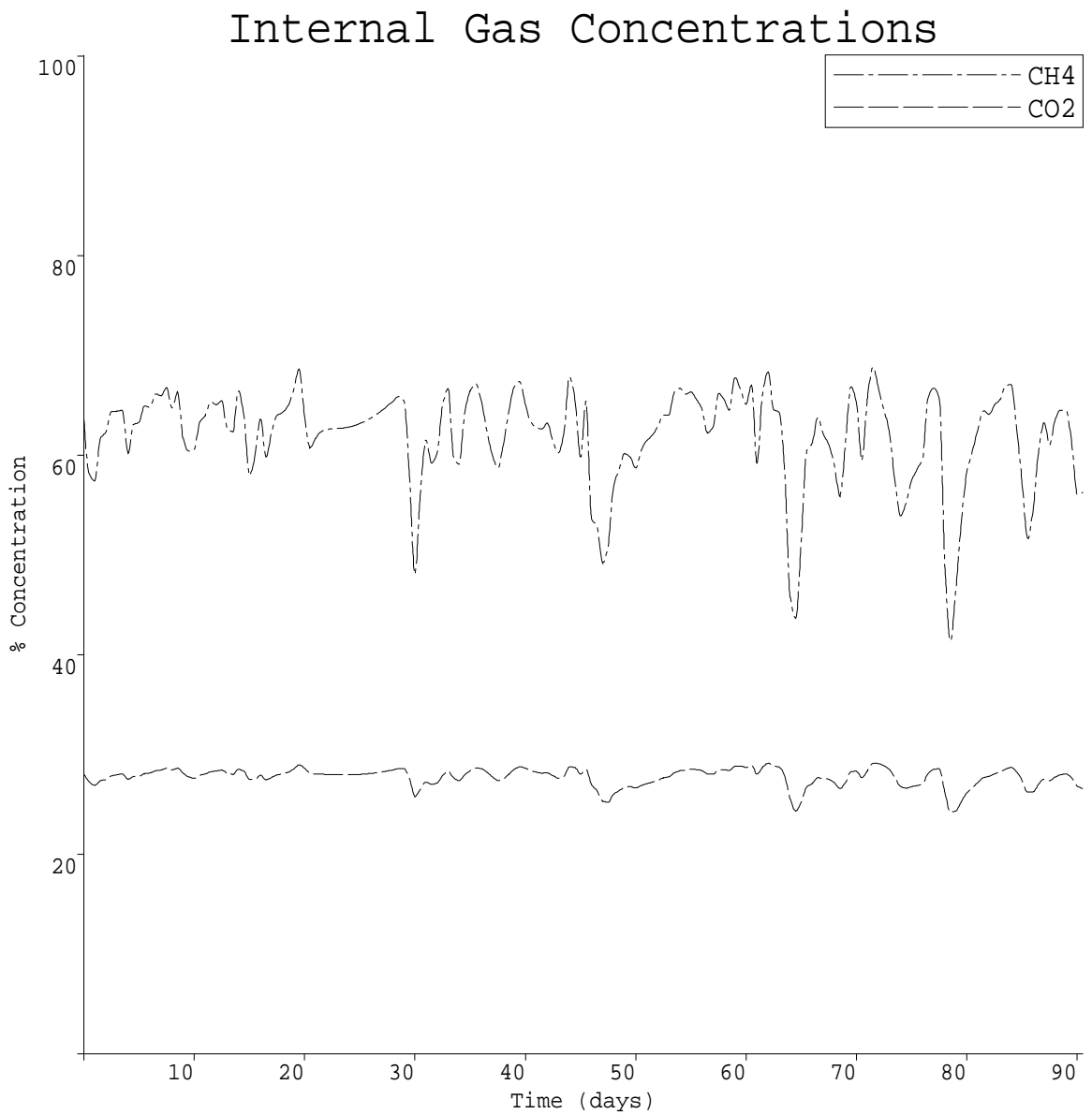
layer	thickness	permability $\theta$	$\varphi$	$\tau$	pH	Prod. $CH_4$	Prod. $CO_2$	
cap	1	$10^{-7}$	0.1	0.1	0.3	5.5	0	0
fill	20	$3 \times 10^{-7}$	0.25	0.1	0.3	6.5	3.0	3.4

The permeability is given in  $\text{m}^2 \text{s}^{-1} \text{Pa}^{-1}$ , and gas production in  $\text{g m}^{-3} \text{d}^{-1}$ . The temperature was taken to be  $15^\circ\text{C}$  throughout.

**Table 4.6 : Simulated Concentrations (%) at 1m Depth.**

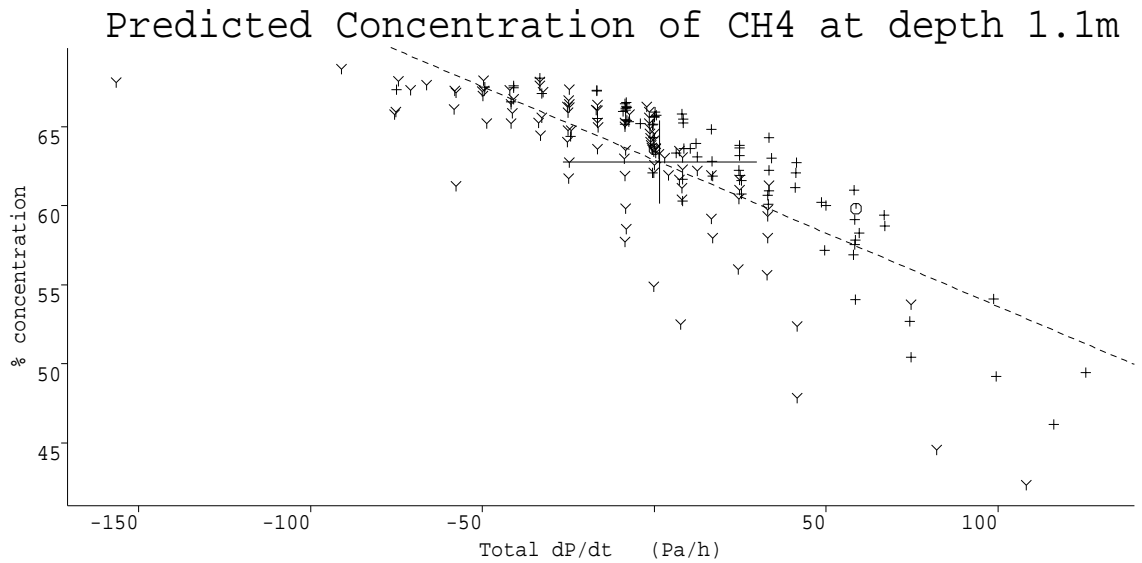
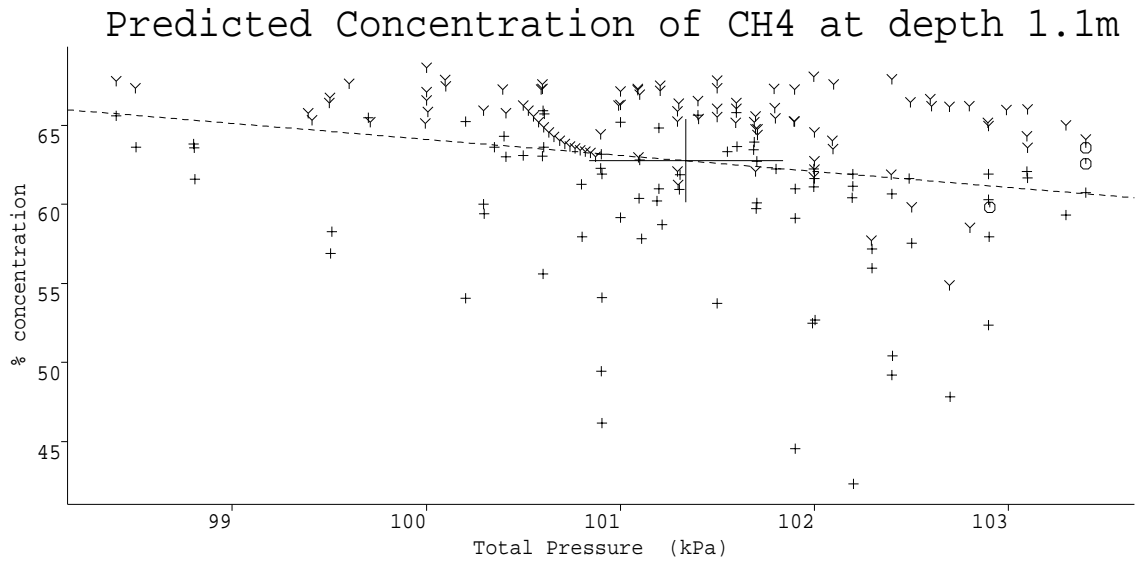
Gas	Minimum	Maximum	Range	Mean	St.Dev	Cor( $P$ )	Cor( $dP/dt$ )
$CH_4$	42.3	68.6	26.3	62.8	4.66	-0.233	-0.788
$CO_2$	24.7	29.1	4.4	28.1	0.80	-0.287	-0.578

Figure 4.15 shows the predicted gas concentrations at the 1 m level. Figures 4.16 and 4.17 illustrate the same data in the form of scatterplots. As with the real data, the concentrations (especially that of carbon-dioxide) fluctuate around a mean level, with only a few exceptional events indicated by the large troughs on the graphs.



**Figure 4.15** Predicted gas concentrations in 1 m borehole.

The graphs for the 1 m borehole are based on the simulated concentrations at a depth of 1.1 m to allow for the fact that the actual wells took gas from a perforated pipe rather than a purely local value.



**Figure 4.16** : Predicted methane concentration in 1 m borehole.

As with the real data, there is not significant evidence of linkage between the instantaneous atmospheric pressure and concentration. Note that, in accordance with the field data, the modelled results show that the same rate of change of atmospheric pressure (for instance  $5\text{KPa hr}^{-1}$ ) can be associated with a wide variety of concentration levels, that the Sleep site does not produce peaks of concentration, and furthermore that all troughs in concentration are associated with falling pressure.

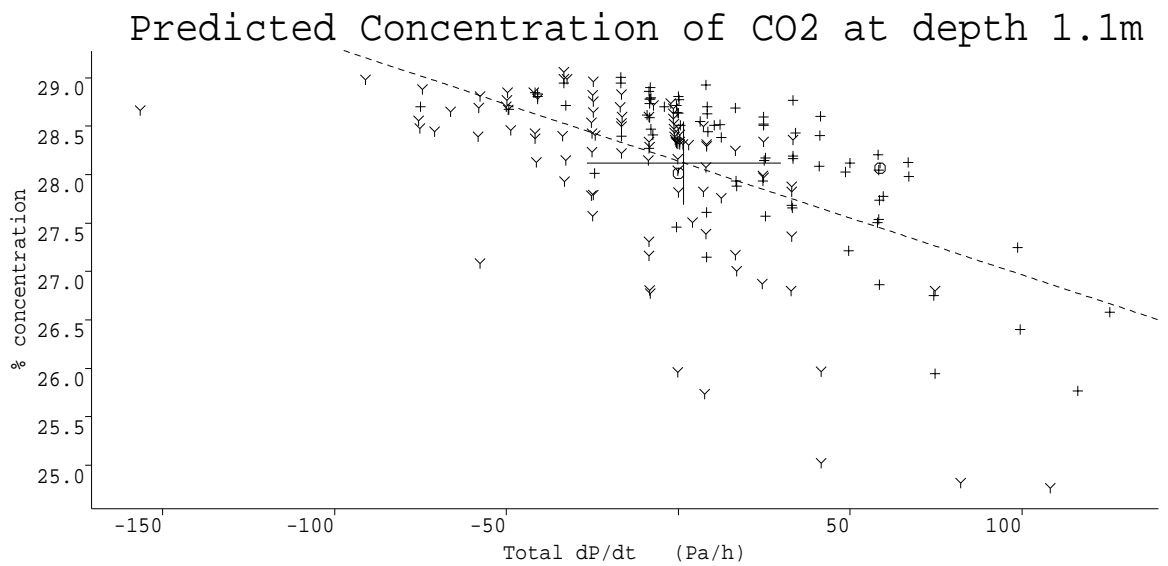
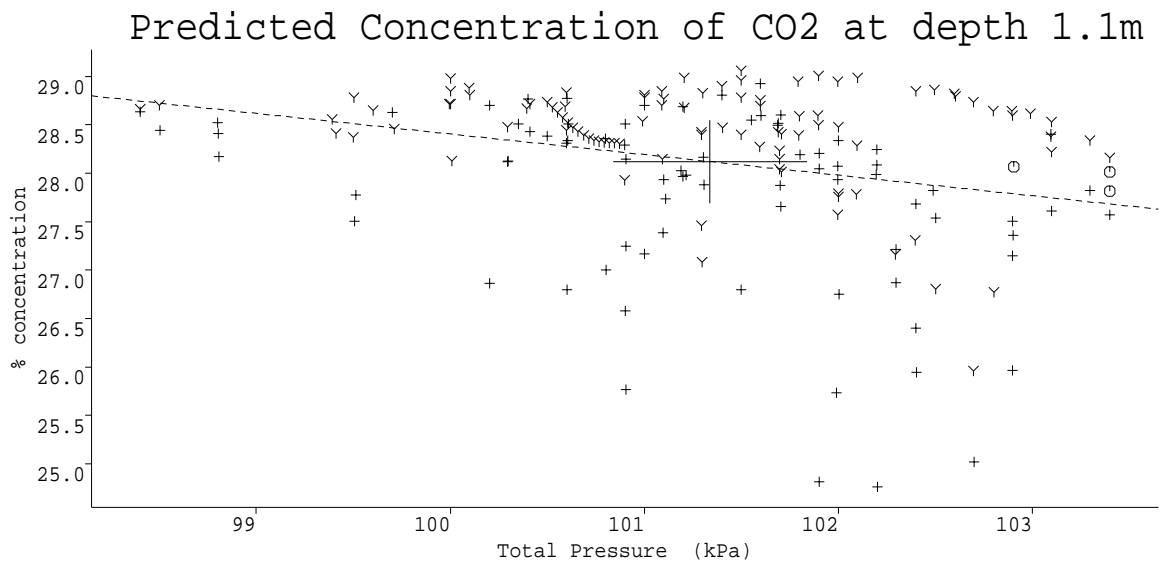


**Figure 4.17** : Predicted carbon-dioxide concentration in 1 m borehole.

Figure 4.18 shows the predicted surface fluxes — which are seen to vary by a factor of 8 for methane and 6 for carbon-dioxide.

**Table 4.7 : Simulated Surface Fluxes.**

Gas	Minimum	Maximum	Range	Mean	St.Dev	Cor( $P$ )	Cor( $dP/dt$ )
$CH_4$	0.97	8.40	7.43	3.76	1.22	-0.256	-0.940
$CO_2$	0.49	2.91	2.42	1.56	0.47	-0.299	-0.931

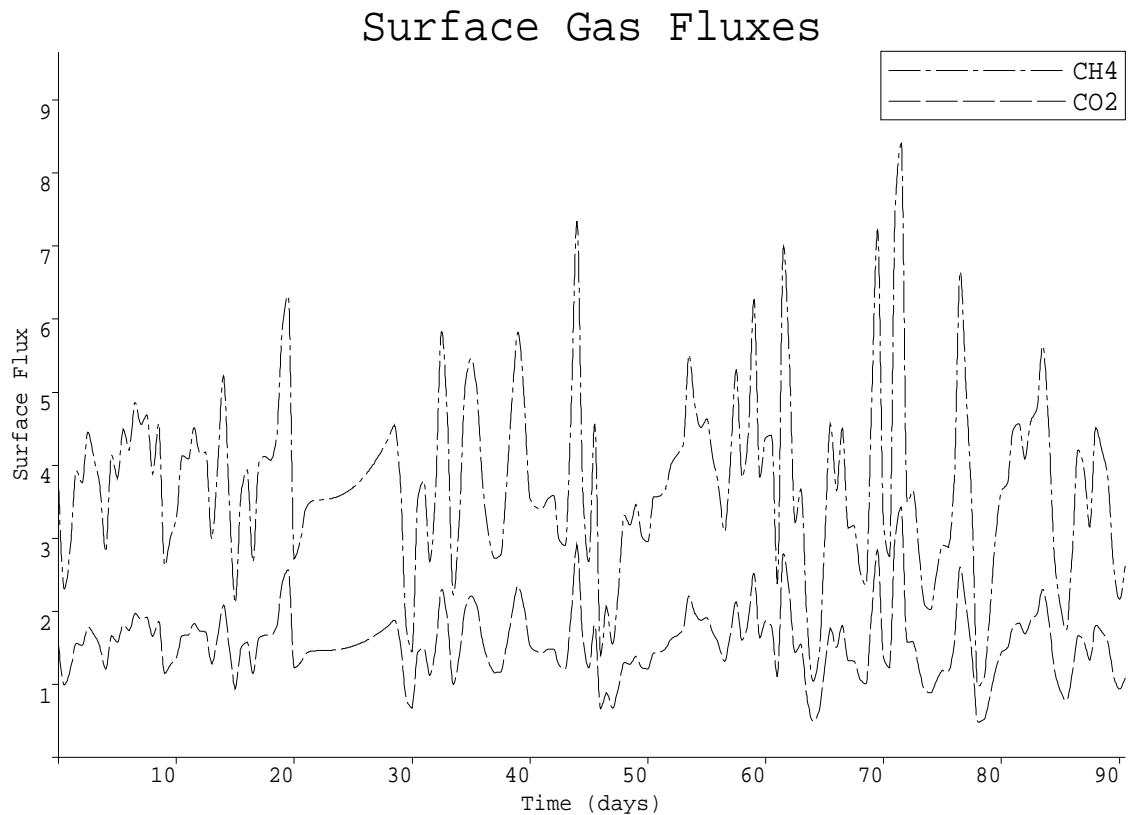


**Figure 4.18 : Predicted surface fluxes at Sleep.**

The predicted surface fluxes are much more strongly linked with the rate of change of pressure than the predicted data for the 1 m concentration, and this can be seen from the statistical correlations in Table 4.7 above. Scatterplots in Figures 4.19 and 4.20 show the near-linear relationship between  $dP/dt$  and vented fluxes.

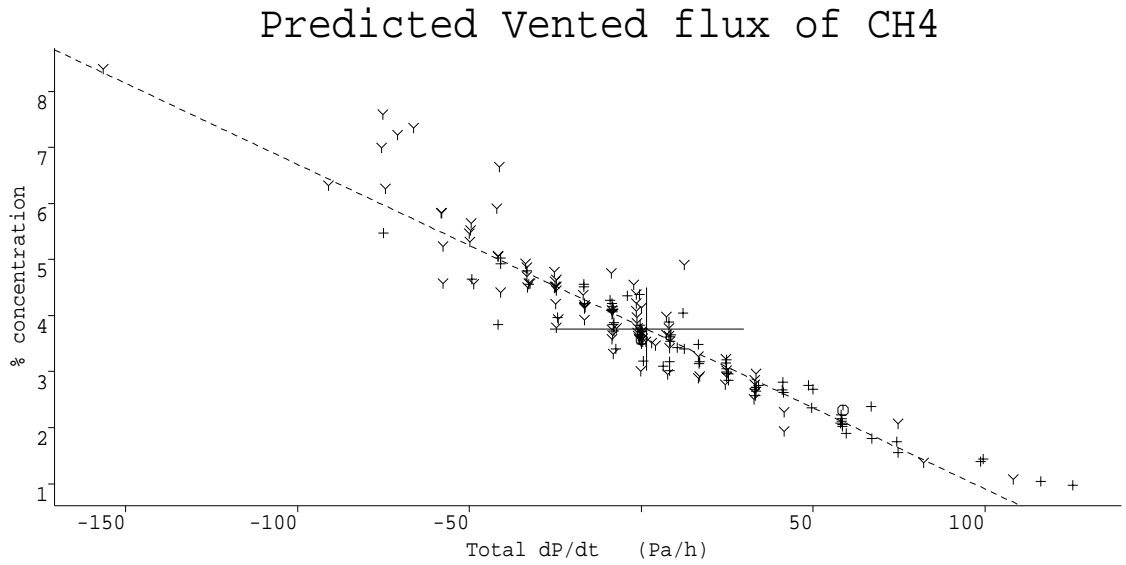
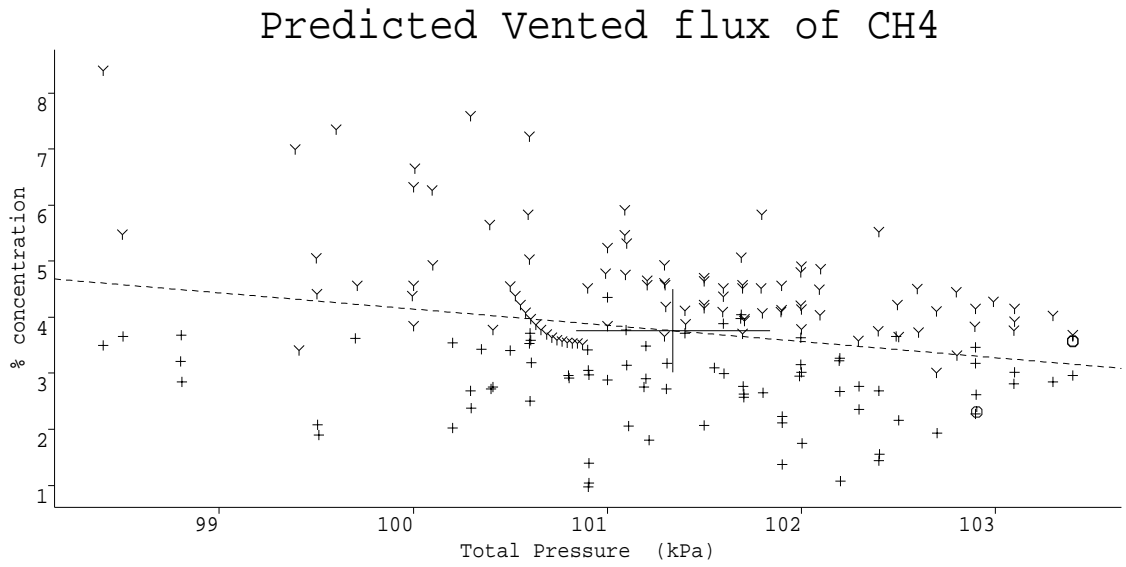


**Figure 4.19 :** Predicted surface flux of CH<sub>4</sub>.

Plot of the modelled gas concentration in the near-surface region (less than 0.3 m below ground) show a correlation with  $dP/dt$  of the same magnitude as the surface fluxes.

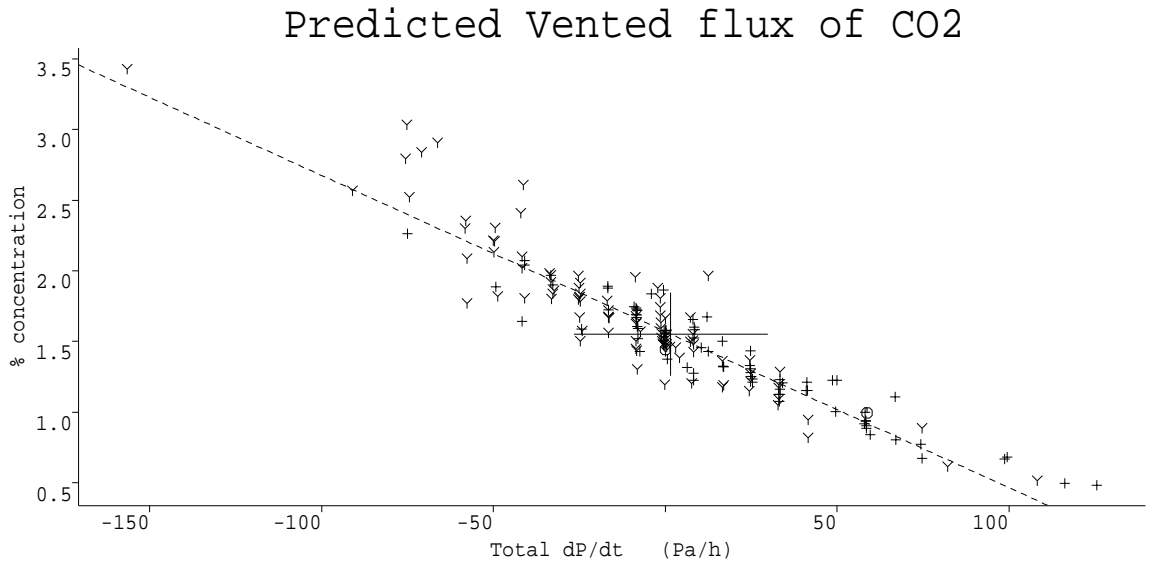
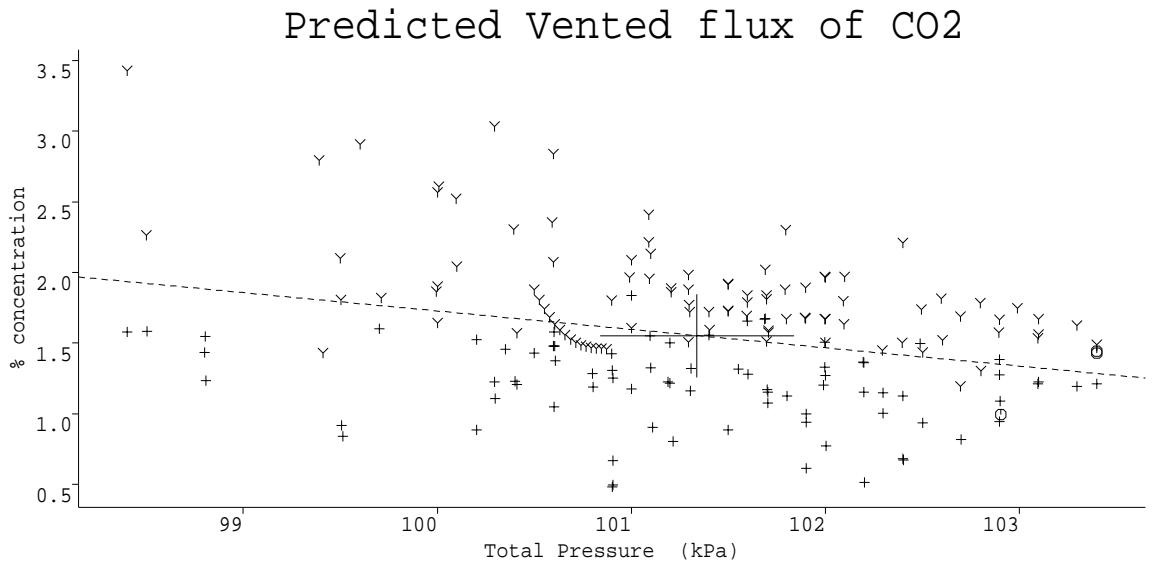


**Figure 4.20 :** Predicted surface flux of  $CO_2$ .



#### 4.6.4 Conclusions on the Sleaf Experiment.

The results demonstrate clearly that internal concentrations vary with time, and that changes in atmospheric pressure are involved as a major contributory factor. Examination of the data shows that all instances of low LFG concentrations occurred during periods of rising atmospheric pressure, and as mentioned previously high concentrations were impossible.

The model is seen to produce results for the internal concentrations which are qualitatively close to the behaviour of the real site, and this gives us confidence that the much larger predicted changes in surface flux at Sleaf are real.

Had the experiment been conducted as originally envisaged (or the site been less vigorously methanogenic), then the observed behaviour should have been much more dramatic. In particular, monitoring nearer to the surface would have allowed more air to enter the site by diffusion, and hence surges in gas concentration would have been detectable. A method of measuring surface flux must be found, since this may vary drastically even though the internal concentrations are almost constantly at 'saturation' levels.

Predictions of internal gas concentration based on  $\chi^2$  methods are seen to be inadequate for this data-set. It is currently normal practice to attempt to infer gas production rates from much smaller data-sets (or even single measurements), and this experiment has proved that such procedures are unreliable. Had a brief site investigation been conducted at Sleaf during one of the periods of rapid atmospheric pressure rise, the investigators would have found  $CH_4$  and  $CO_2$  concentrations of about 20% and 10%, (rather than the average values of 65% and 25%), and hence concluded wrongly that the site is relatively inactive.

The only way to assess a site properly is to gather a large data-set (at least the size of the Sleaf data) and perform a simple statistical analysis in terms of means, extrema and standard deviations as done in Appendix 4B. The graphical method devised herein of illustrating gas concentrations as scatterplots is a very useful way of characterizing site emissions, and we recommend that it be adopted as a standard method of presenting monitoring results.

## 4.7 Overall Conclusions on Gas Monitoring.

The following conclusions can be drawn from the results of the computer simulations

[1] The composition of vented gas can exhibit large fluctuations even though the internal generation rates are steady.

[2] Although the effects are complex, the size of the changes is likely to increase as the moisture content of the site rises, the pH of the leachate increases, or the void fraction decreases.

[3] The size of the stoichiometric fluctuations will increase as gas production decreases. This means that gas composition measurements from older sites and regions adjacent to landfills are especially prone to mis-interpretation.

[4] The size of the stoichiometric fluctuations is greatest near to the site surface.

[5] Gas composition exhibits hysteresis — it has a ‘history’ which must be known to make sense of any new measurement.

[6] It is impossible to gauge the state of degradation of a site from measurements of gas composition taken at a single time or at too infrequent intervals.

[7] The frequency with which much historical gas data has been gathered renders it of little value for risk assessment purposes.

[8] Future monitoring programmes must make provision for a period of frequent (at least daily) monitoring of gas composition and external weather to evaluate the variability at each monitoring location.

The experiment at Sleaf Landfill provides evidence in favour of [1], [4], [5], [6], [7] and [8], but can say nothing about the other model predictions. Frequent simultaneous monitoring of site variables is the only way to perform an accurate assessment of landfill characteristics, and this data should be analysed using the simple statistical and graphical methods shown in this Chapter.

Note finally that while volumetric and compositional fluctuations are real and of a significant magnitude, they are unlikely to be responsible for all the apparent short-term changes in landfill emissions, and should not be used as a blanket excuse to cover faulty equipment or inadequate monitoring.

## **Chapter 5 : Gas Extraction Systems.**

Modern landfills generate large amounts of gas which has the potential to escape from the site and pose a hazard in the surrounding region. Site operators must make provision to prevent this form of contamination when designing and running a disposal facility, and the increasing size of landfills coupled with more stringent regulations has meant that some form of gas extraction system has become necessary.

Early gas extraction systems consisted of a few wells attached to a single pump, but today sites are operating which contain several pumps and hundreds of wells grouped into one or more distinct networks (eg. Merseyside in the U.K.). However, these larger installations continue to be designed on a rule-of-thumb basis derived from experience with smaller systems, and this may result in systems which are either ineffective or inefficient. Some installations are using computers to do automatic load-balancing, but there is no guarantee that such systems make maximum use of every well, or that the site layout is optimally designed beforehand.

### **5.1 Introduction to Yield Reduction Coefficients.**

The specification of the pumps and pipes in an extraction system can be determined in advance of installation from laboratory tests, but the nature of the landfill interior means that the performance of a well can only accurately be gauged through field trials. The empirical basis of the methods for assessing well characteristics has led to the concept of 'radius of influence' (ROI) as a single parameter relating gas yield to applied suction.

Most practical extraction schemes consist of several wells, and they will interact with each other — any gas removed by one well obviously reduces the amount available to the others. This means that the effective radius of influence of a well depends on the status of any neighbouring wells. In the first part of this Chapter we quantify this interaction between wells by introducing a parameter called the 'yield reduction coefficient' (YRC) which gives a numerical value for the degree to which one well affects another, enabling the flux through any single well to be expressed in terms of the suction pressures at all of the wells. Some theoretical calculations are performed to indicate the primary factors which determine the YRCs governing a system of wells.

### 5.1.1 Mathematical Formulation.

Writing  $W_i$  as the extraction pressure at  $i$ th well, and  $V_i$  as the gas flux from it, the following relation is derived in Chapter 3: of the extraction pressures  $W_1, \dots, W_M$  thus

$$V_i = \alpha_i + \beta_i \left( W_i - \sum_{j \neq i} \mu_{ij} W_j \right), \quad (1)$$

where  $\alpha_i$ ,  $\beta_i$  and  $\mu_{ij}$  are constants depending on the physical characteristics of the site.

From equation (1) it can be seen that if the suction pressure  $W_j$  at well  $j$  is increased by  $p$ , then the yield at well  $i$  decreases by the same amount as would occur if  $W_j$  were held constant and  $W_i$  were instead reduced by  $\mu_{ij}p$ . For instance, if  $\mu_{AB} = 0.15$  then an increase in extraction pressure of 200 Pa at well  $B$  causes the same decrease in flux at well  $A$  as if the suction at the latter were reduced by 30 Pa.

Thus  $\mu_{ij}$  quantifies the effect of changing the pressure at well  $j$  on the yield produced by its neighbour well  $i$ . We therefore define the parameter  $\mu_{ij}$  as the yield reduction coefficient at well  $i$  due to well  $j$ . The greater the interaction between two wells, the larger the YRC will be.

Note that the YRCs depend only on the physical properties of the site, and are not affected by the rate of gas generation.

### 5.1.2 General Theoretical Relationships.

In Appendix 5B the approach of the previous section is applied to the particular case of predicting the flow regime within a rectangular containment landfill containing a network of vertical cylindrical wells. In the following sections we consider some of the results produced by a computer program evaluating this system and show how the YRC values are influenced by the characteristics of a site.

For clarity we first look at a site containing only 2 wells, labelled  $A$  and  $B$ , identical in each case except for the particular characteristic being discussed. Numerous simulation runs produced the following guidelines:

- [1] As the separation of the wells increases, the YRCs decrease.
- [2] Increasing the depth of the perforated sections (but not their overall length) results in the YRCs increasing.
- [3] If well  $A$  is situated nearer to an impermeable landfill boundary than well  $B$  then  $\mu_{AB} > \mu_{BA}$  indicating that well  $B$  has a greater influence on well  $A$  than vice versa.
- [4] As the vertical permeability decreases, the YRCs increase.
- [5] As the horizontal permeability decreases, the YRCs decrease.

[6] If the perforated section of well  $A$  is located at a shallower depth than that of well  $B$  then  $\mu_{AB} > \mu_{BA}$ .

[7] If the length of the perforated section of well  $A$  increases then  $\mu_{AB}$  increases slightly while  $\mu_{BA}$  increases by a much larger factor.

[8] If the radius of the perforated section of well  $A$  increases then  $\mu_{AB}$  increases slightly while  $\mu_{BA}$  increases by a much larger factor.

[9] If the thickness of the cap is increased, or its permeability decreased, then the YRCs increase.

### 5.1.3 Relationships For Large Sites.

When the two wells are a sufficiently distant from the site boundaries (at least 3 times the separation between them), it is possible to formulate the relationships given in the preceding section in a more precise manner. These dependencies are illustrated in figures 5.1–5.4 for the particular case of a homogeneous 25 m deep site of side length 600 m.

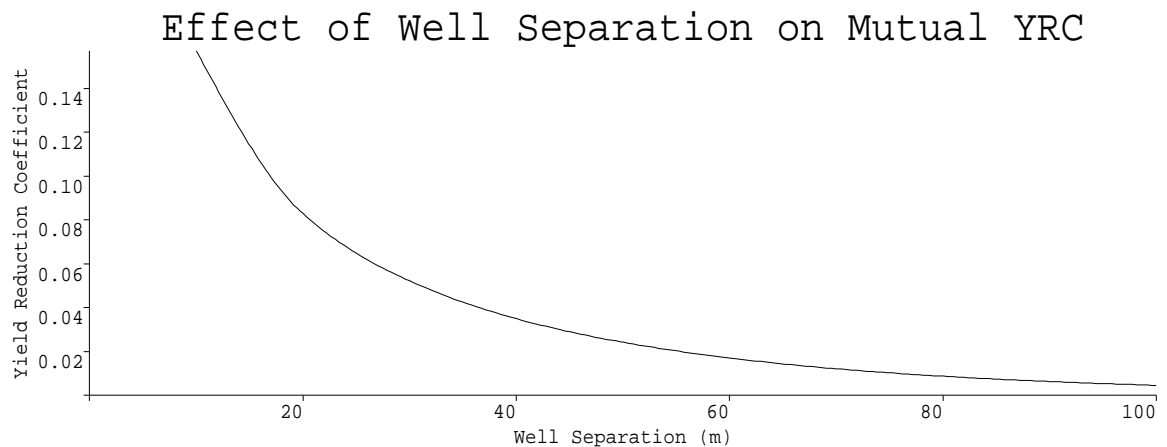
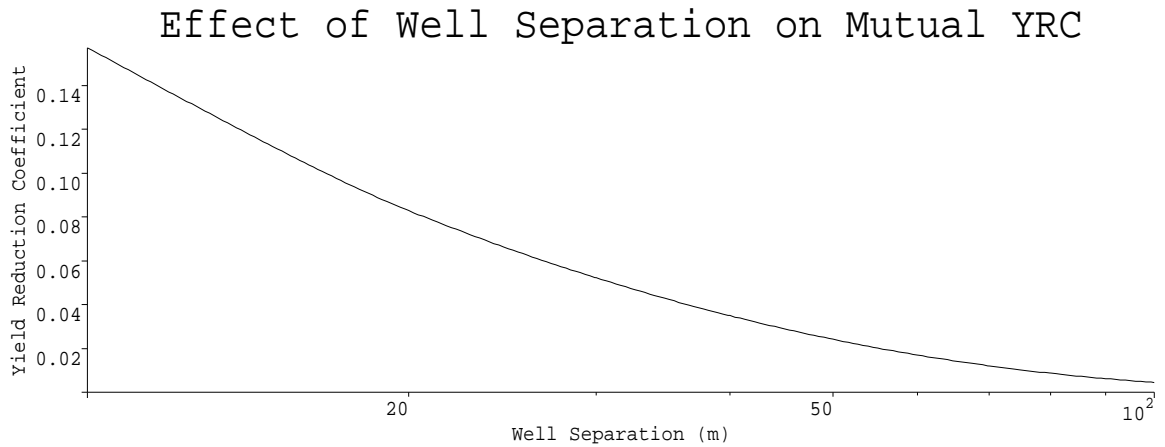


**Figure 5.1** : Relationship of YRC to well separation.

Figures 5.1 and 5.2 show that the relationship between well separation and YRC can be approximated by a decreasing exponential function of distance, except when the wells are extremely close together, or when they approach impermeable boundaries. Hence, if  $\sigma$  is the separation distance between the wells, the YRCs follow the proportionality

$$\mu \propto e^{-k\sigma}, \quad (2)$$

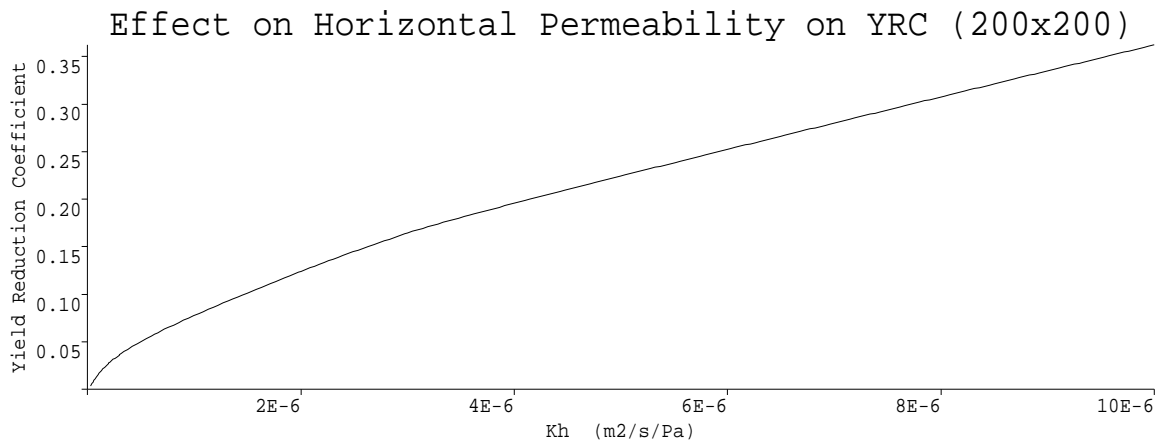
where the coefficient  $k$  depends on the construction of the wells and the site characteristics.



**Figure 5.2 :** Relationship of YRC to well separation.

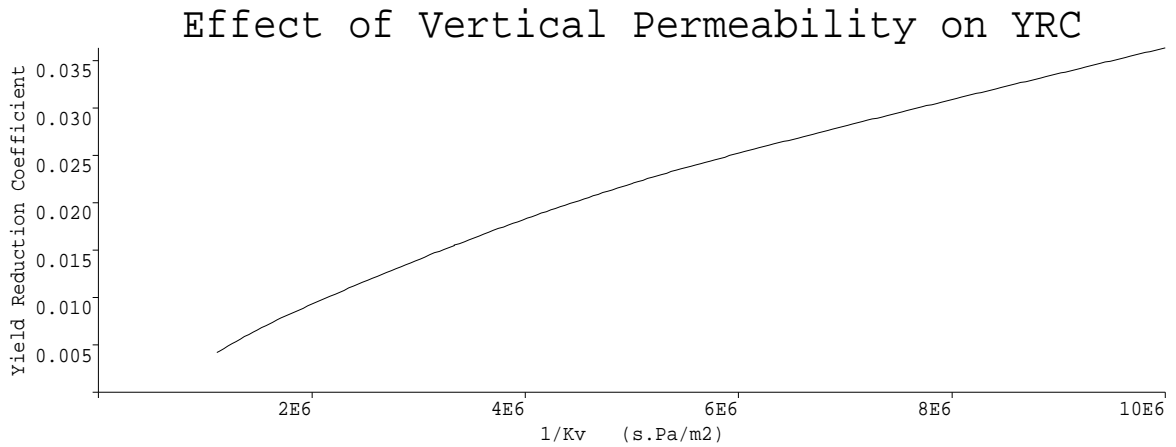
Figure 5.3 demonstrates that the YRC increases linearly with increasing horizontal permeability  $K_h$ . Conversely there is a reciprocal correspondence between the YRC and the vertical permeability  $K_v$ , giving the relationship

$$\mu \propto \frac{K_h}{K_v}. \quad (3)$$



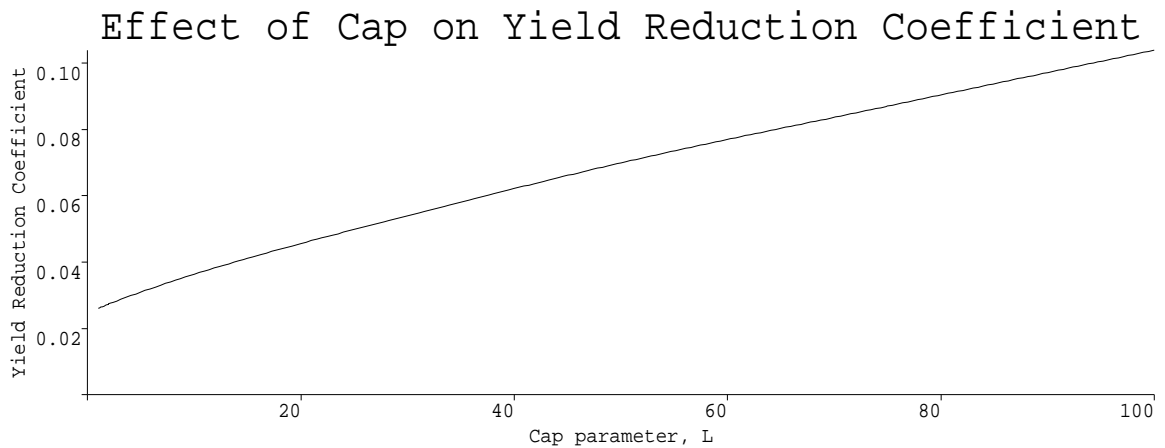
**Figure 5.3 :** Relationship of YRC to  $K_h$ .

Figure 5.4 shows that the YRC is inversely proportional to the vertical permeability of the landfill strata.



**Figure 5.4 :** Relationship of YRC to  $1/K_v$ .

Figure 5.5 indicates that there is a linear increase in the YRC as the resistance to flow of the cap decreases (ie. as its thickness increases or permeability decreases). The capping parameter is defined as  $L = lK_v/K_l$  where  $l$  is the thickness of the cap, and  $K_l$  is its vertical permeability.



**Figure 5.5 :** Relationship of YRC to capping parameter  $L$ .

The introduction of additional wells will alter the slopes of these graphs but not their form — except when the new boreholes are very close to the original pair, in which case the local geometry of the wells becomes significant.

### 5.1.4 Multiple Well Sites.

As extra wells are introduced into a landfill, all of the YRCs will change — generally decreasing, this effect being greatest for those wells nearest to the new one. Conversely the YRCs will increase when one of the wells is removed or blocked.

For illustration, consider a rectangular site having 4 wells, as shown in Figure 5.5. Take  $x, y$  axes centred on the lower left-hand corner, let the site be 100 by 90 m of depth 25 m, and locate wells A—D at horizontal co-ordinates (25, 30), (75, 30), (75, 70) and (25, 70) respectively. Assume that the horizontal permeability  $3 \times 10^{-7} \text{ m}^2 \text{ s}^{-1} \text{ Pa}^{-1}$ , vertical permeability  $10^{-7}$ , and that there is a 1 m thick cap of permeability  $10^{-8}$ . The perforated sections of the wells are 5 m long, extending from depth 15 m to 20 m. Wells A, C, and D have radius 0.25 m, and well B has radius 0.4 m.

Table 5.1 shows the YRC values expected from this arrangement (which has been completed by writing  $\mu_{ii} = -1$ ). Note that except for the identically constructed and symmetrically located wells C and D, no pair of the wells have the same influence on each other — ie.  $\mu_{ij} \neq \mu_{ji}$  usually.

**Table 5.1 : Yield Reduction Coefficients for 4-Well Site.**

$\mu_{AA} = -1$	$\mu_{AB} = 0.048$	$\mu_{AC} = 0.029$	$\mu_{AD} = 0.062$
$\mu_{BA} = 0.043$	$\mu_{BB} = -1$	$\mu_{BC} = 0.063$	$\mu_{BD} = 0.030$
$\mu_{CA} = 0.030$	$\mu_{CB} = 0.072$	$\mu_{CC} = -1$	$\mu_{CD} = 0.046$
$\mu_{DA} = 0.063$	$\mu_{DB} = 0.034$	$\mu_{DC} = 0.046$	$\mu_{DD} = -1$

Table 5.2 shows the new YRCs if well D is removed (or becomes blocked). A comparison of Tables 5.1 and 5.2 shows some of the effects listed at the beginning of this section, in particular all of the YRCs between the other wells have risen.



**Table 5.2 : Yield Reduction Coefficients for 3-Well Site.**

$\mu_{AA} = -1$	$\mu_{AB} = 0.050$	$\mu_{AC} = 0.033$
$\mu_{BA} = 0.045$	$\mu_{BB} = -1$	$\mu_{BC} = 0.064$
$\mu_{CA} = 0.033$	$\mu_{CB} = 0.074$	$\mu_{CC} = -1$

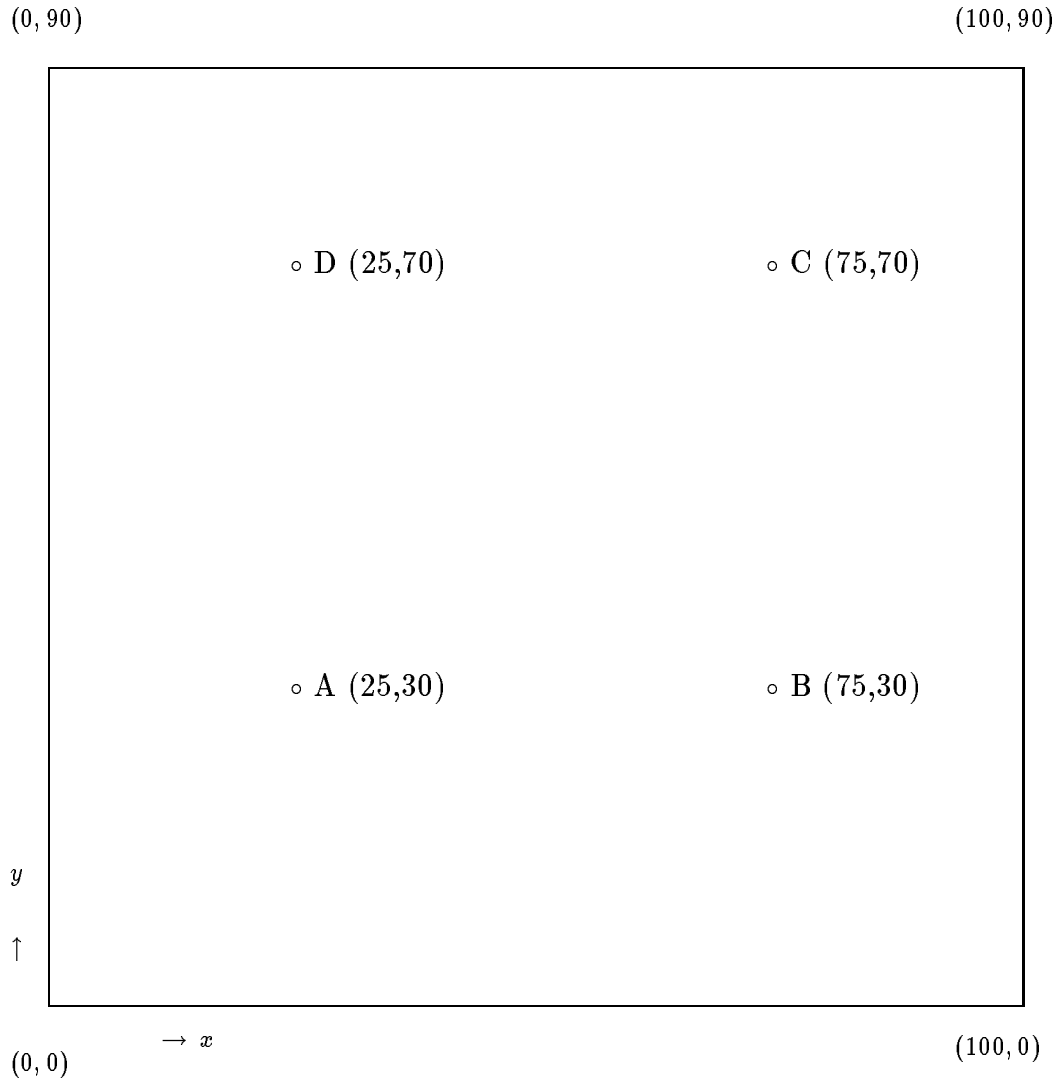


Figure 5.5 : Plan of Model Landfill for YRC Calculations.

### **5.1.5 Conclusion on YRCs.**

To precisely determine the YRCs for a real site would require as many pumping trials as there are wells, and this would be impractical on a large site having perhaps a hundred wells. The problem would be reduced if the wells were connected in clusters, in each of which the wells are always at the same extraction pressure — since each cluster may then be treated as a single well. Additionally a well/cluster will only be significantly affected by its nearest neighbours, so simultaneous pumping trials could be carried out on different regions within the site.

Of more immediate benefit is the identification and quantification of changes in YRC with respect to separation, location, permeability and well construction. Knowledge of these trends should enable landfill operators to transfer field experience gained from present sites to future ones with more accuracy.

The usefulness of YRCs is demonstrated in the next section, where they allow complex calculations on interacting networks of wells to be performed rapidly without the need to do a full underground flow analysis. Without YRCs it would be impractical to predict the gas fluxes within an extraction system.

## 5.2 Introduction to Extraction Networks.

This section demonstrates a methodology whereby the complex interactions occurring in large networks can be calculated quantitatively. This allows different schemes to be compared before installation, in addition to which the effects of changing gas production and component failures can be assessed in advance.

### 5.2.1 Strategy.

The components making up a gas extraction system can be broadly categorised as either pumps, wells or pipes depending on whether they remove gas from the system, introduce it, or convey it. Under this classification a valve is considered as a pipe with variable flow resistance, and a breach open to atmosphere acts as an infinite capacity pump working at a fixed extraction pressure.

A networked extraction system is assumed to consist of  $N_e$  extraction pumps (numbered  $1, 2, \dots, N_e$ ),  $N_w$  wells, and  $N_p$  pipes joined together at  $N_c$  junctions called connection nodes. All of the items attached to any particular connection node are assumed to be working at the same pressure.

Our strategy was to consider each of these generic components in turn and to reduce their properties to individual governing equations expressed in terms of observable pressures and gas fluxes. Having derived these separate relations they can then be linked together by looking at the connection nodes between the components, thus producing a system of equations specifying the behaviour of the network at all points within it. Some example solutions are given to demonstrate the application of the procedure.

### 5.2.2 Extraction Pumps.

The principle characteristic of an extraction pump is that it removes gas by maintaining the node to which it is connected at a lower pressure than adjacent sections of the network. For an extraction pump working at a constant speed, the deficit pressure it produces will depend on the amount of gas flowing through it.

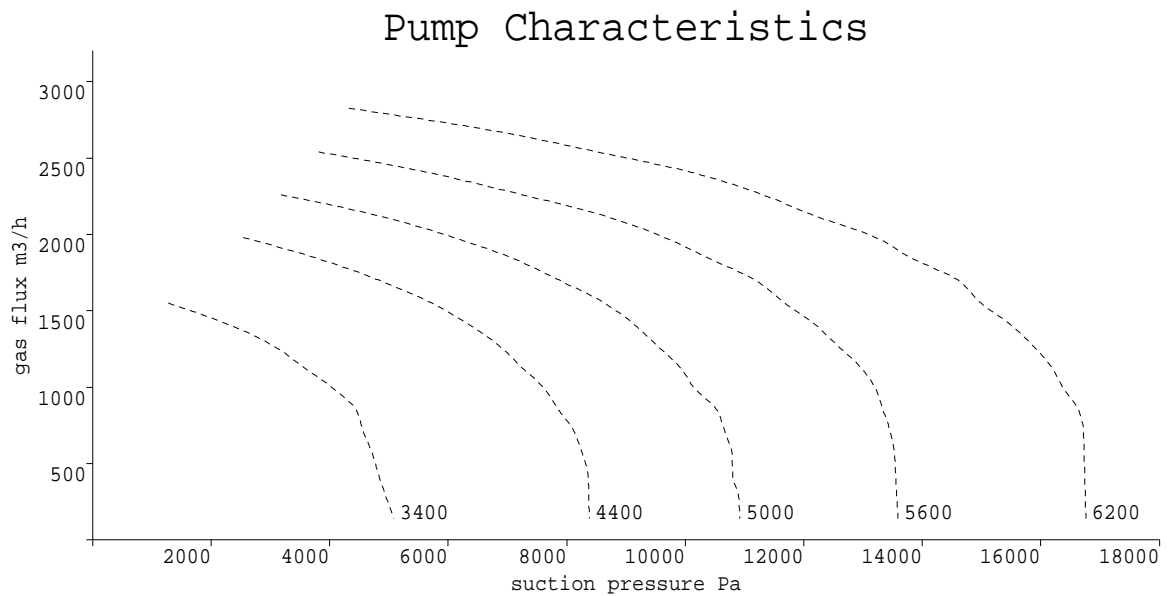


**Figure 5.6 :** Extraction capacity of pumps against applied suction.

Figure 5.6 illustrates pressure/flux curves for a typical extractor fan working at several different speeds (which are given in terms of motor r.p.m. beside each line). The curves demonstrate the existence of a relation

$$F_i^e = \Psi_i(P_k), \quad i = 1, \dots, N_e, \quad (4)$$

where  $F_i^e$  is the flux through extractor  $i$  working at pressure  $P_k$ , with  $k$  being the number of the node to which the pump is connected. The functions  $\Psi_i$  can be obtained from calibration experiments or manufacturer's data.

### 5.2.3 Wells.

The salient feature of a well is that it introduces gas into the network from the surrounding landfill. Describing the behaviour of a set of wells is more complex than for pumps due to their mutual interaction within the interior of the landfill. For instance, increasing the suction pressure at any particular well will result in a decrease in the amount of gas extracted by its neighbours even if the pressures at the latter are held constant. Hence the flux  $F_i^w$  from a well depends on the pressures at all of the  $N_w$  wells in the site.

We have previously shown that under the conditions of Darcy flow, each flux relation may be approximated as a linear function of the well pressures thus

$$F_i^w = C_i + D_i \left( P_j - \sum_{k \neq j} \mu_{jk} P_k \right), \quad i = 1, \dots, N_w, \quad (5)$$

where well  $i$  is connected to node  $j$ , with  $C_i$ ,  $D_i$ , and  $\mu_{jk}$  being dependent only on the sub-surface site characteristics.

Note that once the locations of the wells have been specified, this formulation eliminates the need to continually recalculate the subterranean pressure field whenever the surface parameters are changed. Since the final equations can only be solved via iterative numerical methods this drastically reduces the computer power required — especially when several alternative networks are being compared.

### 5.2.4 Pipes.

Within a pipe the gas flux is determined by the geometry of the pipe and the pressure difference between its ends. Each pipe will have some associated function  $\Phi_i$  describing this relationship so that

$$F_i^p = \Phi_i (P_{kA} - P_{kB}), \quad i = 1, \dots, N_p, \quad (6)$$

where  $F_i^p$  is the flux along pipe  $i$  in the  $A \rightarrow B$  direction, and  $P_{kA}$ ,  $P_{kB}$  are the pressures at the nodes connected to ends  $A$  and  $B$  respectively (which are labelled arbitrarily). Note that  $P_{kA} > P_{kB}$  implies that gas is flowing towards end  $B$ . Figure 5.7 illustrates the gas flux induced in smooth HDPE\* pipes of different diameters (ranging from 125 mm to 500 mm) by applying a pressure gradient across their ends.

---

\* High density polyethylene is a common material for landfill pipes.

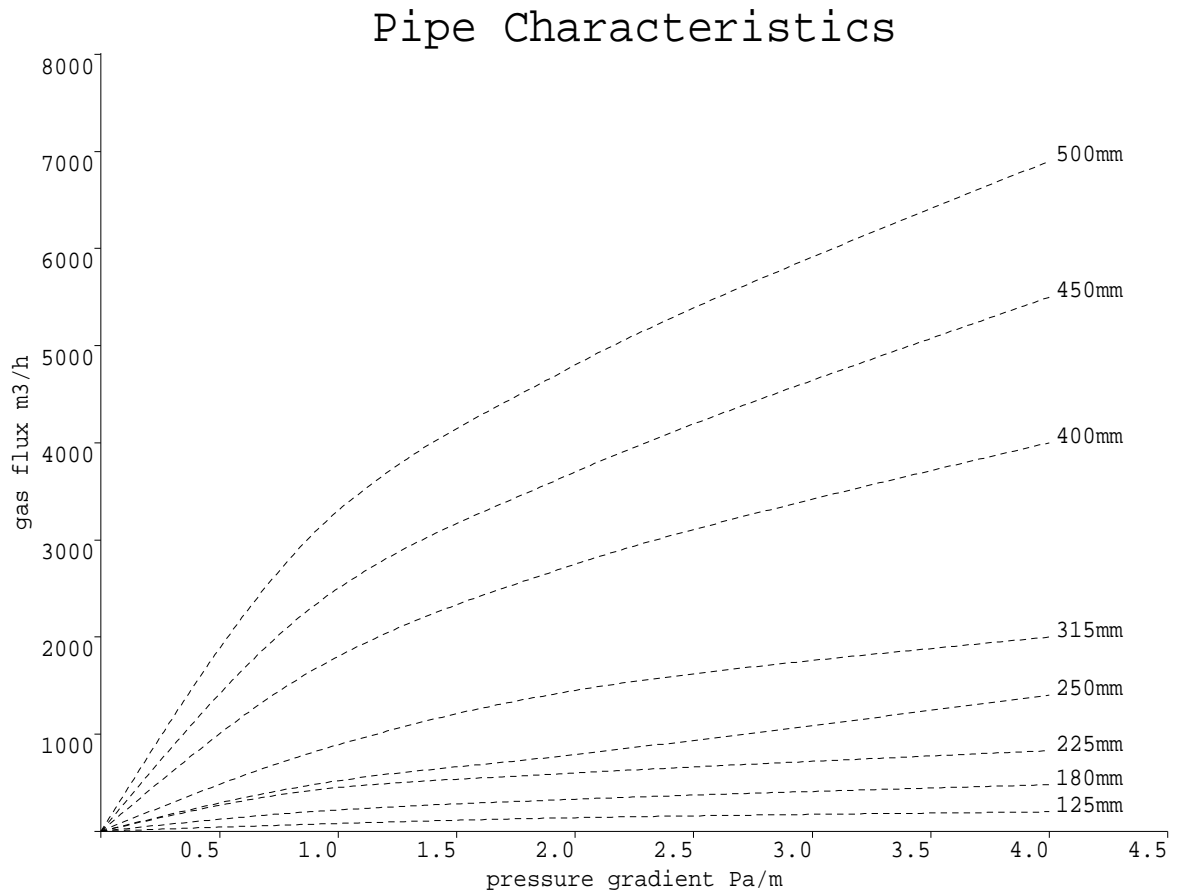


**Figure 5.7 :** Flux through HDPE pipes as a function of applied pressure gradient.

Mechanisms such as valves and flame traps can be characterised in the same way as pipes, since their only influence on gas flow is to retard its velocity. Complications such as entrained water flow within a pipe can be incorporated into the functions  $\Phi_i$ , and cause no extra difficulty provided that it remains monotonic (ie. applying a greater pressure gradient always results in higher flux).

### 5.2.5 Connection Nodes.

All the components attached to the same connection node must be at the same pressure, but this condition has already been implicitly imposed by the use of the nodal pressures in equations (13—15). The other property of a node is that the gas flux into it must be equal to the gas flow out, and this gives the required  $N_c$  additional equations thus

$$\sum_{k \in E_i} F_k^e + \sum_{k \in A_i} F_k^p = \sum_{k \in W_i} F_k^w + \sum_{k \in B_i} F_k^p, \quad i = 1, \dots, N_c, \quad (7)$$

where  $E_i$  is the set of pumps connected directly to the  $i$ th node,  $W_i$  is the set of wells connected,  $A_i$  is the set of pipes having end  $A$  connected, and  $B_i$  is the set of pipes having end  $B$  connected to node  $i$ .

### 5.2.6 Solution.

We now have a set of  $N_e + N_w + N_p + N_c$  equations which completely describes the flow within an extraction network. The well coefficients  $C_i$ ,  $D_i$  and  $\mu_{ij}$  can be either determined from field trials, or else estimated using a three-dimensional underground gas flow model. The pump parameters  $\Phi_i$  may be obtained from manufacturers specifications, as can the  $\Psi_i$  functions describing the pipes (with appropriate modification to allow for any water entrapment).

The resulting equations form a large non-linear set, necessitating an iterative numerical solution. The Newton-Raphson method was selected for this, and is described in Appendix 5A.

### 5.2.7 Examples.

To illustrate the use of this method we will perform a failure analysis on a hypothetical landfill, examining how the gas-flow pattern will change when some of the connecting pipes are damaged.

Consider a square site of length 400 m and depth 25 m, producing 8000 m<sup>3</sup> of gas per hour, and suppose that the main consideration at this landfill is to prevent off-site gas migration. A typical configuration for this purpose would be to dig a series of extraction wells around its border at 50 m intervals, connecting them via short spurs to a ring-main pipe — as illustrated in Figure 5.8. For additional safety (as will be shown below) a relief pipe could be used to link opposite sides of the site.



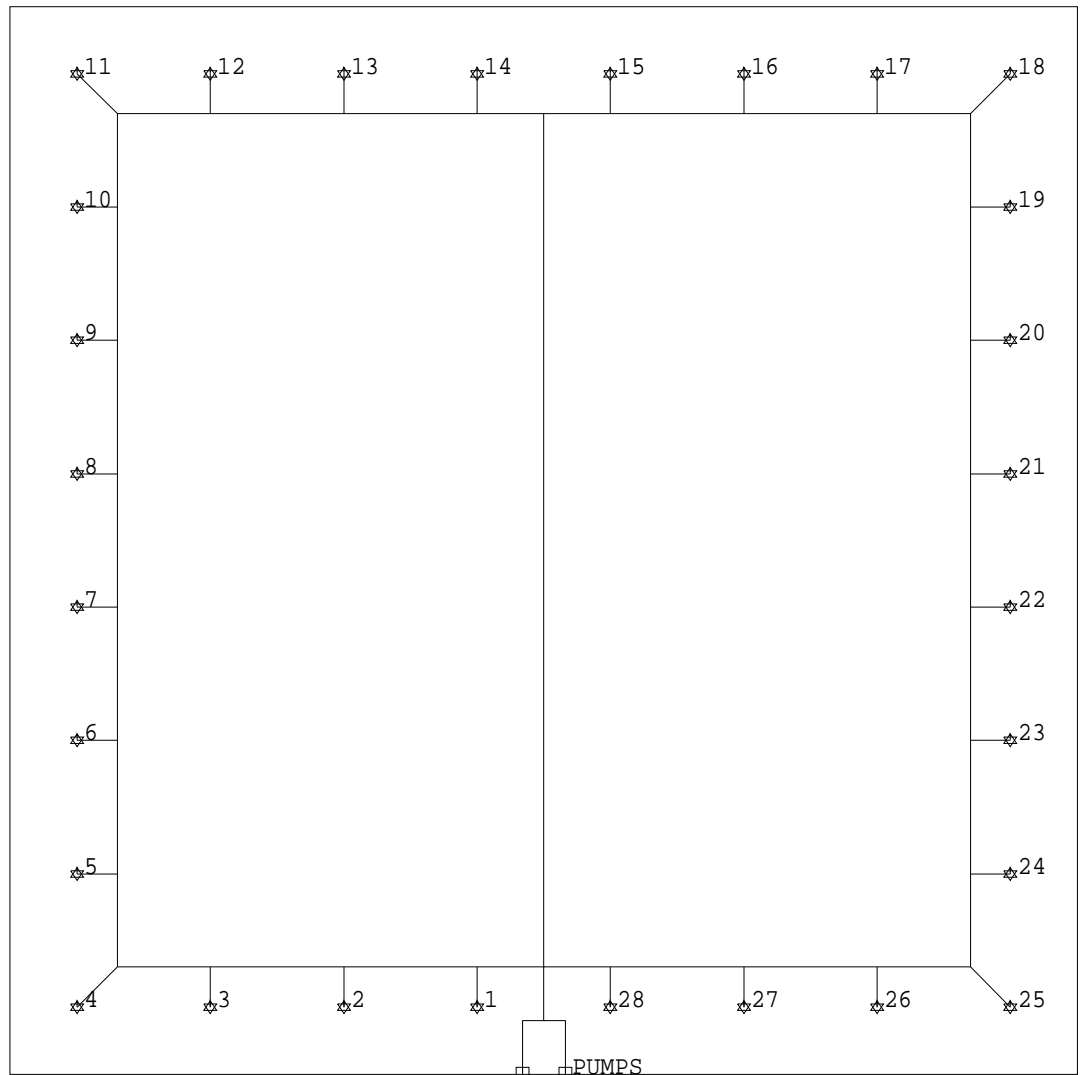


**Figure 5.8 :** Site configuration for extraction calculations.

For reasons of safety and convenience, several pumps are usually located at a single place rather than distributed across the site. The example shows two pumps connected to the ring-main, operating according to the suction-flux relation shown in Figure 5.6 for 5600rpm. Typical HDPE pipe diameters used in such sites are 315 mm for the links connecting the pumps and the central relief pipe to the ring-main, 180 mm for the ring-main itself, and 125 mm for the individual spurs collecting gas from the 28 wells.

The site and installation are designed be fairly typical of medium-sized layouts currently being emplaced in the U.K. To simplify the comparison we assume that the site is fairly homogenous, and that the the horizontal and vertical permeabilities are  $3 \times 10^{-7}$  and  $10^{-6} \text{ m}^2 \text{ Pa}^{-1} \text{ s}^{-1}$  respectively. Then for wells of diameter 30 cm, with perforated sections extending from 15 m to 20 m depth, the well-flux coefficients in Equation (2) are  $\alpha = 2.6 \times 10^1 \text{ m}^3 \text{ hr}^{-1}$  and  $\beta = 2.8 \times 10^{-2} \text{ m}^3 \text{ hr}^{-1} \text{ Pa}^{-1}$ . The YRCs between adjacent wells are calculated to be approximately 0.05, with the YRCs between more distant wells negligible.

The extraction pressures and gas fluxes at each of the wells in the site are given as histograms in Figure 5.9. Note that the flux from each of the wells is similar since the pipe network is able to spread the suction fairly evenly.

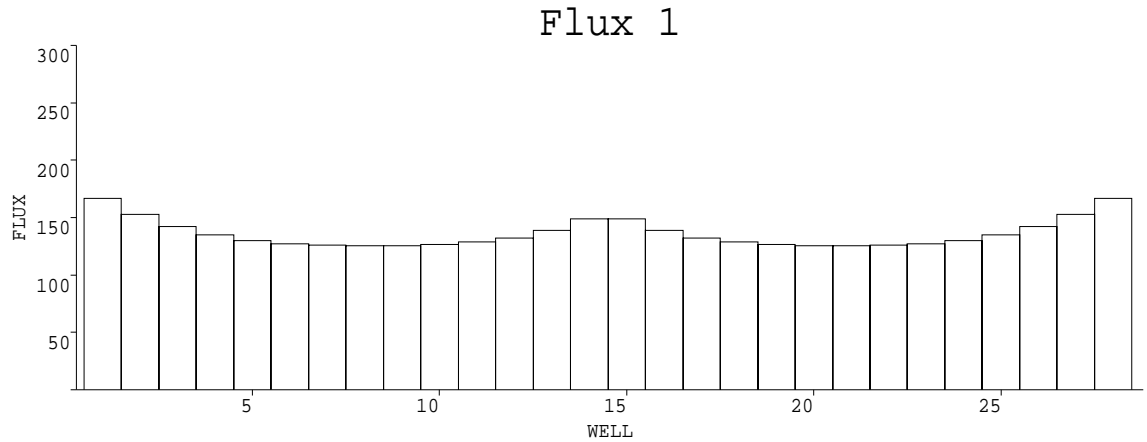


**Figure 5.9** : Full site.

If the central relief pipe had been omitted, then the pressure distribution across the site would be less even, as shown in Figure 5.10. To cope with this, valves would have to be adjusted on the well spurs and the pumps turned up to compensate for the extra drag caused by this.

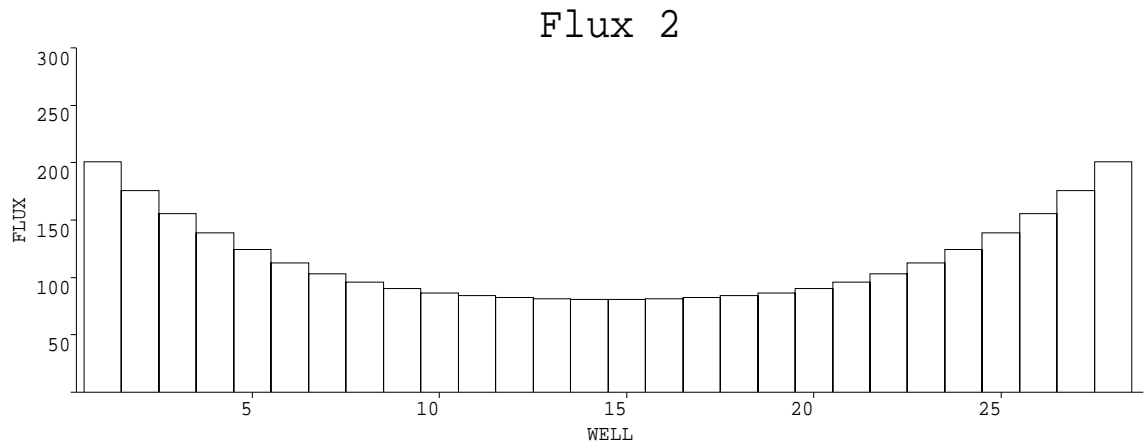


**Figure 5.10** : Full site without relief pipe.

The effect of a failure on the section of the ring-main between wells 13 and 14 is shown in Figure 5.11, and the corresponding fluxes in the absence of the relief pipe are illustrated in Figure 5.12. In this case, the relief pipe prevents any loss of suction in wells 14–28, so that the integrity of the safety system is compromised over a much small region than is the case in its absence.

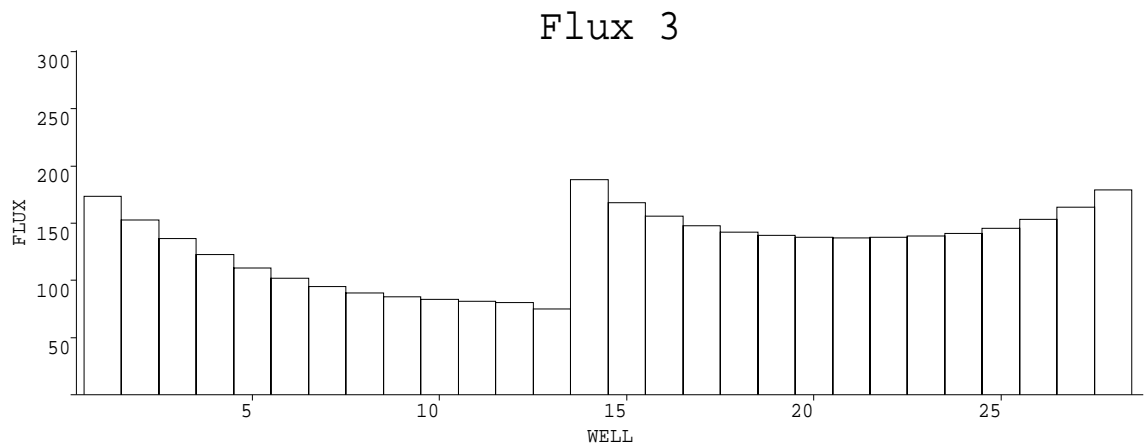


**Figure 5.11** : Failure between wells 13 and 14.

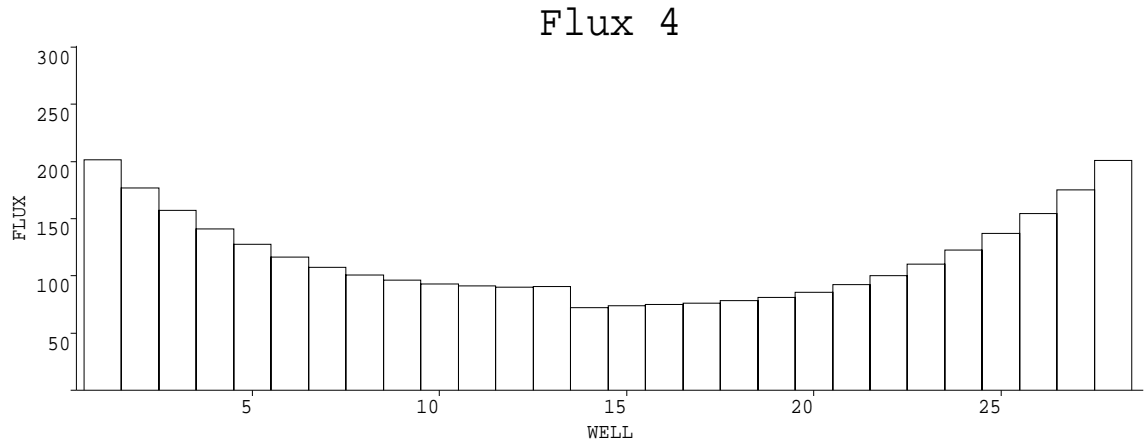


**Figure 5.12 :** Failure between wells 13 and 14, without relief pipe.

The worst case for a single pipe failure occurs when the blockage is near to the point at which the extractors are connected to the ring main. Figure 5.13 shows the effect of a blockage in the pipe between wells 1 and 2, with Figure 5.14 showing the corresponding fluxes in the absence of the relief pipe. Note that the flux from well 2 is substantially less than that from well 3 — this is because the former is much nearer to well 1 which now has a very strong suction applied and is thus able to ‘steal’ a lot of gas from well 2.

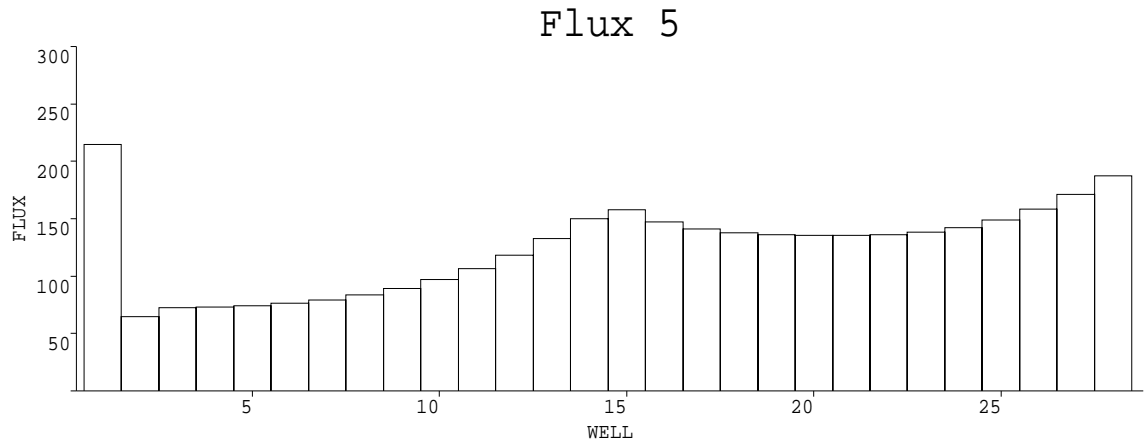


**Figure 5.13 :** Failure between wells 1 and 2.

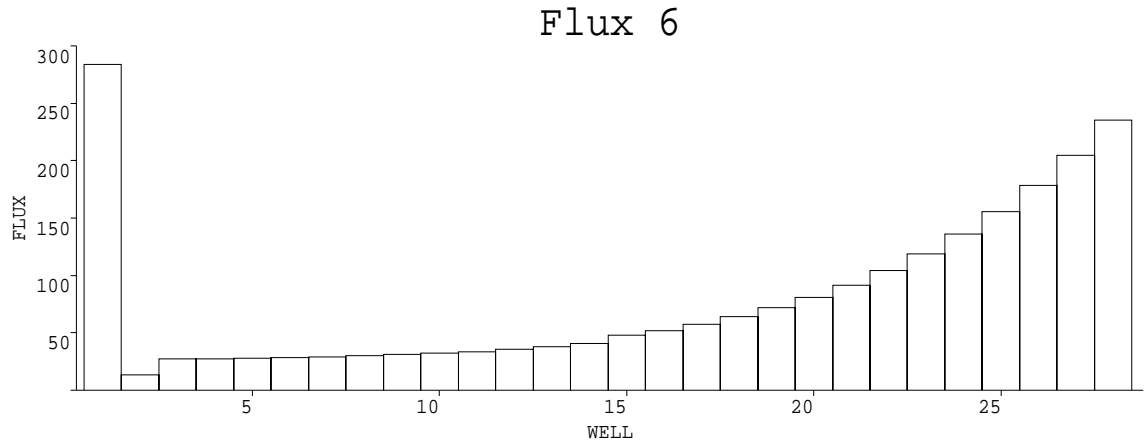


**Figure 5.14** : Failure between wells 1 and 2, without relief pipe.

### 5.2.8 Suggested Further Developments.

The examples illustrated show only a basic scheme, and there are a number of additional engineering components which may be incorporated into a site.

Booster pumps may be used to aid gas flow through very long routes, and in this case the function  $\Phi$  will relate the flux through the pump to the difference in the pressures at the two nodes to which it is connected. This type of pump has the same mathematical formulation as a pipe.

Generators exert a back-pressure on the incoming gas and a fraction of the pumps suction must be expended to overcome this. Such a situation can be treated by modelling the extraction pump as a booster pump which forces gas into a pipe (having the drag-inducing properties of the generator) which then vents to atmosphere.

Condensation ‘knock-out’ pots are used to remove moisture from wet gas, and may be treated as pipes if the incoming gas is not too moist. However, in the case of very wet gas they must be treated as a new category — since they both impede gas flow and alter the total amount of gas in the system. In long pipes some condensation may take place in cold weather, so it may be more appropriate to treat such a pipe as an extended knock-out pot. Since the gas velocity is known at all points it would be possible to calculate changes in its temperature as it moves from wells to pumps, and hence to determine the amount of condensation likely to take place at any location.

### **5.3 Conclusion on Extraction Networks.**

There is no theoretical limit to the complexity of a site which can be modelled by a computer program based on this method. Without modification the procedure can cope with multiple networks being installed on the same site — for instance a utilisation scheme surrounded by a second unconnected network which over-sucks to prevent gas excursion.

To fully exploit the power of the model requires more detailed attention to monitoring individual extraction wells that is common practice. However, if the user can estimate the well yield parameters roughly (either from measurements or previous experience) then the program will be able to produce valuable information about the comparative effectiveness of various installations.

The example simulation given above consisted of a total of 153 simultaneous equations (28 wells, 61 nodes, 2 pumps and 62 pipes), and the algorithm required under 1.2 seconds to parse and solve them on a Vax6000. This makes the program fast enough to be used by engineers on an interactive basis.

With additional development work and the creation of a larger database describing landfill components this system could be an invaluable tool for site planners and operators.

## **Chapter 6 : The Methanogenic Ecosystem.**

### **6.1 Introduction.**

Immediately following its deposition within a landfill most of the organic fraction of solid waste will begin to undergo degradation through chemical and bacterial action. In the earliest phase this takes place via aerobic metabolic pathways (i.e. reactions which consume oxygen), but as more material is added and overlying strata begin to significantly impede the flow of oxygen into the landfill then the dominant reactions within the interior will become anaerobic. After the first year or so of decomposition the major gaseous products are normally carbon dioxide and methane, and the reactions producing them will continue at a gradually decreasing rate for at least fifteen, and often upwards of fifty, years. It is generally accepted that the majority of the degradable waste will decompose during this latter phase.

The onset of large-scale methane production is of great importance when managing a site, both in terms of its environmental impact and the commercial opportunities for its exploitation. Before this occurs the gas vented is largely carbon dioxide with an admixture of hydrogen, and the leachate (the liquid formed within the site during degradation) is highly acidic. When the methane producing phase is entered, hydrogen ceases to be found in the gas, and the leachate becomes much less acidic (and consequently less harmful in the event it escapes). The methanogenic bacteria responsible for this are regarded as being amongst the least-robust species found within a domestic landfill, and sometimes fail entirely to develop.

Hence the primary aim of this section of the model is to predict the conditions under which methanogenesis is able to become established, to estimate the time required for this to happen, and to investigate methods of influencing this period.

The difficulties in gathering detailed information on the composition of wastes deposited at a particular site make it impossible to produce specific predictions of the site's future behaviour — in addition to which the computer time required would be prohibitive. Instead effort was concentrated on producing a generic model to identify the primary in-situ interactions and any feasible methods of controlling them. The advantage of modelling over experimentation for these purposes is that there are no uncontrollable factors and full information is available when trying to understand simulation results.

The changing composition of municipal wastes and the trends toward greater materials recycling and sorting (in accordance with current UK and EC waste management policies) are likely to have a major influence on the nature of the residues being landfilled. The

model allows the consequences of changes in waste input and management to be explored before such sites are constructed.

## 6.2 Methodology.

The actual reactions occurring within a landfill are too numerous and complex to model precisely. To make the problem manageable, the substances involved must be grouped into a number of generic categories and the system phrased in terms of these. It is thought that the most important metabolic pathway in municipal waste decomposition is fermentation of the primary substrates (mainly paper and vegetative matter) to sugars and alcohols followed by their conversion to carboxylic acids, which may then break down to produce methane. Figure 6.1 illustrates the divisions that were chosen as being the best simple representation of this system, with the arrows indicating the overall direction of mass conversion. Data derived from samples of landfill waste and leachate was used to estimate an empirical formula for each of the composite substances, and the proportions in which they transformed to one another were based on simple chemical relations (see below).

The multiphase nature of the landfill environment and the influence of biological factors upon degradation introduce significant complications. The former introduces spatial variability into the problem and the latter makes application of standard chemical kinetic theory highly unreliable. The action of the bacteria within a site is a primary mechanism regulating its temperature, chemical composition and physical structure (ie. the saturation, permeability and density) and these factors in turn determine the viability of the many microbial species present.





**Figure 6.1** : Modelled biochemical processes.

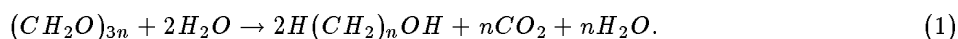
The initial phases of decomposition and acidogenesis are carried out by a large, ill-defined group of species, whose diversity makes the processes fairly robust so that they are probably found in all sites. By contrast, Archer & Fielding (1986) claim there are only a handful of common methanogenic varieties (the archaeobacteria), and that these are more sensitive to adverse conditions, being significantly slower growing than most of the other types and sometimes failing entirely to survive. Considering their different behaviours, and that the level of organics potentially able to escape from a site is crucially

dependent on the amount of acids consumed by methane production, it was decided to model the populations of methanogenic bacteria explicitly and treat the earlier processes as being dependent purely on the instantaneous state of substrate/nutrient availability (thus assuming that the size of their populations will adapt very rapidly to the local steady-state level).

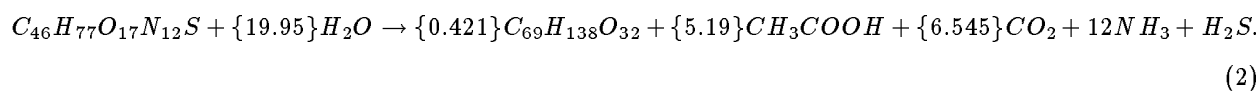
### 6.3 Idealised Reactions.

The reactions relating the transformation of mass between the substances were taken to be as below. We are not asserting that these are the precise reactions occurring, only that they provide a plausible way to relate the mass transference between compounds (see Appendix 6A for further justification).

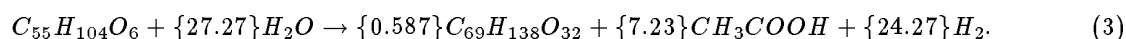
Hydrolysis and fermentation of carbohydrate,  $n = 1, \dots$



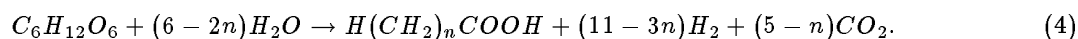
Degradation\* of proteins, the intermediate stage of deamination being ignored



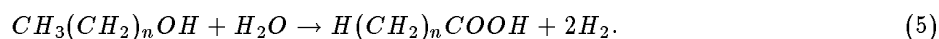
Degradation of fats, the intermediate stage of hydrolysis being ignored



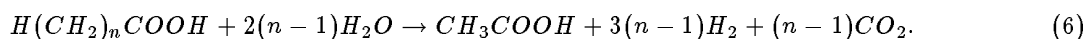
Acidogenesis from glucose



Acidogenesis from the alcohols



Breakdown of carboxylic acids,  $n = 2, 3, 4, 5$



Breakdown of acetic acid



Consumption of hydrogen




---

\* The brackets  $\{ \}$  indicate approximate values. Since the reactions are not precise they would require large coefficients to balance them exactly.

## 6.4 Transport Equations.

Several of the major reactive components within a landfill can exist in both gaseous and dissolved states. To allow for these transferences the interior was assumed to be divided into three overlapping zones; water, gas and solid waste — occupying volume fractions  $\theta$ ,  $\varphi$ , and  $1 - (\theta + \varphi)$  respectively.

Our combined set of transport equations for a single chemical species are thus

$$\frac{\partial}{\partial t}(M_\theta) + \underline{v} \cdot \nabla (M_\theta/\theta) = \text{div}(\underline{E} \nabla M_\theta) + q - Q, \quad (9)$$

$$\varphi \frac{\partial}{\partial t}(M_\varphi) = \text{div}(M_\varphi \underline{K} \cdot \nabla P) + \varphi Q, \quad (10)$$

where  $M_\varphi$ ,  $M_\theta$  are the masses of compound present in each state per unit volume of the landfill,  $\underline{v}$  is the imposed Darcy water velocity,  $\underline{E}$  the combined diffusion and dispersion tensor,  $\underline{K}$  the gas permeability tensor and  $P$  the gas pressure within the voids.  $q$  represents the net rate of formation of the compound within the liquid media, and  $Q$  represents the evolution of dissolved gases from the leachate. For a solute such as acetic acid, with no gaseous form, the  $Q$  term vanishes and equation (10) is irrelevant.

Even if  $q$  and  $Q$  were known precisely, the pair (9,10) is difficult to solve for a single solute, and since several interacting compounds are present the extended set of equations is insoluble by current analytical methods. In view of this complexity and the difficulty of interpreting the results of a full numerical solution it is necessary to verify the biochemical relations before introducing spatial variability.\* To do this the landfill is assumed to be a ‘well mixed’ reactor, so that our equations reduce to

$$\frac{d}{dt}(M) = q - Q + \Omega, \quad (11)$$

$$\frac{d}{dt}(\theta\rho) = Q - V, \quad (12)$$

where  $M$  is the total dissolved mass,  $\rho$  the density of the gas phase,  $V$  represents the rate of gas venting when the system exceeds atmospheric pressure, and  $\Omega$  is the flux of solute in and out of the landfill due to a prescribed water flow ( $V$  and  $\Omega$  thus compensate for the boundary conditions lost during the simplification).

The dissolved and gaseous components of a solute are, provided it does not react chemically with water, related by Henry’s law (see Chapter 3). No suitable data was available with which to predict the rate of gas evolution/solution when the system is not in equilibrium, and this process is also likely to be greatly influenced by local factors such

---

\* The project had not proceeded to this latter stage by its termination date.

as the area of the liquid-gas interface — so a sensitivity analysis of the effect of different forms for  $Q$  was carried out by performing a series of numerical simulations in which the liquid and gas phases were allowed to proceed almost independently, being brought into exact equilibrium once every  $\tau$  hours — where  $\tau$  is the period in which half the excess gas would be vented in the absence of further production.

## 6.5 Rate Controlling Factors.

In order to model the biochemical degradation it is necessary to derive expressions for the rates at which each of the major individual processes are taking place. Most of the important reactions are performed by bacteria within the site and this prevents standard chemical results being applied — for instance, above 60 °C the mesophilic methanogens seem to become extinct (or are rendered inactive) and the cleavage of acetate via reaction (7) usually ceases. A survey of the literature indicated that the primary influences on anaerobic bacterial activity are temperature, pH, Eh, substrate availability, moisture level, oxygen content, trace nutrients and the presence of toxins.

The possible presence of energetically-advantaged sulphate-reducing bacteria (which may out-compete the methanogens for hydrogen) was allowed for by assuming that any sulphate produced was immediately metabolized to sulphide. Aerobic methane-consuming species were neglected (since they require oxygen and are thus normally found only in a shallow surface zone) since although they may alter the apparent temperature and rate/concentration of gas production as measured at the surface, it is assumed that they do not appreciably influence the real internal generation rate (with which this part of the model is concerned).

As degradation proceeds the solid primary substrates will be broken down and their volume and strength decreases. Some settlement will occur, but at a lesser rate than the waste decomposition suggests, and to simplify the model it was assumed that this settlement can be ignored during the first year. The solid volume occupied was thus taken to be proportional to the mass remaining as a fraction of that originally present. As new void space is created the evolved gas is easily able to fill it, so that no allowance is necessary for air being drawn in.

### 6.5.1 Primary Decomposition.

The initial degradation by fermentation, hydrolysis and glycolysis can take place via a large number of metabolic pathways depending on the exact chemical composition of the substrate, and little is known of them individually. Instead of laboratory data it is necessary to rely on more empirical information from sewage digester and landfill measurements, and it was decided to extend the approach of Hoeks (1983) as the best way to make use of this. The waste is categorised as a mixture of four principal components: carbohydrates, proteins, fats and biologically inert materials (masses  $G_1, \dots, G_4$  say), and the first three of these are further divided into slow, medium and readily degradable groups. This division of waste into ten groups allows considerable flexibility when specifying the initial composition of the simulated landfill.

To introduce feedback into the model the decomposition rates of each sub-category were taken to be functions of temperature, pH and the local water saturation level (though no allowance could be made for the increased mobility of nutrients in wetter regions).

Using mainly digester data from Coleman et al. (1985) and Huang et al. (1985), together with general microbiological principles (for the behaviour above  $55^\circ\text{C}$ ), the normalised rate of reaction with temperature was assumed to be as in Figure 6.2.

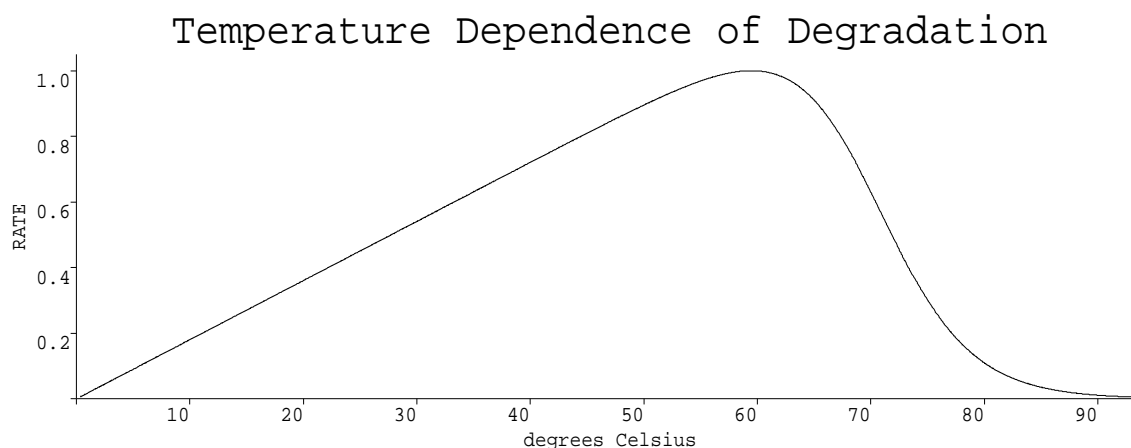


**Figure 6.2** : Normalised modelled rate of degradation vs. temperature.

Quantitative information on the pH behaviour of the main landfill bacteria under field conditions is sparse outside of the range  $5.5 < \text{pH} < 7.5$ . The ‘bell-shaped’ plot of figure 6.3 represents an empirical estimate of this dependency.

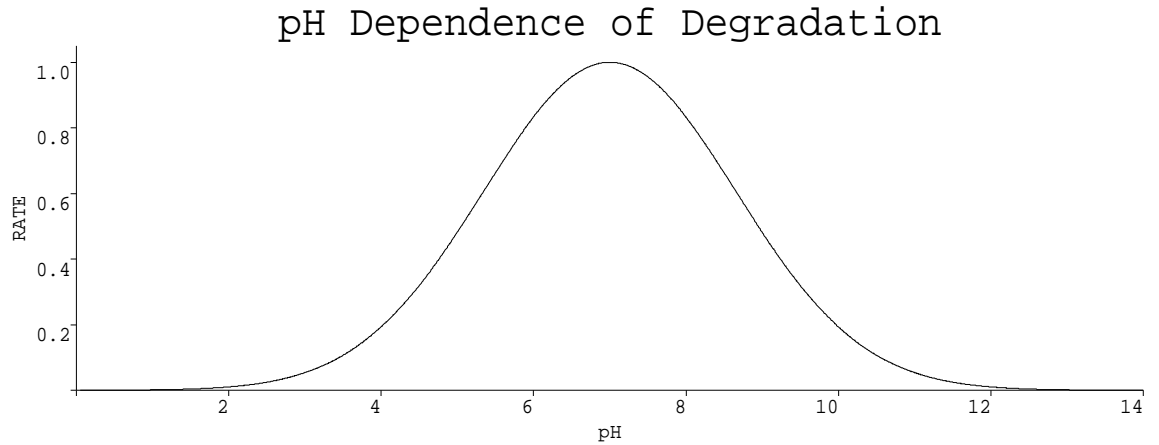


**Figure 6.3** : Normalised modelled rate of degradation vs. pH.

Most of the degradative bacteria require an aqueous environment, and it seems reasonable that the area of waste open to decomposition is related to the degree of saturation. In the absence of quantitative information this dependency was chosen to be directly proportional to the fraction of water present compared to its maximum saturated value. Particle size is also important, but this is not quantified for unprocessed waste, and we do not include it as a separate factor.

Combining these factors, one proposes that the mass of the  $i$ th type of waste, of decay category  $j$ , obeys the first order equation

$$\frac{d}{dt}(G_{ij}) = -\nu_j \xi(T, pH, \varphi) G_{ij}, \quad (13)$$

with the  $\nu_j$  being empirical rate constants (in  $s^{-1}$ ), and

$$\xi(T, pH, \beta) = \frac{T\varphi \exp(-\{pH - 7\}^2 \ln(4/3))}{\varphi_{max} \{1 + \exp(T/4 - 18)\}}, \quad (14)$$

with  $T$  being the temperature in Celsius. Then choosing

$$\nu_1 = 6.29 \times 10^{-10}, \quad \nu_2 = 1.26 \times 10^{-10}, \quad \nu_3 = 2.10 \times 10^{-11} \text{ } ^\circ\text{C}^{-1} \text{ s}^{-1}, \quad (15, 16, 17)$$

means that under constant conditions of  $T = 35 \text{ } ^\circ\text{C}$ ,  $pH = 7$ ,  $\varphi = \varphi_{max}$  the three types of waste would have half lives of 1, 5, and 30 years respectively. Findikakis & Leckie (1979) suggest that fast, medium and slowly degradable wastes might be present in the relative proportions of 15%, 55% and 30% in fresh waste — though their definition of the categories varies between sites.

### 6.5.2 Secondary Degradation.

The carbohydrate materials are modelled as breaking down into soluble sugars and alcohols (in the ratio of 2:1 by mass) and thence to carboxylic acids, whereas this intermediate stage is neglected for the proteinaceous and fatty materials. The levels of sugars observed are small compared to the acid concentrations so that the associated bacterial populations seem to respond rapidly to changes in substrate availability. This phase of acidogenesis was treated as a simple reaction, with the rate of utilisation proportional to the combined glucose/alcohol concentration  $Z_b$  thus

$$\frac{dZ_b}{dt} = -\lambda_b Z_b, \quad (18)$$

taking  $\lambda_b = 8 \times 10^{-6} \text{ s}^{-1}$  so that in the absence of further sugar/alcohol production it has a 'half-life' of one day.

It is useful to distinguish acetic acid from the longer chain carboxylic acids (represented by a composite formula) since the latter are not observed to form a direct substrate for methanogenesis (substances such as formate have been assumed to be insignificant). The primary substrates and glucose/alcohol solutes are modelled as decomposing directly into acetic acid and the composite acid in the ratio of 1:2 by mass, and the succeeding process whereby the long chain acids break down into acetic acid is treated separately. It is thought that this latter acetogenesis is inhibited greatly by the presence of dissolved hydrogen, and that this may be the dominating factor determining its velocity. Numerical data concerning this effect is scarce, though Archer & Harris (1986) assert that a 'well established' methanogenic system usually has around  $0.2 \mu\text{g dm}^{-3}$  dissolved hydrogen, whereas the peak partial pressure observed is about 30kPa which corresponds to  $0.3 \text{mg dm}^{-3}$  at  $30^\circ\text{C}$ . This relation is especially difficult to analyse due to the formation of syntrophic flocs (social aggregations) of methanogens and acidogens, which means that the concentration levels perceived by the bacteria may be quite different from the average measured solution values.

In the absence of quantitative information, the free energy equation was used as a qualitative guideline, noting that one mole of the composite acid decomposes to produce 4.63 moles of hydrogen, and the level of carbon dioxide is relatively constant. The relation assumed was

$$\frac{dX_A}{dt} = -\lambda_A X_A \max \left\{ 0, \ln \left( \frac{Z_A}{Z_a Z_h^{4.63}} \right) \right\}, \quad (19)$$

where  $Z_h$ ,  $Z_a$  and  $Z_A$  are the dissolved concentrations of hydrogen, acetic and composite acid in  $\text{mg dm}^{-3}$ ,  $X_A$  being the dissolved mass of composite acid in  $\text{mg dm}^{-3}$  of the total landfill volume. Choosing  $\lambda_A = 2.78 \times 10^{-8} \text{ s}^{-1}$  means that when  $Z_a = Z_A$  and  $Z_h = 1.35 \times 10^{-4} \text{mg dm}^{-3}$  the composite acid will have a 'half-life' of one week in the absence of further production.

### 6.5.3 Methanogenesis.

The methanogenic bacteria were modelled as two distinct species, labelled ‘*a*’ (acetoclastic) and ‘*h*’ (hydrogen consuming) which gain their energy from reactions (7) and (8) respectively — though some species have been observed to perform both. The masses of these species are denoted by  $X_a$ , and  $X_h$   $\text{mg dm}^{-3}$ . These species are not strongly motile (some researchers suggest they are static) and may be modelled as a simple solute using equation (9), so that they obey (11) in the simplified case. Pirt (1975) asserts that their reproductive behaviour may be described by

$$\frac{dX_a}{dt} = (Y_a E_a - k_{ad}) X_a, \quad \frac{dX_h}{dt} = (Y_h E_h - k_{hd}) X_h, \quad (20, 21)$$

where  $Y$  is the growth yield coefficient (the mass of bacteria produced per mass of substrate consumed),  $E$  the rate of substrate utilisation, and  $k_d$  the endogenous death rate which allows for such factors as maintenance energy. The magnitudes of  $Y$  and  $k_d$  will vary with the environment but their form seems unknown, so they were assigned the constant values  $Y_h = 0.3$ ,  $k_{hd} = 0.022 \text{ d}^{-1} = k_{ad}$  and  $Y_a = 0.048$  using the data of Lawrence & McCarty (1969). The rate of substrate utilisation was assumed to follow Monod’s law (though Farquhar & Rovers (1973) qualify this by indicating that it may be inaccurate for acetate concentrations above  $3000 \text{ mg dm}^{-3}$ ), with the half-velocity and maximum rate governed by non-substrate factors.

Information is lacking regarding the functional form of  $E$ , but figures 6.4 and 6.5 show the observed behaviour of methane production with temperature and pH, and we assumed this followed the activity of the methanogens and fitted functions to the curves. A special study was commissioned at Strathclyde University (Watson-Craik and Goldie, 1991) to investigate the effect of pH and temperature on methanogens, and this is detailed in Appendix 6B. The temperature results echoed the general literature, while the pH experiments indicated that the bacteria are significantly more tolerant of acidic conditions than is normally assumed. The data available provide no way to differentiate between the behaviours of the various species of methanogens so the temperature and pH dependency were taken to be the same for both of the types. It was impossible to assess the relative importance of direct substrate inhibition versus indirect pH-inhibition effects in the acetoclastic reactions.



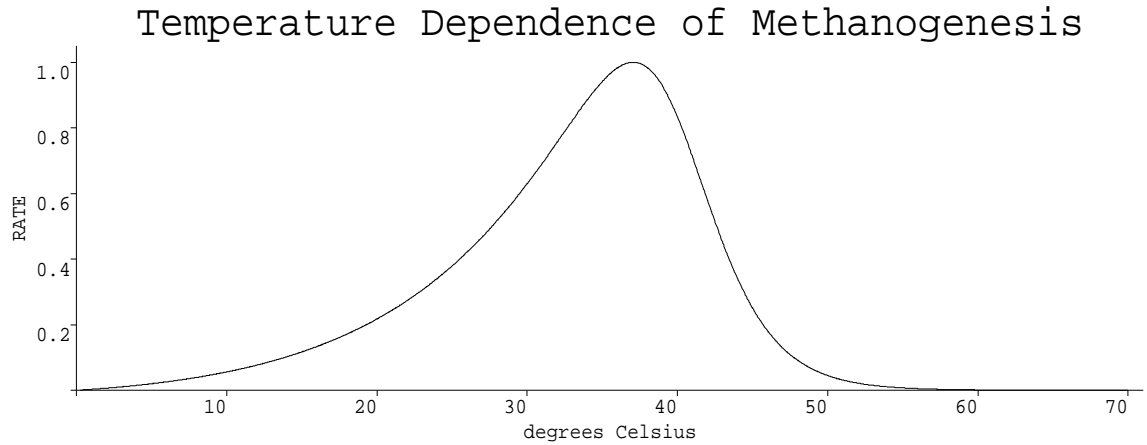


**Figure 6.4 :** Normalised modelled rate of methanogenesis vs. temperature.

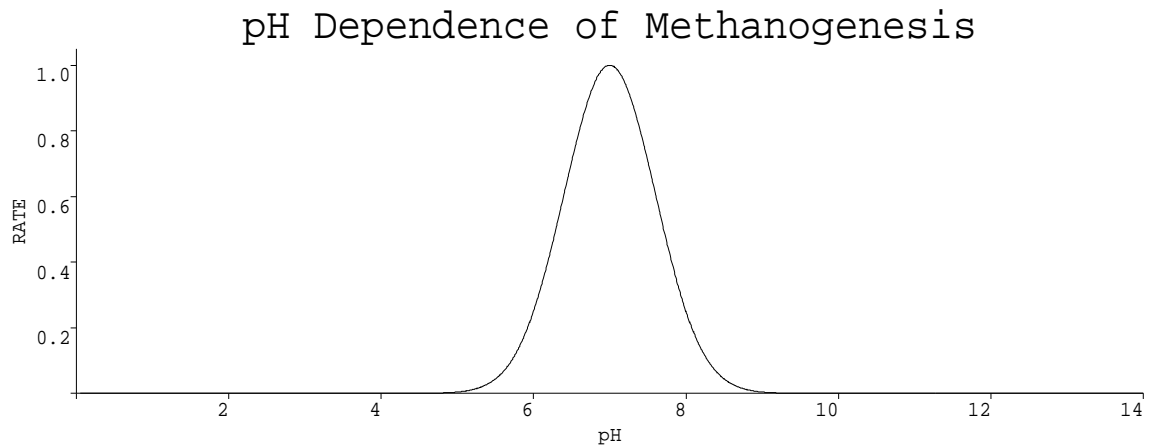


**Figure 6.5 :** Normalised modelled rate of methanogenesis vs. pH.

The half velocities  $K_i$  in Monod's law were taken from Zinder (1984) as  $K_h = 0.005 \text{ mg dm}^{-3} \text{ H}_2$  (it being observed that the modelled carbon dioxide was always present in excess), and for the acetate consumers a temperature dependency was included using data from Lawrence & McCarty (1969) to give

$$K_a = \begin{cases} 869 \text{ mg dm}^{-3}, & T \leq 25^\circ\text{C}; \\ \text{linear interpolation}, & 25 < T < 35; \\ 172 \text{ mg dm}^{-3}, & T \geq 35^\circ\text{C}, \end{cases} \quad (22)$$

where the additional value  $K_a = 333 \text{ mg dm}^{-3}$  at  $30^\circ\text{C}$  was also used for the intermediate interpolation. The overall form of  $E$  used was therefore

$$E_i = E_{max,i} \frac{Z_i \exp\left(- (pH - 7)^2 \ln(4)\right) (e^{-aT} - e^{-bT})}{(K_i + Z_i)(1 + e^{-c(T-d)})}, \quad (23)$$

where  $Z_i$  is the dissolved concentration of substrate for the  $i$  bacteria, and  $K_i$  is the Monod half-velocity. The coefficients  $a$ ,  $b$ ,  $c$  and  $d$  are used to fit the curve of figure 6.4, and have the values 0.08, 0.05, 0.45 and 40.0 respectively. The absolute maximum rates of consumption under optimum conditions were taken to be  $E_{max,m} = 1.86 \text{ d}^{-1}$  and  $E_{max,M} = 8.0 \text{ d}^{-1}$ .

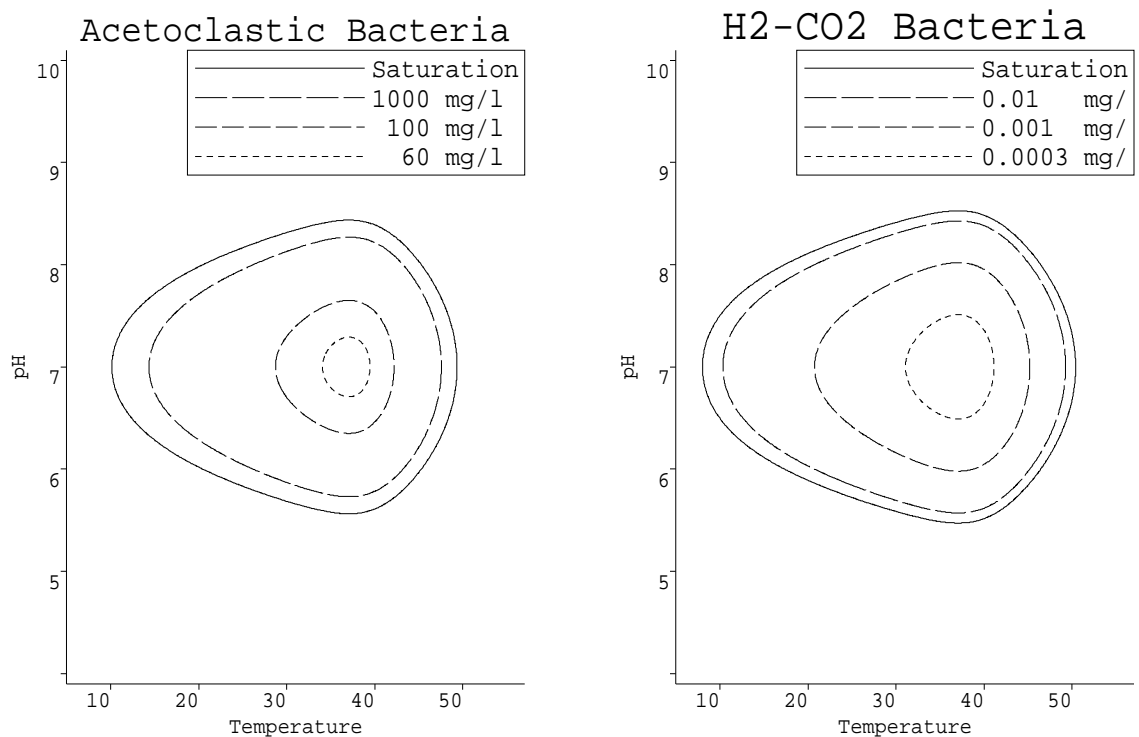


**Figure 6.6 :** Region of viability of methanogenic bacteria.

Figure 6.6 shows the regions of the pH-temperature range under which the two generic species of methanogenic bacteria are viable (ie. the term  $EY - k_d$  is positive) at different levels of substrate concentration. Although the viability contour at saturation levels is larger for the hydrogen-consuming bacteria, this does not indicate that they are more robust in general.

#### **6.5.4 Other Factors.**

The effects of oxygen and toxins were also considered, but the present model is too simple to include their effects in a consistent manner — for instance we have not modelled the facultative anaerobic bacteria which would provide a mechanism for the removal of trace oxygen. The Eh level (ie. the value of the redox-potential) is assumed to be favourable for methanogenesis, as a consequence of our statement that the facultative anaerobes have removed all the oxygen, and so Eh has not been included as a parameter. Accordingly it is assumed that no oxygen is present in the system and there are no unusual toxins other than those normally present (the effects of which are implicitly incorporated in the the growth yields and reaction rates).

## 6.6 pH Regulating Mechanisms.

The pH of the liquid within a landfill exerts a major influence on most of the processes occurring therein, though the mechanisms are often obscure and indirect. If we consider a solution containing only the organic acids shown in figure 6.1, then there is no substrate level at which the methanogens are viable — since as the acetate concentration increases, the pH decreases rendering the bacteria inactive. Ammonia is the only major alkali produced during the degradation of household waste, but it is not present in sufficient quantities to raise the pH to neutral levels.

The results of our simulations together with analyses of leachate samples indicate that the crucial stabilizing influence is the presence of alkali and alkaline metallic cations (positively charged ions within the liquid) which are generated from the biologically inert materials. During the initial anaerobic phase large amounts of organic acids within the leachate act on the metallic and mineral fractions of the waste, causing a rapid release of cations and thereby retarding the decrease of the pH. The main metallic ions found are  $\text{Na}^+$ ,  $\text{K}^+$ ,  $\text{Ca}^{2+}$  and  $\text{Fe}^{2+}$  (the latter being present only in relatively sulphur-free systems) typically in concentrations of 100 to 2000  $\text{mg dm}^{-3}$  each.

Sodium (and likewise potassium, which can be considered with it because of their similar properties) is extremely soluble, so that once their ions are formed they are unlikely to be precipitated. Sodium alone cannot be responsible for the observed buffering, since a concentration of it high enough to neutralize the peak acid levels would probably create an initial highly alkali environment — and even if this was not lethal to the bacteria, then once methanogenesis was established at a near-neutral pH, the residual acid level would be higher than normally observed.

The solubility of calcium varies drastically over the pH range 4–8 (assuming it is in equilibrium with solid calcium carbonate and gaseous carbon-dioxide at 50kPa) and increases as the pH decreases, so that large quantities can dissolve to counteract high acid concentrations. However, by itself, it is too insoluble above pH=6 to produce the final neutral leachate observed.

Accordingly the model suggests that the landfill ecosystem requires both ‘permanent’ sodium buffering (which persists at neutral pH levels) together with ‘variable’ calcium buffering (which increases enormously as the leachate becomes more acid) if the methanogens are to prosper. This pH dependent nature of the cation concentration greatly enhances the homeostatic influence of the bacteria, and allows them to maintain the leachate in a near-neutral state while still having adequately high levels of acid present to act as substrate. The model incorporates this dual buffering mechanism by assuming

that there are finite reservoirs of sodium carbonate and calcium carbonate present in the waste (possibly being supplied by building materials and soil). The sodium carbonate is assumed to dissolve at an exponentially decreasing rate, and the rate of the calcium solution/precipitation reaction is taken to be such that any imbalance decreases with a specified half-life in the absence of other chemical changes.

## 6.7 An Example Simulation.

The final set of equations was integrated numerically using a Fortran program employing backward differentiation (Gear's Method) and forward differencing.

To demonstrate the type of results obtainable using this model consider a particular case. Take a landfill composed of waste having initially  $150\text{g dm}^{-3}$  carbohydrate,  $30\text{g dm}^{-3}$  protein,  $20\text{g dm}^{-3}$  fat and  $450\text{g dm}^{-3}$  of non-degradable materials, with each of the putrescible compounds divided in the ratio 1:11:8 between the rapid, medium and slow decay rate categories. The initial dissolved and gaseous concentrations of  $\text{CH}_4$ ,  $\text{H}_2$ ,  $\text{O}_2$ ,  $\text{H}_2\text{S}$ ,  $\text{NH}_3$ , acetic acid, carboxylic acids, alcohol and glucose were taken as zero with the atmosphere 20%  $\text{CO}_2$  and 80%  $\text{N}_2$  (a reasonable starting point under the assumption that aerobic reactions had just finished depleting the oxygen). A population of  $10^{-2}\text{mg dm}^{-3}$  of each of the methanogenic species was assumed to be resident at the commencement of the anaerobic phase. The gas venting period,  $\tau$ , was set to 1 hour.

The fractional water input was taken to be  $10^{-5}\text{dm}^3\text{dm}^{-3}\text{hr}^{-1}$  of clean water, with an equal outflow of leachate. The half-life for calcium equilibration was taken as 6 hours. It was assumed that the inert waste contained  $500\text{mg dm}^{-3}$  of sodium, and that this passed into solution with a half-life of 100 hours, ultimately giving a dissolved concentration of  $1650\text{mg dm}^{-3}$  within the leachate.

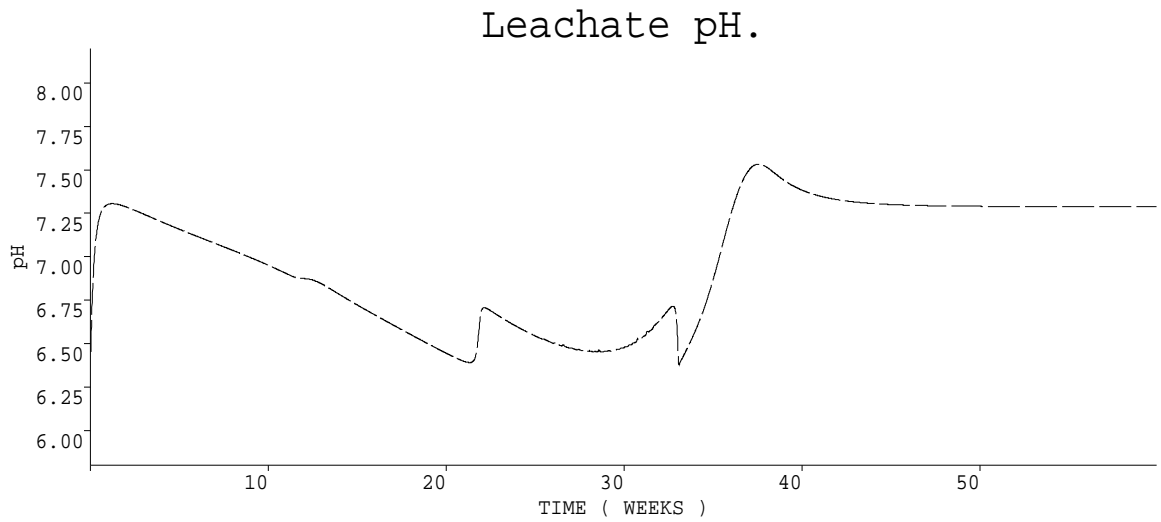


**Figure 6.7 :** Leachate pH during simulation.

The leachate's pH during the 14 month simulation is shown in Figure 6.7. Figure 6.8 records the levels of acid, acetate and alcohol/sugar in the leachate, with Figure 6.9 illustrating the corresponding methanogenic populations. Note that the void fraction occupied by water is 0.3, so that the actual leachate concentrations are 3.3 times the mass per  $\text{dm}^3$  illustrated in Figures 6.8 and 6.9.

Phase plane analysis predicts that a system consisting of only one species of bacteria with activity obeying Monod's Law, together with their substrate which is being produced at a constant rate, has a single non-zero critical point, which is a stable node. This behaviour seems to carry over to our more complex system.

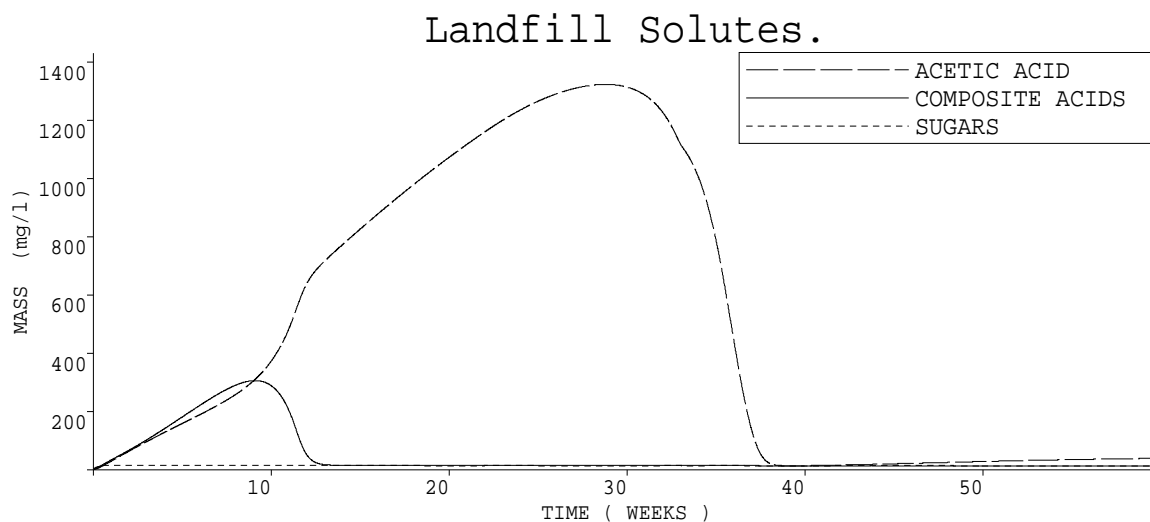


Figure 6.8 : Dissolved concentrations of sugar/alcohol, acetic acid, and carboxylic acids.

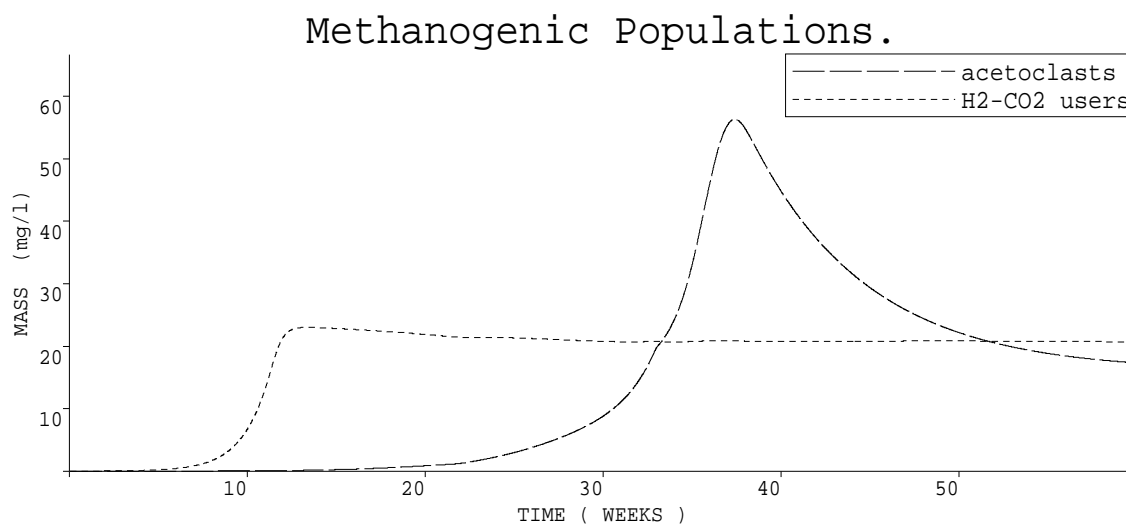
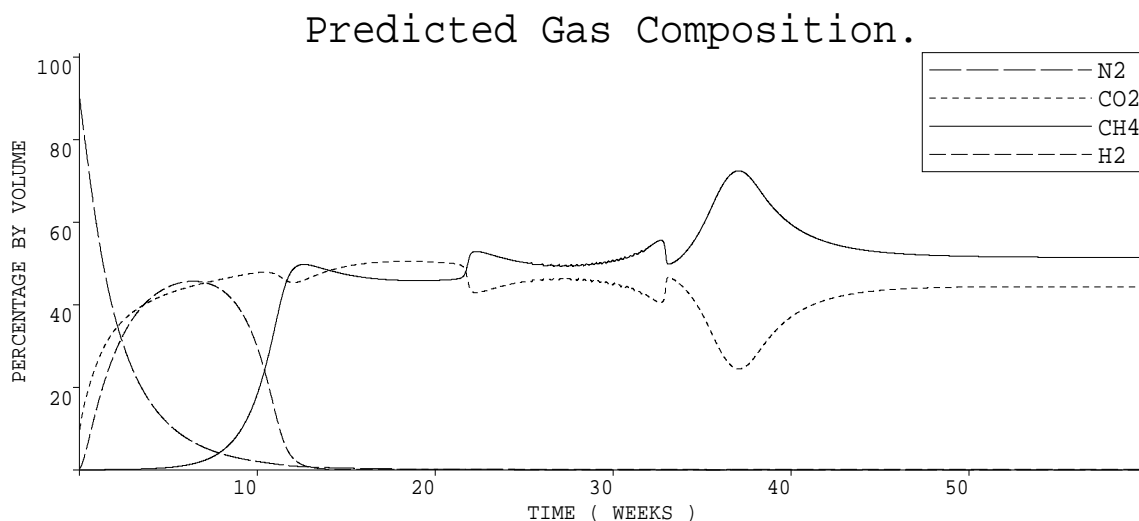


Figure 6.9 : Populations of methanogenic bacteria.

Figure 6.10 shows the daily averages of the partial pressures of the gas being vented from the model landfill.

The gases initially present inside the site are flushed out within the first 10 weeks, as can be seen from the decrease in the partial pressure of nitrogen.

At about 16 weeks the population of  $H_2/CO_2$  consuming bacteria has grown large enough to assimilate all of the hydrogen being produced, and the gas is no longer vented in significant quantities. At the same time the first methane production is observed.



**Figure 6.10 :** Partial pressures of landfill gas during simulation.

By week 30 the population of acetoclastic methanogens has increased sufficiently that it can consume all of the acetate being produced and make inroads on the amount stored in the leachate. The large ‘food reserve’ in the form of dissolved acetate causes the population to over-shoot, and a slow decline to a stable steady-state population is observed in the subsequent period.

The rapid rise in pH caused by the removal of acetic acid from solution greatly increases the solubility of carbonate, and there is a short period when the partial pressure of  $CO_2$  is reduced due to additional carbonate being retained in the liquid. Although both  $CH_4$  and  $CO_2$  production are greatly elevated during this short time, the apparent alteration in the ratio of their partial pressures is entirely due to the solubility effect and not caused by biological mechanisms.



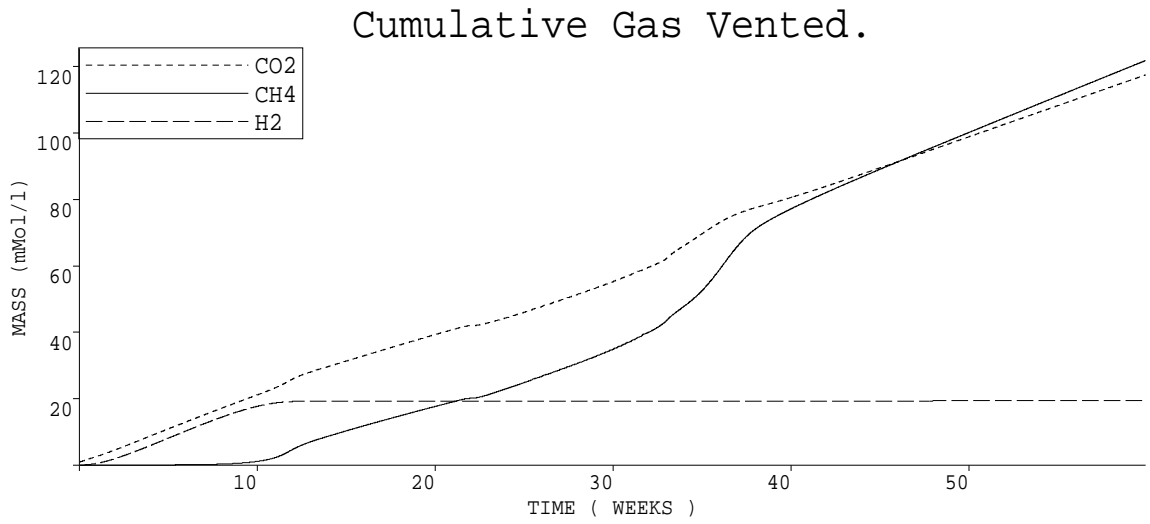


**Figure 6.11 :** Total yields of vented metabolic gases.

Figure 6.11 gives the cumulative molar masses of methane, carbon dioxide and hydrogen which have been vented during the simulation.

## 6.8 Discussion.

In all cases where both species of methanogens (ie. the acetoclasts and the hydrogen consumers) are able to survive, they eventually reach an equilibrium population where substrates are consumed as fast as they are produced, and the degrading waste is being converted to carbon dioxide and methane in a roughly 1:1 molar ratio.

In some actual mature sites a gas composition of more than 50% methane is sustained over a period of years. An overall mass balance on our equations in Appendix 6A shows that carbon dioxide is never generated in lesser quantities than methane from carbohydrates, with a small excess of methane being produced during fat degradation (provided the process goes to completion). Examination of the simulated leachate concentrations reveals that a fraction of the carbonate is being stored in the leachate to provide buffering capacity, and another portion is flushed away as water passes through the system. The relative insolubility of methane results in very little of it being involved in these physical processes, so that almost all of it is out-gassed immediately.

The model predicts a higher concentration of hydrogen during the early phase than is typically observed (the partial pressure in real sites would not normally be expected to exceed 20%) but with spatial variation this may disappear due to averaging as different sections of the site pass through the hydrogen generating phase at different times — however anecdotal evidence describes some sites as being capable of generation up to 40% hydrogen for short periods. The rate equations (13,18,19) are over simplified, and one would like to replace them by explicit bacterial (or fungal) populations when sufficient data becomes available.

Diffusion limitations within the liquid mean that the levels of dissolved gases present in the water held within the smaller waste pores (eg. soaked into paper) may be well above the equilibrium values predicted from Henry's law. This dissolved concentration is highly relevant to bacterial metabolism, but until experimental evidence is produced the magnitude of any excess cannot be estimated. The volume of water inflow/outflow prescribed in the above simulations had a negligible effect on the landfill reactions.

Increasing the amount of readily-degradable waste above that assumed in our example simulation does not speed up the establishment of methanogenesis, since the pre-methanogenic substrate levels already greatly exceed the Monod half-velocities after the first few days. Indeed if there is too much readily-degradable waste present then the initial acid production will be so high that the methanogens are killed (or rendered inactive) by low pH before the population has time to increase.

At some landfills taking pulverized waste which has gone through an initial aerobic

phase, it has been observed that methanogenesis is established faster, and it could be that the high rate of aerobic degradation (which does not yield acids) removes much of the readily-degradable substrate and prevents damagingly high initial acid concentrations in these sites. Similarly the higher initial temperature may reduce the disparity between the rates of development of the methanogens and the other degradative bacteria (see the comments below on thermal regulation).

Field observations generally do not distinguish whether methanogenesis from acetate cleavage or from carbon dioxide reduction comes first, and it is commonly supposed that both processes start at about the same time. The two modelled bacteria are partially coupled in that an increase in the consumption of one will speed up the composite acid degradation and produce more substrate for both species. An alternative explanation for the apparent simultaneity of both forms of methanogenesis lies in the ability of some species to derive energy both from acetate and hydrogen via reactions (7) and (8). Such bacteria could develop rapidly on the more favourable substrate, then when this becomes depleted there will be a large population available to consume the other substrate. Before this effect can be modelled some basic microbiological research on the switching mechanisms and critical concentrations will be necessary. Each doubling of the size of the initial seed populations (up to about  $0.1 \text{ mg dm}^{-3}$ ) results in a linear decrease in their establishment time.

Once the bacteria are firmly established, they maintained the pH at about 7.4, which is fairly typical of a site during the methanogenic stage. During simulations in which the temperature or the amount of sodium present was reduced, this final value decreased towards neutrality. Low alkali metal (ie. the elements found in groups I and II of the periodic table) concentrations are frequently associated with a failure of methanogenesis to develop, and this has been attributed to some of these metals being essential nutrients for the bacteria. However the model implies that there is another effect in that low alkali metal concentrations mean the leachate is poorly buffered against the carboxylic acids so that the pH may fall too quickly for the methanogenic population to reach a self-regulating size. These pH-raising effects of sodium, potassium and calcium may be more important than their nutritional aspects, since the levels required for adequate buffering are above those at which the bacterium's nutritional requirements are satisfied. Some experimental work is required to assess the availability of these metals within waste, and the rate at which they come into solution — which, if they are initially bound within the organic fraction of the waste, will be affected by the amount of degradation which has taken place, and perhaps also by any initial aerobic phase.

The transitions between periods of near steady-state conditions are more sudden than found in actual landfill observations, and this is probably caused by the neglect of spatial variations under the 'well mixed' approximation. In real sites the initial methanogenic populations would be distributed unevenly so that separate regions tend to pass through each growth stage at different times, with diffusion further smoothing the process. The heterogeneous nature of the landfill medium provides a large number of micro-environments, some of which will be more suitable for methanogenesis than an average well-mixed system, and this makes the reactions more robust than our model indicates.

## **6.9 Extensions to the Ecosystem Model.**

Several extensions to the main model were explored during the later stages of the project.

### **6.9.1 Thermal Regulation.**

Site temperature is known to be an important factor in the establishment of methanogenesis, and although the main model uses ambient temperature as a factor in the rate functions, it did not make provision for the effect on the site due to the heat generated by the reactions. Accordingly an extended version was created in which the thermal yields of the main reactions were used to increase site temperature, and heat loss by conduction, evaporation and convection was simulated using functions which attempted to approximate the 3-dimensional nature of a real site. The thermal yields used are given in Appendix 3A.

Unfortunately the simulations performed with this extended model never proved satisfactory, with the temperature either rising or decreasing at faster rates than seemed reasonable. This problem was thought to be caused by an inability to accurately approximate the effects of spatial variability using our thermal-loss functions, particularly as regards heat flows due to evaporation. It seems that thermal feedback effects within a landfill cannot be realistically incorporated without introducing a spatial dimension.

The results from the thermal simulations of Chapter 7 (which were initiated after the biological model) later showed that the effect of anaerobic degradation on site temperature is very small over the periods (up to a year) in which methanogenesis begins. This information give us confidence that the neglect of thermal feedback in the main biological model does not affect the results obtained using it, nor the conclusions drawn therefrom,

### **6.9.2 Mutation.**

To investigate the possibilities of a single species of methanogens being able to metabolize both acetate and hydrogen, a constant mutation rate was postulated at which the acetoclasts and hydrogen-users turned into one another. The effect of this was primarily to handicap the faster growing species, with relatively little benefit to the slower growing type (the two species alternately occupied either role according to the initial conditions). This behaviour seems detrimental to the methanogens, and our conclusion is that if the same species is able to use both substrates then its preferred metabolic pathway is dependant on the actual concentrations of substrate present.

### 6.9.3 Inclusion of Propionate and Butyrate.

An alternative biochemical scheme was explored in which the hypothetical intermediate metabolic stage of sugar/alcohol production was omitted, and the primary substrates assumed to break down into a mixture of propionate and butyrate. The effect of taking the primary carbohydrate to have the empirical formula of starch rather than glucose was also investigated. Appendix 6A gives the empirical formulae used in the alternate scheme.

It was found that the alternate model behaved qualitatively in a similar fashion to the main model, and that the important factors were again the rate of primary degradation and of methanogenesis, with the interchanges between the intermediate metabolites playing only a minor role. This may be an artifact of the modelling assumptions, but we feel it is more likely that it reflects the true state of the system.

### 6.9.4 Spatial Effects.

After investigating the programming problems involved, it was concluded that an extension of the full model to include spatial effects could be carried out most efficiently by adapting the software developed in Chapters 4 and 7 for multi-species gas flow. In addition to the programming issues, a significant increase in computer power is required to introduce dimensional effects. The main example of this Chapter required about 15 minutes CPU time on a Vax6000, so that to extend this to a 1-dimensional simulation with similar resolution to the gas composition examples of Chapter 4 (35 nodes) would require at least 10 hours. For an extension to 3-dimensions, using similar resolution to the gas enhancement model of Chapter 7 (a grid of  $20 \times 20 \times 20$  nodes) would require over 3 months for a single run of the program.

Considering this, the introduction of even 1-dimensional effects did not seem worth attempting until some of the biological and chemical problems highlighted by the model (such as the ability of single methanogens to metabolize both acetate and hydrogen, and the rate of transfer of gas molecules between phases) have been satisfactorily resolved by experimentation.

## 6.10 Conclusions.

When subjected to a variety of initial and ‘boundary’ conditions our model responded in a sensible fashion and eventually settled down to some steady state, though without methanogenesis under the harsher starting regimes — such as those with too low a temperature or insufficient alkali metal buffering. Given the amount of variance between real landfill sites, the behaviour of this model falls well within the range of observed characteristics.

The lack of data which prevents fully incorporating feedback effects into the pH and temperature means that the model has little predictive power regarding primary degradation — we make no claim to estimate the total gas production potential — however the simpler nature of methanogenesis means that useful information can be extracted about the interdependencies of the latter processes.

It would be highly beneficial to conduct further experimental research on the alkali metal leaching, temperature and gas evolution functions. It may be useful to compare sites which are rich/poor in calcium, and do/do not contain refuse which has undergone aerobic pre-composting. Additional modelling work would be valuable to explore the effects of spatial dependency on isolated subsets of the ecosystem, investigating such things as the rate at which a methanogenic region can spread to adjacent areas.

## Chapter 7 : Temperature and Moisture.

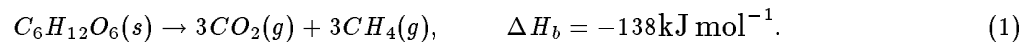
The internal temperature of landfills has long been thought to be one of the primary factors affecting their behaviour. This Chapter explores the physical processes controlling landfill temperature.

### 7.1 Natural Warming of Landfills.

The internal temperature of landfill sites increases as a result of heat released by the exothermic decomposition reactions, until an equilibrium is reached when heat production equals losses to the surroundings. In this section we consider basic models to calculate the rate of this warming (or cooling if the site has initially been heated above the equilibrium point by aerobic activity) and explain how it is affected by various factors including emplacement temperature and site geometry.

#### 7.1.1 Energy Calculations for Natural Warming

First we consider the thermodynamics of the degradation reactions whilst ignoring any spatial variability. This is the equivalent of a homogeneous, perfectly insulated cell and so gives us an estimate of the maximum possible rate of warming. Our analysis concentrates on the primary degradation pathway in landfills, ie. the anaerobic breakdown of carbohydrates to carbon dioxide and methane gases.



The value  $\Delta H_b$  is the standard enthalpy of combustion, ie. the enthalpy change per mole when the reaction is performed at 25 °C. Having determined how much energy is released by the anaerobic breakdown of glucose under 'standard' conditions, we must discover how the energy is used. The energy balance can be summarised by

$$\begin{aligned} \text{Energy released by methanogenesis} &= \text{energy used to heat waste} \\ &+ \text{energy used to evaporate water} + \text{energy lost to surroundings} \end{aligned} \quad (2)$$

As an initial estimate we shall assume that the heat lost to the surroundings is negligible in comparison with the other two terms. This will produce an upper limit on the rate of warming of a landfill.

Considering the above energy balance per mole of landfill gas (LFG) produced, equation (1) shows that six moles of an equimolar mixture of LFG are produced by per mole of glucose and so  $23\text{kJ mol}^{-1}$  of energy is released. We assume that all gas inside a landfill is saturated with water, so for each mole of LFG produced the requisite amount of water



must be evaporated to saturate it: the saturation level being highly dependent on the temperature. Let  $N(T)$  be the number of moles of water vapour needed to saturate 1 mole of LFG at temperature  $T$ , which is illustrated in Figure 7.1 below.  $N(T)$  can be calculated from the saturated vapour pressure of water, data for which is taken from the CRC Handbook, according to the formula

$$N(T) = \frac{Svp(T)}{P_A - SvP(T)}. \quad (3)$$

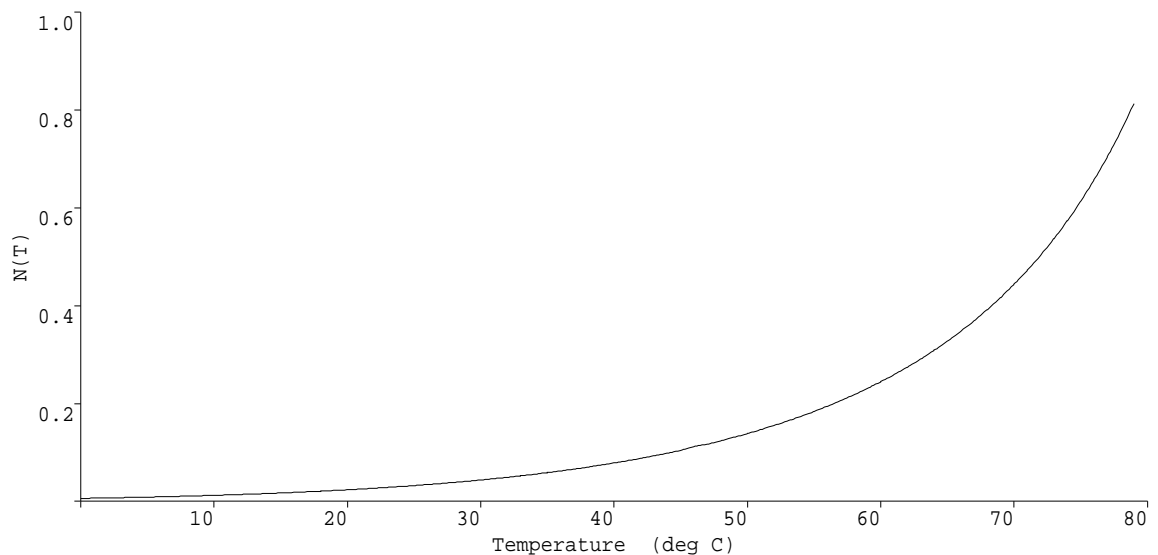


**Figure 7.1 :** Number of moles ( $N$ ) of water vapour required to saturate 1 mole of LFG

The standard enthalpy of vaporization,  $\Delta H_{vap}$ , (the enthalpy change per mole when pure water at 1 atmosphere pressure vapourises to gas at the same pressure) is also temperature dependent, but far less so, varying between  $40.66\text{kJ mol}^{-1}$  at  $100^\circ\text{C}$  and  $44.02\text{kJ mol}^{-1}$  at  $25^\circ\text{C}$  (data for  $\Delta H_{vap}(T)$  is taken from Atkins). The energy used to heat the waste can be expressed as  $c\Delta T$ , where  $c$  is the heat capacity of the waste and  $\Delta T$  is the temperature rise produced.

If we now approximate the values of the various enthalpies under the conditions prevalent in the landfill by their values under standard conditions, we obtain the equation

$$23000 = c\Delta T + N(T)\Delta H_{vap}(T). \quad (4)$$

We define  $M(T)$  as the fraction of the energy released by methanogenesis that is used to heat the landfill (shown in Figure 7.2), so that

$$M(T) = 1 - N(T)\Delta H_{vap}(T)/23000. \quad (5)$$

Using these relations, the temperature rise per mole of gas liberated per  $\text{m}^3$  is

$$\Delta T = 23000M(T)/c. \quad (6)$$

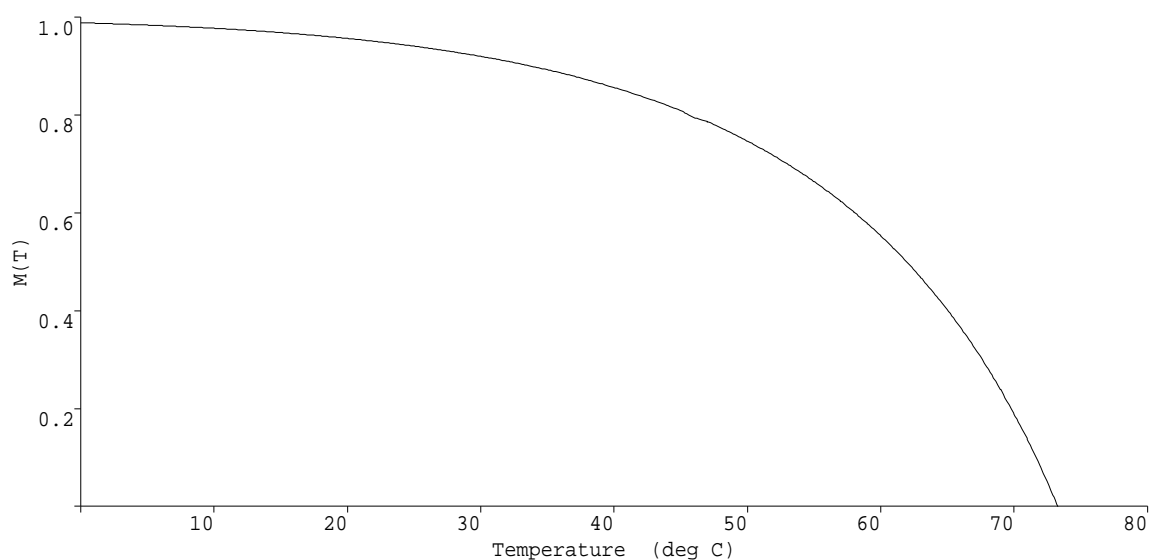


**Figure 7.2 :** Fraction of energy ( $M$ ) released that is used to warm landfill

### 7.1.2 Maximum attainable temperature

The theoretical maximum possible temperature that may be achieved in a fully anaerobic landfill under the above assumptions is the one for which  $M(T) = 0$ , since at this point all the energy released is required to saturate the gas being produced. This temperature is  $73^\circ\text{C}$ . Since we have neglected conductive heat losses this means that any landfill approaching  $70^\circ\text{C}$  cannot be completely anaerobic. The occurrence of such temperatures in sites (especially shallow ones) is an indicator that oxygen is reaching the interior, and operators should check for over-pumping and cracks in the cover material.

### 7.1.3 Rate of temperature rise

The rate of temperature rise is dependent on two factors.

[1] The temperature — this determines how much of the heat released by methanogenesis is used to warm the waste.

[2] The rate of gas production — this determines the rate at which heat is released.

We consider some examples to illustrate this.

### 7.1.4 Example 1 : Constant Rate of Gas Generation.

Suppose we have a site with temperature less than 20 °C (so that  $M(T) \approx 1$ ), and a constant gas generation rate of  $10 \text{ m}^3 \text{ m}^{-3} \text{ yr}^{-1}$ . (equivalent to 400 moles of gas per cubic metre of waste per year). The heat capacity of waste is approximately  $2.2 \text{ MJ m}^{-3} \text{ K}^{-1}$ , so using equation (6) the maximum expected temperature rise of the waste over a year will be

$$\Delta T = \frac{400 \times 23000}{2.2 \times 10^6} \approx 4 \text{ }^\circ\text{C}. \quad (7)$$

### 7.1.5 Example 2 : Temperature Dependent Rate of Gas Generation.

Rather than specifying a fixed gas generation rate, we may allow it to be dependent on temperature. With this assumption the two conditions influencing the rate of temperature rise reduce to one, ie. the rate of temperature rise is solely dependent on the temperature.

$$c \frac{dT}{dt} = 23000M(T) \times 40Q_v(T), \quad (8)$$

where  $Q_v(T)$  is the volumetric gas generation rate (measured in  $\text{m}^3 \text{ m}^{-3} \text{ s}^{-1}$ , noting that 40 moles of LFG occupy approximately one cubic metre at typical landfill temperatures). The generation rate is here assumed to be linear with temperature, so that  $Q_v(T) = Q_{v0}T/T_{max}$ , so that the rate of warming is proportional to the value of  $T \times M(T)$  which is shown in Figure 7.3.

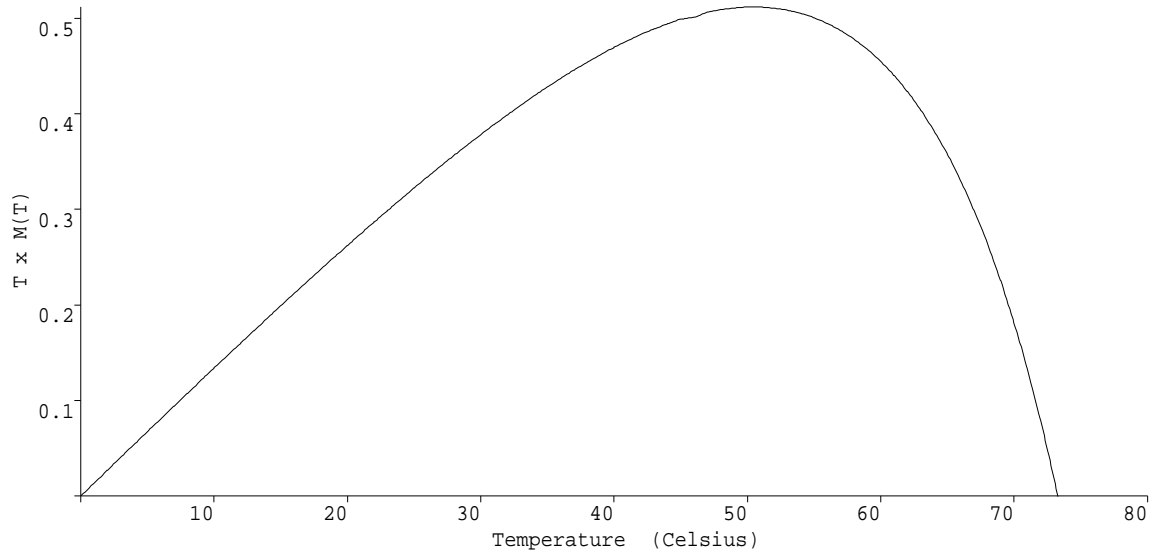


**Figure 7.3 :** Variation of rate of warming with temperature,  $T \times M(T)$ .

Given a value for  $Q_{v0}$  and the present temperature, then the temperature at any future time can be found by integrating equation (8) numerically.

## 7.2 1-Dimensional Model.

Having arrived at a set of theoretical results for the case where there is no heat loss to the surroundings, we now need to introduce spatial variability into our model so that some more practical situations may be tackled.

The first step is to consider only variation with  $z$ , depth below the landfill surface, since this is the dimension with which the most marked changes in temperature occur. This leads to a dramatic simplification in the equations that we must solve. We simplify further assuming the moisture content remains constant, but we continue to model liquid heat convection by allowing a seepage flux,  $v$ . The gas flow model is now directly soluble, with the gas flux ( $u$ ) at any point being the integral of the net production below it. This gives the heat flow equation

$$C \frac{\partial T}{\partial t} = h_v \frac{\partial^2 T}{\partial z^2} + (c_g u + c_w v) \frac{\partial T}{\partial z} + H_0 R + L_0 E, \quad (9)$$

where  $h_v$  is the vertical component of the thermal conductivity. The degradation rate  $R$  is modelled as a function of  $T$ , as shown in Figure 7.4, using data obtained from laboratory experiments (see Chapter 6 on the Biological Model).

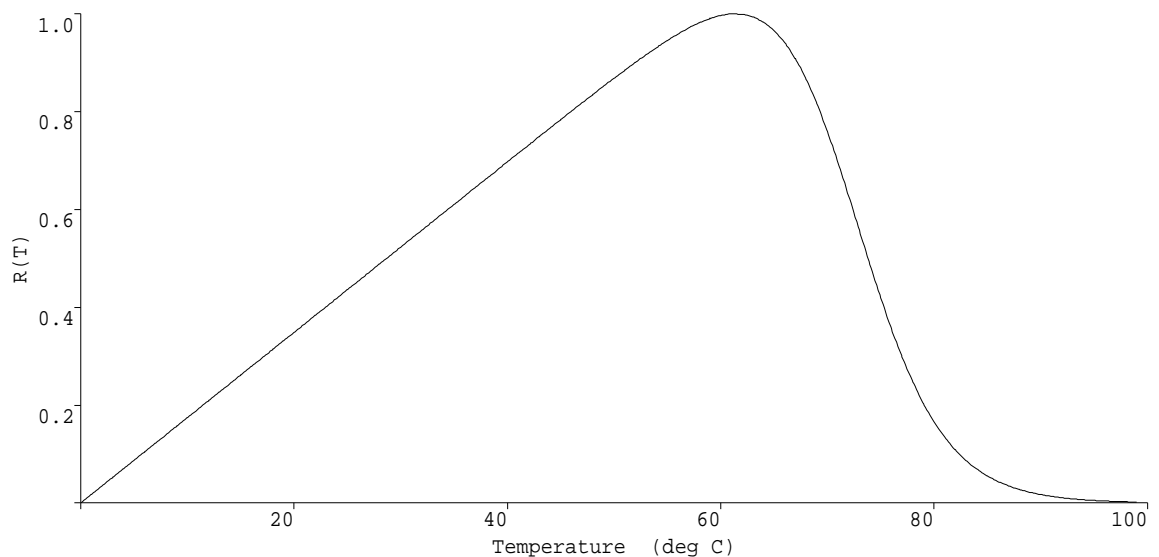


**Figure 7.4** : Dependence of degradation rate on temperature.

### 7.2.1 Results

Numerous runs of the model show that the depth of a site greatly influences both the rate of warming of the site and the final temperature that it reaches. In all cases however the rate of warming is fairly slow, only a few degrees per year. This leads us to conclude that the early temperature of any particular site depends to a large degree on the temperature reached during the initial stage of aerobic degradation.

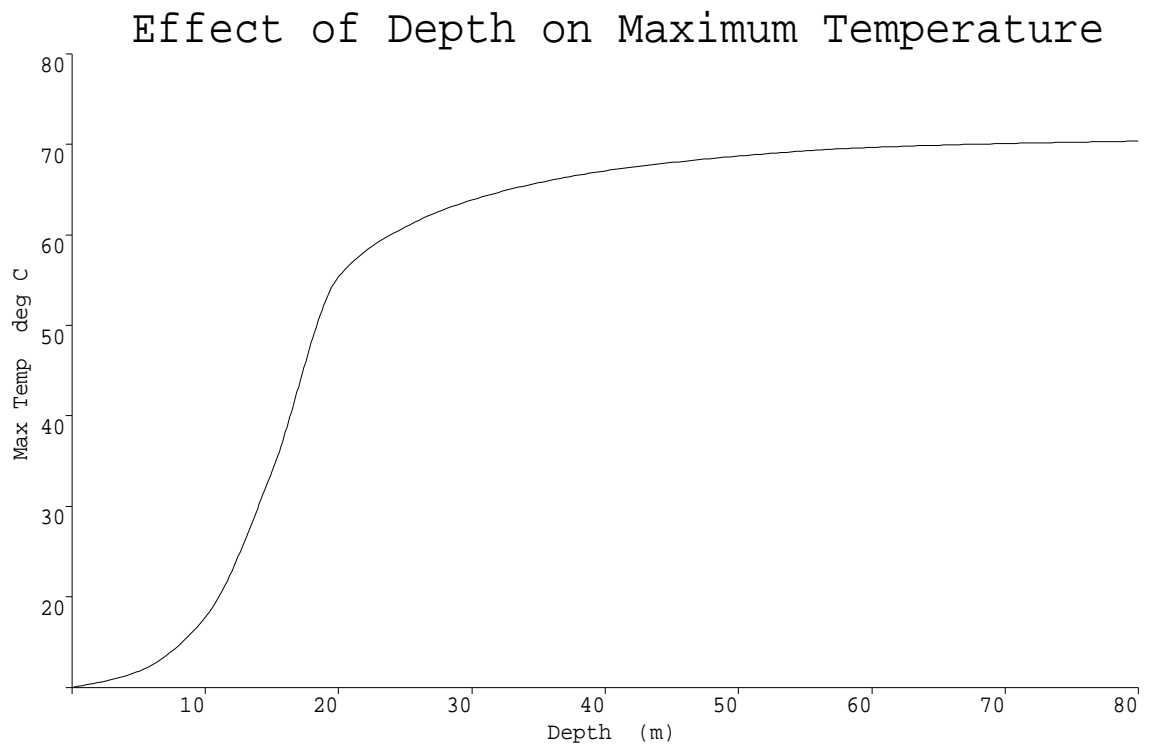


**Figure 7.5 :** Dependence of maximum equilibrium temperature on site depth

Figure 7.5 shows how the maximum internal temperature achieved by model sites depends on their depth (assuming each site obeys the same degradation formula and has unlimited time for warming).

## Maximum Temperature Evolution

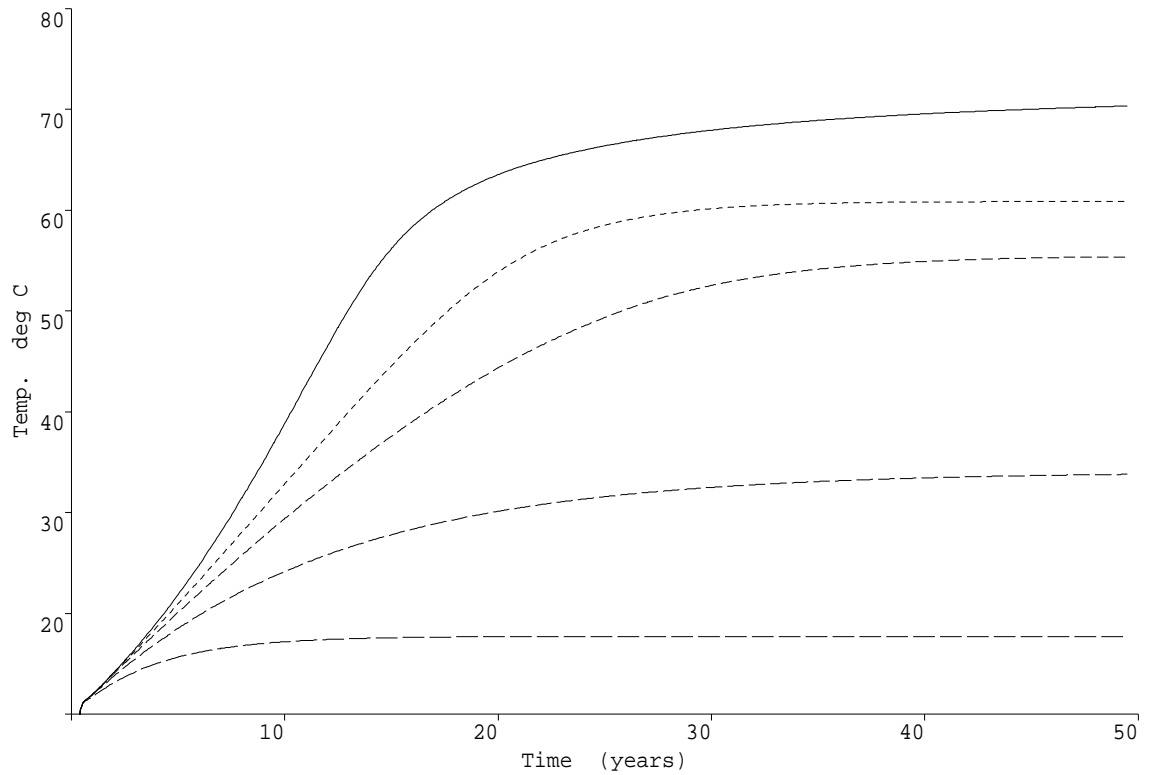


**Figure 7.6 : Maximum evolution.**

-----	10 metres
-----	15 metres
-----	20 metres
-----	25 metres
-----	80 metres

Figure 7.6 demonstrates how the maximum internal temperature in sites of different depths would evolve if there was sufficient substrate. The surface and initial temperature of the sites was assumed to be 10°C, which is the average annual ambient temperature in the U.K.

Figure 7.7 shows the fraction of a site (based on the same simulation results as Figure 7.6) which is above a particular temperature. Thus it can be seen that about 50% of a 15 m deep site exceeds 30°C, whereas 85% of a 20 m deep landfill is above that temperature.

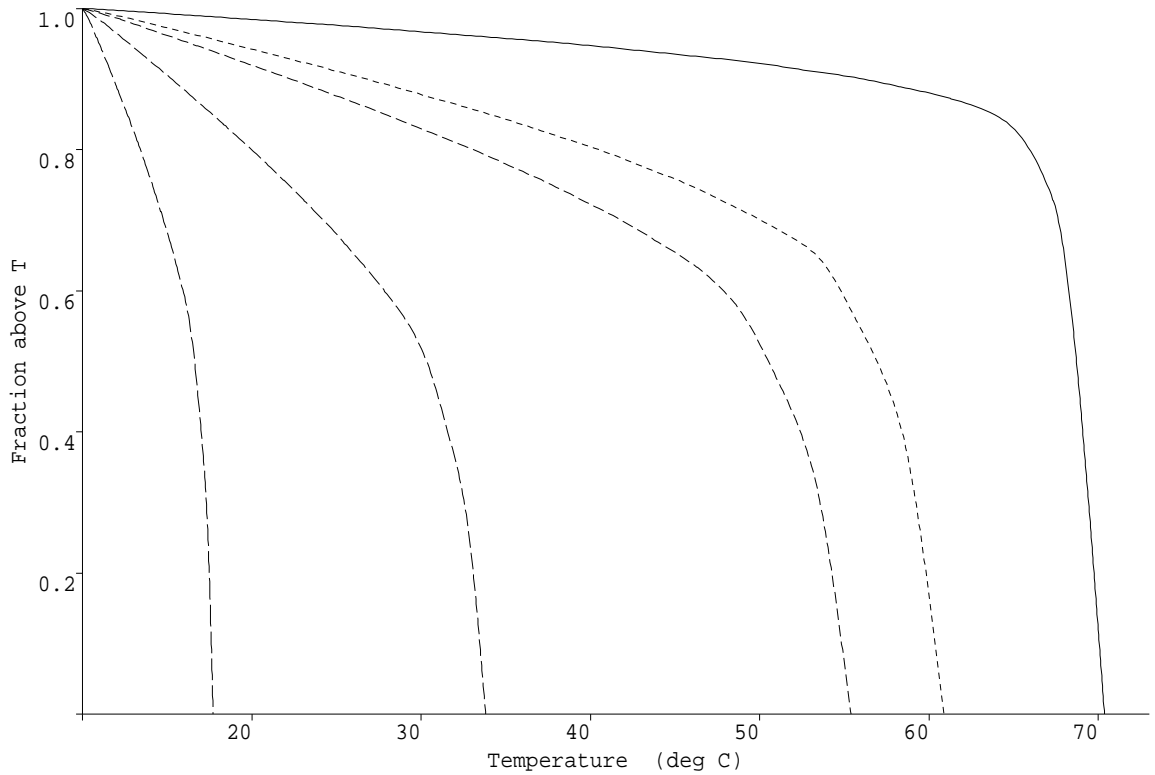


**Figure 7.7 :** Fraction of site above various temperatures.

-----	10 metres
- - - - -	15 metres
-----	20 metres
- - - - -	25 metres
-----	80 metres

When considering these results it should be remembered that the degradation rate, as modelled, only depends on temperature. Other factors such as the availability of sufficient degradable materials are not taken into account. Reaction rates, and therefore peak achievable temperatures, would thus be expected to be somewhat below those predicted here when the site ages — and this is dealt with in the next section.

Considering the curves of Figures 7.6 and 7.7, we recommend that sites should have a minimum depth of 15 m, and preferably greater than 20 m.



### 7.3 Combined Model of Heat, Gas and Moisture Flow.

In order to investigate different strategies for controlling the moisture content of landfills we need to consider a combined model for the flows of heat, gas and moisture within the site. This is derived in Chapter 3. Although it is only practicable to compute solutions to a one dimensional model, this degree of complexity is sufficient to yield valuable results.

#### 7.3.1 Reaction Rate

We now model the rate of degradation within the landfill as a function of both temperature and moisture content. Assuming that these two factors act independently, the reaction rate  $R$  can be written as the product of two functions  $R(T, \theta) = R_1(T)R_2(\theta)$ . The same temperature dependence curve is used as in previous sections, and the assumed dependence of reaction rate on moisture content is illustrated in Figure 7.8 below.

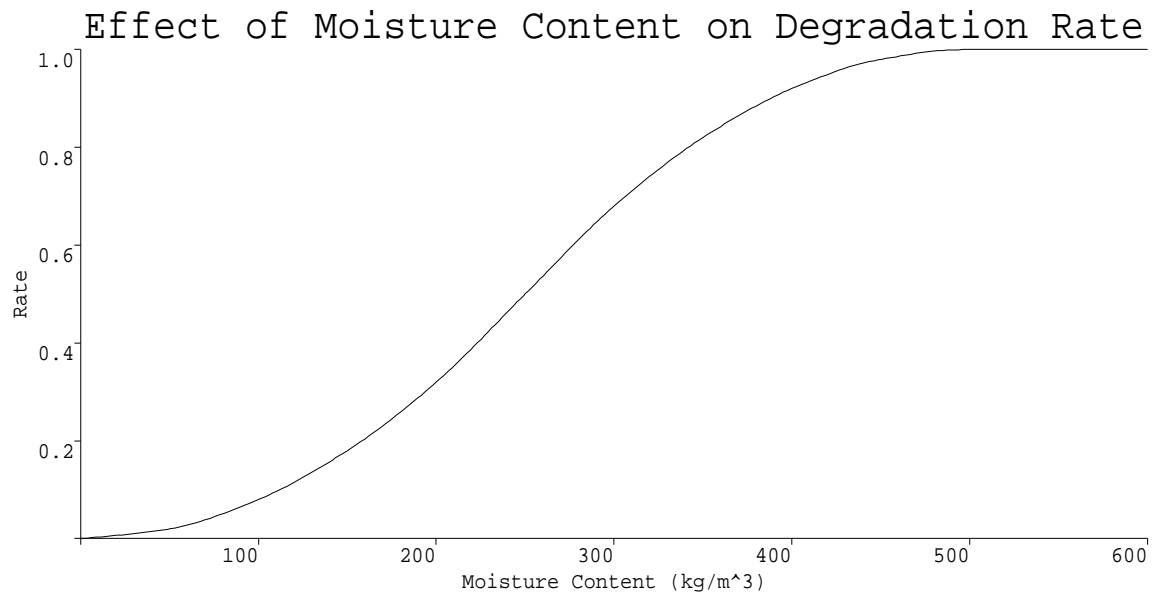


**Figure 7.8** : Modelled dependency of reaction rate on moisture content.

To investigate the behaviour of a site over its active lifetime rather than over a relatively short period (such as that required for the establishment of methanogenesis in Chapter 7), the model must be adapted to take account of the changes occurring in the waste due to decomposition. This is done by introducing an extra factor  $R_3(A)$  in the rate determining equation thus

$$R(T, \theta, A) = R_1(T)R_2(\theta)R_3(A). \quad (10)$$

The form of  $R_3$  is derived using the same assumptions as Chapter 6, so that the waste is divided into three fractions: fast, medium and slowly degradable — labelled  $G_1, G_2, G_3$  respectively, with no attempt to segregate them further by composition. Each type decays independently with its own rate constant  $\mu_j$ , and the net decay rate is shown in Figure 7.9 as a function<sup>†</sup> of the active fraction  $A$  (ie. the proportion of the original degradable waste remaining) defined below.

$$A = 1 - \frac{\text{Total Gas Produced so far}}{\text{Maximum Possible Gas Yield}}, \quad A(z, t) = 1 - \frac{1}{Y_{max}} \int_0^t Q(z, \tau) d\tau. \quad (11, 12)$$

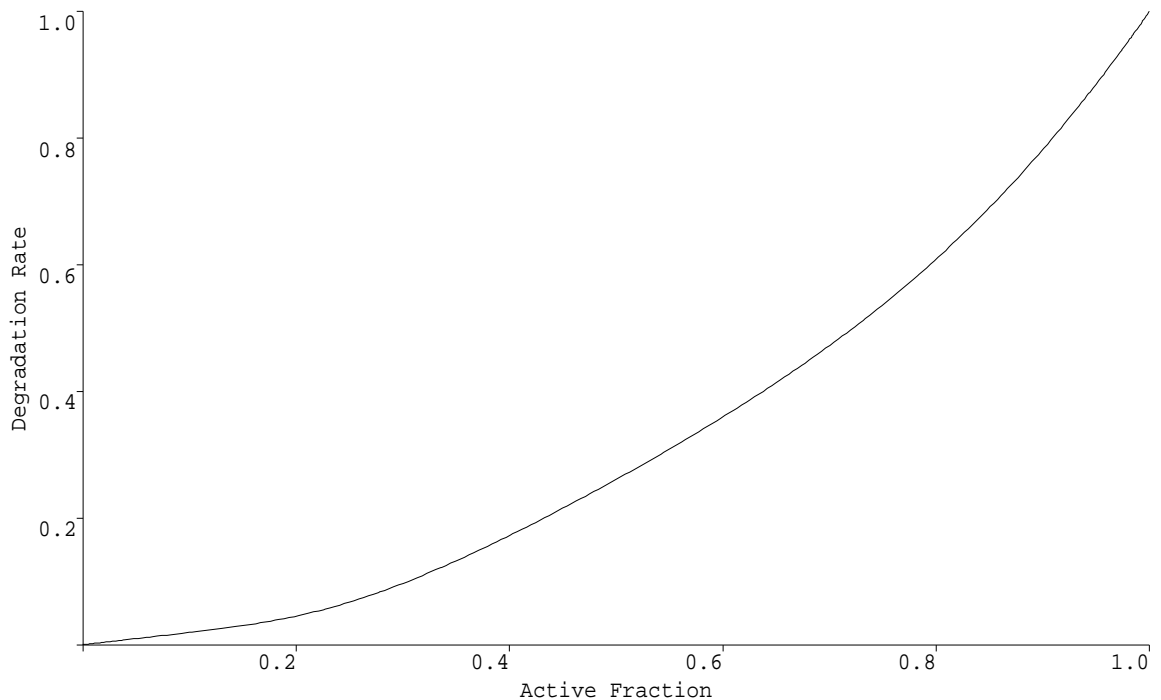


**Figure 7.9 :** Modelled dependency of reaction rate as a function of active fraction  $A$ .

In computing the curve shown in Figure 7.9 we have assumed the same waste types as in the main example of Chapter 6, so that the fast, medium and slowly degradable materials are present in the relative proportions of 5%, 55%, 40% in fresh waste and have half-lives in the ratio 1:5:30. Hence the examples given below show the possible types of

<sup>†</sup> The decay rate  $R_3$  may be related to the active fraction  $A$  by the pair of parametric equations  $A = \sum_j G_j \exp(-\mu_j \tau)$ ,  $R_3 = \sum_j \mu_j G_j \exp(-\mu_j \tau) / \sum_j G_j$ .

long-term behaviour which could occur in the site described in Chapter 6 under different water management regimes.

### **7.3.2 Long-term Comparison of Wet and Dry Sites.**

A key policy question in the management of landfills is whether (or to what degree) rainwater should be excluded from sites. This determines the whole character and future behaviour of a site. Here we use our model to investigate the effects of each strategy in the long term, and discuss the advantages and disadvantages of each strategy.

Two examples are given, which show the way that the same site would react if the amount of rainwater which is allowed to penetrate the cap (and only that parameter) is changed.

### **7.3.3 Wet Sites.**

Wet sites will obviously produce more leachate (than dry sites), but they also have a larger gas production rate and consequently a shorter time to completion. If the leachate and gas migration problems can be dealt with, wet sites would be ideal for gas exploitation schemes.

As an example we consider a site with a 20 m depth of waste, on a clay foundation (nominally 10 m thick) and with a 1 m thick clay cap. The initial waste temperature is 25 °C, the initial water content 20% by volume (ie. 200 kg m<sup>-3</sup>), and the penetration rate of water through the cap is 1 mm d<sup>-1</sup>. The maximum possible gas yield is taken to be 200 kg m<sup>-3</sup>.

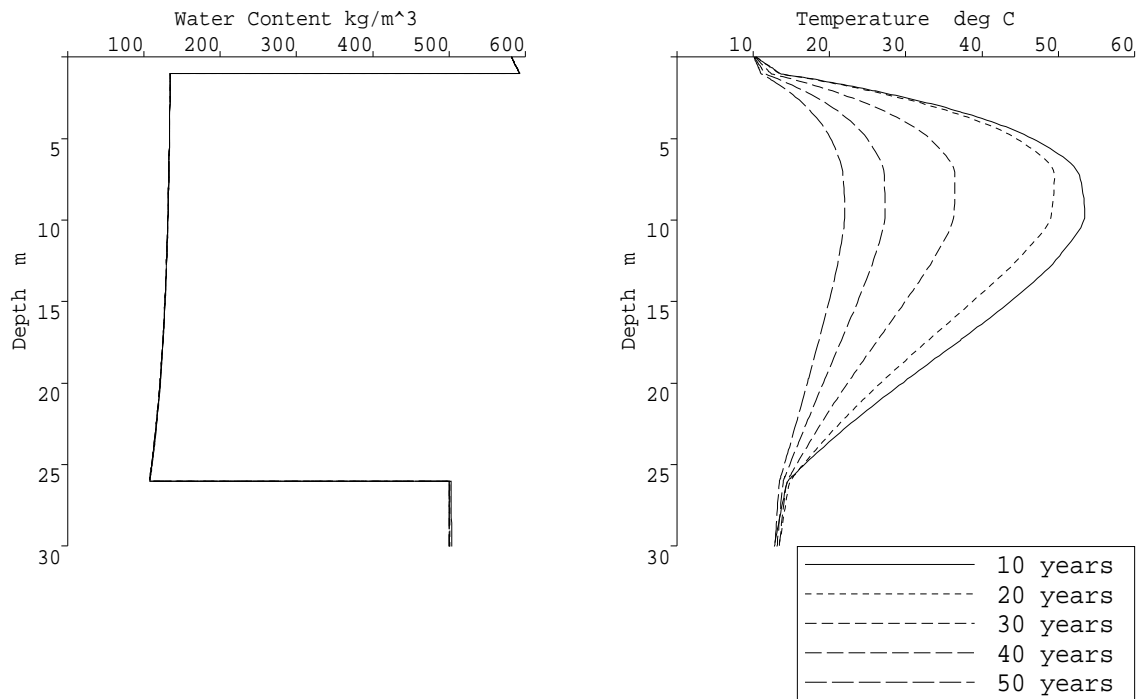


**Figure 10 :** Temperature and water levels in wet site.

Figure 7.10 shows the temperature and water content throughout the life of the site. There is an initial rapid warming period, after which a high temperature is maintained until the degradation nears completion when the reaction rate and temperature fall. Figure 7.11 shows the amount of undegraded waste remaining at the end of the 50 year period and the variation of the gas production with time. These demonstrate clearly that the drop in the activity of the site is caused by the depletion of substrate. (The discontinuities in the water content occur at the waste/clay interfaces due to their differing porous properties).

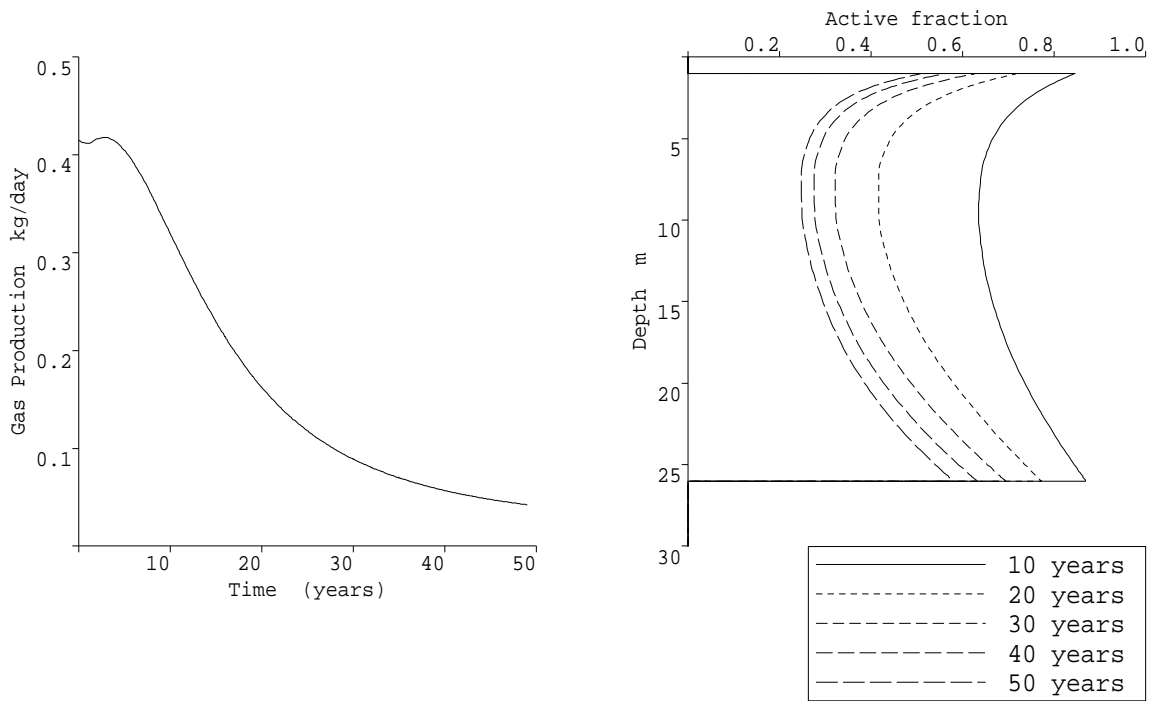


Figure 7.11 : Gas production and active fraction in wet site.

### 7.3.4 Dry Sites.

Dry sites with their low levels of leachate and gas production pose fewer problems in their management. However they offer little potential for power generation and remain active (even if only at a low level) for longer periods, thus requiring extra expenditure on monitoring.

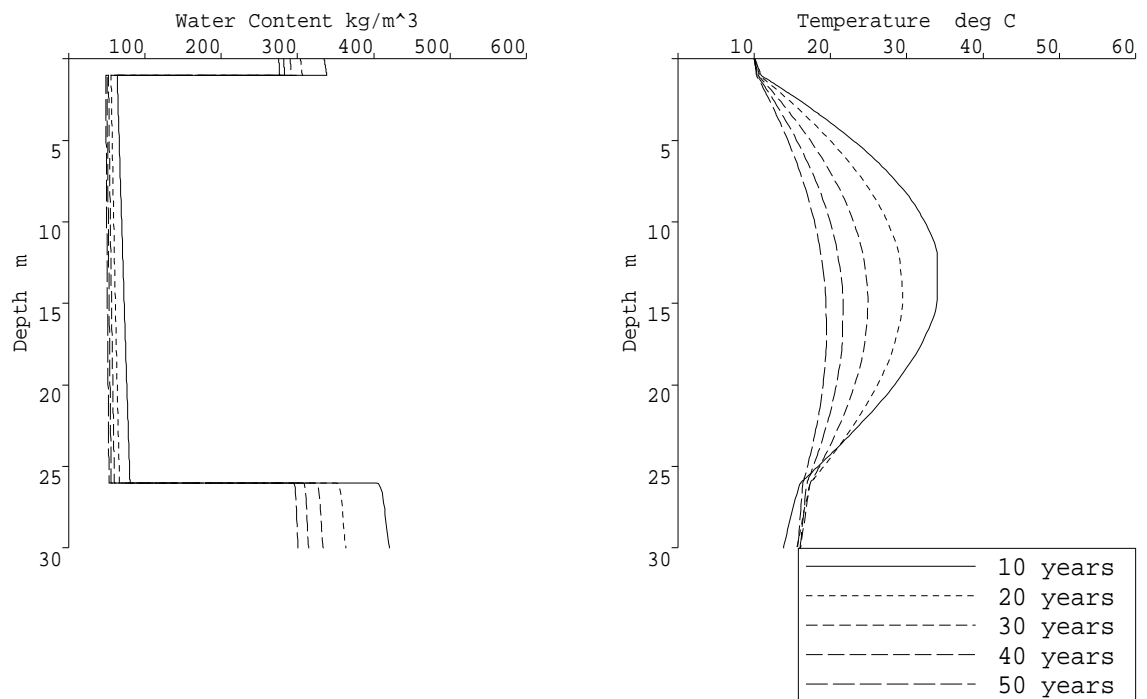


Figure 7.12 : Water levels and temperature in dry site.

Figure 7.12 illustrates the results for our model site with an infiltration rate of 0.1 mm/day. Here, although the site warms initially, the reaction rate slows as the water drains and consequently the temperature drops again. After 50 years the temperature and gas production are similar to the wet site, but in this case it is the lack of water rather than the lack of degradable waste that halts the reaction. Figure 7.13 shows that the waste in the site has only degraded slightly by comparison with the same site under wet conditions.

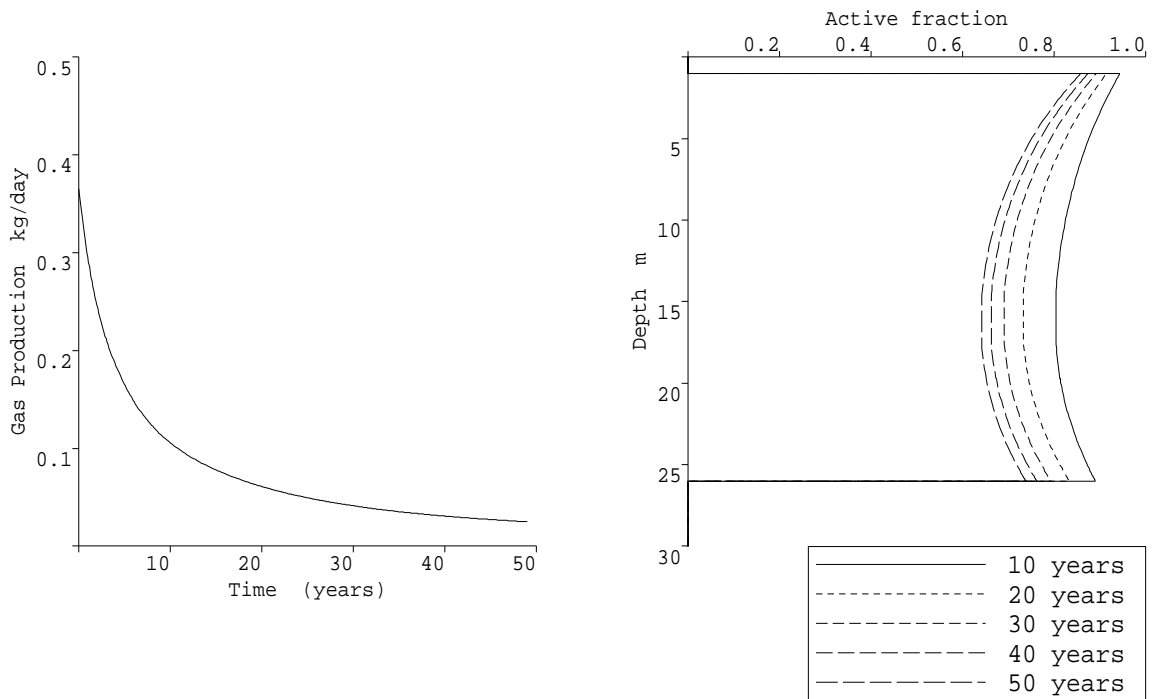


Figure 7.13 : Gas production and active fraction in dry site.

If a completely dry site could be created, by preventing any water from penetrating the cap, it might be possible to limit degradation to the initial aerobic phase. This would eliminate LFG and leachate problems. However such a site would retain the potential to turn methanogenic should the cap develop leaks, thus leaving a huge legacy of sites potentially capable of generating leachate and gas for many decades.

### 7.3.5 Conclusion on Optimum Site Moisture Levels.

It is our opinion that it would be far easier, safer and (ultimately) less expensive to use landfills to process waste now, rather than creating sarcophagi to be forgotten about until problems inevitably arise. This requires that the internal moisture levels be managed so as to create optimum conditions for methanogenesis thereby eliminating the potential hazards as quickly as possible.

The results of our simulations indicate that dry sites cannot fulfil this aim, and that water management strategies aimed at creating a dessicated interior will produce ‘time-bomb’ sites rather than safe repositories. We therefore recommend that site moisture is maintained at sufficiently high levels that it does not become a limiting factor for degradation.

## 7.4 Enhancing Methane Production.

The easiest way to dispose of the unwanted methane is to burn it off in a flare, releasing a great deal of heat which is lost to the atmosphere. At some large sites however the gas is used as a fuel to power electricity generators, thus turning a troublesome waste product into a valuable source of income. It is usually economic factors that decide whether or not the gas is utilised in this way. At small sites the revenue that would be produced by installing generators is not sufficient to justify the large capital costs incurred in doing so, whereas at larger sites the payback times are much shorter. Hence there is a threshold above which it is economically viable to exploit the landfill gas. This threshold is not strictly a measure of the site's size but also of the rate at which it is producing methane.

This section proposes a scheme for exploiting the landfill gas at those sites where flows are below the current threshold for profitable electricity generation. Whilst there are existing examples of other small scale projects these tend to be fairly specialised and may not be suitable to the majority of sites. The scheme discussed here involves using the heat produced by burning the gas to warm the landfill site itself. This would increase gas production in the site, possibly to a level above the threshold, when electricity generation could begin. Of course, this scheme need not be confined to those sites below the profitability threshold but could also be used to make viable generation projects even more lucrative.

In accordance with the policy advocated at the end of the previous section, our proposed technique will also reduce the long-term environmental impact of a site by increasing the rate of degradation and hence shortening the time to final completion.



#### **7.4.1 Outline of Scheme.**

In order to make the basic idea of raising the site temperature practicable, an efficient way of distributing around the site the heat produced by burning the methane must be found. The model has been used to simulate the effect of splitting the extracted landfill gas into two parts, the first of which is burned in order to heat a water bath through which the second fraction is passed. This second fraction emerges from the water bath both warm and saturated with water vapour and is pumped back into the site. When this hot, saturated gas encounters a cooler region of the landfill, it will cool and will therefore be able to hold less vapour (see Figure 7.1). The excess vapour will condense, releasing latent heat which warms the landfill. In this way the landfill becomes hotter and more moist, both of which help to increase the gas production rate.

It should be noted that if the returned gas encounters a warmer region of the landfill the opposite effect will occur: water will evaporate and the region will cool. Hence by controlling the temperature of the gas pumped into the site, the model predicts that we can control the temperature of that region of the site which is within the radius of influence of the injecting well. In principle this should enable the optimum temperature for the methanogenic bacteria to be achieved and maintained.

#### **7.4.2 Large Sites**

The strategy as explained so far is most likely to be applicable to completed sites where the gas flow rates are not quite sufficient to warrant exploitation. Large sites would enable and require more sophisticated management of the methane resource with a balance being struck between one of three uses:

- [1] burned to heat the water bath,
- [2] passed through the water bath and pumped back into the site,
- [3] utilised for electricity generation, etc.

The proportion of the gas put to each use would vary throughout the lifetime of the landfill, with all gas being split between fractions 1 and 2 initially until the desired flows are reached. Once levels of production are sufficiently high, utilisation would commence. At this stage however it would still be possible to use some gas to bring areas of more recently deposited waste up to the optimum temperature.

There are many other potential advantages using the scheme proposed above. These include:

- [1] The use of warmed landfill gas to heat the site maintains the anaerobic environment required by the methanogenic bacteria and does not reduce the quality (methane content)

of the gas yield.

[2] Faster reaction rates imply shorter times to completion. Once gas yields drop below economically acceptable limits the generators could be moved to another site.

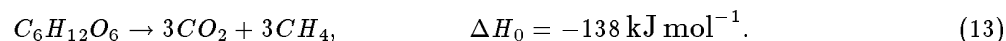
[3] The pumps and wells would be required to extract the gas for safety reasons in any case.

[4] The system would be flexible: the gas flow pattern could be changed simply by changing wells from extracting gas to injecting hot gas.

[5] The increased gas velocities inside the site would help to transport other materials through the site. This might allow pollutants (eg. hydrogen sulphide) to be removed by solution in the water bath, and could also help to relieve problems of non-homogeneity such as perched water tables.

### 7.4.3 Energy Calculations

A landfill, if left undisturbed, will gradually warm up since the process which produces methane from carbohydrates is exothermic. However this warming is very slow as only a small amount of heat is released (as shown earlier in this Chapter).



The combustion of methane is much more exothermic, hence the plan to use this reaction to heat the landfill.



The heat of combustion can be used to calculate the energy available from the gas. An achievable gas generation rate for a mature landfill is  $2 \times 10^{-3} \text{ m}^3 \text{ m}^{-3} \text{ hr}^{-1}$ . So the amount of methane produced per cubic metre per day is  $24 \text{ dm}^3$ , which is approximately one mole. Burning this in air releases  $890 \text{ kJ}$  of energy, so the potential rate of heat output is calculated to be approximately  $10 \text{ W m}^{-3}$  of waste. The efficiency of the generators must now be taken into consideration to calculate the potential generation capacity.

#### 7.4.4 Mathematical Model

Since most sites are constructed of cells separated by clay walls, we model an individual cell of width  $w$ , length  $l$  and depth  $d$ , containing  $N$  vertical extraction wells at horizontal coordinates  $(x_i, y_i)$ .

In order to be able to examine the effects of different well positions and arrangements we must retain the full three dimensional geometry of the model derived in Chapter 3. As is stated there, this requires us to make some other simplification in order to reduce the problem to a manageable size. We therefore model temperature and gas pressure and treat the moisture content as being a uniform constant throughout the site. Hence our model is

$$\frac{\partial \rho_g}{\partial t} = \text{div}(\underline{v}\rho_g) + Q_0 R(T) + E + W, \quad (15)$$

$$C \frac{\partial T}{\partial t} = \text{div}(\mathbf{N} \cdot \nabla T) + \rho c_g \underline{u} \cdot \nabla T + H_0 R(T) - L_0 E. \quad (16)$$

Details of the method of solution of this model are given in Appendix 5B.

#### 7.4.5 Simulation Results

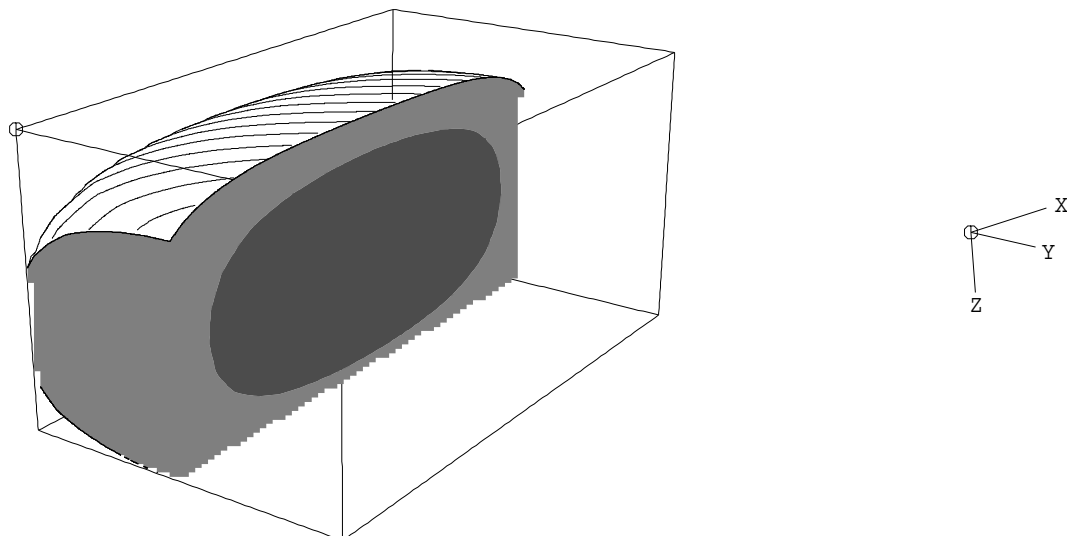
We now use the model to examine various arrangements of pumps within the landfill cell, to assess their effectiveness for a range of other parameters. The way that the wells, both injection and extraction, are arranged in the site will greatly affect the effectiveness of the scheme. The criteria by which the layout is designed are:

- [1] No gas should escape from the site, both for reasons of safety and efficiency.
- [2] The temperature distribution achieved should be as even as possible.
- [3] As few wells should be drilled as possible, in order to keep installation costs low.
- [4] The injection and extraction pressures should be as low as possible, in order to keep running costs low. This might mean using very large diameter wells.

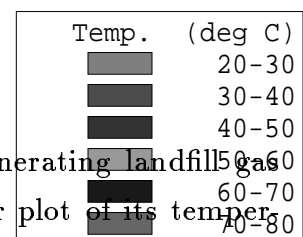
Obviously consideration of [3] and [4] will lead to compromises being necessary in finding the best layout for a particular site.

### 7.4.6 Example

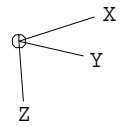
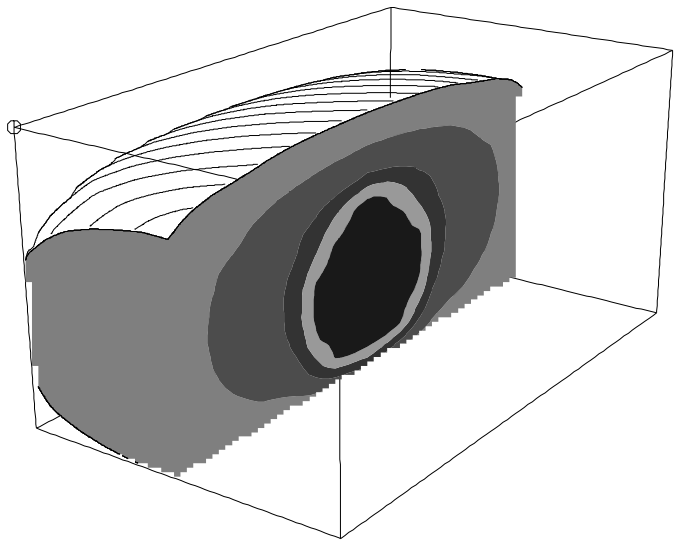
As an illustrative example we consider a site 40 m × 24 m × 20 m deep (approximately the size of a test cell at the Brogborough site). After trying various configurations it was found that a suitable layout would be a large bore injection well in the centre of the site at  $(x, y)$  coordinates (20,12) and towards the bottom (say with the perforated part of the well between depths of 12 m and 18 m), with two smaller extraction wells symmetrically placed either side at (8,12) and (32,12). These extraction wells are placed less deeply than the injection wells, both to ensure no leakage and to draw hot gas up through the site.









**Figure 7.14** : Initial site temperature.



Initially the site has an average temperature of 27°C and is generating landfill gas at a rate of 15.3 m<sup>3</sup> hr<sup>-1</sup>. Figure 7.14 shows a 3-dimensional contour plot of its temperature distribution. Hot saturated gas at 65°C is then pumped in through the central well at a rate of 216 m<sup>3</sup> hr<sup>-1</sup>, requiring an injection pressure of 20k Pa. This rate of pumping is maintained throughout the trial simulation. If the heating were perfectly efficient only 6.5 m<sup>3</sup> hr<sup>-1</sup> of the gas generated would be needed to heat the water bath, so even in practice it should be possible to utilize some of the gas immediately.



**Figure 7.15 : Temperature after 30 days.**

Temp. (deg C)	
20-30	
30-40	
40-50	
50-60	
60-70	
70-80	

After 30 days the area around the injection well has been heated to the optimum temperature (see Figure 7.15). This raises the average temperature to 29°C and the gas yield to 16 m<sup>3</sup> hr<sup>-1</sup>.

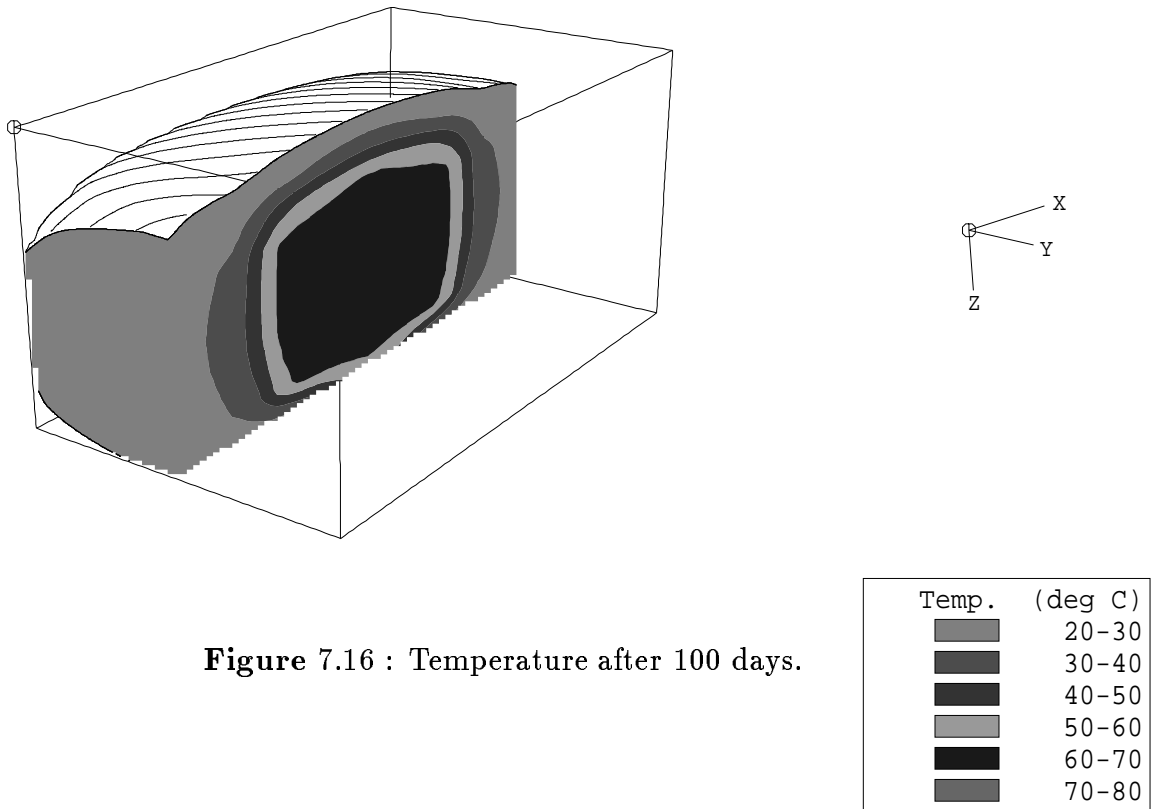


**Figure 7.16 :** Temperature after 100 days.

Figure 7.16 shows that after 100 days the area of optimum temperature has spread further, raising the average temperature to 34 °C and the gas yield to 18 m<sup>3</sup> hr<sup>-1</sup>.

One year after recirculation was started the region at optimum temperature has spread to cover most of the site. By this time the temperature around the extraction wells has risen, so slightly less energy is used in heating the gas extracted to the required 65 °C. The average temperature has been raised to 44 °C and the gas yield to 22 m<sup>3</sup> hr<sup>-1</sup>, an increase of almost 50% over the original gas production rate.

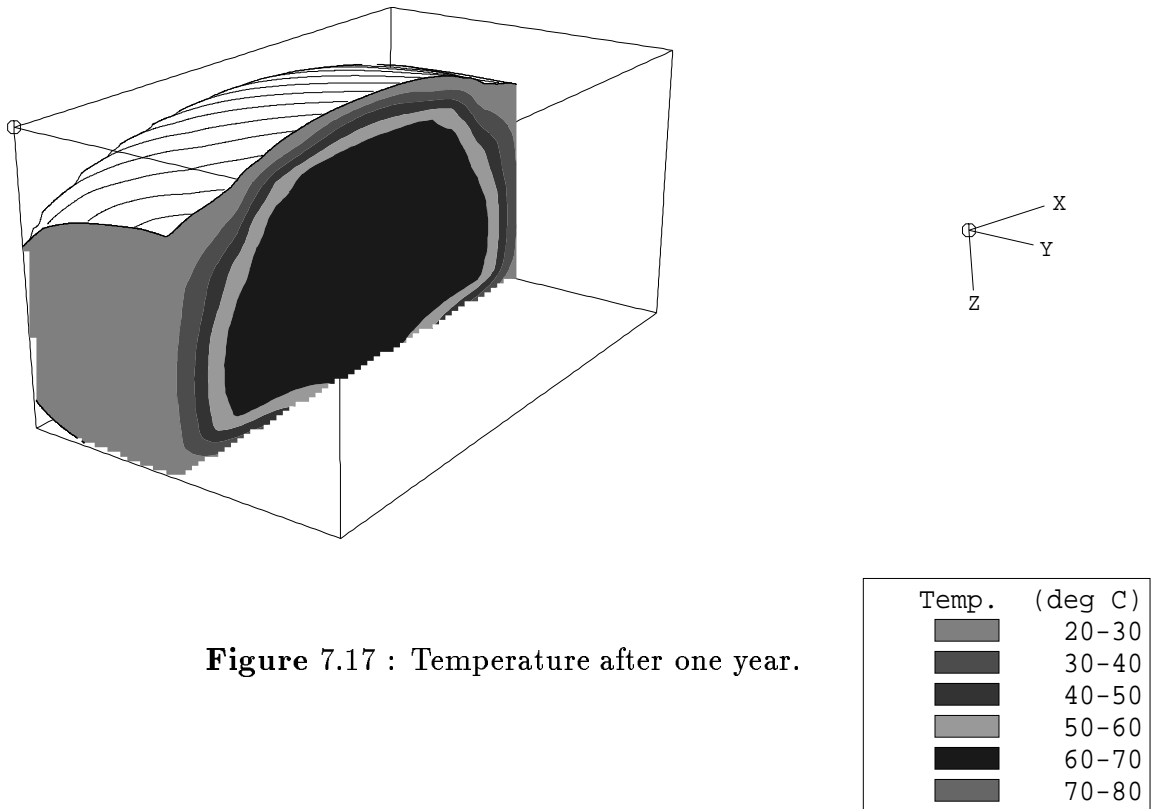


**Figure 7.17 :** Temperature after one year.

**7.4.7 Conclusions on Enhancing Methane Production.**

The simulation results indicate that the proposed scheme to recycle hot gas through the landfill could be successful in raising temperatures in the site, and it may be possible to raise them to thermophilic levels ( $\approx 60^{\circ}\text{C}$ ). This should raise gas production significantly whilst in the mesophilic range and although no data are available on the growth rates of thermophilic bacteria, their maximum production rate is thought to be several times higher than that of mesophiles.

Note that no account has been taken of the fact that the increased moisture levels within the site should boost gas production rates even further, so that the effect should be even more favourable than predicted above.

## **Chapter 8 : Additional Topics.**

### **8.1 Introduction.**

This Chapter gathers together topics which were considered during the course of the investigation, but not felt sufficiently developed to warrant individual treatment.

### **8.2 Settlement.**

Part of the original project brief was to look at the available data on landfill settlement, attempting to explain the major factors effecting its rate and magnitude, and if possible to produce a predictive model based on them.

However, whilst there is a general perception in the industry that a great deal of information is available regarding settlement, none of it is useful for our purposes. All of the monitoring that has been done to date (in the U.K.) has consisted of measuring the degree to which the surface height of a given site decreases over time. Nothing is usually known of the landfill interior, nor of the extent to which different layers within the site have been compressed and displaced. Construction companies involved in building on landfill sites were contacted and they revealed that they either excavated the waste before beginning, or else drove piles through the site to support the weight. There is a total absence of experimental evidence regarding the structural properties of waste.

The first step in predicting waste settlement must be an experimental determination of the bulk modulus of various types of fill — ie. the degree to which a given load will compress them. This is currently being carried out (September 1992) by the Department of the Environment, but no results were available at the time of writing. Ideally, such experiments should investigate several categories of waste and mixtures thereof, both fresh and decomposed, so that a table can be constructed relating waste composition to its structural properties. Such data would be immensely helpful to site planners, and could be used to develop a predictive model as originally hoped.



### **8.3 Methane Oxidation.**

Aerobic bacteria within soil are capable of oxidizing methane escaping from landfills. The rates of breakdown depend on local conditions such as moisture, temperature, diffusion pathways, population size and methane/oxygen availability.

Properly applied these microbes could provide a means of limiting methane migration, and a brief investigation was conducted into the feasibility of modelling their behaviour. It was concluded that most of the required parameters had already been incorporated into existing models within the project, and that the major hindrance to progress was lack of data regarding the metabolism of the actual bacteria, in particular how they respond to different dissolved concentrations of methane and oxygen. Given a specifically designed laboratory experiment, it should be quite straightforward to model methane oxidation and produce recommendations for enhancing it.

### **8.4 Moisture Flow in a Doubly-Porous Medium.**

Observations of water flow in landfills suggest that it may not always obey a Darcy's Law — which is unsurprising in view of the highly heterogeneous nature of waste. Two phenomena in particular are difficult to reconcile without introducing a high degree of non-linearity into the basic porous medium type model:

[1] The landfill may be fairly wet over its entire depth without any region being fully saturated.

[2] Leachate production at the base of the landfill can increase within hours of water being applied at the top surface (eg. heavy rainfall), whilst most of the time the flows are very small.

### 8.4.1 One Dimensional Doubly-Porous Model.

To reconcile the existence of long-term stable states with the ability to respond rapidly to transient conditions, we attempted to construct a doubly-porous model for landfill water flow.

The concept of a doubly-porous medium is that it consists of two over-lapping media with different physical properties. One of these media, the macropores, represents the large flow channels in the overall system such as the gaps between large waste particles. The other media, called the micropores, has a smaller length-scale and models the tiny interstices within the ‘solid’ material — for instance, the interior of a soggy mass of paper would be considered as part of the micropores. The flow in each of these two ‘sub-media’ is considered separately, and they are coupled only by the transfer of moisture between them.

A general model for doubly-porous flow in three dimensions is developed in Young, 1989. Due to computational limits our numerical results were restricted to one dimension (depth  $z$ ), and so only a reduced model is considered here. This takes the form of a pair of partial differential equations in  $\alpha(z, t)$  and  $\beta(z, t)$ , which are the volume fractions of water in the macropores and micropores respectively. These equations are

$$\begin{aligned}\frac{\partial \alpha}{\partial t} &= -\frac{\partial v_\alpha}{\partial z} + \Upsilon + q_\alpha, \\ \frac{\partial \beta}{\partial t} &= -\frac{\partial v_\beta}{\partial z} - \Upsilon + q_\beta,\end{aligned}\tag{1, 2}$$

where  $\Upsilon$  is the intermedia transfer function representing the rate at which water moves from the micropores into the macropores, and  $q_\alpha, q_\beta$  are the rates of moisture generation from biochemical processes (this model did not include vapour transport).

The vertical Darcy fluid velocities  $v_\alpha$  and  $v_\beta$  are computed from moisture potentials  $\psi_\alpha$  and  $\psi_\beta$  as follows

$$v_\alpha = K_\alpha \alpha^m \frac{\partial \psi_\alpha}{\partial z}, \quad \psi_\alpha = h_\alpha \alpha^{-b} + z - d_\alpha,\tag{3, 4}$$

$$v_\beta = K_\beta \beta^m \frac{\partial \psi_\beta}{\partial z}, \quad \psi_\beta = h_\beta \beta^{-b} + z - d_\beta,\tag{5, 6}$$

with  $K_\alpha$  and  $K_\beta$  being the Darcian moisture-flow permeability coefficients. The values of  $b$  and  $m$  depend on the nature of the medium, and for soils are generally chosen so that  $m \approx 2b + 3$ .

### 8.4.2 Intermedia Transfer Function

The intermedia transfer function  $\Upsilon$  is difficult to estimate and we suggest

$$\Upsilon = \begin{cases} -K_{\alpha\beta} \left( \frac{\alpha}{\gamma_s - \gamma_f} \right)^{c_\alpha}; & 0 < \beta < \gamma_a, \\ -K_{\alpha\beta} \left\{ \left( \frac{\alpha}{\gamma_s - \gamma_f} \right)^{c_\alpha} - \left( \frac{\beta - \gamma_a}{\gamma_f - \gamma_a} \right)^{c_\beta} \right\}; & \gamma_a < \beta, \end{cases} \quad (7)$$

as a trial solution, for some values of the constants  $K_{\alpha\beta}$ ,  $c_\alpha$  and  $c_\beta$ . The terms  $\gamma_a$ ,  $\gamma_f$  and  $\gamma_s$  represent the moisture levels at the absorptive, field and saturation capacities of the waste respectively.

If we choose  $c_\alpha = c_\beta$  (and denote their common value as  $c$ ) then when the absorption capacity ( $\gamma_a$ ) is reached, the equilibrium water distribution ( $\Upsilon = 0$ ) is one in which the excess moisture is divided proportionally between the remaining capacity in the micro- and macropores. Taking  $c \neq 1$  would make the rate of intermedia transfer depend explicitly on the saturations themselves and not simply on the deviation from equilibrium. Since neither of  $c > 1$  nor  $c < 1$  seem more likely,  $c = 1$  was used for all the calculations.

### 8.4.3 Boundary Conditions

The conditions at the external boundaries may take the form of either

- [1] known saturation (eg. fully saturated :  $\alpha = \gamma_s - \gamma_f$ ,  $\beta = \gamma_f$ ), or
- [2] known flux (eg. no flux :  $\frac{\partial \alpha}{\partial z} = 0$ ,  $\frac{\partial \beta}{\partial z} = 0$ ).

Landfills generally have a layered structure consisting of alternate levels of waste and fill material used for daily cover (typically soil or clay). Water movement in the homogeneous filler strata is best modelled as in a ordinary porous medium (with moisture fraction  $\theta$  and potential  $\psi_f$ , say). Three conditions are then necessary at each inter-layer boundary. One of these conditions must be conservation of water flux across the boundary, but the other two involve interpretation of the overall (or average) potential in a doubly-porous medium.

Gas generation within a landfill ensures that the landfill is very rarely fully saturated with water. In the partially saturated case the flows of gas and water are partially uncoupled with the water movement being assumed dominant. To combine gas movement with this doubly-porous model, it is suggested that water flow is solved first and the gas occupies the remaining volume.

#### 8.4.4 Wetting Example.

Numerical solutions to the model were found using our finite element method (see Appendix 3A) with purely implicit time stepping. The transient response of the model is illustrated by considering a 10m deep site, which is initially uniformly wet, and has free drainage at the base.

The first shows a site getting wetter due to moisture infiltration from the surface, and the second demonstrates how a site might drain if it was capped so that no water could enter from the surface. The transient is initiated by changing the flux at the landfill surface, which causes a rapid reaction in the macropores, followed by a slower response from the micropores as they take up water and the equilibrium between the two phases is regained.

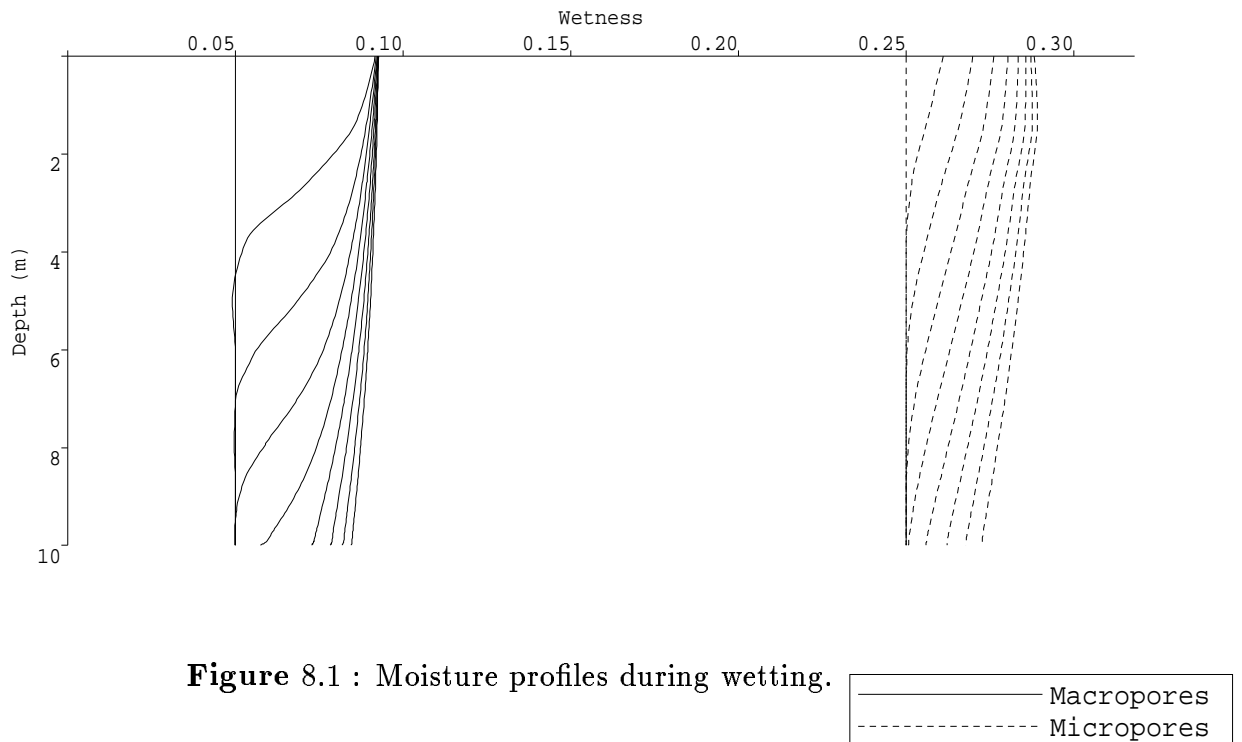
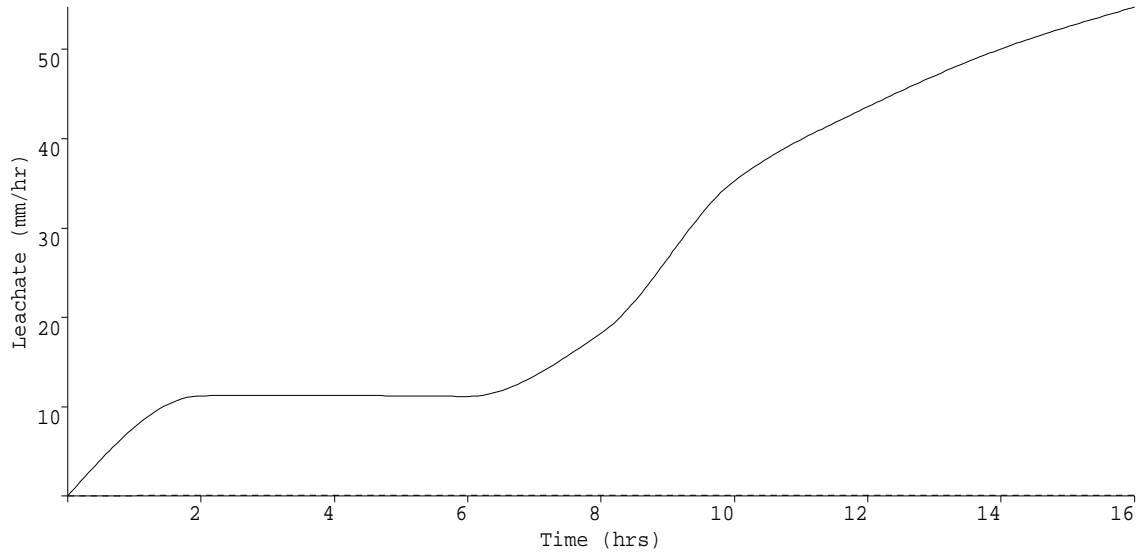


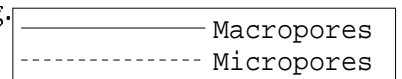
Figure 8.1 : Moisture profiles during wetting.

— Macropores  
- - - Micropores

The increase in the flux of surface water causes a 'wetting front' to move down the site as seen in Figure 8.1 (in which the multiple lines show the moisture profile at equally spaced time intervals).



**Figure 8.2 :** Flux at base of site during wetting.



The wetting front gradually becomes less pronounced, but the time at which it reaches the base of the landfill is still easily identified by the rapid increase in leachate production illustrated in Figure 8.2. The nature of the front is also illustrated by Figure 8.3 which clearly demonstrates the transition between the two equilibria states being made at different times at varying depths.

# Macropore Wetness

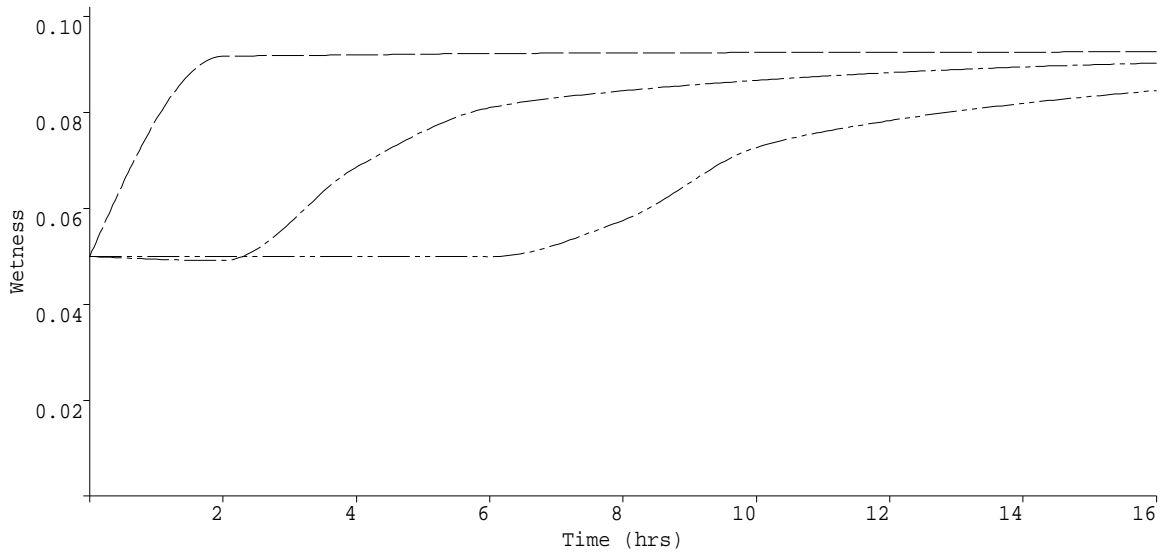
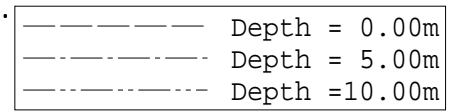
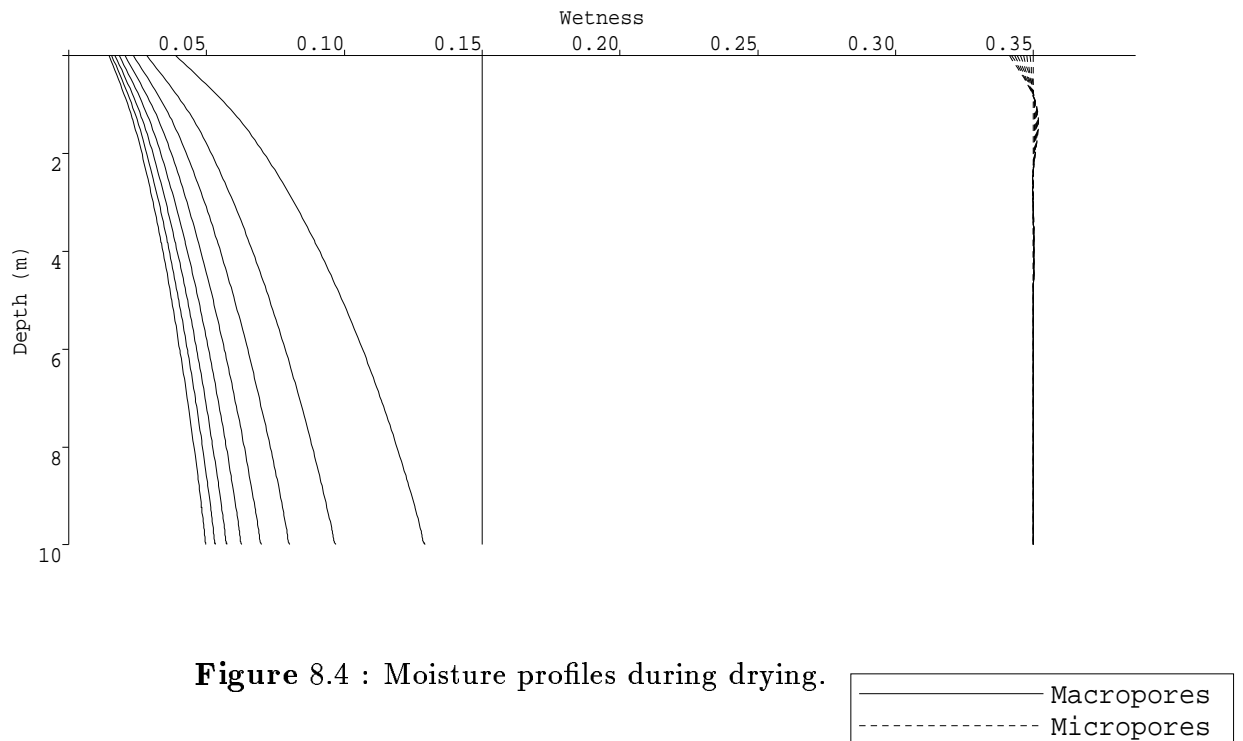


**Figure 8.3 : Macropores during wetting.**



### 8.4.5 Draining Example.

As a second example we consider the same site, but starting at a higher uniform moisture level. The site is assumed to be sufficiently well capped that no new water can enter from the surface



Notable in this example is the ‘reluctance’ of the micropores to release any moisture, illustrated in Figure 8.4. Again the reaction in the macropores is very rapid, with large volumes of water draining away causing the huge bulge in leachate production seen in Figure 8.5. The micropores retain almost all their original moisture over the short time period examined, as shown by Figure 8.6.

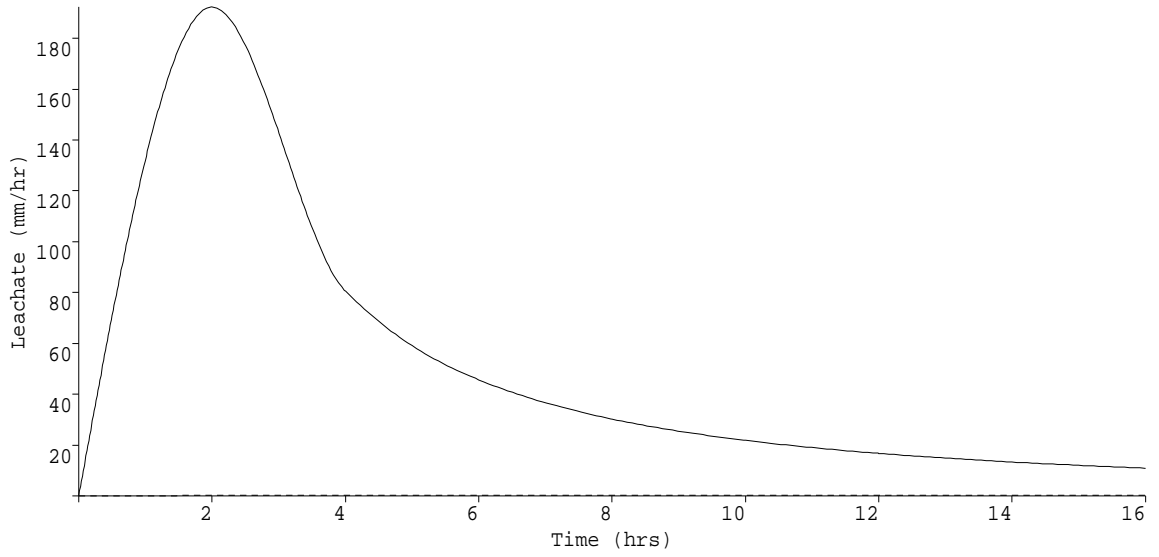
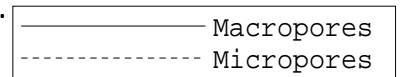


**Figure 8.5 : Flux at base of site during drying.**



### Macropore Wetness

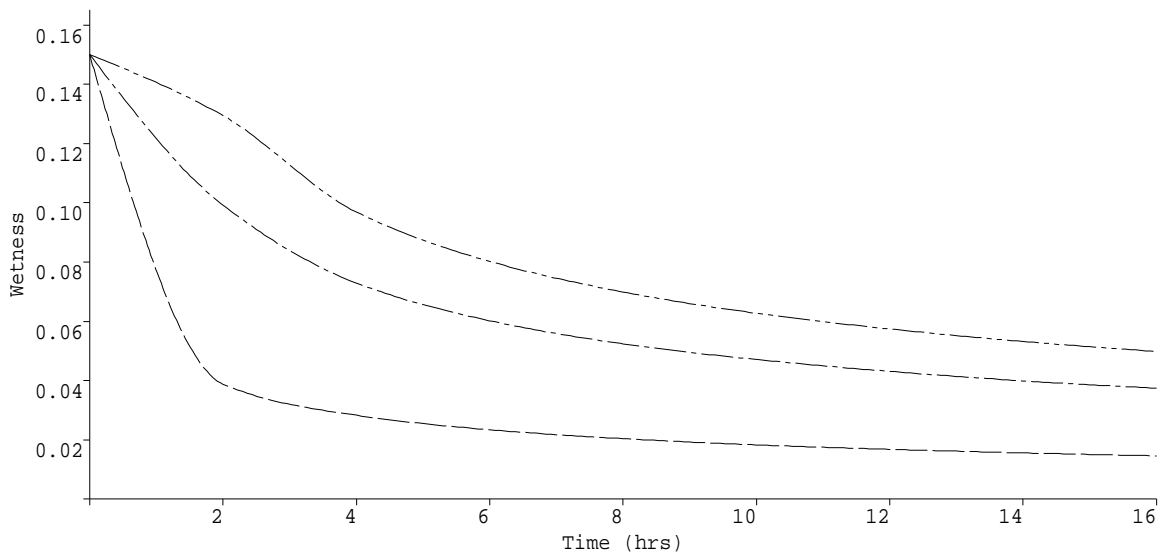
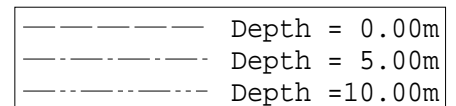


**Figure 8.6 : Macropores during drying.**





#### **8.4.6 Conclusion on Doubly-Porous Media.**

The most attractive aspect of the doubly-porous model for flow in landfills is the intuitive notion that it is in some sense more true to what is actually happening inside the site than a more conventional, but highly non-linear model. However, although the model can illustrate qualitatively some of the behaviour seen in landfills, it inevitably suffers from requiring twice the amount of data as well as some arbitrary intermedia transfer function. At present it is an exploratory tool rather than a predictive system, but the rapid drainage of the macropores suggests that for a capped landfill (so that there are no sharp transients at the site boundaries) the long-term water movement can be adequately modelled by a singly porous system.

## **Chapter 9 : Overall Summary.**

This final Chapter gathers together some of the main results from the report, and presents recommendations for further research.

### **9.1 Gas Monitoring.**

Some recent experimental evidence has suggested that there is a linkage between atmospheric pressure effects and the quantity and composition of landfill gas. Chapter 4 explored this issue to determine to what extent current gas monitoring practices represent a reliable method of determining the status and safety of a site. The model demonstrated a fundamental physical mechanism, common to all sites, which is able to cause such changes even though gas production is constant.

The main theme of this Chapter was to demonstrate that the rate of change of atmospheric pressure is much more important than the actual pressure itself.

#### **9.1.1 Volumetric Changes.**

The model's results show that the void fraction is more important than the permeability for determining changes in gas yield, and that differing values for the horizontal and vertical permeabilities influence where the gas escapes rather than how much is vented. The simulations give the following results for changes in volumetric gas yield:

[1] When the atmospheric pressure is steady, the rate of gas venting is constant and independent of the pressure.

[2] When the atmospheric pressure is rising, the rate of venting decreases by an amount proportional to the rate at which the pressure is rising.

[3] When the atmospheric pressure is falling, the rate of venting increases by an amount proportional to the rate at which the pressure is falling.

The implications of these results are that gas emissions on or adjacent to landfill sites are highest during times of rapid atmospheric pressure decrease. Also, the total amount of extra gas vented over any period is proportional to the total decrease in pressure. This effect will enhance the build up of methane and carbon dioxide concentrations in confined or poorly ventilated spaces during such periods, greatly enhancing the risk of explosions and asphyxiation.

### 9.1.2 Compositional Changes.

A more complex model was used to investigate compositional changes in landfill gas due to variations in atmospheric pressure. The following main conclusions were drawn from the results of the computer simulations

[1] The composition of vented gas can exhibit large fluctuations even though the internal generation rates are steady.

[2] Although the effects are complex, the size of the changes is likely to increase as the moisture content of the site rises, the pH of the leachate increases, or the void fraction decreases.

[3] The size of the compositional fluctuations will increase as gas production decreases. This means that gas composition measurements from older sites and regions adjacent to landfills are especially prone to mis-interpretation.

[4] The size of the compositional fluctuations is greatest near to the site surface.

[5] Gas composition exhibits hysteresis — it has a ‘history’ which must be known to make sense of any new measurement.

[6] It is impossible to gauge the state of degradation of a site from measurements of gas composition taken at a single time or at too infrequent intervals.

[7] The frequency with which much historical gas data has been gathered renders it of little value for risk assessment purposes.

[8] Future monitoring programmes must make provision for a period of frequent (at least daily) monitoring of gas composition and external weather to evaluate the variability at each monitoring location.

A field experiment was conducted at Sleaf landfill, and agreed with the model predictions regarding points [1], [4], [5], [6], [7] and [8], but could say nothing about the other items. However, the degree of agreement between the model and the tested predictions leads us to believe that [2] and [3] are essentially correct also.

In particular, in accordance with the field data, the model results show that the same rate of change of atmospheric pressure (for instance  $5\text{kPa hr}^{-1}$ ) can be associated with a wide variety of concentration levels, that the Sleaf site does not produce peaks of concentration, and furthermore that all instances of low LFG concentrations occur during periods of rising atmospheric pressure (high LFG concentrations being impossible due to the nature of the site). The similarity between the models behaviour and the sub-surface field data gives us confidence that the much larger predicted changes in surface flux are real.

Note that the permeability makes little difference to the stoichiometric behaviour,

because it affects only the gas velocity, and cannot cause the individual molecules to be vented in a different order. The gas composition is influenced not just by the instantaneous pressure changes, but also by the history of the weather over the preceding days or weeks which determines the initial position of the molecules of the individual component gases. As a result, the time-scale for gas composition to approach equilibrium under steady external conditions is several weeks, whereas the net internal pressure reaches equilibrium within a matter of hours.

Any trace gases produced within the landfill are subject to the same mechanisms as the  $CO_2$  and  $CH_4$  molecules, and will therefore show analogous alterations in concentration. Highly soluble gases, such as  $H_2S$ , should show less variation than relatively insoluble gases like  $H_2$ . Since the compositional variations decrease with depth, to assess the actual relative fractions of gas being generated it is necessary to draw samples from deep within a landfill.

It would be useful to repeat the Sleaf experiment on a site with lower gas generation rates using monitoring points nearer to the surface. A method of measuring surface flux should be found, since this may vary drastically even when the internal concentrations are almost constantly at 'saturation' levels. A laboratory experiment to investigate the tortuosity coefficient for waste would be useful.

### **9.1.3 Recommendations for Future Monitoring Practises.**

The existence of these short term variations mean that the prevailing barometric conditions should always be taken into account when using field data to assess gas generation rates and pollution hazards, and pressure data must be collected simultaneously with other readings. Since continuous barometric pressure monitors are cheap, all sites ought to have one installed immediately. As a general guideline, the model suggests that if only a small number of measurements can be made then they should be conducted during periods when the atmospheric pressure is falling — ideally when it has been falling for several days to allow  $CH_4$  and  $CO_2$  to migrate to the surface. With more resources, a period of frequent monitoring should be undertaken to assess the range of behaviours possible to a site, covering an interval sufficiently long that there are several rapid falls and rises in atmospheric pressure. Ideally some form of continuous (at least daily) monitoring should be installed in sites for the majority of their active phase.

Predictions of internal gas concentration based on  $\chi^2$  methods are seen to be inadequate for the Sleaf data-set. It is currently normal practice to attempt to infer gas production rates from much smaller data-sets (or even single measurements), and this experiment has proved that such procedures are unreliable. The only way to assess a site properly

is to gather a large data-set (at least the size of our Sleaf data) and perform a simple statistical analysis in terms of means, extrema, Standard Deviations, and (for the near surface) Correlation coefficients. Our graphical method of illustrating gas concentrations as scatterplots is a very useful way of characterizing site emissions, and I would recommend that it be adopted as a standard method of presenting monitoring results.

#### **9.1.4 The Effect of Aquifers within a Site.**

The model simulations indicated that the presence of aquifers can cause enrichment of the methane content and some lowering of internal pressure. The magnitudes of these effects cannot be determined without additional experimental evidence, particularly the rate at which gas molecules pass into and out of aqueous solution.

## 9.2 Network Pumping Installations.

This section develops a computer program which may be used by site operators to assess the efficiency of a gas extraction system while a site is still in the planning stage.

### 9.2.1 Yield Reduction Coefficients.

Most practical extraction schemes consist of several wells, which will interact with each other, so that the effective ROI of a well depends on the status of any neighbouring wells. We have quantified this interaction by introducing a parameter called the ‘yield reduction coefficient’ (YRC), which enables the flux through any single well to be expressed as a function of the suction pressures at all of the wells ( $\mu_{ij}$  measures the extent to which well  $j$  reduces the yield from well  $i$ ). For instance, if the YRC at well  $A$  due well  $B$  is 0.15 ( $\mu_{AB} = 0.15$ ) then an increase in extraction pressure of 100 Pa at well  $B$  causes the same decrease in flux at well  $A$  as if the suction at the latter were reduced by 15 Pa.

The YRCs depend only on the physical properties of the site, and are not affected by the rate of gas generation. The model predicts the following properties for the YRCs between two identical wells, labelled  $A$  and  $B$ :

- [1] As the separation of the wells increases, the YRCs decrease.
- [2] Increasing the depth of the perforated sections (but not their overall length) results in the YRCs increasing.
- [3] If well  $A$  is situated nearer to an impermeable landfill boundary than well  $B$  then  $\mu_{AB} > \mu_{BA}$  indicating that well  $B$  has a greater influence on well  $A$  than vice versa.
- [4] As the vertical permeability decreases, the YRCs increase.
- [5] As the horizontal permeability decreases, the YRCs decrease.
- [6] If the perforated section of well  $A$  is located at a shallower depth than that of well  $B$  then  $\mu_{AB} > \mu_{BA}$ .
- [7] If the length of the perforated section of well  $A$  increases then  $\mu_{AB}$  increases slightly while  $\mu_{BA}$  increases by a much larger factor.
- [8] If the radius of the perforated section of well  $A$  increases then  $\mu_{AB}$  increases slightly while  $\mu_{BA}$  increases by a much larger factor.
- [9] If the thickness of the cap is increased, or its permeability decreased, then the YRCs increase.

When the two wells are a sufficiently distant from the site boundaries, it is possible to formulate these relationships in a more precise manner. Firstly, the YRCs decrease exponentially with distance, except when the wells are extremely close together, or when they are near to impermeable boundaries. The YRCs increase linearly with increasing

horizontal permeability, and are inversely proportional to the vertical permeability of the landfill strata. There is a linear increase in the YRC as the resistance to flow of the cap decreases.

As extra wells are introduced into a landfill, all of the YRCs will change — generally decreasing, this effect being greatest for those wells nearest to the new one. Conversely the YRCs will increase when one of the wells is removed or blocked.

To precisely determine the YRCs for a real site by experimentation would require as many pumping trials as there are wells, which would be impractical on a site having many wells, though the problem is reduced if the wells are connected in clusters, (assuming each cluster is at the same extraction pressure). Additionally a well/cluster will only be significantly affected by its nearest neighbours, so simultaneous pumping trials could be carried out on different regions within the site.

Our quantification of changes in YRC with respect to separation, location, permeability and well construction should enable landfill operators to transfer field experience gained from present sites to future ones with more accuracy. However, we feel that a field trial (involving say 3 wells and 5 pumping tests) is required to validate the model, so that engineers have sufficient confidence in it to use the generated predictions.

### **9.2.2 Comparison of Surface Installations.**

The Network Pumping model allows different gas extraction schemes to be compared before installation, and the effects of changing gas production and component failures to be assessed in advance. Without the concept of YRCs developed in this project, limitations in computer power would make it impractical to predict the gas fluxes within an extraction system.

To fully exploit the power of the model requires more detailed attention to monitoring individual extraction wells that is common practice. However, if the user can estimate the well yield parameters roughly (either from measurements or previous experience) then the program will be able to produce valuable information about the comparative effectiveness of various installations. For instance, in addition to illustrating the program, the simulation results demonstrate the usefulness of installing relief pipes — both for everyday use and as a contingency against failures elsewhere. We feel that it would be useful to perform a further series of model calculations to compare generic site layouts (such as ‘radial’, ‘daisy chain’, ‘clustered’ and ‘herring-bone’).

Several extensions are possible to the basic model, and these would require calibration experiments if manufacturers were unable to supply the relevant data. For instance,

attaching generators causes a back-pressure, booster pumps may be used to aid gas flow through very long routes, condensation ‘knock-out pots’, valves and flame traps cause pressure drops, and entrained water may interfere with flow. In long pipes some condensation may take place in cold weather, but since the gas velocity is known at all points it would be possible to calculate the rate at which it cools on the way to the pumps, and hence to determine the amount of condensation likely to take place at any location (and thus the potential for blockages and ice-plugs).

There is no theoretical limit to the complexity of a site which can be modelled by the computer program. Without modification the procedure can cope with multiple networks being installed on the same site — for instance a utilisation scheme surrounded by a second un-connected network which over-sucks to prevent gas excursion. The program devised during the project is fast enough to be used by engineers on an interactive basis. With additional development work and the creation of a larger database describing landfill components this system would be an invaluable tool for site planners and operators.

### **9.3 Biological Processes.**

The action of the bacteria within a site is a primary mechanism regulating its temperature, chemical composition and physical structure (ie. the saturation, permeability and density) and these factors in turn determine the viability of the many microbial species present. One of the primary goals of the project was therefore to develop a model to study the establishment of the landfill ecosystem, and in particular the methanogens since they seem to be more sensitive to adverse conditions than the other species.

When the model was subjected to a variety of initial conditions it responded in a sensible fashion and eventually settled down to some steady state, though without methanogenesis under the harsher starting regimes. Given the amount of variance between real landfill sites, the behaviour of this model falls well within the range of observed characteristics.

The lack of data which prevented fully incorporating feedback effects into the pH and temperature means that the model has little predictive power regarding acidogenesis. In particular, we were forced to incorporate the ‘standard’ division of waste into three different ‘half-life’ categories. However the simpler nature of methanogenesis allows much useful information to be extracted about it. The inclusion of spatial effects did not seem worth attempting until some of the biological and chemical problems highlighted by the model have been satisfactorily resolved by experimentation.



### **9.3.1 Laboratory Study.**

A special study at Strathclyde University (Watson-Craik and Goldie, 1991) found that the temperature behaviour of methanogens agreed with the literature, but that the bacteria are significantly more tolerant of acidic pH conditions than is normally assumed. It was impossible to assess the relative importance of direct substrate inhibition versus indirect pH-inhibition effects in the acetoclastic reactions. It would be valuable to extend the scope of these experiments.

Also, it would be valuable to conduct experiments on the effects of moisture content within waste, especially as the newer containment landfills may have quite arid interiors while laboratory studies have generally confined themselves to very wet waste for reasons of speed and convenience.

Field observations generally do not distinguish whether methanogenesis from acetate cleavage or carbon dioxide reduction comes first. Knowledge of the links between these two processes would be useful — for instance it may be that monitoring hydrogen concentration can provide information about the establishment of acetate cleavage and hence give early warning of sites behaviour. This is especially important if both reactions are performed by the same species, in which case microbiological research on the switching mechanisms and critical concentrations should be carried out.

### **9.3.2 Thermal Effects.**

It seems that thermal feedback effects within a landfill cannot be realistically incorporated into a model without introducing a spatial dimension. However, calculations indicate that during the critical period in which methanogenesis is established (or fails) anaerobic decomposition is producing insufficient heat (under typical U.K. conditions — see the section in Chapter 7 on gas enhancement) to significantly change the temperature in any case.

### **9.3.3 Aerobic Pre-digestion.**

Increasing the amount of readily-degradable waste indefinitely does not increase the rate of the establishment of methanogenesis, and indeed if there is too much readily-degradable waste present then the initial acid production will kill the methanogens.

At some landfills taking pulverized waste which has gone through an initial aerobic phase, it has been observed that methanogenesis is established faster, and this may be due to the high rate of aerobic degradation removing much of the readily-degradable substrate and/or the higher initial temperature (and possibly also due to increased availability of metals — see below). Some experimentation is required here, as it may be beneficial to adopt a policy of exposing some or all of landfill waste to oxygen before infilling.

### **9.3.4 The Influence of Metals.**

Low alkali metal concentrations are frequently associated with a failure of methanogenesis to develop, and this has been attributed to some of these metals being essential nutrients for the bacteria. The model shows that low alkali metal concentrations mean the leachate is poorly buffered against the carboxylic acids so that the pH may fall too quickly for the methanogenic population to reach a self-regulating size, and furthermore that this effect is more important than nutritional aspects, since the levels required for adequate buffering are above those at which the bacterium's nutritional requirements are satisfied. Also, the model implies that the landfill system requires both 'permanent' buffering (cations which remain in solution at neutral pH levels) together with 'variable' buffering (cations whose solubility increases enormously as the leachate becomes more acid) if the methanogens are to prosper.

This pH dependent nature of the cation concentration greatly enhances the homeostatic influence of the bacteria, and allows them to maintain the leachate in a near-neutral state while still having adequately high levels of acid present to act as substrate. Some experimental work is required to assess the availability of alkali metals within waste, and the rate at which they come into solution — which, if they are initially bound within the organic fraction of the waste, will be affected by the amount of degradation which has taken place, and perhaps also by any initial aerobic phase.

### **9.3.5 Diffusion.**

Diffusion limitations within the liquid mean that the levels of dissolved gases present in the water held within the smaller waste pores (eg. soaked into paper) will be above the equilibrium values predicted from Henry's law, and could even be several times higher. The dissolved concentration is highly relevant to bacterial metabolism, and the present practise of inferring bacterial activity using gas samples from the void space has not been validated experimentally, and is therefore unsound. A laboratory experiment is essential to determine the rate at which gas molecules are evolved from the waste mass and pass across the liquid-gas interface — an initial step would to isolate samples of waste in a vacuum chamber to determine the amount of dissolved gas actually held within them. This data is also required to improve our models of Chapters 4 and 7.

## **9.4 Thermal Regulation.**

The internal temperature of landfills has long been thought to be one of the primary factors affecting their behaviour. Chapter 7 explored the physical and biological processes controlling landfill temperature.

### **9.4.1 Natural Warming of Landfills.**

First we considered the thermodynamics of the degradation reactions whilst ignoring spatial variability to give an estimate of the maximum possible rate of warming. It was assumed that all gas inside a landfill is saturated with water, so that for each mole of LFG produced the requisite amount of water must be evaporated to saturate it (this amount being highly dependent on the temperature). Under these assumptions, the theoretical maximum temperature that may be achieved in a fully anaerobic landfill is 73°C.

This implies that any landfill approaching 70°C cannot be completely anaerobic. The occurrence of such temperatures in sites (especially shallow ones) is an indicator that oxygen is reaching the interior, and operators should check for over-pumping and cracks in the cover material.

#### **9.4.2 Rate of Temperature Rise.**

The depth of a site greatly influences both the rate of warming of the site and the final temperature that it reaches. Numerous runs of the model show that the rate of warming is fairly slow, only a few degrees per year. We conclude that the early temperature of any particular site depends to a large degree on the temperature reached during the earlier stage of aerobic degradation, and that methods of raising this initial value should be investigated.

Consideration of insulation effects leads us to recommend that sites should have a minimum depth of 15 m, and preferably greater than 20 m.

#### **9.4.3 Long-term Comparison of Wet and Dry Sites.**

A key question in the management of landfills is whether (or to what degree) rainwater should be excluded from sites, and the model was used to investigate this. In order to investigate different strategies for controlling the moisture content of landfills we need to consider a combined model for the flows of heat, gas and moisture within the site. An age factor was incorporated to allow for the changes occurring in the waste due to decomposition.

The model predicts that wet sites undergo an initial rapid warming period, after which a high temperature is maintained until the degradation nears completion when the reaction rate and temperature fall. The model shows clearly that the cause of the drop in the activity of the site is the reduction of waste mass through anaerobic degradation. After 50 years the temperature and gas production of a dry site is similar to that of a wet site, but in this case the model indicates that it is the lack of water rather than the lack of degradable waste that halts the reaction, and adding water (which may happen accidentally if the cap cracks) restarts the processes once again.

Dry landfills with their low levels of leachate and gas production pose fewer problems in their management than wet sites. However they offer little potential for power generation and remain active (even if only at a low level) for longer periods, thus requiring extra expenditure on monitoring. It is our opinion that it would be far easier, safer and (ultimately) less expensive to use wet landfills to process the waste now.

#### **9.4.4 Enhancing Methane Production**

It is usually economic factors that decide whether or not LFG is utilised or simply flared off. This section proposed a scheme for exploiting the landfill gas at those sites where flows are below the current threshold for profitable electricity generation. The scheme involves using the heat produced by burning some of the gas to warm the landfill site itself, thus raising the internal temperature and thereby increasing the rate of gas production. By re-injecting unburnt heated LFG into the site, the anaerobic environment is not compromised and the quality of the gas yield is maintained.

In addition to controlling the temperature within the radius of influence of the injection well, the process allows the moisture level within a site to be regulated by introducing or excluding water vapour. The model predicts that the increased temperature and controlled moisture should enable the optimum environment for the methanogenic bacteria to be achieved and maintained. The faster reaction rates would give shorter completion times, and the large throughput of gas could be used to 'scrub' some of the pollutants out of the waste before they could reach the leachate.

We feel that this scheme should be carried out on a trial basis after some smaller scale experiments. Firstly it is necessary to carry out pumping trials to investigate the forces required to re-inject gas into a landfill, and also some laboratory work is needed to assess the response of methanogens to rapidly rising temperatures and the possibility of establishing a thermophilic culture.

### **9.5 Miscellaneous Topics.**

#### **9.5.1 Settlement.**

At present there is no useful scientific evidence with which a model of landfill settlement can be constructed. As a preliminary step, an experimental determination of the bulk modulus of various types of fill is required, ideally investigating several categories of waste and mixtures thereof, both fresh and decomposed, so that a table can be constructed relating the physical properties of waste to its composition. Such data could be used to develop a predictive model as originally envisaged.

### **9.5.2 Methane Oxidation.**

Aerobic bacteria within soil are capable of oxidizing methane escaping from landfills, and properly applied could provide a means of limiting methane migration. It was concluded that most of the parameters required to model the processes are already known, and that a laboratory experiment is required to determine the metabolic parameters of the bacteria.

### **9.5.3 Doubly-Porous Media.**

The doubly-porous water flow model can illustrate qualitatively some of the behaviour seen in landfills, but due to difficulties in obtaining calibration data (in particular the rate at which water moves between the major and minor voids) it cannot be used as a predictive tool. The results suggest that for a capped landfill the long-term water movement can be adequately modelled by a more standard singly-porous approximation.

## **9.6 Afterword.**

This project can only be considered successful if its conclusions are widely disseminated and acted upon.

## Appendix 3A : Finite Element Algorithm.

In this appendix we give a brief sketch of the numerical algorithm used to solve equation (3.11), a more rigorous treatment of finite element methods may be found in Davies (1980). The extensions for convection terms are simple.

Our aim is to find solutions  $P$  of the  $2^{ND}$  order parabolic equation

$$C \frac{\partial A}{\partial t} = \frac{\partial}{\partial z} \left( D \frac{\partial A}{\partial z} \right) + G, \quad (1)$$

where  $t$  is time,  $z$  is depth, and  $C, D, G$  are functions of  $z, t, A$ . The equation is to be solved on the region  $0 < z < d$  subject to initial and boundary conditions, with the latter possibly varying with  $t$ . We divide this region into  $n-1$  elements by taking  $n$  points  $0 = d_1 < d_2 < \dots < d_n = d$  across the depth, and attempt to represent  $P$  as a piecewise linear function, of the form

$$P(t, z) = \sum_{i=1}^n A_i(t) \Lambda_i(z), \quad (2)$$

where the  $\Lambda_i$  are triangular ‘hat-functions’, defined as

$$\Lambda_i(z) = \begin{cases} \frac{z - d_{i-1}}{l_{i-1}}, & d_{i-1} < z \leq d_i; \\ \frac{d_{i+1} - z}{l_i}, & d_i \leq z < d_{i+1}; \\ 0, & \text{elsewhere,} \end{cases} \quad (3)$$

with  $l_i = d_{i+1} - d_i$  being the length of the  $i$ th element. Thus the value of our approximation to  $P$  at the  $i$ th node is exactly  $A_i(t)$ , with  $P$  changing linearly between the nodes. The use of these triangular basis functions gives good mass conservation in regions where  $P$  varies sharply with  $z$ . Given a set of coefficients  $A_1^{(0)}, \dots, A_n^{(0)}$  which describe  $P$  at time  $t_0$ , we wish to compute another set  $A_1, \dots, A_n$  to approximate  $P$  at the later time  $t_0 + h$ , and this may be done as follows :

Multiply (1) by  $\Lambda_j$  and integrate (using the method of ‘parts’) over the full depth to get the exact expression

$$\int_0^d C \frac{\partial P}{\partial t} \Lambda_j dz = \left[ D \frac{\partial P}{\partial z} \Lambda_j \right]_0^d - \int_0^d D \frac{\partial P}{\partial z} \Lambda_j' dz + \int_0^d G \Lambda_j dz. \quad (4)$$

Assume next that  $C, D, G$  are approximately constant across each of the elements, so that  $C \approx C_i$  for  $d_i < z < d_{i+1}$  etc. Substitute (2) into (4) using (3), noting that  $\Lambda_i$  and  $\Lambda_j$  have no interaction when  $i$  and  $j$  differ by more than  $\pm 1$ , to get the equation

$$\begin{aligned} \frac{1}{6} l_{j-1} C_{j-1} \frac{\partial A_{j-1}}{\partial t} + \frac{1}{3} l_{j-1} C_{j-1} \frac{\partial A_j}{\partial t} + \frac{1}{3} l_j C_j \frac{\partial A_j}{\partial t} + \frac{1}{6} l_j C_j \frac{\partial A_{j+1}}{\partial t} &= \left[ D \frac{\partial P}{\partial z} \Lambda_j \right]_{z=0}^d \\ + \frac{1}{l_{j-1}} D_{j-1} A_{j-1} - \frac{1}{l_{j-1}} D_{j-1} A_j - \frac{1}{l_j} D_j A_j + \frac{1}{l_j} D_j A_{j+1} + \frac{1}{2} l_{j-1} G_{j-1} + \frac{1}{2} l_j G_j. \end{aligned} \quad (5)$$

The time derivative  $\frac{\partial A_i}{\partial t}$  may be approximated by the formula

$$\frac{\partial A_i}{\partial t} \approx \frac{A_i - A_i^{(0)}}{h}, \quad (6)$$

and for an internal node ( $j = 2, \dots, n-1$ ) the contribution from the boundary terms vanishes, to give the recurrence relation

$$\begin{aligned} & \left( \frac{l_{j-1}C_{j-1}}{6h} - \frac{D_{j-1}}{l_{j-1}} \right) A_{j-1} + \left( \frac{l_{j-1}C_{j-1}}{3h} + \frac{D_{j-1}}{l_{j-1}} + \frac{l_j C_j}{3h} + \frac{D_j}{l_j} \right) A_j + \left( \frac{l_j C_j}{6h} - \frac{D_j}{l_j} \right) A_{j+1} \\ & = \frac{l_{j-1}C_{j-1}}{6h} A_{j-1}^{(0)} + \left( \frac{l_{j-1}C_{j-1}}{3h} + \frac{l_j C_j}{3h} \right) A_j^{(0)} + \frac{l_j C_j}{6h} A_{j+1}^{(0)} + \frac{1}{2} l_{j-1} G_{j-1} + \frac{1}{2} l_j G_j. \end{aligned} \quad (7)$$

At the end  $z = 0$ ,  $P$  must have the known value  $P_{atm}$ , and this is imposed on our solution by fixing

$$A_1 = P_{atm}. \quad (8)$$

At the lower end, it is assumed that there is no gas flux through the landfill base, so that

$$D \frac{\partial P}{\partial z} = 0 \quad \text{at} \quad z = d, \quad (9)$$

and using equation (12) this corresponds to

$$\left( \frac{l_{n-1}C_{n-1}}{6h} - \frac{D_{n-1}}{l_{n-1}} \right) A_{n-1} + \left( \frac{l_{n-1}C_{n-1}}{3h} + \frac{D_{n-1}}{l_{n-1}} \right) A_n = \frac{l_{n-1}C_{n-1}}{6h} A_{n-1}^{(0)} + \frac{l_{n-1}C_{n-1}}{3h} A_n^{(0)} + \frac{1}{2} l_{n-1} G_{n-1}. \quad (10)$$

The relations (8,9,10) form a tri-diagonal system of  $n$  simultaneous linear equations for the variables  $A_1, \dots, A_n$  and these may be solved by Gaussian elimination.



## Appendix 3B : 3-Dimensional ADI Method.

The Alternating Direction Implicit method is based on the idea of operator splitting, whereby a difference equation with several implicit steps is approximated by several sub-equations which each have only a single implicit step.

The basic equation under discussion is

$$C \frac{\partial \Phi}{\partial t} + (\underline{V} \cdot \nabla) \Phi = \text{div}(\underline{D} \nabla \Phi) + F \Phi + G, \quad (1)$$

where  $C$ ,  $\underline{D}$ ,  $\underline{V}$ ,  $F$  and  $G$  are independent of  $t$  and  $\varphi$ . The diffusion tensor  $\underline{D}$  is assumed to be in diagonal form, so that equation (1) may be expanded as

$$C \frac{\partial \Phi}{\partial t} = \frac{\partial}{\partial x} \left( D_1 \frac{\partial \Phi}{\partial x} \right) + \frac{\partial}{\partial y} \left( D_2 \frac{\partial \Phi}{\partial y} \right) + \frac{\partial}{\partial z} \left( D_3 \frac{\partial \Phi}{\partial z} \right) - V_1 \frac{\partial \Phi}{\partial x} - V_2 \frac{\partial \Phi}{\partial y} - V_3 \frac{\partial \Phi}{\partial z} + F \Phi + G, \quad (2)$$

taking  $\underline{r} = (x, y, z) = (x_1, x_2, x_3)$  to be a triad of right-handed orthonormal axes. We seek to solve this on a rectilinear domain  $\Omega$  defined as

$$\Omega = \{ \underline{r} | a_1 < x_1 < b_1 \cap a_2 < x_2 < b_2 \cap a_3 < x_3 < b_3 \} = \Omega_1 \times \Omega_2 \times \Omega_3, \quad (3)$$

subject to a mixture of Dirichlet, Neumann, Radiation and Flux boundary conditions.

### 3B.1 Basic ADI Algorithm.

Define the operator  $\Lambda_i$  as

$$\Lambda_i(\psi) = \frac{\partial}{\partial x_i} \left( D_i \frac{\partial \psi}{\partial x_i} \right) - V_i \frac{\partial \psi}{\partial x_i} + \frac{1}{3} F \psi, \quad (4)$$

then equation (1) becomes

$$C \frac{\partial \Phi}{\partial t} = \Lambda_1(\Phi) + \Lambda_2(\Phi) + \Lambda_3(\Phi) + G. \quad (5)$$

Divide  $\Omega$  by a rectilinear mesh and let  $\varphi$  be a discretisation of  $\Phi$  upon this mesh, and  $\mathcal{L}$  a finite difference operator, such that

$$\varphi \approx \Phi, \quad \mathcal{L}_i(\varphi) \approx \Lambda_i(\Phi). \quad (6)$$

then a semi-implicit difference equation approximating (1) can be written as

$$C \frac{\varphi^* - \varphi^\emptyset}{\delta t} = \sum_{i=1}^3 \left( \theta_i \mathcal{L}_i(\varphi^*) + (1 - \theta_i) \mathcal{L}_i(\varphi^\emptyset) \right) + G, \quad (7)$$

where each the superscripts ‘\*’ and ‘ $\emptyset$ ’ refer to the new and old values of  $\varphi$ , and the  $\theta_i$  are constants in the range  $[0, 1]$ . Note that for  $\theta_i = 0$  the method is fully explicit along the  $x_i$  axis, and for  $\theta_i = 1$  the method is fully implicit along the  $x_i$  axis.

This may be decomposed into 3 consecutive operations over the pseudo-time intervals  $[\emptyset, \emptyset_1]$ ,  $[\emptyset_1, \emptyset_2]$ ,  $[\emptyset_2, *]$ , so that during the overall updating process  $\varphi$  passes through two intermediate stages  $\varphi^\emptyset \rightarrow \varphi^{\emptyset_1} \rightarrow \varphi^{\emptyset_2} \rightarrow \varphi^*$ , thus

$$\begin{aligned} \frac{C}{\delta t} (\varphi^{\emptyset_1} - \varphi^\emptyset) &= \theta_{11} \mathcal{L}_1(\varphi^{\emptyset_1}) + \theta_{12} \mathcal{L}_2(\varphi^\emptyset) + \theta_{13} \mathcal{L}_3(\varphi^\emptyset) + \tau_1 G, \\ \frac{C}{\delta t} (\varphi^{\emptyset_2} - \varphi^{\emptyset_1}) &= \theta_{21} \mathcal{L}_1(\varphi^{\emptyset_1}) + \theta_{22} \mathcal{L}_2(\varphi^{\emptyset_2}) + \theta_{23} \mathcal{L}_3(\varphi^{\emptyset_1}) + \tau_2 G, \\ \frac{C}{\delta t} (\varphi^* - \varphi^{\emptyset_2}) &= \theta_{31} \mathcal{L}_1(\varphi^{\emptyset_2}) + \theta_{32} \mathcal{L}_2(\varphi^{\emptyset_2}) + \theta_{33} \mathcal{L}_3(\varphi^*) + \tau_3 G \end{aligned} \quad (8)$$

where

$$\tau_i = \frac{\theta_{i1} + \theta_{i2} + \theta_{i3}}{3}, \quad \theta_i = \theta_{ii}, \quad \sum_{j=1}^3 \theta_{ji} = 1. \quad (9)$$

### 3B.1.1 Form of the $\mathcal{L}$ Operator

The  $\mathcal{L}$  symbol is a difference operator in one space dimension along the  $x_i$  axis. We subdivide this axis  $\Omega_i$  into  $K$  parts, labelling the junction nodes as  $z_0, z_1, \dots, z_{K-1}$ , and writing

$$h_j = z_j - z_{j-1}, \quad \text{for } j = 1, \dots, K-1. \quad (10)$$

Denoting the value of  $\varphi$  at  $z_k$  by  $U_k$  for clarity, allows  $\mathcal{L}$  to be decomposed as follows: use central differencing for the diffusion term\* to give

$$\begin{aligned} \frac{\partial}{\partial x} \left( D \frac{\partial U}{\partial x} \right) &\approx \frac{D_k \frac{U_{k+1} - U_k}{h_{k+1}} - D_{k-1} \frac{U_k - U_{k-1}}{h_k}}{\frac{1}{2}(h_{k+1} + h_k)}, \\ &= \frac{2D_k}{h_{k+1}(h_{k+1} + h_k)} U_{k+1} - \left( \frac{2D_k}{h_{k+1}(h_{k+1} + h_k)} + \frac{2D_{k-1}}{h_k(h_{k+1} + h_k)} \right) U_k + \frac{2D_{k-1}}{h_k(h_{k+1} + h_k)} U_{k-1}, \\ &= \alpha_k D_k U_{k+1} - (\alpha_k D_k + \beta_k D_{k-1}) U_k + \beta_k D_{k-1} U_{k-1}, \quad \text{say.} \end{aligned} \quad (11)$$

where  $D_k$  is the average value of  $D$  across  $z_k, z_{k+1}$ . Upwind differencing is employed with the convection term thus

$$V \frac{\partial U}{\partial x} \approx \begin{cases} V_k \frac{U_k - U_{k-1}}{h_k}, & \text{for } V_k > 0; \\ V_k \frac{U_{k+1} - U_k}{h_{k+1}}, & \text{for } V_k < 0; \end{cases} \quad (12)$$

noting that  $V(z_k) = V_k > 0$  corresponds to flow in the positive direction. The remaining part of  $\mathcal{L}$  is simply

$$\frac{1}{3} F U_k. \quad (13)$$

Using the formulation of (11,12,13) means that the implicit sections of (8) form a tri-diagonal system, and the explicit sections may simply be evaluated immediately from the known function values.

---

\* We use  $D_j$  to denote the mid-point/mean value of  $D$  between  $z_j$  and  $z_{j+1}$ .

## **Appendix 4A : The Loscoe Explosion.**

The explosion at Loscoe in 1986 brought the dangers of uncontrolled landfill gas migration dramatically to public attention, and it has figured prominently in discussions about landfill hazards ever since.

However, despite a public inquiry the exact reason for the explosion was never determined. The weather was suggested as a probable cause, but there had been little gas monitoring prior to the explosion and this hypothesis could not be substantiated. In this Appendix we apply the computer model of Chapter 4 to this event.

## 4A.1 Events at Loscoe.

The landfill site at Loscoe had previously been used as a brick quarry for over a century, and during this period housing developments had come to surround it on all sides. After the closure of the brickworks, a licence was granted for limited tipping which began in 1974. This licence was extended, so that when disposal ceased in 1982 the site contained 200,000 tonnes of waste, almost 60,000 tonnes of which were domestic and commercial wastes.

After closure the site was capped and some landscaping work carried out. However there was no active ventilation installed, so that the cap encouraged gas to migrate laterally along adjacent strata. From 1981 onwards several nearby residents began to notice unusual changes in patches of soil, particularly the death of vegetation and local heating, and eventually these were reported to the District Council. As first it was assumed that a coal seam was responsible, but by 1985 an analysis of the gas composition had thrown suspicion onto the landfill. On 24th March, 1986, a gas explosion completely demolished 51 Clarke Avenue.

After the incident a considerable site investigation was carried out. It was estimated that the landfill was producing over 1300 m<sup>3</sup> of gas per day, and surface measurements near the demolished region showed levels of methane ranging from 0.025% to 32.9% over the following month, with carbon dioxide varying between 0.1% and 30.1% over the same time.

The main gas migration pathway between the landfill and the explosion is likely to have been a 60 m long block of sandstone which inclined upwards from the side of the landfill towards the surface at Clarke Avenue. Using the best available data for the physical properties of this slab, we have used the model to estimate the volumes and concentrations of gases moving through it during the period prior to the incident.

Figure 5A.1 shows the atmospheric pressure over Loscoe during 60 days covering February and March 1986, together with the simulated gas flux passing through the sandstone layer and out of the ground surface during the same period. Note the sudden large drop in barometric pressure on day 52 when the explosion occurred, and the simultaneous surge in gas movement — this surge is five times the average level, and over twice the size of the largest of the other peaks.

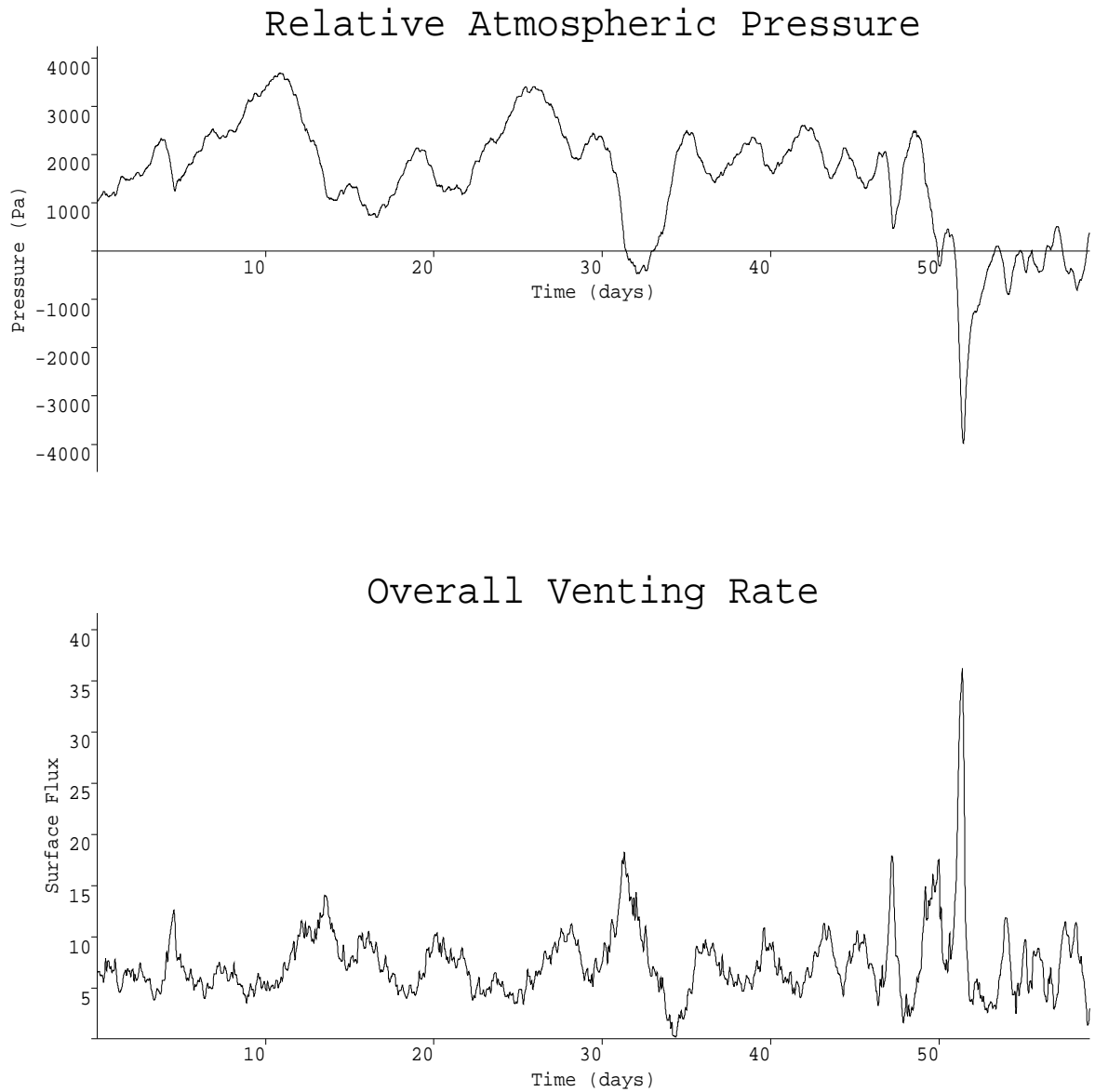


**Figure 4A.1 :** Barometric pressure and predicted surface flux at Loscoe.

Compositional predictions show that the fraction of methane in the gas would also have been raised slightly, but this is much less significant than the total flux increase. Thus, all other factors being equal, the computer reconstruction provides very strong support for the belief that a sudden drop in atmospheric pressure was the primary trigger factor for the explosion.

## Appendix 4B : Experimental Results from Sleep.

This appendix tabulates results from the gas monitoring program at Sleep Landfill. The Standard Deviation of the gas concentration measurements  $\{C_1, C_2, \dots, C_N\}$  is defined as

$$\text{St.Dev} = \sqrt{\frac{\sum_{i=1}^N (C_i - \bar{C})^2}{N}}, \quad (1)$$

where  $\bar{C}$  is the mean  $\sum C_i/N$  of the sample. The correlations given are those between the gas concentration and either the atmospheric pressure ( $P_i$ ) or its rate of change ( $dP_i/dt$ ), thus

$$\text{Cor}(P) = \frac{\sum_{i=1}^N (C_i - \bar{C})(P_i - \bar{P})}{\sqrt{\sum_{i=1}^N (C_i - \bar{C})^2 \sum_{i=1}^N (P_i - \bar{P})^2}}. \quad (2)$$

with a similar formula for  $\text{Cor}(dP/dt)$ . Note that  $\text{Cor} = \pm 1$  implies that there is a pure linear relationship between the two sets of variables, and lesser values (i.e. closer to zero) indicate that a linear fit is less applicable. A positive value for  $\text{Cor}(P)$  indicates that high gas concentrations tend to be associated with period of high atmospheric pressure, whereas a negative value means that high gas concentrations are more common when the atmospheric pressure is below average.

**Table 4B.1 : Total Pressure Against Depth.**

Depth	Minimum	Maximum	Range	Mean	St.Dev	Cor( $P$ )	Cor( $dP/dt$ )
1	982	1034	52	1013.5	11.3	0.995	0.375
2	982	1033	51	1012.9	11.5	0.992	0.385
5	983	1033	50	1013.2	11.3	0.995	0.390

**Table 4B.2 : Methane % Concentration Against Depth.**

Depth	Minimum	Maximum	Range	Mean	St.Dev	Cor( $P$ )	Cor( $dP/dt$ )
1	15.7	72	56.3	62.97	6.71	-0.040	-0.336
2	33.4	75.5	42.1	65.5	3.72	-0.107	-0.180
5	23.9	69.8	45.9	61.1	4.38	-0.060	-0.059

**Table 4B.3 : Carbon Dioxide % Concentration Against Depth.**

Depth	Minimum	Maximum	Range	Mean	St.Dev	Cor( <i>P</i> )	Cor( <i>dP/dt</i> )
1	6.5	29.1	22.6	24.5	2.71	-0.090	-0.162
2	12.8	27.1	14.3	24.3	1.34	-0.104	-0.023
5	11.4	31.2	19.8	28.1	2.04	-0.009	-0.032

**Table 4B.4 : Oxygen % Concentration Against Depth.**

Depth	Minimum	Maximum	Range	Mean	St.Dev	Cor( <i>P</i> )	Cor( <i>dP/dt</i> )
1	0.4	15.2	14.8	0.88	1.59	0.022	0.200
2	0.3	10.0	9.7	0.619	0.81	0.004	0.063
5	0.2	11.9	11.7	0.696	1.167	0.013	0.096

**Table 4B.5 : % Concentrations at 1m Depth.**

Gas	Minimum	Maximum	Range	Mean	St.Dev	Cor( <i>P</i> )	Cor( <i>dP/dt</i> )
<i>CH</i> <sub>4</sub>	15.7	72	56.3	62.97	6.71	-0.040	-0.336
<i>CO</i> <sub>2</sub>	6.5	29.1	22.6	24.5	2.71	-0.104	-0.023
<i>O</i> <sub>2</sub>	0.4	15.2	14.8	0.88	1.59	0.022	0.200

**Table 4B.6 : % Concentrations at 2m Depth.**

Gas	Minimum	Maximum	Range	Mean	St.Dev	Cor( <i>P</i> )	Cor( <i>dP/dt</i> )
<i>CH</i> <sub>4</sub>	33.4	75.5	42.1	65.5	3.72	-0.107	-0.180
<i>CO</i> <sub>2</sub>	12.8	27.1	14.3	24.3	1.34	-0.104	-0.023
<i>O</i> <sub>2</sub>	0.3	10.0	9.7	0.619	0.81	0.004	0.063



**Table 4B.7 : % Concentrations at 5m Depth.**

Gas	Minimum	Maximum	Range	Mean	St.Dev	Cor( $P$ )	Cor( $dP/dt$ )
$CH_4$	23.9	69.8	45.9	61.1	4.38	-0.060	-0.059
$CO_2$	11.4	31.2	19.8	28.1	2.04	-0.009	-0.032
$O_2$	0.2	11.9	11.7	0.696	1.167	0.013	0.096

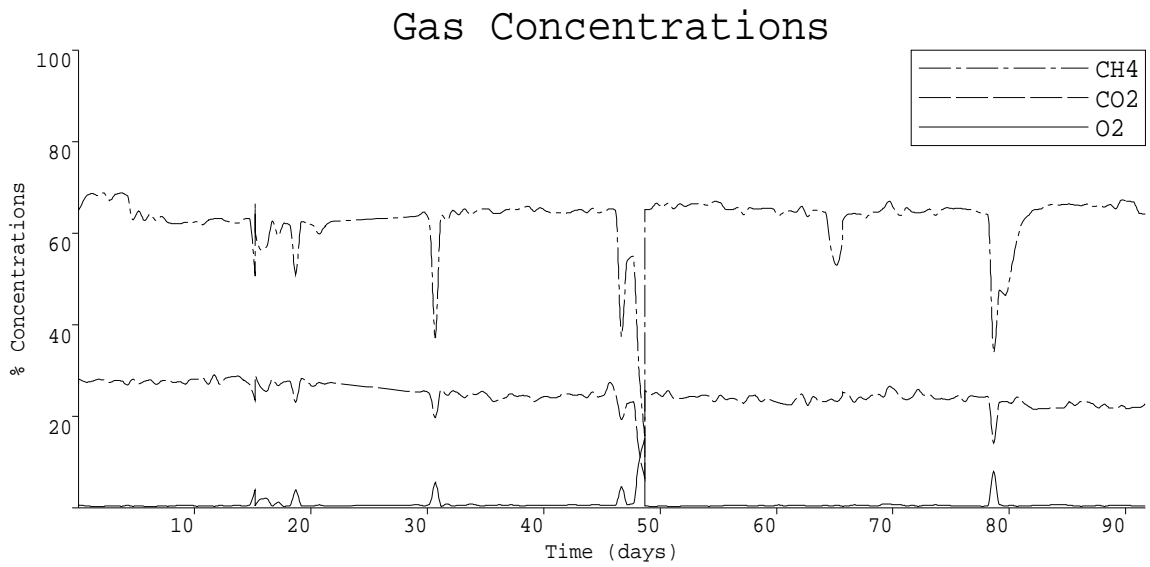
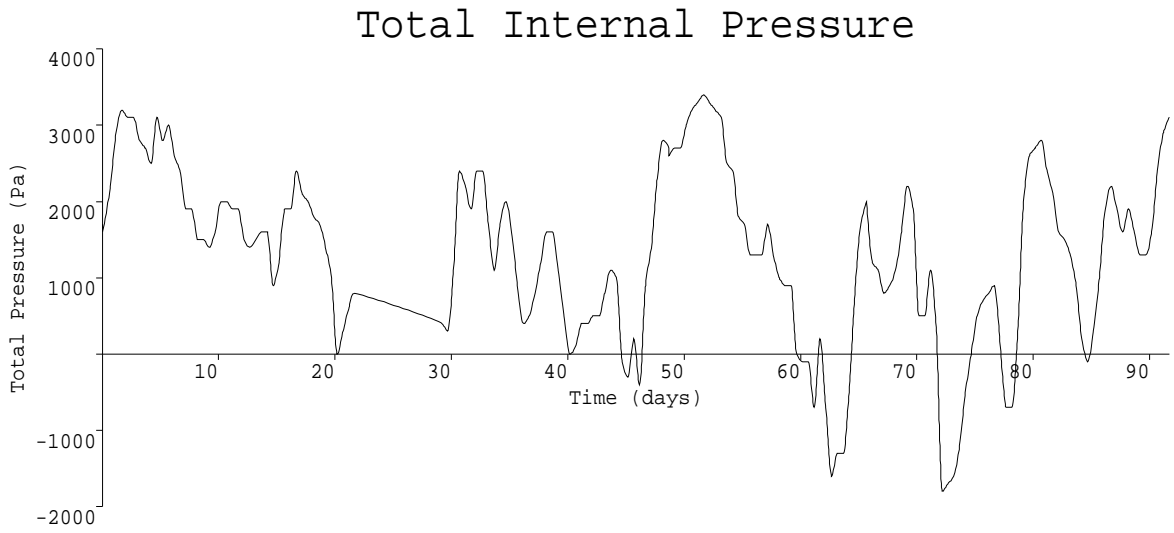


**Figure 4B.1 : Gas pressures within borehole at 1 m depth.**

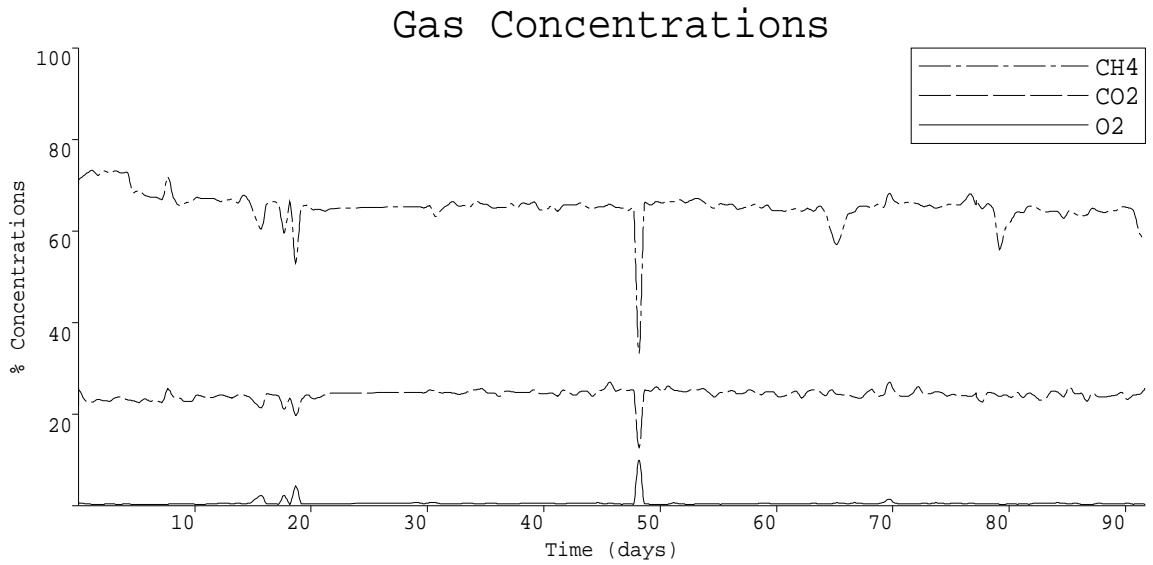
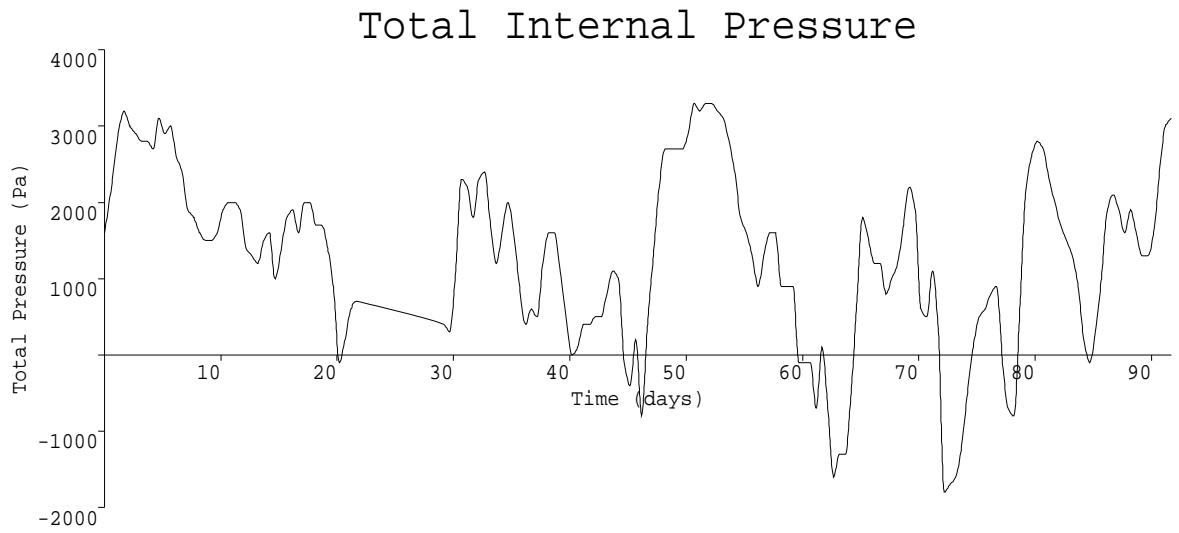


**Figure 4B.2 :** Gas pressures within borehole at 2 m depth.

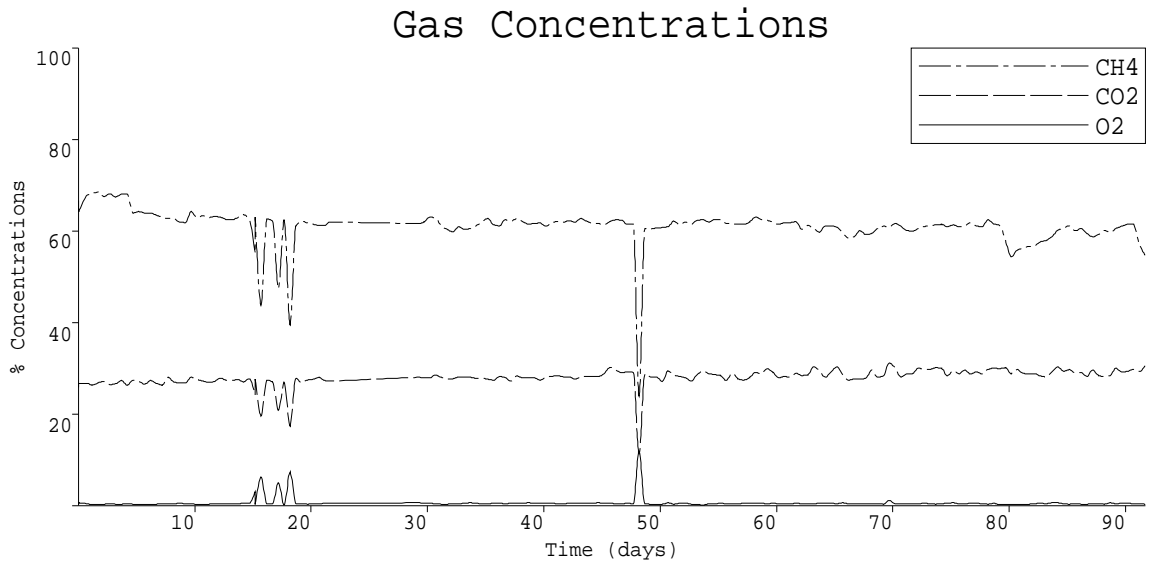
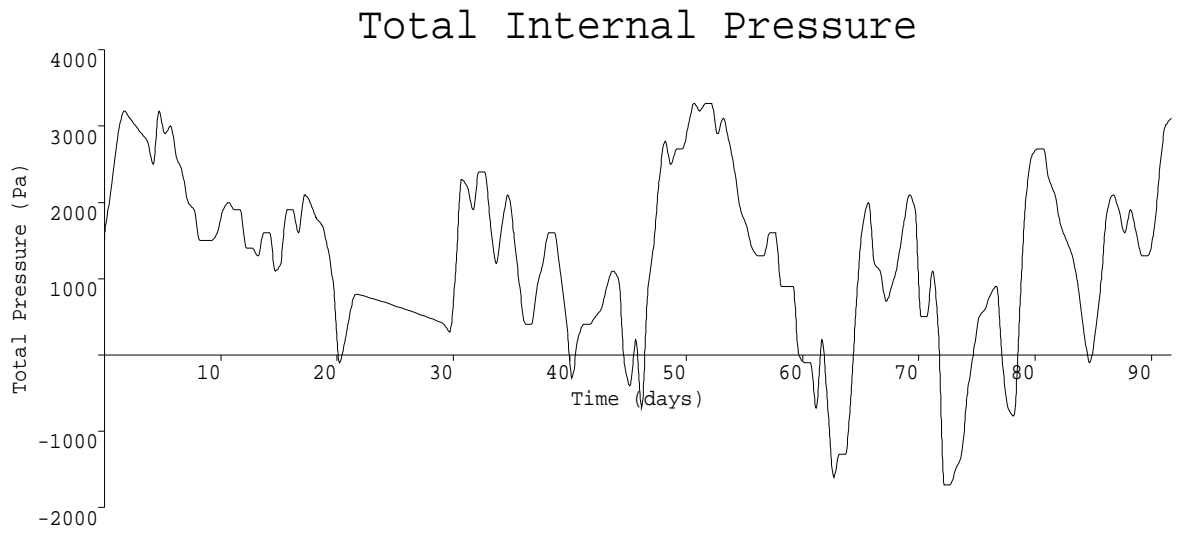


**Figure 4B.3 :** Gas pressures within borehole at 5 m depth.

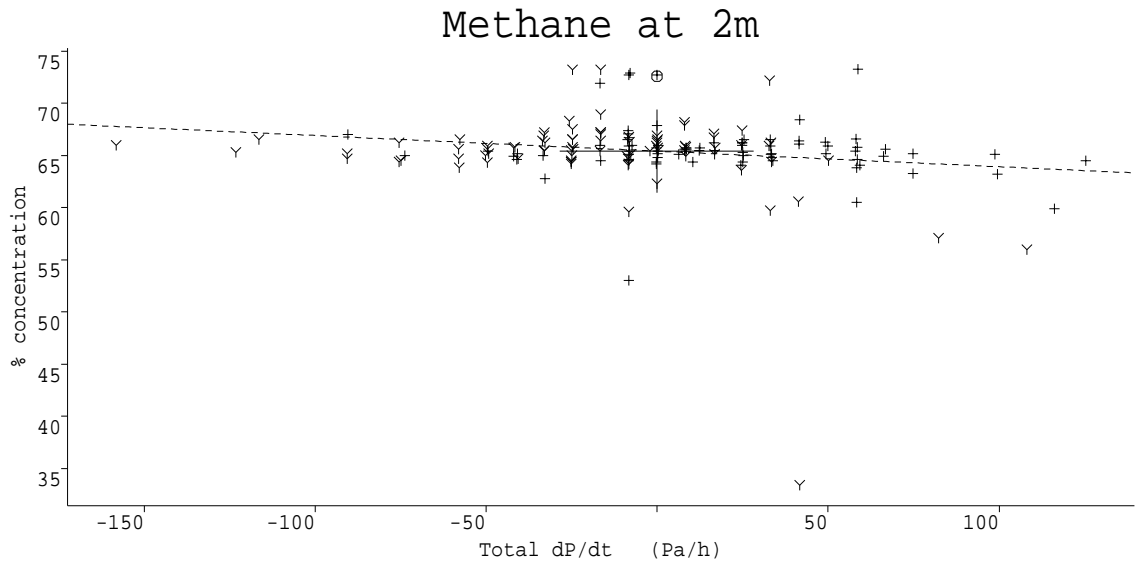
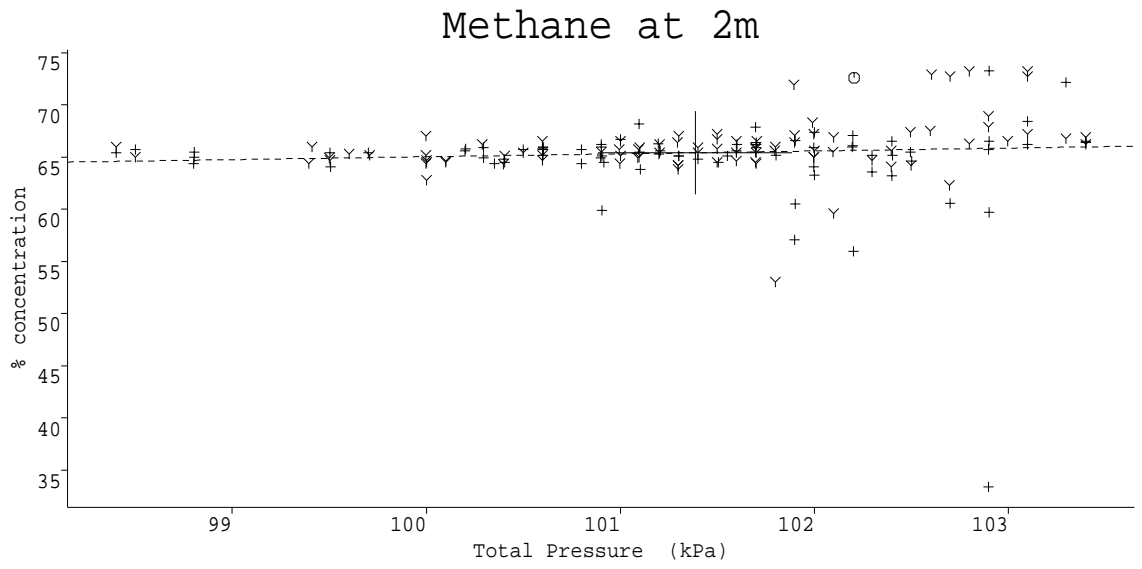


**Figure 4B.4 : Methane at 2m Depth.**

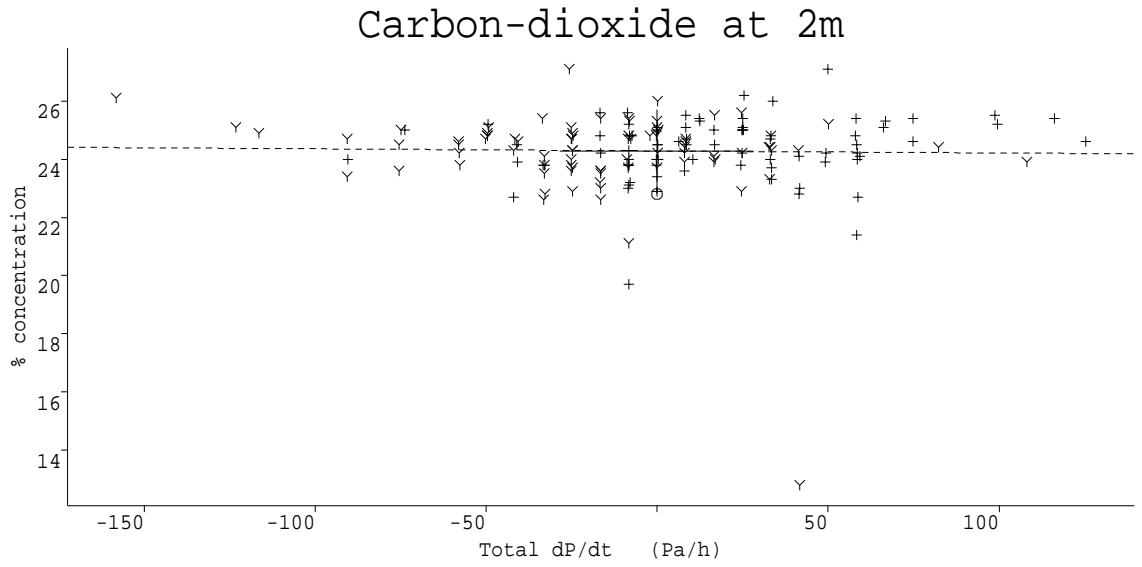
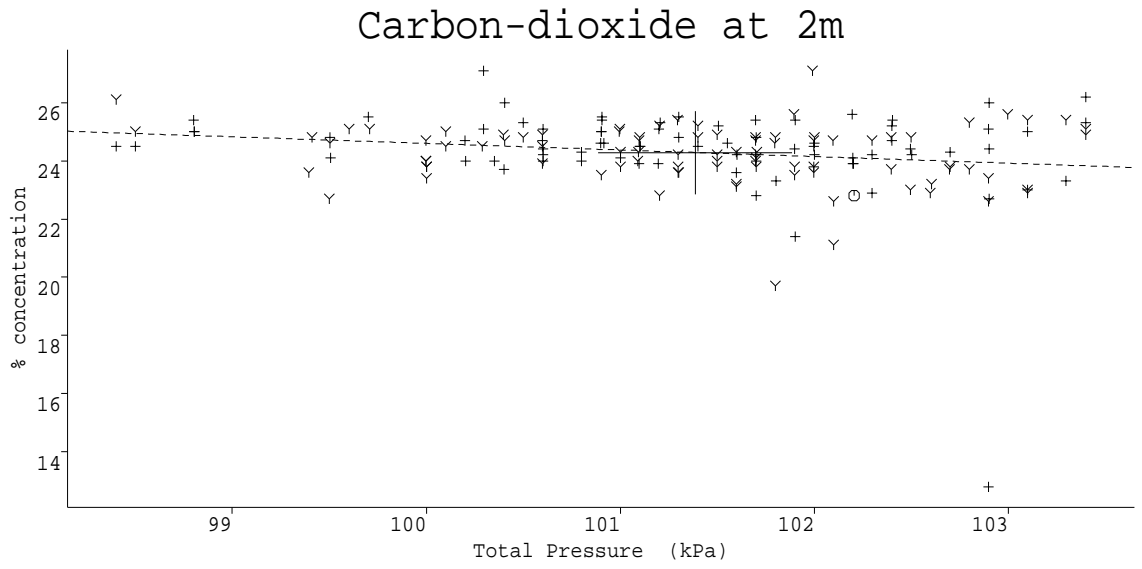


**Figure 4B.5 : Carbon-dioxide at 2m Depth.**

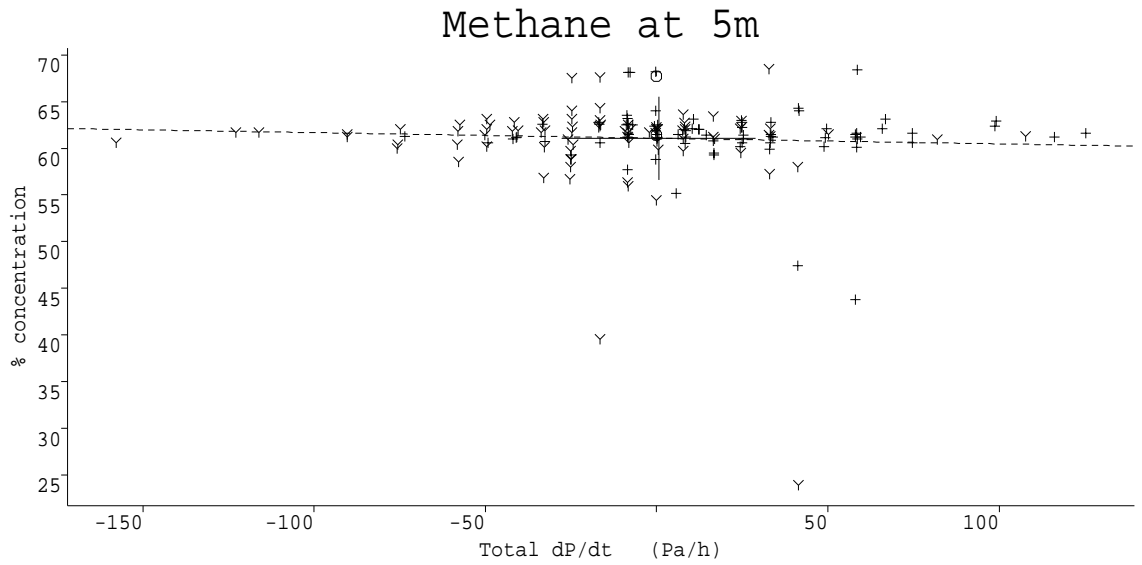
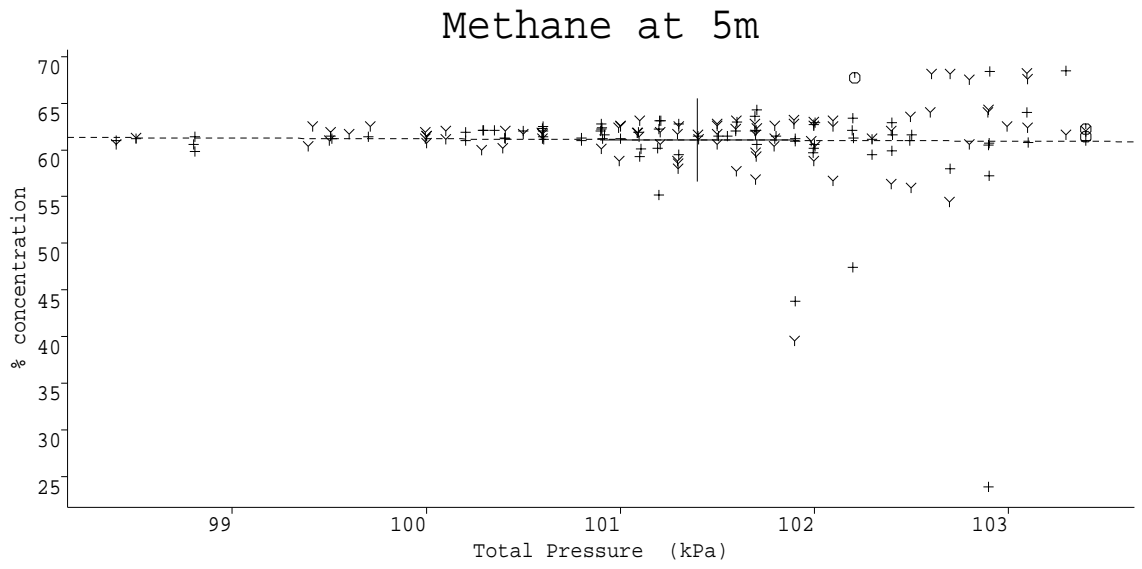


**Figure 4B.6 : Methane at 5m Depth.**

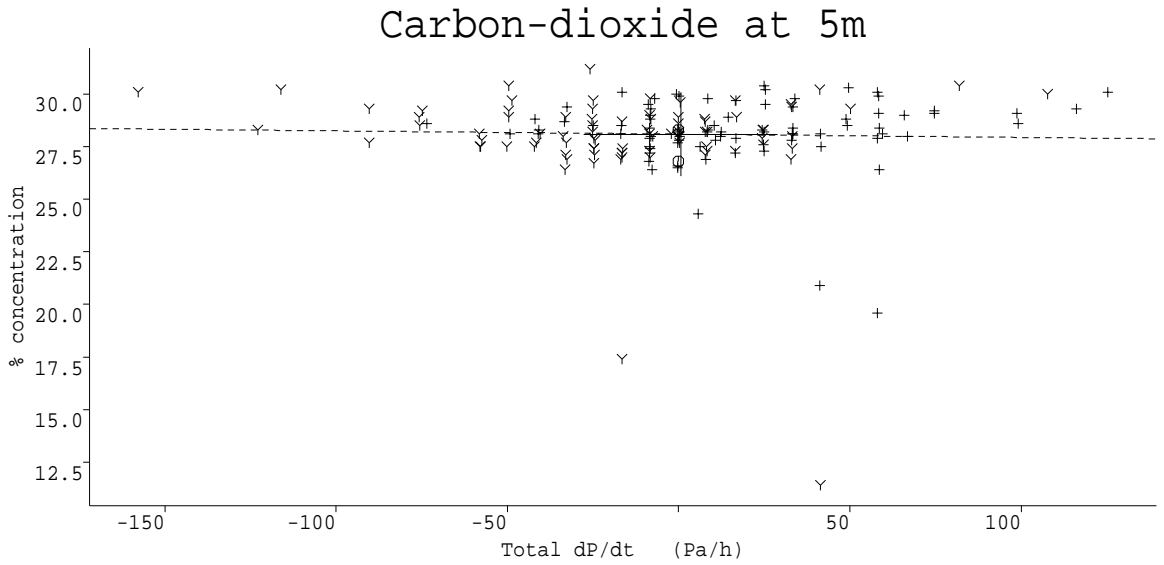
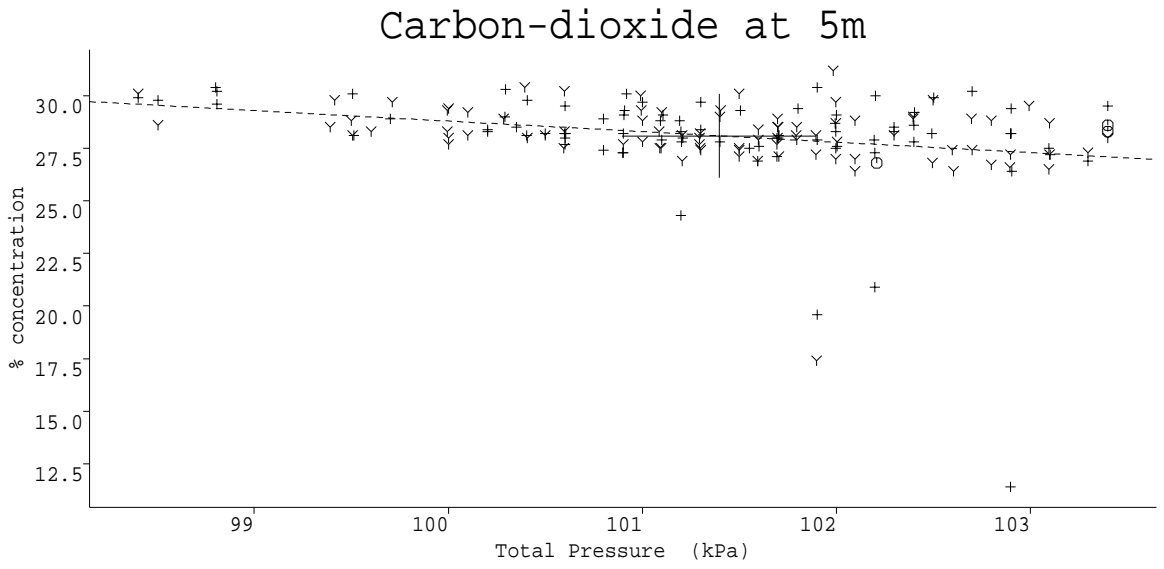


**Figure 4B.7 : Carbon-dioxide at 5m Depth.**

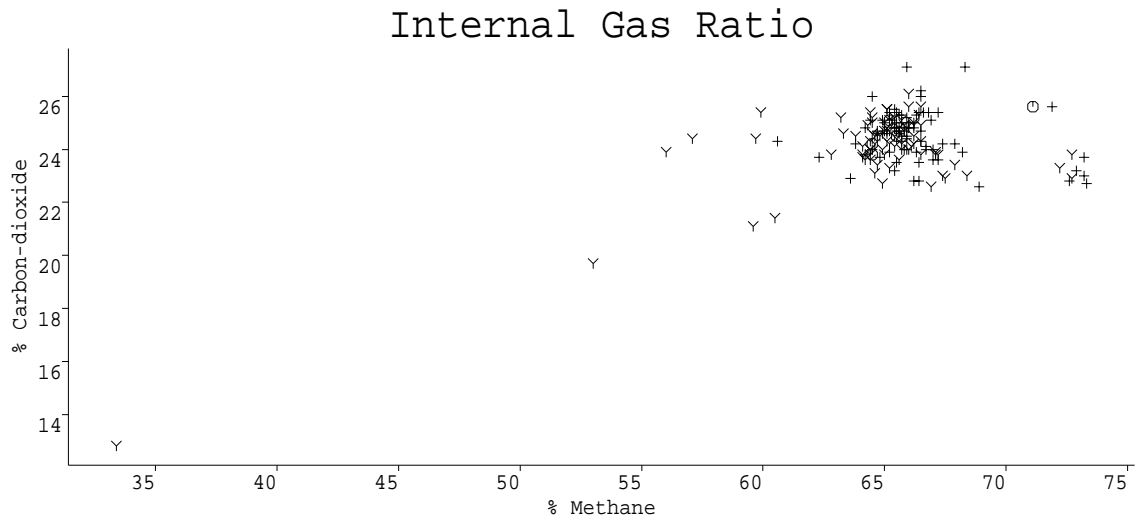


**Figure 4B.8 :** Carbon-dioxide versus methane in 2m borehole.

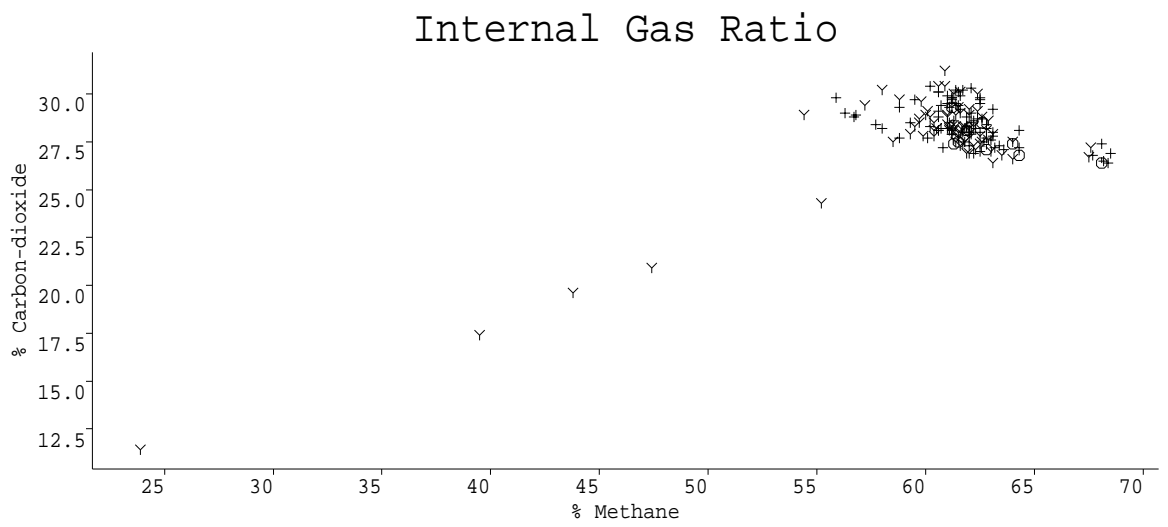


**Figure 4B.9 :** Carbon-dioxide versus methane in 5m borehole.



## Appendix 5A : Solution of Network Equations.

For convenience we re-write equations (5.4—5.7) in the form

$$G_i = \begin{cases} F_i^e - \Psi_i(P_k), & i = 1, \dots, N_e; \\ F_j^w - C_j - D_j(P_k + \sum_{k \neq j} P_j), & i = j + N_e, \quad j = 1, \dots, N_w; \\ F_j^p - \Phi_j(P_{kA} - P_{kB}), & i = j + N_e + N_w, \quad j = 1, \dots, N_p; \\ \sum_{k \in E_j} F_k^e + \sum_{k \in A_j} F_k^p - \sum_{k \in W_j} F_k^w - \sum_{k \in B_j} F_k^p, & i = j + N_e + N_w + N_p, \quad j = 1, \dots, N_c; \end{cases} \quad (1)$$

and re-label the variables as follows

$$\underline{x} = (x_1, \dots, x_N) = (F_1^e, \dots, F_{N_p}^e, F_1^w, \dots, F_{N_w}^w, F_1^p, \dots, F_{N_p}^p, P_1, \dots, P_{N_c}), \quad (2)$$

where  $N = N_e + N_w + N_p + N_c$ , giving the system of simultaneous equations

$$G_i(x_1, x_2, \dots, x_N) = 0, \quad i = 1, \dots, N. \quad (3)$$

This system may be solved using a Newton-Raphson scheme described below (for more details see Fletcher, 1980) which, since the functions  $\Psi$  and  $\Phi$  are monotonic, should converge well provided a suitable initial trial solution is chosen. The actual program interpolates the values of  $\Psi$  and  $\Phi$  from data points using cubic splines.

Suppose that  $\underline{z} = (z_1, \dots, z_N)$  is the solution of (3) and let  $\underline{h} = (h_1, \dots, h_N)$  be the deviation from this of a trial solution, then we can write

$$G_i(\underline{z} + \underline{h}) = G_i(\underline{z}) + \sum_{k=1}^N h_k \frac{\partial G_i}{\partial x_k}(\underline{z}) + O(h_k^2). \quad (4)$$

Assuming that  $h_k$  is sufficiently small the term  $O(h_k^2)$  can be neglected, and since  $G_i(\underline{z}) = 0$  this leaves a set of  $N$  simultaneous linear equations

$$G_i(\underline{z} + \underline{h}) = \frac{\partial G_i}{\partial x_1} \hat{h}_1 + \frac{\partial G_i}{\partial x_2} \hat{h}_2 + \dots + \frac{\partial G_i}{\partial x_N} \hat{h}_N, \quad i = 1, \dots, N. \quad (5)$$

the solution  $\hat{\underline{h}}$  being approximately equal to  $\underline{h}$ . The vector  $\hat{\underline{h}}$  may be subtracted from  $\underline{z} + \underline{h}$  to yield a new trial solution, and the process repeated until it converges sufficiently close to  $\underline{z}$ . Written in matrix form this system looks like

$$\begin{pmatrix} \mathbf{A} & \mathbf{B} \\ \mathbf{C} & \mathbf{0} \end{pmatrix} \begin{pmatrix} h_1 \\ h_2 \\ \vdots \\ h_N \end{pmatrix} = \begin{pmatrix} G_1 \\ G_2 \\ \vdots \\ G_N \end{pmatrix}_{(\underline{z}+\underline{h})}, \quad (6)$$

where  $\mathbf{A}$ ,  $\mathbf{B}$ ,  $\mathbf{C}$  and  $\mathbf{0}$  are matrices. The order of writing  $x_1, \dots, x_N$  and the form of  $G_i$  result in several simplifications since  $\mathbf{A}$  is an identity matrix of dimension  $N_e + N_w + N_p$ ,  $\mathbf{C}$  is sparse with scattered entries of  $\pm 1$  and zeroes elsewhere, and  $\mathbf{0}$  is the zero matrix.

Since the four sub-matrices have different formats they are most efficiently represented by differing structures in the computer program (only  $\mathbf{D}$  needs to be stored fully). This means that pivoted Gaussian elimination, rather than the more usual LU-decomposition, is the optimum algorithm for solving the system in an economical fashion.

## Appendix 5B : Analytical Gas Flow Solution.

Consider a rectangular region of waste which is generating gas and contains  $M$  vertical cylindrical boreholes. Take Cartesian axes  $x, y, z$  with  $z$  vertically downwards. Let the  $M$  wells be at horizontal co-ordinates  $(x_i, y_i)$ , with collection zones (typically perforated sections) between depths  $z_{i1}$  and  $z_{i2}$ . This satisfies the condition that the wells occupy only a tiny proportion of the landfill volume and thus (if blocked) would not significantly impede the flow due to the other wells.

Then equation (6.1) for the deviation from atmospheric pressure becomes

$$K_h \frac{\partial^2 P}{\partial x^2} + K_h \frac{\partial^2 P}{\partial y^2} + K_v \frac{\partial^2 P}{\partial z^2} + Q(x, y, z) = \sum_{i=1}^M v_i(z) \delta(x - x_i) \delta(y - y_i), \quad (1)$$

where  $K_h, K_v$  are the horizontal and vertical permeabilities, and  $v_i(z)$  is the strength of the  $i$ th well, defined as the mass of gas extracted per unit length per unit time.

$$v_i(z) = \begin{cases} \frac{V_i(U_i + s^4)}{2(U_i + 1/5)}, & z_{i1} < z < z_{i2}; \\ 0, & \text{otherwise.} \end{cases} \quad (2)$$

where  $s$  is defined on  $(z_{i1}, z_{i2})$  by  $s = (2z - z_{i2} - z_{i1}) / (z_{i2} - z_{i1})$ , and  $U_i \approx 1.65$  is an adjustable parameter which ensures that the pressure is roughly constant along the length of the well.

## 5B.1 Separable Solution by Transforms.

Let the landfill have length  $w_1$ , breadth  $w_2$ , and depth  $d$ , with impermeable base and sides, and a capped top of thickness  $l$  and permeability  $K_l$ . Hence the rate of gas migration through the site walls depends only on either the pressure, the pressure gradient, or a sum of the two, so that equation (6.3) can be expanded to give the boundary conditions

$$\frac{\partial P}{\partial x} = 0 \text{ on } x = 0, w_1; \quad \frac{\partial P}{\partial y} = 0 \text{ on } y = 0, w_2; \quad \frac{\partial P}{\partial z} = 0 \text{ on } z = d, \quad (3)$$

$$L \frac{\partial P}{\partial z} = P \text{ on } z = 0, \quad L = \frac{lK_v}{K_l}. \quad (4)$$

The problem can be broken down by considering the pressure as the sum of several parts,

$$P(x, y, z) = P_0(x, y, z) + \sum_{i=1}^M P_i(x, y, z), \quad (5)$$

where  $P_0$  is the solution in the absence of any wells and  $P_i$  is the perturbation caused by the  $i$ th well. Substituting expression (A5) into (A1) shows that the the background pressure  $P_0$  can be found by solving

$$K_h \frac{\partial^2 P_0}{\partial x^2} + K_h \frac{\partial^2 P_0}{\partial y^2} + K_v \frac{\partial^2 P_0}{\partial z^2} + Q(x, y, z) = 0, \quad (6)$$

which may be done using a Green's function. The other components of the overall pressure field satisfy the relation

$$K_h \frac{\partial^2 P_i}{\partial x^2} + K_h \frac{\partial^2 P_i}{\partial y^2} + K_v \frac{\partial^2 P_i}{\partial z^2} = v_i(z) \delta(x - x_i) \delta(y - y_i). \quad (7)$$

where  $\delta$  represents the Dirac delta function. The equation for  $P_i$  is solved by taking finite cosine transforms in first  $x$  then  $y$ , defining

$$g_{i,m,n}(z) = \int_0^{w_2} \left\{ \int_0^{w_1} P_i(x, y, z) \cos(\lambda_n x) dx \right\} \cos(\mu_m y) dy, \quad \lambda_n = \frac{n\pi}{w_1}, \quad \mu_m = \frac{m\pi}{w_2}, \quad (8)$$

with the result that

$$g_{i,m,n}(z) = \begin{cases} A_1 e^{\nu_{m,n} z} + B_1 e^{-\nu_{m,n} z}; & 0 < z < z_{i,1} \\ A_2 e^{\nu_{m,n} z} + B_2 e^{-\nu_{m,n} z} - \frac{V_i \cos(\lambda x_i) \cos(\mu y_i)}{2\nu_{m,n}^2 K_v (U_i + 1/5)} \left( U_i + s^4 + \frac{12s^2 \xi_i^2}{\nu_{m,n}^2} + \frac{24\xi_i^4}{\nu_{m,n}^4} \right), & z_{i,1} < z < z_{i,2}; \\ A_3 e^{\nu_{m,n} z} + B_3 e^{-\nu_{m,n} z}, & z_{i,2} < z < d; \end{cases} \quad (9)$$

where  $\nu_{m,n}^2 = K_h(\mu_m^2 + \lambda_n^2)/K_v$ , and  $\xi_i = 2/(z_{i,2} - z_{i,1})$ . The  $A$ 's and  $B$ 's are constants determined by the continuity of  $g_{i,m,n}$  and  $g'_{i,m,n}$  at  $z_{i,1}$  and  $z_{i,2}$  and the two external boundary conditions on  $z = 0, d$ . Sequentially inverting the transforms gives

$$P_i(x, y, z) = \frac{1}{wl} \left\{ g_{i,0,0} + 2 \sum_{m=1}^{\infty} g_{i,m,0}(z) \cos\left(\frac{m\pi y}{w_2}\right) + 2 \sum_{n=1}^{\infty} g_{i,0,n}(z) \cos\left(\frac{n\pi x}{w_1}\right) + 4 \sum_{n=1}^{\infty} \sum_{m=1}^{\infty} g_{i,m,n}(z) \cos\left(\frac{m\pi y}{w_2}\right) \cos\left(\frac{n\pi x}{w_1}\right) \right\}. \quad (10)$$

The linear boundary and continuity conditions on  $g_{i,m,n}$  mean that all of the  $A_1, \dots, B_3$  will be multiples of  $V_i$ , and (A5) can be rewritten as

$$P_i(x, y, z) = V_i F_i(x, y, z), \quad \Rightarrow \quad P = P_0 + \sum_{i=1}^M V_i F_i, \quad (11)$$

as indicated in the main text. This expression gives the pressure in terms of the amount of gas being extracted by each well — whereas we require the opposite relation.

Define  $\bar{F}_{i,j}$ ,  $W_j$  and  $\bar{P}_{0,j}$  as the mean values of  $F_i$ ,  $P$  and  $P_0$  respectively evaluated over the interface where the perforated section of well  $j$  meets the landfill. Hence  $W_i$  is the pressure at the  $i$ th well, and we have  $M$  equations which can be written as

$$\begin{pmatrix} \bar{F}_{1,1} & \bar{F}_{1,2} & \dots & \bar{F}_{1,M} \\ \bar{F}_{2,1} & \bar{F}_{2,2} & \dots & \dots \\ \vdots & \vdots & \ddots & \vdots \\ \bar{F}_{M,1} & \bar{F}_{M,2} & \dots & \bar{F}_{M,M} \end{pmatrix} \begin{pmatrix} V_1 \\ V_2 \\ \vdots \\ V_n \end{pmatrix} = \begin{pmatrix} W_1 \\ W_2 \\ \vdots \\ W_M \end{pmatrix} - \begin{pmatrix} \bar{P}_{0,1} \\ \bar{P}_{0,2} \\ \vdots \\ \bar{P}_{0,M} \end{pmatrix}, \quad (12)$$

The matrix of  $\bar{F}_{i,j}$  entries has an inverse, with entries  $h_{ij}$  say, and pre-multiplying (A12) by this inverse gives the final solution

$$V_i = \alpha_i + \sum_{j=1}^M h_{ij} W_j, \quad \alpha_i = - \sum_{j=1}^M h_{ij} \bar{P}_{0,j}, \quad i = 1, \dots, M. \quad (13)$$

Writing  $\beta_i = h_{ii}$  and  $\mu_{ij} = -h_{ij}/\beta_i$  produces the relationship proposed in the main text, and gives  $\mu_{ii} = -1$ .

### 5B.1.1 Convergence of Series for $P_i$

A convergence estimate is required for the series for  $P_i$ , in order to know how many terms are required for accurate numerical evaluation. The vertical distance  $z_{i,c}(z)$  of a point from the nearest end of the  $i$ th pump is the primary factor determining the convergence rate.

$$z_c = \min(|z - z_{i,1}|, |z - z_{i,2}|). \quad (14)$$

If  $z \in [z_{i,1}, z_{i,2}]$  convergence is much slower than otherwise, since the particular integral from equation (9) is then zero.

When  $z \notin [z_{i,1}, z_{i,2}]$ , then if the computer evaluation neglects all terms such that

$$\nu_{m,n}^2 = \frac{m^2}{l^2} + \frac{n^2}{w^2} < R^2 \quad (15)$$

the error ( $P_{i,R}^*$ ) caused by this satisfies the relation

$$P_{i,R}^* < \frac{V_i}{\pi k_h} E_1(\pi h z_c R), \quad (16)$$

where  $E_1$  is the Exponential Integral function, described in Abramowitz & Stegan (1964).

For the case where  $z \in [z_{i,1}, z_{i,2}]$  the solution does not converge at the  $\delta$  function singularity. Then an approximation to the error caused by ignoring terms with  $\nu_{m,n} > R$  is

$$P_{i,R}^* \approx \frac{V_i}{2\pi^2 k_h} \int_R^\infty \frac{1}{r} \sin(r x_c) dr. \quad (17)$$

where  $x_{i,c}$  is the horizontal distance to the singularity. Hence best results are obtained from choosing  $R$  so that the integral is zero. These values are given by Abramowitz & Stegan, and are approximately  $x_c R = (n + \frac{1}{2})\pi$ .

## Appendix 6A : Biochemical Approximations.

The composite substances were grouped to reflect the fashion in which they are assumed to break down, rather than according to more sophisticated biochemical definitions.

### 6A.1 Main Biochemical Scheme.

Carbohydrates : This is any substance having the formula



it was assumed to decompose into dissolved glucose and alcohols.

Proteins : This formula is based on an rough statistic that an 'average' protein contains 50% carbon, 25% oxygen, 15% nitrogen, 7% hydrogen and 3% sulphur by weight.



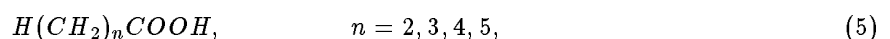
Fats : The wide variety of landfill waste makes this substance especially hard to formulate, and it was decided to take it as being composed of equal quantities of palmitic, stearic and oleic residues.



Acetic Acid : This is treated separately from the other acids because of its importance in methanogenesis.



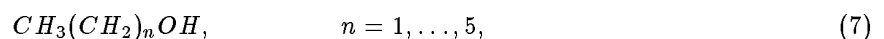
Carboxylic Acids : These are assumed to be an equal mixture by weight of the propionic, butyric, valeric and caproic species. The absence of the longer chain acids is compensated for by having more of the latter two types than are normally found. These have the group formulae



which may be combined to yield an empirical approximation for the composite carboxylic acid



Alcohols : The formula for alcohol was picked so that it would decompose to acetic acid and the composite carboxylic acid in the proportions of 1:2 by weight. It is thus a mixture of substances with the description



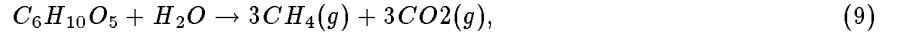
having an overall empirical approximation

$$C_{507}H_{1320}O_{153}. \quad (8)$$

## 6A.2 Alternative Biochemical Schemes.

This section details the alternative schemes considered during the biological modelling, and gives the calculated energy values associated with them as used in the thermal-feedback modelling. The values of  $\Delta G^\ominus$  and  $\Delta H^\ominus$  are given in  $\text{KJ mol}^{-1}$ .

Overall methanogenic reaction

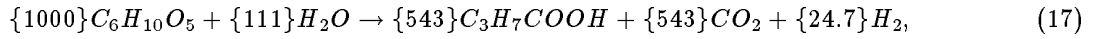
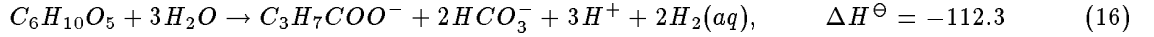
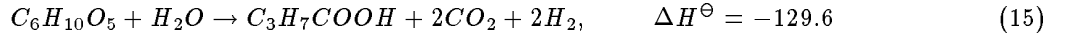
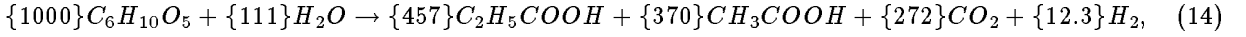
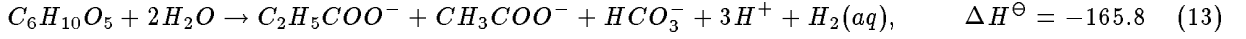
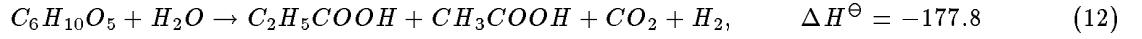


The free energy equations for the breakdown of butanoic and propanoic acids respectively are

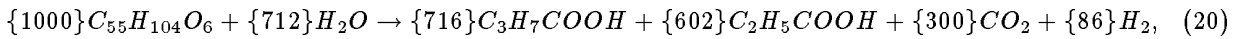
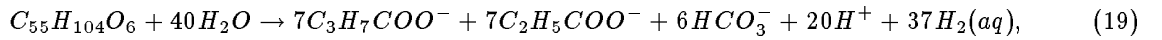
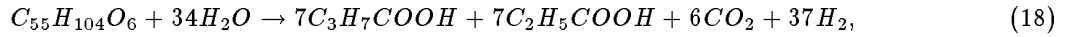
$$\Delta G = \Delta G^\ominus - RT \ln \left( \frac{[Ac^-]^2[H^+][H_2]^2}{[C_3H_7COO^-]} \right) \quad (10)$$

$$\Delta G = \Delta G^\ominus - RT \ln \left( \frac{[Ac^-][HCO_3^-][H^+][H_2]^3}{[C_2H_5COO^-]} \right) \quad (11)$$

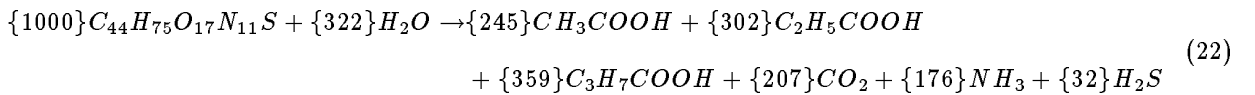
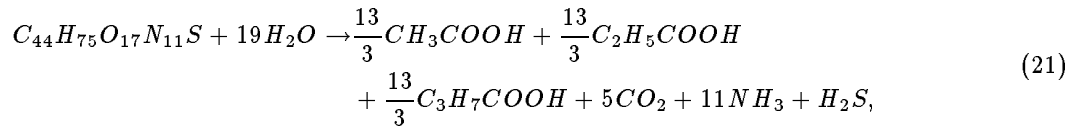
Starch to butanoic, propanoic and acetic acids, plus carbon dioxide and hydrogen.



Fat to equimolar mixture of butanoic and propanoic acids



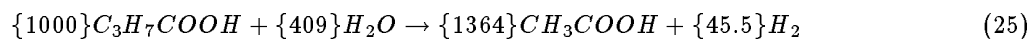
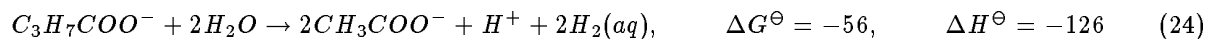
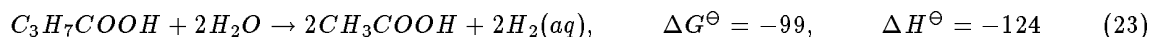
Protein to equimolar mixture of butanoic, propanoic and acetic acids



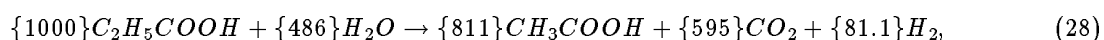
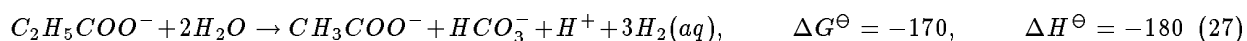
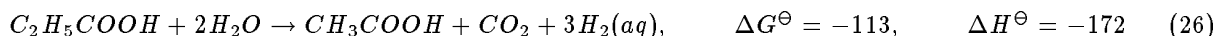


### 6A.2.1 Acetogenic and Methanogenic Reactions.

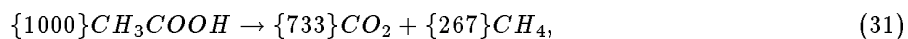
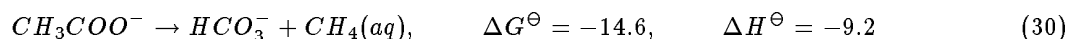
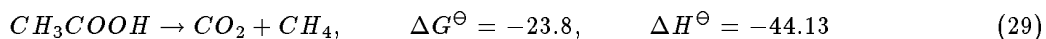
Butanoate to acetate



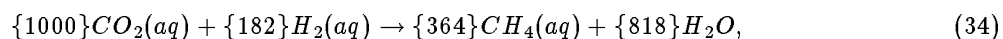
Propanoate to acetate



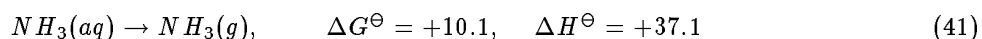
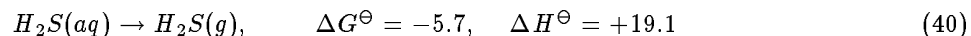
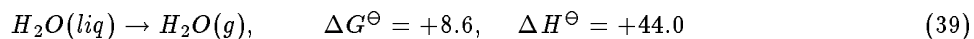
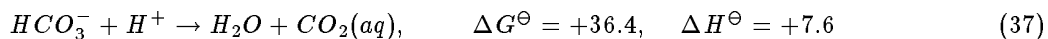
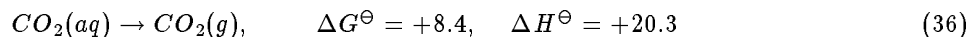
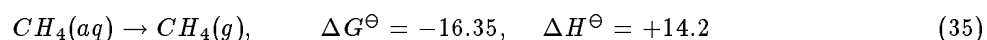
Acetate to methane



Reduction of carbon dioxide to methane



### 6A.3 Thermal Parameters for Gas Evolution.



## **Appendix 6B : Effects of Temperature and pH.**

This Appendix summarises the work performed by Dr. Irene Watson-Craik and Sandra Goldie at the Department of Bioscience and Biotechnology in the University of Strathclyde. The full report is entitled “The Effects of Incubation Temperatures and pH on the Refuse Methanogenic Fermentation”.

The main aims of this 10-week project were to investigate the effects of temperature, low leachate pH and high volatile fatty acid (particularly acetate) concentrations. The experiments were designed to produce data both on methane release rates, and the turnover of intermediate metabolites.

### **6B.1 Effects of Temperature.**

Experiments were conducted at intervals of 5 °C from 10 °C to 50 °C.

#### **6B.1.1 Experiment.**

Triplicate closed culture bottles (500 ml) were filled with 20 g waste and 150 ml phosphate buffer. To eliminate problems due to substrate availability, some of the bottles were supplemented with 1 ml sodium acetate after 29 days. The buffer maintained the pH at around 6.5.

The bottles were initially over-gassed with OFN (oxygen free nitrogen) and at regular intervals (3–6 days) headspace samples (50 µl) were withdrawn through the subbaseals for GC (gas chromatograph) analysis. After gas analysis the bottles were again over-gassed with OFN. At intervals of 5–7 days small liquid samples (0.9 ml) were withdrawn from one randomly-selected bottle at each temperature and the concentrations of acetate, propionate, butyrate and valerate determined by GC.

### **6B.1.2 Results.**

No significant rates of methane release were recorded at incubation temperatures below 20 °C within 43 days (NAS, no acetate supplementation) or 36 days (AS). With a lag period arbitrarily defined as the time required to achieve a headspace methane concentration of 0.2 μmol ml<sup>-1</sup>, the shortest lags were recorded at 35 °C.

The maximum rates of methane release were 1.72 mmol d<sup>-1</sup> at 35 °C (NAS) or 1.99 mmol d<sup>-1</sup> at 30 °C (AS). Although the maximum release rates were comparable in the NAS and AS cultures, methane release rates from replicate bottles varied considerably, presumably due to heterogeneities in the small waste samples.

Acetate was usually the VFA present in the highest concentrations. At temperatures below 25 °C the concentrations of all the acids (particularly acetate) increased with time, suggesting that acidogenesis and acetogenesis are less sensitive to low temperatures than methanogenesis (a similar effect was observed above 40 °C).

At incubation temperatures of 30 °C and 35 °C acetate concentrations initially increased then decreased significantly, presumably due to elevated methane release rates, and a week later methane production also declined probably due to substrate limitation.

### **6B.2 Effects of pH and Organic Acid Concentration.**

Experiments were conducted at pH intervals of 0.5 from 5.5 to 8.

#### **6B.2.1 Experiment.**

Triplicate closed-culture bottles were set up as for the temperature investigation, with the phosphate buffer adjusted to provide pH values over the range 5.5–8.0. The NAS bottles had 150 ml of phosphate solution added, whereas the AS bottles had 140 ml. After 26 days, 10 ml of either 0.15M or 1.50M sodium acetate solutions were added to the AS cultures. All the bottles were incubated at 30 °C.

### 6B.2.2 Results.

The pH effects over the interval 5.5–8.0 were seen to be less than the temperature effects over the range 10–50°C. Significant methane release rates were recorded in the NAS cultures over the range 5.5–7.5. Variations in lag-time were also less, with no significant differences observed over the interval 6.0–7.5.

This investigation, together with other experiments carried out by Dr. Watson-Craik, indicates that methanogens have much broader pH optima than generally quoted in the literature. Methane release rates seem comparable over from pH 6.0 to 7.5, with a minor reduction at 5.5 and a significant at 8.0.

It was unclear whether acidogenesis and acetogenesis were also partially inhibited, since elevated VFA concentrations were observed in some of the duplicate bottles at the ends of the pH range tested, but not in others. Immediately after the addition of the acetate supplements there was a 1–2 day period of reduced methane production, and the introduction of oxygen dissolved in the liquid supplement was suggested as a likely explanation.

There was no evidence of methanogenic inhibition due to the acetate supplementation in the pH range 6–7. This corresponds to peak acetate concentrations of 100 mmol (equivalent to 5000 mg l<sup>-1</sup>) and it is therefore thought unlikely that methanogenesis in landfill sites is inhibited by high acetate levels *per se*.

### 6B.3 Analysis of Landfill Waste Used in Experiment.

Below is the analysis of the 2 kg waste sample (from the Wilderness Landfill, Bishopriggs) used for the bottle experiments. All units are  $\text{mg kg}^{-1}$  except where stated.

pH	6.76	Cd	<0.1
TOC	27.2%	Cr	8
calorific value	4227 $\text{J g}^{-1}$	As	<0.1
moisture content	32.3%	Pb	59
cellulose	33.3%	Hg	<0.1
lignin	9.92%	Cu	296
fluoride	26.2	Ni	102
chloride	650.8	Zn	114
nitrate	2.9	B	17
phosphate	87.4	Fe	44480
sulphate	1484.0	Mn	268
carbonate	25.1%	Al	16590
VFA	26	Ti	172
		V	494
		Mo	1
		Sb	<0.1
		Mg	5695
		Na	28
		K	36
		Ca	24650

## Appendix 7A : Solution of Gas Flow Equations.

It has been observed that the permeability of landfills to gas flow is often much greater in a horizontal direction than in a vertical direction. The problem considered here is the flow of gas under pumping in such a landfill (using cylindrical polars with axial symmetry). A small parameter  $\varepsilon = K_v/K_h$  is introduced and the solution for the pressure obtained as a series

$$P(r, z) = P_0(r, z) + \varepsilon P_1(r, z) + O(\varepsilon^2). \quad (1)$$

The equation governing gas flow under the above conditions is

$$\frac{1}{r} \frac{\partial}{\partial r} \left( r \frac{\partial P}{\partial r} \right) + \varepsilon \frac{\partial^2 P}{\partial z^2} + H(z) \delta(r) = 0. \quad (2)$$

where  $H(z)$  represents the pumping from the line  $r = 0$  and need not be continuous. A crucial factor in solving (1) is the magnitude of this pumping term which must be consistent with any boundary conditions applied.

### 7A.1 Sealed Site.

Use of a no flux condition at  $r = a$  say, forces  $H(z) = O(\varepsilon)$ . This can be seen from solving (1) to  $O(1)$ . If  $H(z)$  is  $O(1)$  the solution is

$$P_0(r, z) = b(z) - \frac{1}{2\pi} H(z) \log r. \quad (3)$$

But imposing  $\frac{\partial P}{\partial r} = 0$  on  $r = a$  requires  $H(z) = 0$ . Hence  $H(z)$  is  $O(\varepsilon)$ , and the first order solution is simply

$$P_0(r, z) = b(z), \quad (4)$$

with  $b(z)$  to be determined by the examination of higher order terms.

Write  $H(z) = \varepsilon H_1(z)$  and consider terms in (1) of order  $\varepsilon$ . This gives

$$\frac{1}{r} \frac{\partial}{\partial r} \left( r \frac{\partial P_1}{\partial r} \right) + \frac{d^2 P_0}{dz^2} + H_1(z) \delta(r) = 0, \quad (5)$$

which can be integrated twice w.r.t.  $r$  to yield the result

$$P_1(r, z) = -\frac{r^2}{4} \frac{d^2 P_0}{dz^2} + c_1(z) \log r + d_1(z), \quad (6)$$

where  $c_1(z) = -\frac{1}{2\pi} H_1(z)$ . Applying the no flux condition on  $r = a$  now provides the required equation for  $P_0$ , ie.

$$\frac{d^2 P_0}{dz^2} = \frac{2}{a^2} c_1(z). \quad (7)$$

This result can be fed back into the equation for  $P_1(r, z)$  to give

$$P_1(r, z) = c_1(z) \left[ \log r - \frac{r^2}{2a^2} \right] + d_1(z). \quad (8)$$

### 7A.1.1 Gas Velocity.

The gas velocity  $\underline{u}$  is given by

$$\begin{aligned}\underline{u} &= \underline{K} \cdot \nabla P = \left( K_h \frac{\partial P}{\partial r}, K_v \frac{\partial P}{\partial z} \right) \\ &= K_h \left( \frac{\partial P}{\partial r}, \varepsilon \frac{\partial P}{\partial z} \right) \\ &= \varepsilon K_h \left( \frac{\partial P_1}{\partial r}, \frac{\partial P_0}{\partial z} \right).\end{aligned}\tag{9}$$

The radial component is found (by differentiating equation (9)) to be

$$u_r = \varepsilon K_h c_1(z) r \left[ \frac{1}{r^2} - \frac{1}{a^2} \right],\tag{10}$$

and the vertical component  $u_z$  is found by integrating the pump strength  $c(z)$ . In areas where there is no pumping ( $c(z) = 0$ ) the velocity is seen to be constant and vertical ( $u_r = 0$ ).

## 7A.2 Practical Problems.

In practice it is virtually impossible to ensure a no flux condition on the boundary  $r = a$ , so a more feasible condition needs to be used. One possibility is the standard leaky boundary condition

$$\frac{L}{a} \frac{\partial P}{\partial r}(a, z) = P(a, z),\tag{11}$$

where  $L$  is a measure of the integrity of the boundary. For large values of  $L$  (ie. if  $L = O(\frac{1}{\varepsilon})$ ) similar gas flow patterns to those in a sealed site are observed.

### 7A.2.1 Slightly Leaky Boundary.

The problem is now considered with the leaky boundary condition (11).

If  $L$  is  $O(1)$  the problem is trivial with the first order velocity being simply  $(\frac{c(z)}{r}, 0)$ . However for  $L = L_1/\varepsilon$  the structure of the no flux solution is retained, and

$$P(r, z) = P_0(z) + \varepsilon P_1(r, z) + O(\varepsilon^2),\tag{12}$$

where

$$\frac{d^2 P_0}{dz^2} - \frac{2}{M} P_0 = \frac{2c_1(z)}{a^2},\tag{13}$$

and

$$P_1(r, z) = -\frac{r^2}{2} \left( \frac{P_0}{L_1} + \frac{c_1}{a^2} \right) + c_1 \log r + d_1(z).\tag{14}$$

### 7A.2.2 Consequences

If the low flux boundary could be achieved in practice the even velocity distribution achieved would be extremely advantageous in any 'hot gas recycling' scheme. A suitable arrangement would be two pumps (one sucking, one blowing) placed at any convenient (x,y) coordinates, but at depths which differ by the greatest possible amount.

## Appendix N : Main Notation.

This appendix lists the variables used for the mathematical models in each Chapter, and the associated sections of Chapter 3.

### **N.1 Notation for Chapter 4.**

$k$	decay factor for gas evolution/solution rate, $s^{-1}$ .
$Q_i$	mass rate at which molecules of gas $i$ are evolved, $kg\ m^{-3}\ s^{-1}$
$t$	time, s
$u$	Darcy water velocity, $m\ s^{-1}$ .
$v$	net Darcy gas velocity, $m\ s^{-1}$ .
$z$	depth co-ordinate, positive downwards, m.
$C_i$	dissolved concentration of solute $i$ , $kg\ m^{-3}$
$D_{ij}^b$	binary diffusion coefficient of gases $i$ and $j$ in free space, $m^2\ s^{-1}$ .
$D_{ij}$	modified binary diffusion/dispersion coefficient of gases $i$ and $j$ , $m^2\ s^{-1}$ .
$E_i$	combined diffusion and dispersion coefficient of gas $i$ , $m^2\ s^{-1}$ .
$E_i^w$	combined diffusion and dispersion coefficient of solute $i$ , $m^2\ s^{-1}$ .
$H$	Henry's constant, $kg\ m^{-3}\ Pa^{-1}$ .
$\underline{K}$	permeability of site to gas flow, $m^2\ s^{-1}\ Pa^{-1}$ .
$K_v$	vertical permeability of site to gas flow, $m^2\ s^{-1}\ Pa^{-1}$ .
$P$	total pressure of gas, Pa.
$P_i$	partial pressure of $i$ th gas, Pa.
$Q$	total rate of gas evolution, $kg\ m^{-3}\ s^{-1}$
$S_i$	rate at which molecules of gas $i$ are created by biochemical activity, $kg\ m^{-3}\ s^{-1}$
$T_{1/2}$	half life for gas evolution/solution, s.
$V$	an arbitrary volume within the landfill.
$\partial V$	surface surrounding volume $V$ .
$\lambda_i$	conversion factors from gas densities to pressures, $Pa\ m^3\ kg^{-1}$
$\varphi$	void fraction occupied by gas.
$\theta$	void fraction occupied by water.
$\rho_i$	density of $i$ th gas, $kg\ m^{-3}$
$\tau, \tau^w$	tortuosities for diffusion in gas and water phases.
$\Omega$	rate of gas evolution/solution, $kg\ m^{-3}\ s^{-1}$ .



## N.2 Notation for Chapter 5.

$A_i, B_i$	the set of pipes having end $A, B$ connected to node $i$ .
$E_i$	the set of extraction pumps connected to node $i$ .
$F_i^e, F_i^w, F_i^p$	fluxes through pumps, wells and pipes.
$\underline{K}$	permeability of landfill.
$K_h, K_v$	horizontal and vertical permeabilities of landfill.
$K_l$	vertical permeability of capping layer.
$L$	capping parameter.
$M$	number of wells in site
$N$	total number of components and nodes in a network.
$N_e, N_w, N_p, N_c$	number of pumps, wells, pipes and nodes in a network.
$p_i$	pressure at point $r_i$ within site, Pa.
$P_i$	pressure at connection node $i$ in Network analysis, Pa.
$P$	deviation of pressure from atmospheric value.
$P_a$	atmospheric pressure.
$P_0, P_1, \dots, P_M$	component parts of pressure field in YRC derivation.
$S$	volume-averaged rate of gas extraction.
$V_i$	rate of gas extraction at well $i$ per unit length.
$W_i$	the set of wells connected to node $i$ .
$l$	thickness of capping layer.
$\underline{r}$	location of a point within site
$\alpha_i$	flux at well $i$ when no suction is applied to any of wells.
$\beta_i$	flux proportionality at well $i$ .
$\varphi$	void fraction available to gas.
$\mu_{ij}$	yield reduction coefficient due to well $j$ acting on well $i$ .
$\Psi_i$	flux function for pump $i$
$\Phi_i$	flux function for pipe $i$ in $A \rightarrow B$ direction.

### N.3 Notation for Chapter 6.

$E$	rate of substrate utilisation in Monod's Law;
$G_{ij}$	mass of the $i$ th primary substrate, of decay speed $j$ ;
$H$	rate of gas evolution from the leachate;
$K_i$	half rate constant in Monod's Law;
$k_d$	endogenous death rate in Monod's law;
$N$	smoothing interval;
$Q$	net rate at which a solute is created by biochemical activity;
$t$	time;
$T$	temperature;
$V$	rate of excess gas venting;
$X_b, X_a, X_A$	mass of alcohol, acetic acid and organic acid per $\text{dm}^3$ ;
$X_a, X_h$	mass of acetoclastic and $H_2$ -methanogens per $\text{dm}^3$ ;
$Y$	growth yield coefficient in Monod's Law;
$Z_i$	concentration of substance $i$ per $\text{dm}^3$ of landfill liquid;
$\theta$	the fractional volumes occupied by water;
$\varphi$	the fractional volumes occupied by gas;
$\nu_j$	empirical decay rate coefficients;
$\rho_h, \rho_c, \rho_g, \rho_n, \rho_l, \rho_s$	the densities of $H_2, CO_2, CH_4, N_2, NH_3$ and $H_2S$ in the void space;
$\Omega$	net rate of water inflow/outflow.

## Appendix R : References.

### **R.1 Publications referred to within this report.**

- [] Abramowitz M., Stegun I.A. (1964)  
“Handbook of Mathematical Functions.”  
Dover Publications, Inc., New York.
- [] Archer D.B., Fielding E.R. (1986)  
In : ‘Effluent Treatment and Disposal.’  
IChemE symposium series No.96, Pergamon Press, pp.331–341.
- [] Archer D.B., Harris J.E. (1986)  
In : ‘Anaerobic bacteria in habitats other than man : Symposium Proceedings.’  
(Barnes E.M., Mead G.C. Eds.)  
Blackwell Scientific Publications, pp.185-223.
- [] Atkins P.W., (1986)  
“Physical Chemistry.” 3rd Edition.  
Oxford University Press.
- [] Bogner J., Vogt M., Moore C., Gartman D., (1987)  
“Gas pressure and concentration gradients at the top of a landfill.”  
Proceedings GRCD 10th International Landfill Gas Symposium.
- [] Chapman S. & Cowling T.G., (1970), ‘The Mathematical Theory of Non-Uniform Gases.’  
(3rd Edition) Cambridge University Press. p343–357.
- [] Coleman P.F., Gupta A.K., Oldham W.K. (1985)  
In : ‘Proceedings of International Conference : New directions and research in waste  
management and residuals management. June 23–28.’ (Jasper S.E. Ed.)  
University of British Columbia, Vol.1, ISBN 0-888-65-350-6. pp.376–391.
- [] Davies A.J. (1980),  
‘The Finite Element Method.’  
Oxford University Press.
- [] Farquhar G.J., Rovers F.A. (1973)  
‘Gas production during refuse decomposition.’  
Water, Air and Soil Pollution, Vol.2, pp.483–495.
- [] Findikakis A.N., Leckie J.C. (1979)  
‘Numerical simulation of gas flows in sanitary landfills.’  
Jou. of the Env.Eng.Div., ASCE, Vol.1, pp.927-945.
- [] Hoeks J. (1983)

- ‘Significance of biogas production in waste tips.’  
Waste Management and Research, Vol.1. pp.323–335.
- [] Huang J-C, Huang Y-J, Ray B.T. (1985)  
In : ‘Proceedings of International Conference : New directions and research in waste management and residuals management. June 23–28.’ (Jasper S.E. Ed.)  
University of British Columbia, Vol.1, ISBN 0-888-65-350-6. pp.582-591.
- [] Lawrence A.W., McCarty P.L. (1969)  
‘Kinetics of methane fermentation in anaerobic treatment.’  
Journal of the Water Pollution Control Federation, Vol.41(2), pp.R1–R17.
- [] Pirt S.J. (1975)  
‘Principles of microbe and cell cultivation.’  
Blackwell Scientific Publications, p.68.
- [] Rettenberger G. (1990)  
“Gas migration: measurement and monitoring.”  
Proceedings Landfill Gas: Energy and Environment ‘90. ISBN 0-7058-1628-1.
- [] Weast R.C.,  
“CRC Handbook of Chemistry and Physics.” 1st Student Edition.  
CRC Press, Inc., Florida.
- [] Young A. (1989)  
‘Mathematical Modelling of Landfill Gas Extraction.’  
Journal of the Environmental Engineering Division of the American Society of Civil Engineers, Vol.115(6), p1073–1087.
- [] Young A. (1990)  
‘Volumetric Changes in Landfill Gas Flux in Response to Variations in Atmospheric Pressure.’  
Waste Management & Research, Vol.8, p379–385.
- [] Zinder S.H. (1984)  
‘Microbiology of anaerobic conversion of organic wastes to methane : recent developments.’  
ASM News, Vol.50(7) pp.294–298.

## **R.2 Publications Associated with CWM039/92.**

- [1] “Mathematical Models for Active Landfills.”  
D.Phil Thesis, Mathematical Institute, Oxford, 1989.
- [2] “Mathematical modelling of landfill degradation.”  
Journal of chemical technology and biotechnology, Vol.46, p189–208, September 1989.
- [3] “Mathematical modelling of landfill gas extraction.”  
Journal of the environmental engineering division, A.S.C.E., Vol.115, No.6, p1073–1087, December 1989.
- [4] “Simulating Methanogenesis in Landfills.”  
Proc. of Landfill Microbiology R&D Workshop, ETSU p62–86, 1990.
- [5] “Volumetric Changes in Landfill Gas Flux in Response to Variations in Atmospheric Pressure.”  
Waste Management and Research., Vol.8, p379–385, 1990.
- [6] “The Landfill Ecosystem.”  
I.M.A. Journal of Mathematics Applied in Biology, Vol.7, p199–217, December 1990.
- [7] “A Model for the Effects of Fluctuations in Atmospheric Pressure on Landfill Gas Migration and Composition.”  
Water, Air and Soil Pollution, 1992.

### **R.2.1 Papers Pending.**

- [8] “Interactions Between Gas Extraction Wells.”
- [9] “Evaluating Network Pumping Strategies for Landfill Gas Installations.”
- [10] “Results of Sleep Investigation.”